# ABSTRACT

Title of dissertation:    Effect of Aggregate Inhomogeneity on Mechanical
                          Properties of Asphalt Mixtures

                          Haleh Azari, Doctor of Philosophy, 2005

Dissertation directed by:    Professor Richard McCuen
                             Department of Civil and Environmental Engineering

Vertical and radial inhomogeneity of asphalt mixture components in laboratory-fabricated specimens have been of concern in asphalt mixture testing because of their potential effect on the mechanical response of the materials. Two important questions needed to be answered. First, can the existence of inhomogeneity in laboratory specimens definitively be distinguished? Second, if inhomogeneity exists, what effect would it have on the performance of asphalt materials?

Several new indices were developed to assess the extent of inhomogeneity. The level of accuracy of the suggested indices was evaluated by testing virtual and real specimens. Computer simulation was used to fabricate virtual specimens with various aggregate structures and to test the indices. The statistical power of the tests and the critical values for tests on the proposed indices were computed. The computed power of the tests indicated that the proposed tests are accurate for the measurement of both vertical and radial inhomogeneity.

Actual specimens, both homogeneous and inhomogeneous, were fabricated to validate the simulation results. The indices of homogeneity were computed from the x-ray computed tomography images of the specimens. Among the proposed indices, the z

index on frequency proportion most clearly distinguished between the homogeneous and inhomogeneous specimens.

The specimens were then subjected to mechanical testing to examine the effect of inhomogeneity on the mechanical performance of the material. The effect of vertical and radial inhomogeneity was examined on compressive and shear properties of the mixtures, respectively. Statistical analyses on the results indicated that the compressive modulus ($E^*$) of homogeneous specimens were slightly but not significantly higher than those of vertically inhomogeneous specimens, and the shear modulus ($G^*$) of homogeneous specimens were significantly lower than those of radially inhomogeneous specimens.

A correlation analysis indicated insignificant correlation between the compressive properties and the index of vertical homogeneity but significant correlation between the shear properties and the index of radial homogeneity. The asphalt mixture was not sensitive to extreme level of vertical inhomogeneity when loaded axially but was responsive to radial inhomogeneity when loaded in shear.

EFFECT OF AGGREGATE INHOMOGENEITY ON MECHANICAL
PROPERTIES OF ASPHALT MIXTURES

by

Haleh Azari

Dissertation submitted to the Faculty of the Graduate School of the
University of Maryland at College Park, in partial fulfillment
of the requirements for the degree of
Doctor of Philosophy
2005

Advisory Committee:

       Professor Richard McCuen
       Professor Sherif Aggour
       Professor Charles Schwartz
       Professor Ahmet Aydilek
       Professor Mohammed Al-Sheikhly

# DEDICATION

I dedicate this dissertation to my wonderful family. Particularly to my husband, Ala, who encouraged me to pursue my Ph.D. and has been understanding and patient during these many years of research, and to our children, who their love and support inspired me to continue to the end. I must also thank my mother who has always supported me emotionally. Finally, I dedicate this work to my late grandmother who always believed in me.

# ACKNOWLEDGEMENTS

# TABLE OF CONTENTS

# LIST OF FIGURES

# LIST OF TABLES

# CHAPTER 1 -  INTRODUCTION

## 1.1  BACKGROUND

Segregation, which is defined as "inhomogeneity" in the internal structure of asphalt mixture specimens, has been of concern in laboratory testing. The internal structure of specimens is characterized by the distribution of the asphalt mixture components such as aggregates, mastic, and voids. Several studies have indirectly aimed to relate the mechanical properties of asphalt mixture specimens to their internal structure. Research on the required minimum dimension of a specimen with respect to aggregate size that provides consistent engineering properties were a means of explaining the effect of internal structure (Witczak et al. 1999). The research showed that, as the minimum dimension of the specimen increased, the consistency of the measured mechanical properties increased. Similarly, Romero and Anderson (2000) associated a high variability in the measured shear properties to the small ratio of the smallest specimen dimension to largest aggregate diameter. It is generally believed that the probability of achieving a homogeneous material increases as the dimensions of the specimen are increased because the aggregates have a better chance of being distributed randomly.

The internal structure of granular materials, which was defined by the distribution and orientation of the grains and the voids, has been shown to have an important influence on the mechanical properties of the material (Oda 1972). It is documented that the aggregate distribution and orientation controls the shear strength and yielding behavior of unbound granular materials (Tobita 1989). Thus, it can be speculated that the

internal structure of an asphalt mixture as a bounded granular material has a significant effect on its stress-strain response.

The effect of field segregation on the performance of the asphalt pavements has been investigated (Chang et al. 2000; Stroup-Gardiner and Brown 1999; AASHTO 1997); however, the effect of segregation (inhomogeneity) on the mechanical performance of laboratory specimens has not been fully examined. Although, this effect has been speculated for a period of time, a tool that quantitatively characterizes the internal structure of asphalt mixture specimens has not been identified. Until recently, imaging techniques have been utilized to study the internal structure of the aggregates and voids (Erikson 1992; Yue 1995; Masad et al. 1998). They developed and applied innovative techniques to quantify the distribution, orientation, shape, and contacts of the coarse aggregates.

Several of the parameters used in characterizing the internal structure of asphalt mixtures have been initiated in other fields of science and their reliability in their intended use has been tested. Examples of this are the parameters for the measurement of orientation of aggregates. These parameters have been successfully applied to the analysis of soil mass particles in the past (Curray 1956; Oda 1972) and recently to asphalt mixture aggregates (Masad 1998). However, the available statistical methods for evaluating the distribution of the aggregates have not been evaluated, and it has not been shown that they provide the accuracy and the reliability required.

## 1.2  PROBLEM STATEMENT

With the advances of the Superpave volumetric mixture design, the use of coarse graded mixtures has become more common. However, coarse graded mixtures are prone

to segregation. The Superpave gyratory compactor itself might also induce segregation. Thus, if segregation occurs during the mixing and compaction process and if it affects the load response of the mixture, then merely because the specimens were prepared according to Superpave volumetric mixture design does not ensure the reliability of the measured mechanical properties.

The mechanical properties of the laboratory compacted specimens, known as local properties, are used as parameters to design a pavement layer or used in the models to predict its performance. In the presence of inhomogeneity, the local mechanical properties will not be representative of the global properties of the material. Using an incorrect parameter can result in either the over-design or under-design of the pavement layer or under-prediction or over-prediction of its performance, with either one being problematic. Therefore, characterizing inhomogeneity in laboratory prepared specimens is essential to understand the material behavior, to better predict performance, and to design a better performing pavement.

Two types of inhomogeneity are probable while preparing laboratory specimens: random and systematic. Random inhomogeneity is caused during aggregate batching and mixture handling. As a result, the sieve sizes that have not been mixed thoroughly would appear as pockets of fine and coarse aggregates in the compacted specimens. Based on empirical knowledge, random inhomogeneity has been held responsible for occasional high variability in the measured mechanical properties. Every now and then, an unexpectedly high or low stiffness value is measured as a specimen is subjected to various modes of loading such as shear, indirect tension, or compression, which is commonly believed to relate to random inhomogeneity.

Systematic inhomogeneity occurs in the process of placing asphalt mixtures into the gyratory mold and the kneading and gyrating process of the gyratory compactor. During these processes, the coarser particles may tend to positions in the bottom and periphery of the gyratory compacted specimens, which creates vertical and radial forms of inhomogeneity, respectively. The properties of systematically inhomogeneous specimens might not be representative of the properties of the material. In this case, the measured properties would not be reliable design and distress prediction parameters.

While identifying both random and systemic inhomogeneity and examining their effect on mechanical response of the mixture are important, the systematic inhomogeneity seems more critical to be characterized. The random inhomogeneity is hypothesized to be the cause of occasional low or high property measurements, which can be disregarded as outliers. Systematic inhomogeneity, on the other hand, has a systematic effect on the property measurements. The measured properties might be consistently skewed in one direction, either lower or higher than the property of homogeneous specimens. In this case, the bias in the property measurements is not recognizable, and therefore, its effect on design and distress prediction will not be taken into account.

## 1.3  GOAL AND OBJECTIVES

Since reliable material characterizations is important for the support of performance prediction models and the design of pavement structures, this study is directed towards quantifying systematic inhomogeneity and examining its effect on the mechanical response of asphalt mixture material. The effect of the variation in aggregate structure on the mechanical properties of an asphalt mixture is investigated. This requires

the measurement of the distribution of aggregates, which is done by an analysis of the images of the specimen cross-sections, captured nondestructively using 3-D x-ray computed tomography (XCT). The measurement of the aggregate distribution necessitates evaluation of existing methods of analysis and the development of new statistical tests using 3-D computer simulation.

The goal of this study was to improve our understanding of the effect of systematic inhomogeneity on the mechanical properties of asphalt mixture specimens. The following objectives follow from this goal:

1.  To develop optimum indices of aggregate homogeneity.

    a.  Identify existing homogeneity indices and evaluate them based on the type of inhomogeneity being distinguished.

    b.  Propose new indices that are best able to characterize inhomogeneity.

    c.  Use simulation to evaluate critical statistics and the power of the tests.

2.  To verify one or more of the optimal indices.

    a.  Develop a procedure for introducing various levels of inhomogeneity into laboratory specimens.

    b.  Use image analysis techniques to compute a precise value of the index for each laboratory specimen.

3.  To show the effect of inhomogeneity on mechanical properties.

    a.  Identify mechanical properties that might be affected by inhomogeneity.

    b.  Test laboratory specimens of various levels of inhomogeneity for mechanical properties.

c. Relate the indices of homogeneity validated at Step 2 to the measured mechanical properties.

## 1.4 IMPLICATIONS OF RESEARCH

Based on the results of this study engineers and technicians will better understand asphalt mixture behavior in the laboratory. This will produce more reliable designs and more realistic performance prediction of asphalt pavement structures and in turn, lower total cost. Knowing that both the level of inhomogeneity is detectable and quantifiable and that the effect of inhomogeneity is observable in mechanical property measurements will motivate technicians to do their best to prepare homogeneous specimens. Also, it will enable engineers to identify the factors that cause inhomogeneity even when care is taken to ensure homogeneity. Factors such as mixing and compaction temperatures and the angle and speed of the gyratory compactors can be reliably examined since the required tools, the test methods, and the specific procedures to be followed will be available. Specific implications for the objectives can also be stated as follows:

1. The development of statistical tests to identify inhomogeneous specimens will provide engineers with methods that can determine the type and the level of inhomogeneity in asphalt-aggregate mixtures. This will lead to a better understanding of the requirements for fabricating homogeneous specimens in the laboratory.

2. The development of a statistical sampling program removes the arbitrariness in the selection of test variables such as the slice face direction and the number and location of the slice faces that are needed for the reliable measurement of homogeneity. By following the standard sampling program, engineers will be

guaranteed that the results obtained at one laboratory is understandable in other laboratories and that the results of research can be reproduced and followed by others.

3. A standard sampling program provides assurance for engineers that the planned experimental design will provide conclusive results and the sampling program will reliably detect the level of homogeneity. For example, if a statistical test indicates that a specimen is homogeneous while the measured mechanical property seems irrational, then it can be stated confidently that factors other than inhomogeneity have caused the irrationality.

4. Showing that computer simulation and image analysis of actual specimens agree, will indicate that simulation is a reasonable mathematical tool to test and measure the indices of homogeneity. This will verify that the statistical indices provide a realistic indication of various levels of inhomogeneity.

5. Simulation validates the adequacy of the number of actual specimens for inhomogeneity testing. For example, a collection of four specimens might not be capable of providing accurate statements about the existence of inhomogeneity.

6. The outcome of the establishment of relationships between the level of homogeneity and the measured mechanical properties will provide a means of estimating the reliability of the measured properties. The reliability of the mechanical results is expected to increase as the level of inhomogeneity in the specimen decreases.

## 1.5  ORGANIZATION OF THE REPORT

This dissertation documents the research aimed at developing indices for the measurement of inhomogeneity that prevails in gyratory compacted asphalt mixture specimens. In addition, the effect of inhomogeneity on the results of commonly used compressive and shear laboratory load tests was investigated. After the introductory discussion in this chapter, a literature review of various concepts utilized in this study is presented is Chapter 2. The models for simulating homogeneous and inhomogeneous specimens are explained in Chapter 3. Chapters 4 and 5 provide the proposed indices for the measurement of vertical and radial inhomogeneity, respectively. In Chapter 6, using Monte Carlo simulation, the critical statistics and the statistical power of the indices are detailed. Chapter 7 discusses the fabrication of homogeneous and inhomogeneous laboratory specimens and the application of x-ray computed tomography and image processing in measuring geometric properties of the aggregates and voids, which are utilized by the selected indices for the measurement of homogeneity (validating results of simulation using laboratory measurements of homogeneity). Chapter 8 presents the results of compressive load tests on homogeneous and inhomogeneous specimens and the correlation between compressive properties and vertical inhomogeneity. Chapter 9 provides the results of shear loads test on homogeneous and inhomogeneous specimens and the correlation between shear properties and radial inhomogeneity. Chapter 10 includes a summary of the research and identifies major conclusions of the research. Chapter 11 includes recommendations for further study.

# CHAPTER 2 - LITERATURE REVIEW

## 2.1 INTRODUCTION

The laboratory testing of asphalt mixture specimens is an important part of research that ultimately will contribute to the improvement of highway pavement serviceability. Performance and design decisions are made based on the results of such laboratory tests in the shear, tension, or compression mode of loading. However, if inhomogeneity was present and it influenced the results of mechanical tests, incorrect design and performance decisions could be made.

Evaluation of the effect of inhomogeneity on mechanical properties of laboratory prepared asphalt mixture specimens requires testing of specimens for both inhomogeneity and mechanical properties. This necessitates the development of the indices that reliably measure inhomogeneity and the selection of the mechanical tests that could be affected by inhomogeneity. This chapter reviews the literature specific to the development of the homogeneity indices, selection of the mechanical tests, and establishing the correlations between the two sets of information. At first a general discussion on the concept of inhomogeneity in laboratory prepared specimens is provided. A review of the existing indices for the measurement of inhomogeneity is presented thereafter. The use of statistical testing in development of new indices and evaluation of the exiting indices is discussed, accordingly. The usefulness of computer simulation in determining the reliability of the indices is overviewed. The concept of nondestructive homogeneity testing of specimens using x-ray computed tomography and image analysis is talked about. Finally, the types of mechanical test that have been commonly used in practice and

are assumed to be useful for evaluation of the performance effect of inhomogeneity is described.

## 2.2  DEFINITION OF INHOMOGENEITY

Inhomogeneity of laboratory prepared specimens is the lack of uniformity in the distribution of various components of asphalt mixture composition, such as aggregates, mastic, and voids. Traditionally called segregation, inhomogeneity might occur during the steps of specimen preparation. Inhomogeneity might be in the form of random clusters or in the form of systematic arrangements in the top, bottom, or along the periphery of the specimens.

The preparation of laboratory specimens includes several steps including batching, mixing, and compaction, while at any one of the steps in the process inhomogeneity can be introduced. Various mechanisms in the preparation of the specimens can impart various forms of aggregate inhomogeneity, specifically vertical, radial, or cluster inhomogeneity. Vertical inhomogeneity is the form that occurs in the process of emptying the mixture in the gyratory mold, when the original gradation gets separated into a finer and a coarser gradation along the depth of the specimen. This phenomenon is believed to be the result of the heavier, coarse aggregates gravitating to the bottom of the mold thus preventing the fine aggregates from sinking. Also, the kneading effort of compaction forces the larger particles to the bottom of the mold.

Radial inhomogeneity is another form that is generally specific to gyratory compacted specimens. For radial inhomogeneity, the original aggregate gradation is radially separated with the finer aggregates being located near the center axis of the specimen. Radial inhomogeneity is often observed in Superpave Gyratory Compacted

specimens because of the rotational movement of the gyratory compactor and the boundary condition imposed by the gyratory mold. Tashman et al. have shown the non-uniform distribution of the air voids in the gyratory compacted specimens in lateral direction (2002), which might have been caused by inhomogeneous distribution of the aggregates.

Cluster inhomogeneity can occur when the differently sized aggregates are not well blended during batching, prior to the mixing with asphalt binder. Thus, a specimen would include pockets of aggregates that are coarser or finer than the design gradation. This form of inhomogeneity has been hypothetically associated to the variability in asphalt mixture mechanical test results.

## 2.3 HOMOGENEITY INDICES

To examine if erroneous decisions are being made with respect to the properties of asphalt material because of inhomogeneity, it is necessary to develop indices that can accurately measure inhomogeneity. Measures of inhomogeneity can be found in various fields of science. Examples are: satellite photographs, geological maps, urban settlement patterns, and microscopic sections of metals, minerals, and cellular tissues. In each of these areas, there is a great need to analyze the distribution of a set of elements within a media, where any such data set is called spatial point pattern (Vincent et al. 1976 and Vincent et al. 1977). Spatial point patterns, which have been commonly examined from 2-dimensional plane sections (Vincent et al. 1983; Hilliard and Anacker 1974), are examined for a variety of reasons. A major reason is that studying the point patterns may be useful in learning more about the phenomena represented and the processes responsible for creating it. The information gained from analysis of spatial point pattern

enables acquiring some initial insights into the phenomena. For example, the finding that objects are spaced differently towards the margins of the media than they are at its center may lead to investigation of the possibility of different forces operating at those locations or of the same forces operating but with different intensities (Ripley 1981).

The information from spatial point pattern also enables examining the correlation between the phenomena and the material behavior. For example, inhomogeneity in spatial point pattern has been accounted for local deficiencies that lead to premature failure of the material (Oda 1972 and Miles 1970). It is possible to build an explanatory model of the point pattern and to use it to drive hypotheses concerning the behavior of the phenomenon (Okabe et al. 1992).

Asphalt mixture as a composite material is also hypothesized to behave as a function of locational properties of its component materials. Therefore, there has been concern to detect and quantify homogeneity of its constituent components. Several indices of homogeneity have been proposed, which were either adopted from the methods that are existed in other fields of science or developed specific for asphalt mixtures. Yue et al. (1995), Masad et al. (1998), and McCuen et al. (2001) have applied a number of these methods to asphalt concrete specimens, while the values of indices of homogeneity were computed from measurements made on vertical and horizontal slice faces through the specimen.

Yet more methods exist in the field of spatial statistics that have been pertained to various areas of science, but their applicability to the asphalt material has not been investigated. Even though the statistical methods are well established and fully elaborated, their success in the asphalt concrete area needs to be examined.

### 2.3.1 Classification of Indices

Numerous indices of homogeneity based on slice face measurements have been proposed. One class of statistics is based on the frequency of particles within a specified area; the quadrat methods are representatives of this class (Diggle 1983). A second class of statistics is based on the distances between the centers of the particle faces or distances of the center of particles to a reference point; nearest-neighbor distance methods are representatives of this class (Diggle et al. 1976). A third class is based on area measurements, with a representative area delineated within each particle face, about each particle face, or enclosed between particle faces; the Voronoi polygon statistic is an example of this class (Okabe et al. 1992, Lin 1997). Each group of indices is linked to different physical property of the composite material (Okabe 1992). The frequency-based methods better define the degree of dispersion of the studied phase, i.e., where particles are more concentrated (Busters et al. 1996). The arrangement of the particles is best described by the distance-based methods, i.e., how the particles are organized spatially (Byth and Ripley 1980). The area-based methods best reveal the amount of the material, i.e., what is the volume fraction of each class size (Besterci et al. 1996).

### 2.3.2 Homogeneity Indices for Asphalt Mixture Specimens

To measure the level of inhomogeneity of a mixture, the quality of the distribution of one or more components of the mixture needs to be evaluated. Since aggregates constitute the major portion of the asphalt mixture, the quality of the distribution of the aggregates is a good indicator of the quality of the distribution of the other components of the mixture such as the air voids and the mastic. If aggregates are distributed inhomogeneously, then the other constituents are more likely to exhibit inhomogeneity.

An assessment of the inhomogeneity of the aggregates should be the most reliable

indicator of specimen inhomogeneity. Therefore, the statistical tests that measure

homogeneity are defined based on geometric measurements of the aggregates. The

general description of the available methods and their advantages and disadvantages are

reviewed briefly.

### 2.3.2.1   *Random Quadrat Test*

One test (or variations thereof), which has been proposed is the quadrat test

(Diggle 1983; Miles 1978; Heltshe and Ritchey 1984; Cressie 1993). The quadrat statistic

is a frequency based descriptive statistic for the measurement of inhomogeneity in

general. The method is based on quadrat sampling of the region of interest. The number

of aggregate centroids located in each quadrat is recorded. From the frequency counts,

the test statistic can be developed. Masad et al. (1998) have utilized the quadrat statistic

described by Cressie (1993) to study the segregated pattern of the aggregates on the faces

of sliced sections of asphalt mixture specimens. The procedure for the application of the

test utilized by Masad (1998) is as follows:

a.  Three vertical slices, 37.5 mm apart, are made on each specimen (Figure 2-1). The
    slice face at the middle of the specimen provides the largest cross-sectional area;
    two additional equally spaced slices are made on both side of the middle slice face.

b.  The aggregates that have a diameter equal to or greater than 2.36 mm are signified
    by their centroids.

c.  One hundred square quadrats are randomly positioned within the cross-section.
    The ratio of the quadrat length to the small dimension of the cross-section is equal

to 1/30. This ratio has been used by Cressie (1993) in other spatial statistic problems.

d.  The number of centroids in each quadrat is counted.

e.  The frequency distribution of the number of particles per quadrat is then formed.

f.  The spatial point pattern is examined by comparison of the quadrat count distribution to a Poisson's distribution. A significant departure of the calculated frequency distribution from a Poisson distribution indicates that the pattern is not spatially random. The degree of departure is then measured by an index based on the quadrat counts. A test statistic ($S_r$) that was developed by David and Moore (1954) is utilized to measure the departure from spatial randomness:

$$S_{ri} = \frac{s_i^2}{\overline{x}_i} - 1 \qquad (2\text{-}1)$$

in which $S_{ri}$ is the measure of deviation of the frequency distribution of the $i^{th}$ slice face from the Poisson distribution; $s_i^2$ is the variance and $\overline{x}_i$ is the mean frequency of the one hundred quadrats on the ith slice face.

g.  For each specimen, the index of homogeneity is the average of the $S_{ri}$ values computed from the three slice faces of the specimen:
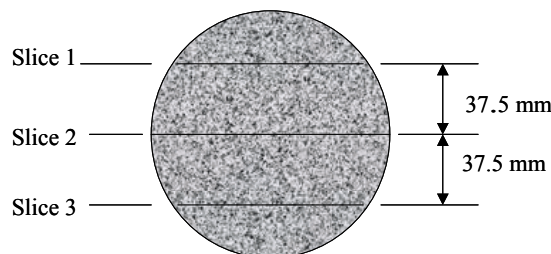


**Figure 2-1. The position of the slices for random quadrat test**

$$S_r = \frac{1}{3} \sum_{i=1}^{3} S_{ri} \qquad\qquad (2\text{-}2)$$

**h.** For a Poisson distribution, the mean and variance are equal. Therefore, the value of $S_r$ in Equation (2-2) would be equal to zero for a truly Poisson process. Values of $S_r$ that are significantly greater than 0 indicate segregation, while values significantly smaller than 0 indicate regularity or a lack of segregation.

**Advantages**: the suggested test statistic is assumed to have a known sampling distribution (Poisson distribution). Therefore, criteria for the comparison of the measured segregation parameters exist.

**Disadvantages**: The suggested quadrat method has several disadvantages: First, since the locations of the quadrats are selected at random, the statistic would be insensitive to the type of inhomogeneity. The quadrat method might indicate whether the specimen is segregated or not but it would not suggest if the segregation pattern is extended vertically or radially.

Second, the null hypothesis ($H_o$) for testing the test statistic $S_r$ is that the frequency is Poisson distributed. From that, one must infer segregation or randomness. This would only be valid when the aggregates are uniform i.e., all one particle size. The method would not be applicable to well-graded aggregates. For well-graded aggregates, a frequency of 1 could occur because it is a large piece of aggregate and other particles would not fit in the quadrat, or one aggregate with a diameter of 2.36 mm is surrounded by particles smaller than 2.36 mm. However, for uniform sized particles, a frequency of 1 is only the result of the quadrat sitting on one particle that got separated from the other particles. This shows that the computed values of $S_r$ must be interpreted differently for uniformly size aggregates and well-graded aggregates. $S_r$ varies within the range of

$-1 \leq S_r \leq \infty$, since $s^2$ can not be less than 0. When every quadrat has the same frequency, then $s^2$ is zero. For well-graded aggregates, the probability of occurrence of $s^2 = 0$ is almost zero even for homogeneous specimens. Also, a large variance is possible when the gradation curve is shallow sloped even if the distribution pattern of the aggregates is homogeneous. This makes $S_r$ a poor test statistic for aggregates with a shallow gradation curve (well graded aggregates).

Third, the quadrat size for sampling of the specimen's slice face is very small. For an asphalt mixture specimen the largest cross-section has dimensions of 150 mm by 150 mm, the ratio of 1 to 30 for the quadrat to the slice face dimensions would yield a quadrat of about 5 mm x 5 mm. For the aggregates that have a diameter in the range of 4.75 mm to 19 mm, the probability of the centroids residing in such a small quadrat seems very small.

Fourth, one hundred 5-mm × 5-mm panels could cover a maximum area less than 11% of the slice face area even if none of the randomly placed quadrats overlapped. The percentage could be much less depending on the amount of overlap. This implies that the estimated frequency may not be a good representation of the population since only a small portion of the slice face is actually sampled. Therefore, it is necessary to have an adequate number of quadrats that will provide a reliable estimate of the particle dispersion.

Fifth, averaging of the parameter, $S_{ri}$, of the three slice faces might not be appropriate. It is more logical to compute a single index from frequency measurements of the three slice faces.

Sixth, the changing cross-section of the slice faces necessitates computation of the frequency intensities rather than use of absolute frequencies. The mean and variance of the frequency intensities are better representatives of the frequency distribution using the changing cross-sections than the absolute frequencies.

### 2.3.2.2   Quartered Quadrant Test

The quartered quadrant method has been suggested by Masad et al. (1998) for testing general forms of inhomogeneity. The test is based on the measurement of the variations in the mean aggregate diameters in the four quadrants of the sampled slice face of a specimen. The test is applied as it follows:

a.  Three vertical slices, 37.5 mm apart, are made on each specimen (Figure 2-1). The slice face at the middle of the specimen provides the largest cross-sectional area; two additional equally spaced slices are made on each side of the middle slice face.

b.  On each slice face, the aggregates that have a diameter equal to or greater than 2.36 mm are identified.

c.  Each vertical slice face is divided into four equal size quadrants, with two located on top of the other two.

d.  On each slice face, the mean diameter ($\overline{q}_j$) of the aggregates in each quadrant is calculated where $j$=1, 2, 3, 4.

e.  On each slice face, the average ($\overline{Q}_i$) and the standard deviation ($s_{Qi}$) of the mean aggregate diameters of the four quadrants is calculated.

f.  For each slice face, The coefficient of variation of the four averages is calculated as follows:

$$S_{qi} = \frac{s_{Qi}}{\overline{Q}_i}\%$$
(2-3)

g.  The segregation index ($S_q$) is defined as the average of the coefficient of variations ($S_{qi}$) of the three slices:

$$S_q = \frac{1}{3}\sum_{i=1}^{3} S_{qi}$$
(2-4)

**Advantages:** Four advantages are associated with this method: First, the method provides the potential for evaluating different patterns of segregation since the location of the quadrants is known. The information regarding the average and standard deviation of the particle diameters in each quadrant reveals the variation in aggregate size in each quarter of the slice face. Comparison of the means and standard deviations could reveal the pattern of the particle arrangements.

Second, the advantage of this method over the random quadrat methods is that rather than dealing with particle frequencies the method takes into consideration the size of the particles. The reduction of the aggregates to their centroids would result in loss of information.

Third, the slice face area that is being tested is completely covered by the quadrants. Under-sampling of the cross-sectional area is avoided since the cross-sectional area is divided into equal panels and all of the panels enter into the calculation of the test statistics.

Fourth, the quadrants are not overlapping; therefore, the information obtained from one quadrant is independent of the other quadrants.

**Disadvantages**: This method has the following disadvantages: First, the critical values of the test statistic ($S_q$) and therefore criteria for distinguishing between condition of

homogeneity and inhomogeneity are not known. Therefore, a reliable decision regarding homogeneity of the specimen based on the calculated value of $S_q$ cannot be made. This disadvantage is overcome by simulating the distribution of the test statistic $S_q$.

Second, by averaging the four mean aggregate diameters associated with the four quadrants, the information regarding the variations in the aggregate diameters within each quadrant would be lost. The four average aggregate diameters of the four quadrants might be the same while the standard deviations would be very different.

Third, four quadrats is an inadequate number of samples to be tested. Sample values of $\overline{Q}_i$ and $s_{Qi}$ have poor accuracy when the number of quadrats is low. The standard error of the mean ($\dfrac{S_e}{\sqrt{n}}$) could result in more accurate estimates of the mixture homogeneity if the slice face is divided into more number of quadrats.

Fourth, the test statistic ($\dfrac{s_{Q_i}}{\overline{Q}_i}$) is indifferent to the type of inhomogeneity. The test statistic is the same if the two low average aggregate diameters correspond to the top quadrants or the alternate quadrants at the top and bottom.

Fifth, the changing cross section of the slice faces necessitates comparison of the frequency densities of the slice faces rather than comparison of absolute frequencies.

Sixth, averaging of the parameter, $S_{ri}$, of the three slice faces might not be appropriate. It is more logical to compute a single index from the means and standard deviations of the frequency densities of the quadrats measured from the three slice faces.

### 2.3.2.3    $C_V$ *Quadrat Test*

$C_V$ quadrat test is a variation of the quadrat test that has been proposed by

McCuen and Azari (2001). For this test, n panels of the same size are placed over the

middle slice face of the specimen and the number of particle faces in each panel is

counted. The mean and standard deviation of the particle counts from the $n$ panels are

computed. The test statistic is the coefficient of variation, denoted as $C_v$, and is equal to

the ratio of the standard deviation to the mean. For a homogeneous specimen each panel

would expect to have nearly the same number of aggregate faces, so the standard

deviation, and therefore $C_v$, would be small. For an inhomogeneous specimen, some

panels would be placed over portions of the specimen dominated by small particles while

other panels would cover areas associated with large particles. Thus, both the standard

deviation and $C_v$ would be relatively large. Using Monte Carlo simulation, the

distributions of $C_v$ for both homogeneous and inhomogeneous specimens were

determined in order to identify the decision criterion. When a computed value of $C_v$

exceeds the decision criterion, the specimen is assumed to have been taken from an

inhomogeneous specimen.

Quadrat sampling requires specification of several variables, including the shape,

size, number, and the placement (systematically located or randomly placed) of the

quadrats (Miles and Davy 1977). McCuen and Azari (2001) used a simulation model to

evaluate the power of the quadrat test and to determine critical values for a 5% level of

significance for various combinations of quadrat size and quadrat number. For each

combination of size and number of the square panels, 50,000 specimens were created by

simulation for both homogeneous and inhomogeneous conditions. The distributions of $C_v$

for both conditions were used to determine the critical values and the corresponding

power of the test. Sample sizes of 10, 20, and 30 panels were tried with the lengths of the

square panels varying from 20 mm to 90 mm. Table 2-1 provides an alternative sampling

scheme which includes various combinations of the panel size and panel number. To

evaluate alternative sampling schemes, in addition to the computed power of the test, the

proportions of the slice face area covered by the area of the panels was considered. For

the middle slice face (150-mm x 150-mm), the area of the slice face was compared to the

product of the number of panels and the area of a panel. Analysis indicated that accuracy

increased as the coverage of the slice face increased. For example, ten 30 mm $\times$ 30 mm

panels would cover an area that is 40% of the slice face area. If any of the randomly

located panels overlap, then less than 40% of the slice face area would be involved in the

testing. The power of the test statistic for this combination was 44%. Accuracy increased

to 57% when the coverage of the slice face by the panels increased to 80%. However, it

was not recommended to use too many panels or have panels with large areas because

then the entire face area may be sampled in a way that the results are not independent.

Thirty 70 mm $\times$ 70 mm panels would cover an area that is 653% of the slice face area,

which implies that each aggregate face might be sampled on the average more than six

times. Obviously, this was not a realistic sampling scheme since the frequency estimates

from each panel would not be independent.

In summary, it was concluded that the power of the test is about equally sensitive

to panel size and the panel number. For the sampling schemes that resulted in small

coverage of the slice face (small panel sizes or small number of panels), the power of the

test was very low. In such cases, only a small portion of the slice face was actually

**Table 2-1. Critical values and the power of the quadrat test as a function of panel length (L) and the number of panels (n)**

| Panel Length (mm) | Critical Values for | | | Test Power for | | |
|---|---|---|---|---|---|---|
| | n=10 | n=20 | n=30 | n=10 | n=20 | n=30 |
| 20 | 0.395 | 0.360 | | 0.25 | 0.37 | |
| 30 | 0.260 | 0.242 | | 0.44 | 0.57 | |
| 40 | 0.194 | 0.183 | | 0.56 | 0.69 | |
| 50 | 0.156 | 0.144 | | 0.63 | 0.75 | |
| 60 | 0.124 | 0.119 | 0.118 | 0.70 | 0.78 | 0.82 |
| 70 | 0.098 | 0.098 | 0.096 | 0.75 | 0.82 | 0.85 |
| 80 | | | 0.078 | | | 0.90 |
| 90 | | | 0.059 | | | 0.96 |

sampled. Accuracy increased with either an increase in the panel area or an increase in the number of panels (see Table 2-1). However, the increase in the power of the test after the coverage of the slice face exceeded 100% did not indicate the increase in the accuracy of the test since the measured frequency from the overlapped panels would not be independent of each other. The optimum power of the test was obtained where the coverage area was approximately 100%, although the actual coverage would be less because of the random sampling. For this situation, the power of the quadrat test at optimum was about 60%, which suggested that the power of the quadrat test for even optimum sampling scheme is relatively low.

**Advantages:** The method offers several advantages: First, the panels are selected large enough to include reasonable number of aggregate centroids. Second, the number of panels is adequate to provide about 100% coverage of the slice face area. Third, the probability distributions of the test statistic for both states of homogeneity and inhomogeneity are known. Therefore, the critical values for the comparison with the measured statistic are available.

**Disadvantages:** Similar to other quadrat methods, because of randomly positioned quadrats, the test is not sensitive to vertical or lateral forms of inhomogeneity, but measures the existence or lack of inhomogeneity in general. To overcome this disadvantage the location of the panels should be linked to the measured frequency. Second, the quadrat test randomly samples from the entire slice face, but the entire face may not be sampled.

### 2.3.2.4 Eccentricity Test

The eccentricity test was suggested by Yue et al. (1995) for the measurement of vertical uniformity. The test involved evaluating the variation of the eccentricity parameter in the vertical direction. The eccentricity parameter were computed from the horizontal cross-sections that were made in equal intervals of 5-mm along the height of the specimen. The mean and residual of the eccentricity values of the cross sections were used as the measure of uniformity. To compute the eccentricity parameter from each horizontal cross-section, the origin of the X- and Y-coordinates were selected at the center of the circular cross-section. The eccentricity parameter is the ratio of the distance between the aggregate centroids and the geometric center of the slice face over the radius of the slice face. For a completely uniform distribution of the aggregates, the eccentricity should be zero on each cross-section and there should be no vertical variation in the eccentricity values of the slice faces.

**Advantages:** The advantage of this method is the potential that the method can offer in the measurement of inhomogeneity. The eccentricity of the aggregates could be a good

indicator of the equilibrium of the aggregates in the mixture if an appropriate test statistic is used.

**Disadvantages:** There are four disadvantages associated with this test: First, the method is not well documented. The authors do not provide mathematical expression on how eccentricity parameter is computed. Second, a zero criterion on eccentricity value that is decided for the state of uniformity does not warranty homogeneity of the specimen. A zero value might correspond to radial segregation where most of the coarse aggregates are arranged along the periphery of the specimen. Third, zero variation in eccentricity values of the cross-sections might correspond to consistent radial segregation that is observed in all cross-sections but not to complete homogeneity. Fourth, the distribution of the eccentricity parameter and the critical values that distinguishes between the state of uniformity and non-uniformity are not known.

### 2.3.2.5 Moment of Inertia Test

This test was also suggested by Yue, et al. (1955) for uniformity evaluation of the aggregate distribution in vertical direction. The origin of the X- and Y-coordinates were selected at the center of horizontal circular cross-sections. A moment of inertia parameter was computed as the ratio of the summation of the moment of inertia of coarse aggregates over the moment of inertia of slice face with respect to the X-axis or the Y-axis. The mean and residual of the moment of inertia ratios of all cross sections were used as the measure of uniformity of the mixture. For a completely uniform distribution of the aggregates, the moments of inertia with respect to X- and Y-axes would be the

same on each cross-section and there would be no vertical variation in the moment of inertia parameter along the height of specimen.

**Advantages:** The advantage of this method is the potential that the method can offer in the measurement of inhomogeneity. The moment of inertia of the aggregates could be a good indicator of the equilibrium of the aggregates in the mixture if an appropriate test statistic is used.

**Disadvantages:** There are four disadvantages associated with this test: First, the method is not well documented. The authors do not provide mathematical expression on how the moment of inertia parameter is computed. Second, the equality of moment of inertia with respect to X- and Y-axis does not warranty homogeneity. This condition might correspond to radial inhomogeneity where arrangement of coarse aggregates along the periphery of the specimens results in equal moment of inertia with respect to X- and Y-axes. Third, the zero variability in the percent moment of inertia of the cross-sections might correspond to consistent radial inhomogeneity but not to complete homogeneity. Fourth, the distribution and the critical values of the moment of inertia parameter were not determined.

### 2.3.2.6   Runs Test

The runs test is a nonparametric method that was traditionally used to test a spatial or temporal sequence for randomness. McCuen and Azari (2001) applied the runs test to evaluate for vertical homogeneity of asphalt mixture specimens. The Runs test assumes equally spaced measurements; therefore, the number of particles in layers of equal thickness is of interest. To develop the distribution of the runs statistic, 5000

homogeneous and 5000 vertically inhomogeneous specimens were simulated. Each specimen was virtually sliced through the diameter, resulting in a rectangular face for homogeneity analysis. The slice face was then divided horizontally into layers of equal thickness and the number of particle centroids in each layer was measured. For a homogeneous specimen, each layer contains approximately the same number of particles, at least within sampling variation. For an inhomogeneous specimen with most of the larger aggregates near the bottom of the specimen, the particle count in the layers decreases with depth. The median frequency was computed, and the frequency in each layer was compared with the median. A frequency above the median was denoted as a "+" sign, while a frequency below the mean was denoted as a "−" sign. A run was defined as a sequence of one or more like symbols. A homogeneous specimen had a mid-number of runs while an inhomogeneous specimen had only a few runs. From the distribution of the runs statistic for homogeneous specimens the critical value for 5 % level of significance was obtained. If for a specimen the number of runs was below the critical number of runs, then the specimen was assumed to be inhomogeneous.

McCuen and Azari (2001) showed that the critical value of the runs test would depend on the number of layers into which the slice face is separated. The number of layers would also influence the power of the test. However, the task of measurement increased as the number of layers was increased. The layers would be thinner and many of the particles would overlap the boundaries of the layers, which made counting the frequencies more difficult. However, the power of a test generally increased as the sample size increased. Therefore, a larger number of layers were desirable as long as the frequency of the particles in each layer did not become too small.

To investigate the relationship between the number of layers and the power of the test, McCuen and Azari (2001) conducted separate simulations of homogeneous and inhomogeneous specimens with different numbers of layers. The results for 5000 simulations for each number of layers are given in Table 2-2. An inhomogeneity was assumed if the calculated number of runs was less then or equal to the critical number of runs. A 5% level of significance was used, but since the number of runs is a discrete random variable and can only take on integer values, the critical value that defined a region of rejection just less than 5% was used. The selected critical value was used with the distribution of runs for the inhomogeneous specimens to compute the probability of the type II error and the power of the test. The values in Table 2-2 indicate that the power increased with increases in the number of layers. For 30 layers, with each layer being 5 mm, the test showed a power of 95%. The power for twenty 7.5mm layers was 90%. Given the size distribution of the particles on the slice face, twenty layers seemed the most practical decision. The 5% gain in power was not justified based on the computation effort and consideration of the particle size relative to the size of the layer.

**Advantages:** The runs test samples systematically from top to bottom and all particles are counted.

**Disadvantages:** The test makes no distinction based on the size of the aggregates, although an inverse relationship between the size of the aggregates and the number of aggregates within an area is expected.

**Table 2-2. Variation of runs test critical values and test power for various number of layers**

| Number of Layers | Critical Number of Runs | Type I Error Probability | Type II Error Probability | Power |
|---|---|---|---|---|
| 10 | 2 | 0.0095 | 0.2805 | 0.7195 |
| 15 | 4 | 0.0200 | 0.1475 | 0.8525 |
| 20 | 6 | 0.0325 | 0.1025 | 0.8975 |
| 25 | 8 | 0.0465 | 0.0760 | 0.9240 |
| 30 | 10 | 0.0445 | 0.0525 | 0.9475 |

### 2.3.2.7  *Average Depth Test*

The average depth test was developed by McCuen and Azari (2001) for the measurement of vertical inhomogeneity. The test was based on sampling of all particles that have a diameter equal to or greater than 2.36 mm in diameter on the vertical slice face that goes through the diameter of the specimen, distinguished between particles of different area-gradation classes. The distance from the top of the specimen to the center point of each particle was measured, and the mean distance for each sieve size was computed. For a homogeneous specimen, the means would be one-half of the specimen height. For an inhomogeneous specimen with the large particles at the bottom of the specimen, the mean distances for the large sieve sizes would be larger than the mean distances for the smaller sieve sizes. A one-way analysis of variance on the means was used to test for equality of the mean distances. The test showed that the means were significantly different, when the specimen was inhomogeneous.

The average-depth test was applied to 25,000 simulated slice faces for both homogeneous and inhomogeneous conditions. The distributions of the analysis of variance F statistic were computed for the two conditions, with the critical F values for

5% and 1% levels of significance determined from the F distribution for the homogeneous condition. The critical values were then used with the distribution of F statistics for inhomogeneous simulated specimens to estimate the corresponding probabilities for type II errors and the power of the test.

The values of the average-depth statistic using computer simulation are given in Table 2-3. The one-sided upper tail of the F distribution for homogeneous specimens was used to obtain the 5% and 1% F values. The lower tail of the F distribution for inhomogeneous conditions was used to compute the probability of the type II error ($\beta$), with the power being equal to 1-$\beta$. When the larger five sieve sizes were used, the power was 92% for the 5% test and 81% for the 1% test. The power of the test when only the four largest gradation levels were used was very poor. Although using more than five sieve sizes increased the power, it drastically increased the computational effort and reduced the reproducibility of the test.

**Advantages:** The advantage of this method is that both size and the location of the aggregates are included in the computation of the index. The more inhomogeneity-relevant information is used the more reliable the test statistic would be.

**Disadvantages:** The disadvantage of the method is that involving only the large aggregates from less than five class sizes would result in not enough aggregates in each class size of one slice face. Including the classes with small size particles will drastically increase the computation time. To overcome this disadvantage, a larger number of slices can be used. This provides enough numbers of particles if only larger classes of aggregates are used.

**Table 2-3. Critical values and test power for the average-depth F-test**

| Test | No. of Gradation Levels | Critical F | | β | | Power | |
|---|---|---|---|---|---|---|---|
| | | α =5% | α =1% | α =5% | α =1% | α =5% | α =1% |
| Average Depth | 5 | 2.31 | 3.39 | 0.083 | 0.195 | 0.917 | 0.805 |
| | 4 | 2.89 | 4.49 | 0.741 | 0.893 | 0.259 | 0.107 |

### 2.3.2.8  *Nearest Neighbor Distance Test*

The nearest neighbor distance test was suggested by McCuen and Azari (2001) for the measurement of vertical inhomogeneity. The nearest-neighbor statistic required separating the middle slice face of the specimen into upper and lower halves and computing the mean distances between the centers of the nearest neighbor particle faces in both halves. The standard parametric two-sample t-test was used to test for a significant difference in the means. For the larger particles in one half of the specimen, a one-tailed test was applied, with the mean distance for one half of the specimen expected to be larger than the mean distance for the other half.

The distribution of the two-sample t statistic for homogeneity was evaluated from 5000 slice face simulations and the distributions compiled for both homogeneous and inhomogeneous specimens. The critical values were obtained from the distributions for levels of significance of 5% and 1%. Since inhomogeneity would yield large values of t, the critical value was obtained from the upper tail of the t statistic for homogeneous conditions. The probability of a type II error was computed from the lower tail of the t distribution for inhomogeneity using the 5% and 1% critical values.

The computational effort was considerably less when only the four largest

gradation levels were used rather than the largest five levels. Separate sets of simulations

were made for both 4 and 5 gradation levels. Fewer than four levels did not yield reliable

values because the gradation distribution dictated a small number of aggregate particles

for the large sieve sizes, which were used to compute the nearest neighbor means.

Table 2-4 contains the results of the simulations. The results suggested that the average

depth test was a powerful test as long as 5 or more gradation levels were used. When four

gradation levels were used, the test provided 63% power at the 5% level of significance

and 36% power at the 1% level. For five gradation levels of significance the power was

essentially 100% for both levels of significance. Thus, the increase in effort required to

evaluate the statistic for five gradation levels was warranted.

 **Advantages:** The advantage of this method is involving the size and relative location of

the aggregates with respect to each other in the computation of the index. The more

inhomogeneity-relevant information is involved, the more accurate index can be

computed.

**Disadvantages:** The disadvantage of the method is that involving only the large

aggregate class sizes would result in not enough aggregates in each class size. However,

including the classes with small size particles will drastically increase the computation

**Table 2-4. Critical values and test power for the nearest neighbor t-test**

| Test | No. of Gradation Levels | Critical t | | $\beta$ | | Power | |
|---|---|---|---|---|---|---|---|
| | | $\alpha = 5\%$ | $\alpha = 1\%$ | $\alpha = 5\%$ | $\alpha = 1\%$ | $\alpha = 5\%$ | $\alpha = 1\%$ |
| **Nearest Neighbor** | 5 | 2.133 | 3.075 | 0.001 | 0.002 | 0.999 | 0.998 |
| | 4 | 2.520 | 3.454 | 0.374 | 0.640 | 0.626 | 0.360 |

time, while involvement of small particles in the measurement of inhomogeneity might not be necessary. Inhomogeneity can be quantified by measuring the changes in properties of either coarse or fine aggregates. Since it is much easier to detect and measure the properties of the coarse particles than the fine particles, it is preferred to emphasize on the coarse aggregates. To overcome the inadequacy of the number of particles when only larger class sizes are involved, a larger number of slice faces can be analyzed. This would provide enough number of particles regardless of inadequacy of the number of aggregates in each class size of a slice face.

### 2.3.2.9   *Inner-Outer Average Diameter*

This method is suggested by Tashman et al. (2001) for the measurement of radial inhomogeneity. The method compares the average diameter of the aggregates that have a diameter equal to or greater than 2.36 mm in the inner and the outer portions of a specimen. Figure 2-2 shows the divisions of a slice face into the inner and outer portions. The division is based on the location of the areas with the highest concentration of the coarse aggregates, which are mainly along the periphery of the gyratory compacted specimen. The procedure for the application of the test is as follows:

  a.   Three vertical slices, 37.5 mm apart, are made on each specimen (Figure 2-1). One slice face is made in the middle of the specimen and two additional equally spaced slices are made, one on each side of the middle slice face.

  b.   Each slice face is divided into inner and outer areas, such that the area of the inner portion is equal to the area of the outer portion (Figure 2-2). The width and the height of the inner rectangular portion is obtained using the following equations:

$$w_i = W_i / \sqrt{2} \tag{2-5}$$

$$h_i = H_i / \sqrt{2} \tag{2-6}$$

where $w_i$ and $h_i$ are the width and the height of the inner portion of the $i^{th}$ slice face, respectively; and $W_i$ and $H_i$ are the width and height of the $i^{th}$ vertical slice face, where $i$=1, 2, 3, respectively. The inner portion is centered within the slice face.

c. On each slice face, the average diameter of the aggregates that have a diameter equal to or greater than 2.36 mm in the outer ($\overline{d}_{ui}$) and in the inner ($\overline{d}_{ni}$) portions are measured.

d. For each slice face, the computed average aggregate diameters are used to compute parameter $S_{li}$ that is a measure of the percent difference between the average aggregate diameters in the inner and in the outer portions:

$$S_{li} = (\frac{\overline{d}_{ui}}{\overline{d}_{ni}} - 1) \times 100\% \tag{2-7}$$
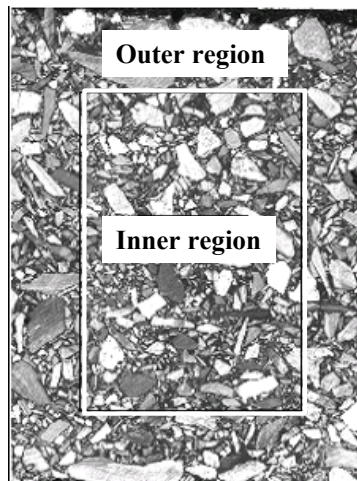


**Figure 2-2. The division of a vertical slice faces for the inner-outer average diameter test**

e. The index of lateral segregation for each specimen is computed as the average of the $S_{li}$ values of the three slice faces:

$$S_l = \frac{1}{3} \sum_{i=1}^{3} S_{li} \qquad (2\text{-}8)$$

The authors explain that a zero value of $S_l$ indicates a lack of radial segregation, while a positive value indicates that more of the coarser aggregates are distributed in the outer portion and a negative value indicates the opposite.

**Disadvantages:** Three disadvantages are associated with this method. First, the distribution of the test statistic for either condition of homogeneity or inhomogeneity is unknown. Therefore, the critical value for the comparison with the computed test statistic for a selected level of significance is not available. Second, the inner and outer portion method is applicable to homogeneity testing of full size gyratory specimens. The test is not applicable to the cut specimens that meet the size requirements of a specific mechanical test such as the Superpave shear test in which the top and bottom portions, which include the coarser aggregates, are cut prior to the shear test. Third, the test statistic based on the existing inner-outer division does not distinguish between the concentration of the coarser aggregates at the top and bottom or at the periphery. Therefore, the test does not exclusively measure the lateral segregation. Fourth, averaging the lateral segregation index values computed from the three slice faces might not be correct since the cross-sections of the slice faces are not the same. The two slice faces at both sides of the middle slice face have smaller width than the middle slice face. Therefore, the aggregate diameters measured from the slice faces should be adjusted based on the area of the slices before they are used in the computation of the index.

### 2.3.3    Independency of the Slices

A cylindrical asphalt mixture specimen is sliced at multiple positions and an index of homogeneity is computed from measurement of geometric properties of the aggregates observed on the slice faces (Masad et al., 1998 and Yue et al., 1995). Obviously, the more the number of slices, the more accurate estimate of homogeneity of the specimen is obtained. However, it seems reasonable to believe that the slices would need to be far enough apart to ensure that any one particle is not part of both slice faces. In other words, the slices should be far enough apart to ensure that the values of the index are made from different pieces of aggregate. It was therefore of interest to know the minimum spacing between the slices. Additionally, it also seems rational that the slices should be made at locations that would ensure slice faces that are large enough to obtain a reasonable number and distribution of aggregates.

McCuen and Azari (2001) used a three-dimensional simulation model of cylindrical specimens to examine the hypothesis of obtaining accurate estimate of homogeneity from independent slice faces. 2500 pairs of cylindrical specimens with each specimen having a diameter of 150-mm and a height of 150-mm were simulated. The following weight gradation curve was used for all specimens: 25, 19, 12.5, 9.5, 4.75, 2.36, 1.18, 0.6, 0.3, 0.15, 0.075 mm with weight fractions passing 1.0, 0.992, 0.828, 0.695, 0.46, 0.31, 0.21, 0.15, 0.11, 0.078, 0.058, respectively. For each pair, one specimen was sliced in three places: ¼ diameter (denoted $x_1$), ½ diameter (center slice denoted $x_2$), and ¾ diameter (denoted $x_3$). This means that the center slice would be 37.5 mm from both of the quarter point slices, which was at least 50% more than the largest particle diameter of 25mm. The second specimen of each pair was only sliced vertically through the center, which was denoted as $x_4$. The second specimen, which had the same

36

design mix gradation as the first specimen, was used as a control specimen since it was known to be independent of the first specimen. The Runs test was applied separately to each of the four faces and the number of runs computed. This yielded four values of the Runs test homogeneity index for each pair of specimens, from which six comparisons of the number of runs was made: (face $x_1$ vs. face $x_2$), ($x_1$ vs. $x_3$), ($x_1$ vs. $x_4$), ($x_2$ vs. $x_3$), ($x_2$ vs. $x_4$), and ($x_3$ vs. $x_4$). Since $x_4$ was from the independent control specimen, then all correlations with $x_4$ should not be statistically different from zero when compared with slices made in the first specimen. If multiple homogeneity indices from the same specimen were independent, then the three comparisons [($x_1$, $x_2$), ($x_1$, $x_3$), and ($x_2$, $x_3$),] should also not be statistically different from zero. In all cases, a significant positive correlation would indicate a lack of independence. Negative correlations and near-zero correlations would indicate independence.

For each of the four slice faces in the 2500 pairs, the Runs test index of homogeneity was computed. Correlation coefficients were computed for each of the six paired comparisons, with the following results: -0.0026 for $x_2$ vs. $x_1$, 0.0087 for $x_2$ vs. $x_3$, -0.0090 for $x_1$ vs. $x_3$, 0.0032 for $x_1$ vs. $x_4$, -0.0042 for $x_2$ vs. $x_4$, and $-0.0205$ for $x_3$ vs. $x_4$. For a one-tailed test of the correlation coefficient, the critical values of the correlation coefficients for 5% and 10% rejection probabilities are 0.0329 and 0.0256, respectively. Since none of the six correlations exceeded even the critical value for 10%, the null hypothesis of zero correlation was accepted for all six comparisons, which led to the conclusion that all of the slice faces gave independent estimates of the Runs test index. These results suggested that for the gradation used, 37.5 mm spacing between the slices was adequate for accurate estimate of homogeneity.

The simulation model was then used to evaluate the hypothesis that slices that are too close to each other would not yield independent estimates of the homogeneity index. For each of these analyses, 2500 additional pairs of specimens were formed, sliced in the same manner as above but not at the same locations, and evaluated for the correlation coefficient between Runs test indices. However, for this analysis, the first specimen of each specimen pair was sliced at the center ($x_2$) and at an offset distance from the center slice; this slice was denoted as the offset slice $x_5$. For example, a second slice may be made at 2 mm from the center slice. Again, the second specimen is used as a control and only sliced through the diameter. Three comparisons were made using the Runs test statistic: ($x_2$ vs. $x_5$), ($x_2$ vs. $x_4$), and ($x_4$ vs. $x_5$). The correlation coefficients from the comparisons are given in Table 2-5 for various offset distances. For a 5% level of significance and a sample size of 2500, the critical correlation coefficient was 0.0329. Therefore, the null hypothesis of zero correlation was accepted for the control specimen versus all of the slices in the first specimen. However, the null hypothesis was rejected for comparisons of the center slice on the first specimen with the offset slice faces of 5 mm or less (see Table 2-5). For small offset distances, the correlation coefficients increased as the distance between the slice faces decreased. These results support the results from the above analysis, suggesting that multiple slices can be made on a single specimen as long as the slice faces are separated by a reasonable distance. A 10-mm offset would be the minimum slice-face separation suggested by the results of Table 2-5. The minimum offset distance would depend on the gradation curve.

For the mix design used for that analysis, the largest particles passed a 25-mm sieve but not the 19 mm sieve. However, the gradation curve was such that less than 1%

**Table 2-5. Correlation coefficients between the runs test statistic for offset slice faces**

| Offset Distance (mm) | $x_4$ vs. $x_2$ (Control vs. Center) | $x_4$ vs. $x_5$ (Control vs. Offset) | $x_2$ vs. $x_4$ (Center vs. Offset) |
|---|---|---|---|
| 2 | -0.0116 | -0.0049 | 0.3776 |
| 3 | -0.0084 | 0.0268 | 0.2234 |
| 5 | 0.0102 | 0.0263 | 0.0895 |
| 10 | -0.0161 | 0.0057 | 0.0038 |
| 15 | 0.0163 | 0.0163 | -0.0042 |
| 20 | -0.0116 | 0.0118 | 0.0100 |
| 25 | 0.0077 | 0.0270 | 0.0086 |
| 30 | -0.0137 | -0.0094 | 0.0008 |
| 35 | 0.0053 | 0.0013 | -0.0274 |
| 37.5 | 0.0032 | -0.0042 | -0.0026 |

of the particles by weight were in this largest gradation class. Also, since the Runs test

measurements were made on the slice faces, where the face area gradation curve indicates

smaller particle diameters than that suggested by the weight gradation curve, the 10-mm

offset distance may be indicative of the aggregates from the larger weight gradation

levels. A larger offset distance would be warranted if the weight gradation had a higher

fraction in the larger sieve sizes. It seemed reasonable to conclude that the offset distance

should be at least equal to the largest sieve size for which 95% of the material passes.

## 2.4 X-RAY COMPUTED TOMOGRAPHY

The computation of homogeneity indices has been conducted on two-dimensional

slice face images of asphalt mixture specimens. Based on stereology, the use of

two-dimensional planer images for characterizing the geometric properties of the

components of a three-dimensional object is efficient in addition to being valid (Mathieu

et al, 1980). In the past, in order to make available the slice face images for the 2D

analyses, the specimens were cut at several locations either horizontally or vertically and

the images of the slice faces captured using a digital camera. Yue et al. (1995) and later

Masad et al. (1998) developed methods for quantifying the aggregate structure using two-dimensional image analyses from the actual slices of specimens.

The actual slicing of the specimens has several disadvantages. First, the cutting destroys the specimen, which prevents the specimens from some forms of mechanical testing. Second, a specimen that is cut in one direction cannot be used for obtaining images from another direction. Third, since it is preferred to mechanically test the same specimens as the ones used for image analysis, the number of cuts that can be made on a specimen is limited by the size requirement for the mechanical test. For example, 50-mm thick circular disks that are required for the Superpave Shear Tester are the result of three slices on a gyratory compacted specimen. These provide only three independent slice faces for image analysis, which is not adequate for making reliable measurements of specimen homogeneity. Fourth, if mechanical testing is not planned, the number of cuts that can be made on a specimen is limited by the thickness of the blade. Fifth, the surface of the specimen that is being prepared for image analysis might get damaged when cutting. Sixth, some mechanical tests, e.g., the axial compression test, do not require cutting of the specimen except trimming of the top and bottom. Therefore, only two slice faces from the top and the bottom are available for the analysis. However, the top and the bottom slices are mostly affected by the boundary condition and may not serve as good representations of the internal structure of the specimen.

With advances in technology, x-ray computed tomography (XCT) made it possible to nondestructively obtain images of the asphalt mixture specimens at any depth and at extremely small intervals. XCT has shown to be valuable tool for characterizing and quantifying the complex macro and microstructure of various materials, including

asphalt concrete. Wang et al. (2002), Ketcham and Carlson (2000), and Shashidhar (2000) utilized XCT to characterize asphalt concrete components. Tashman et al. (2005) has used the x-ray tomography images to quantify air void distribution and to analyze damage evolution under loading. Landis et al. (2003) aimed at quantifying microstructure-property relationships for cement based materials using x-ray CT.

The XCT system consists of a continuous x-ray source, a digital detector to obtain data, a processor for data reconstruction, and a processor for data display (Figure 2-3). The procedure produces a series of cross-sectional images of an object from a number of projections. A thin plane layer of a 3D object, referred to as a slice, is isolated by the synchronized movement of the beam source and the detector. During this synchronized motion, x-ray beam projection data are obtained for the particular image plane from many different angles. Each slice image corresponds to a finite thickness of material, and by acquiring a series of adjacent slices an entire volume can be described (Figure 2-4).
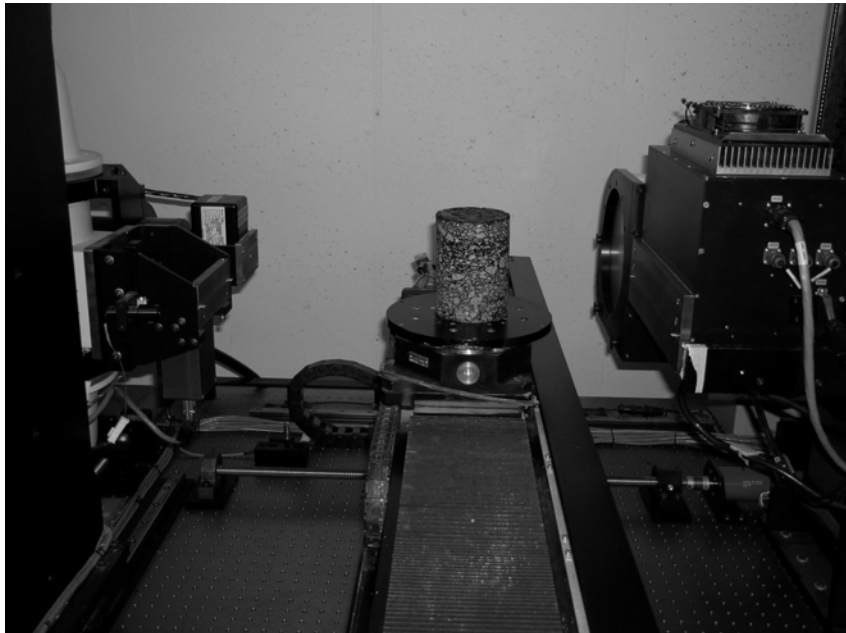


**Figure 2-3. Computed x-ray tomography system**

XCT works based on relating the changes in intensity of x-rays (particles or photon beams) to the density of the object as x-rays penetrate through the object. The gray level of the pixels in CT images, also called CT values or numbers; reflect the x-ray attenuation that is primarily a function of density. The atomic number and the spectrum of x-ray energies also play factors in the x-ray absorption of the material. If the area enclosed by a pixel contains multiple materials (or voids), the net x-ray attenuation is a complexly weighted mean of the attenuations of the different materials. Pixel CT values are also affected by the x-ray spot size, detector spacing, and data acquisition protocol.

Briefly, x-ray computed tomography could be described as follows. The x-rays from the source go through the specimen and are received by the detector. As the x-rays passes through the specimen, their intensity is reduced as a function of the density of the material. The construction of the cross-sectional images is based on the intensity of the x-rays as the detector receives them. Different intensity levels of the x-rays then result in
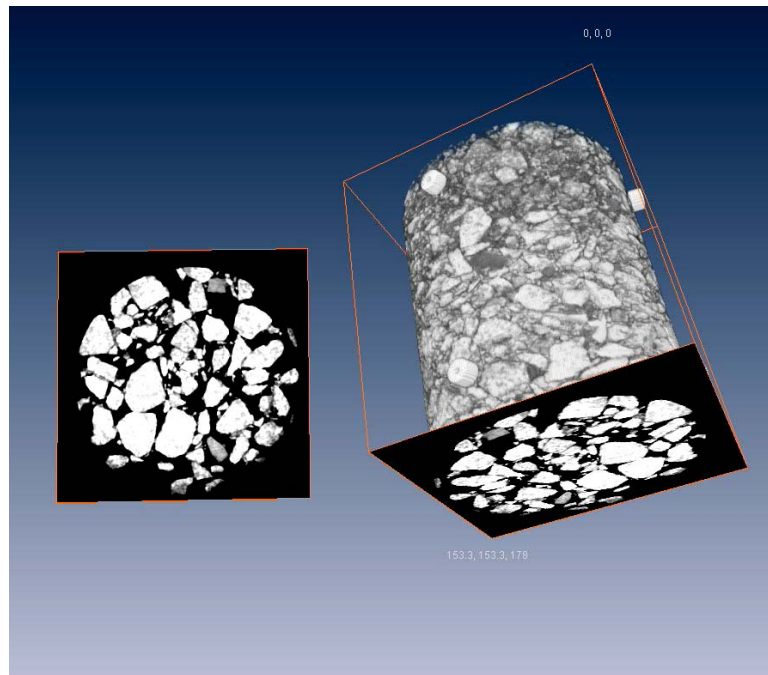


**Figure 2-4. 3-D reconstruction of an asphalt mixture specimen using series of adjacent slices**

different shades of gray on the scanned images. CT is highly sensitive to small density differences between the component materials. Therefore, in the scanned images, each constituent material can easily be isolated for further examination and analysis.

Figure 2-5 shows a two dimensional CT image of an asphalt concrete specimen. The figure clearly shows the three phases of asphalt concrete material: aggregates, mastic, and air. Since the intensity of each pixel is proportional to object density, air voids with the lowest density are black while the solids vary from dark to light gray depending on relative densities. The intensity differences in the image are sufficient to clearly distinguish aggregates from mastic.

## 2.5 IMAGE ANALYSIS

### 2.5.1 Image Processing Techniques

Digital image processing is a fairly mature field that has produced a wealth of analysis tools for extracting quantitative information. Image analysis requires image processing software, which visualizes the image data and provides the tools for processing of the images. The image processing and analysis steps include length scale calibration, thresholding, object recognition, and automated area calculations (Russ 1999 and Wojnar 1998), which can be structured in nine steps:

The first step of image processing is the length scale calibration. This involves determination of a calibration factor that converts the object measurements in pixels to other measurement units such as micron or millimeter. By default, spatial measurements are expressed in terms of pixels. To report the measurements in terms of millimeters the spatial scale needs to be calibrated by assigning a certain number of pixels to a known length in millimeters.
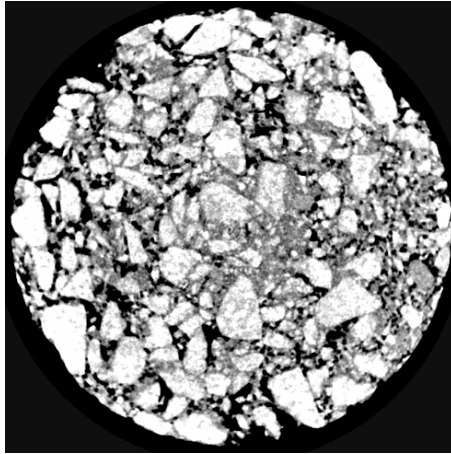
**Figure 2-5. An example of x-ray computed tomography image**

The second step is the image filtering. Several filters could be applied to enhance the contrast and visibility of the image. This will provide better delineation of the edges of the aggregates and more clearly show the separation of the adjacent aggregates.

The third operation is thresholding. The improved image is reduced to a binary image by a thresholding operation. Image thresholding consists of separating different phases in the image through pixel intensity-based criteria. In asphalt mixture images the three phases are aggregates, voids, and mastic. Image thresholding sets pixel intensities that represent the boundary between each of the three phases. Therefore, two threshold values are required to separate the three phases. That is, all pixels with intensities above the upper threshold are considered aggregates, below the lower threshold is considered voids, and between the lower and upper threshold values are considered mastic. The result of this operation is a binary (black and white) image showing only two phases: the phase of interest and every thing else. An example of this is shown in Figure 2-6.
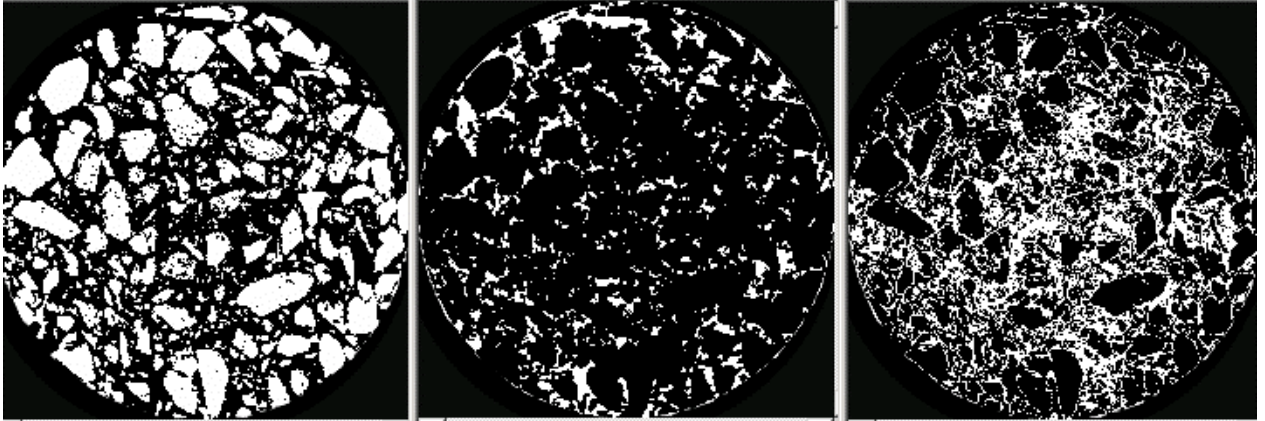
**Figure 2-6. Threshold images of the aggregates, air voids, and the mastic**

Fourth, the aggregates might need to be separated in the binary image since in the process of thresholding two or more aggregates might have been identified as one piece. The limited watershed technique has been commonly used for separating the aggregates.

Fifth, particles smaller than a specific size, i.e. 2.36 mm in diameter, are eliminated. Including very small aggregates would make the analysis more complicated and decline the precision of the measurements.

Sixth, additional thresholding provides a new image with particles larger than the specified size separated and particles smaller than the specified size trimmed out. The new binary image is used for the measurement of geometric properties.

Seventh, important characteristics such as the area, frequency, diameter, centroid locations, and the angle of orientation of each individual aggregate are measured.

Eight, based on the geometric data obtained in step seven, additional features of the aggregates such as the centroid-to-centroid distances of the aggregates, are calculated.

Ninth, a statistical interpretation of the data from step eight quantifies the level of inhomogeneity of the cross-section being analyzed.

## 2.5.2   Accuracy of Image Analysis

The accuracy of measurements taken from a slice face using image processing techniques is highly dependent on the quality of the images and the validity of the images as representations of the actual samples (Russ 1994). Images with low resolutions and not enough contrast are not easy to analyze. Manual measurements, which are subject to errors, are required to measure the characteristics from these images. This is time consuming and is imprecise in comparison to automatic measurements.

There are several problems associated with the images acquired using x-ray computed tomography, with two of the commonly encountered problems addressed here. The first problem is the ring artifact, which is the appearing of concentric rings centered on the scanned images. This problem can sometimes be very intense so that they interfere with the measurement of components of interest such as air or aggregates. The ring artifact problem is caused by the change in the response of the detectors due to the changes in scanning conditions, such as changes in temperature or beam strength. These factors can be overcome by carefully controlling experimental conditions or by frequent calibrations. The ring artifact can also be addressed at the scanning stage with conducting a wedge calibration using a material of similar attenuating properties to the scanned objects.  The wedge calibration is a process that establishes the characteristics of the x-ray signals as read by the detectors under scanning (Ketcham and Carlson, 2001).

The second problem with XCT images is the beam-hardening that causes the edges of the object to appear brighter than the center, even if the material is the same through out. This makes the detection of the objects at the edges of the specimens very difficult since the threshold value that is selected based on the pixel intensities of the middle portion is too low for the edges. The beam-hardening problem is caused by less

attenuation of the x-ray beams at the edges than in the middle of the object. This is because the thickness of the object that x-rays go through is much less at the edges than in the middle. The x-ray beams, which are absorbed in proportion to the thickness of the object, are less absorbed at the edges and are received at more intensity by the detector. There are several techniques that can alleviate the beam-hardening artifact. The most effective technique is to correct the raw data at the data processing stage before the reconstruction stage. The correction converts each raw scan data to a non-beam hardened equivalent data (Ketcham and Carlson, 2001).

## 2.6  STATISTICAL ANALYSIS OF IMAGING MEASUREMENTS

Statistical tools are widely used in interpreting image analysis data. Statistical analyses are generally being carried out by exporting the measured data to a spreadsheet program or a more specialized data analysis program. Generally the analysis involves the comparison of two or more sets of measurement data to determine whether the two samples can be distinguished from each other. The comparison can be made on means, standard deviations, or the distributions of the two samples (Russ 1999).

To compare the means of two populations relative to the standard deviations and sizes of the two populations, a two-sample t-test can be used. For more than two populations, the same comparison can be performed using a one-way analysis of variance (ANOVA) test. If the distribution of the population is different from that which underlies the test, then nonparametric tests, such as the Kolmogorov-Smirnoff test, can be applied (Russ 1999). The Runs test, which is an example of nonparametric test, can be used to test the randomness of the location of aggregates in space. These tests generally require

less effort to apply but they require a larger sample size for an equivalent confidence to the corresponding parametric test (McCuen 1985).

## 2.7  SIMULATION

Image analysis and simulation are tightly bonded together. It is difficult to reach the desired precision using only image analyses of a limited number of laboratory-made specimens. Additionally, the real values of the estimated parameters are never known with real structures. On the contrary, a precise analysis of a structure can be easily achieved using simulation. Various microstructures and some processes leading to microstructure alteration can be developed using computer simulation. Any simulated structure is well defined and all the necessary parameters can be evaluated precisely. The exact values of the parameters can then be used for comparison with the results obtained from the verification process using image analysis. This gives the necessary information concerning the precision and bias of the procedures being verified (Wojnor 1998).

Simulation is very effective in the modeling of granular structures. Simulation can be easily performed to create randomly packed or intentionally distributed to have inhomogeneous granular structures. Considerable care must be taken to ensure that simulation procedures give a reliable representation of the underlying processes (Diggle 1977).

### 2.7.1  Monte Carlo Simulation

Where an analytical-experimental study of a system is not adequate or is impossible, the probabilistic nature of a system output can be studied using the Monte Carlo simulation (McCuen 1985). The Monte Carlo method provides approximate

solutions to a variety of mathematical problems by performing statistical sampling experiments on a computer (Sobel 1994). The Monte Carlo simulation is a set of methods that are utilized for inexpensively testing engineering systems by mimicking their real behavior (Ayyub and McCuen 1997). The main purpose of the simulation methods is to develop a computer-based analytical model that can be used in predicting the behavior of a system. The simulation of a probabilistic system provides the tools for examining the expected response of the system for a wide variety of inputs and system conditions (McCuen 1985). The model is then evaluated based on the data measured from the system using many simulation runs. The random selection of parameters should be based on the probability distribution of the respective parameter. For example, if the input is the value of a random variable having a normal distribution with a mean of $\mu_o$ and standard deviation of $\sigma_o$, then the random number generator must be capable of generating random numbers for this density function. The generated values are then input to the model and the output values are computed. In order to evaluate the behavior of the system, statistical methods are applied to compute the moments and the distribution type of the system output (Ayyub and McCuen 1997).

The Monte Carlo simulation involves several steps. First, a clear definition of the system being modeled must be developed; second, the ability to generate uniform random numbers should be achieved; third, the uniform numbers must be transformed to the probability density function of the population of the input variables; fourth, the model must be evaluated; fifth, a statistical analysis of the output must be performed; and sixth, the simulation efficiency and convergence must be evaluated. The definition of the system should indicate the boundaries of the system, input parameters, output measures,

and models that relate the input to the output parameters. The values of some inputs are generated randomly using Monte Carlo simulation, with consideration of the uncertainty of the model and the data variability. The generated input values are then input to the model to obtain a computed output measure. N simulation cycles are made to obtain N responses of the system. Statistical methods can then be applied to identify the distribution and parameters. The convergence of the simulation methods can be investigated by examining the expected values of the output parameters and the variability in the output values (Ayyub and McCuen 1997).

Simulation has been widely used in different disciplines of science and technology. Statistical analyses of the spatial distribution of the features of a point pattern have been particularly facilitated by the use of simulation. Diggle et al. (1976) used Monte Carlo methods to simulate two nonrandom population models and investigated the power of the statistics proposed by Holgate (1965) and Besag and Gleaves (1974). Heltshe and Ritchey (1984) have generated various spatial patterns and various sampling procedures for testing the power of the quadrat method using Monte Carlo simulation. Nolan and Kavanagh (1993) have used computer simulation to produce gravitationally stable random loose and random close packing of lattices consisting of equal sized spheres. Using simulation, they evaluated the packing density, the mean coordination numbers (number of contacts) and the radial distribution function. Meakin and Jullien (1991) applied simulation models to investigate the surface and internal structure of the systems formed by particle deposit processes. They also used their model to study the segregation of particles of different sizes in the sedimentation process. Diggle (1979)

simulated several tests of spatial randomness to provide insight into the suitability of various models for different mapped patterns.

### 2.7.2 Advantages and Disadvantages of Simulation

Simulation is widely used in engineering decision making. It is a popular modeling tool because it enables working with a representation of the system when dealing with the real system is impossible or too costly. A few additional reasons for using simulation as a modeling tool are:

1. Simulation enables gathering of the applicable data systematically.

2. Simulation enables the model parameters, variables, and initial conditions to be controlled, which is often not possible with the real system (Ayyub and McCuen 1997).

3. The simulation of a complex system determines which variables are important and how they are related. This will eventually lead to successful analytic formulations.

4. Simulation enables experiments to be replicated.

5. Simulation is the only tool that gives the complete probability distribution of the output of the process when information on only mean and variance is not adequate.

6. A simulation can be performed to evaluate an uncertain analytic solution.

7. Using simulation, prediction of future performance may be accomplished.

8. Simulation is less expensive and less time consuming than many forms of experiments.

9. Simulation is an informative tool since it gives an insight of the system being studied.

f.   Simulation allows the scaling of the time and space of the problem to be changed

to more convenient scales.

Computer simulation of the aggregate structure in asphalt concrete specimens, in

particular, has numerous advantages. First, it enables computer generation and analysis of

specimens with different aggregate structures without the cost and effort required to form

and analyze laboratory specimens. Second, computer simulation enables alternative

indices of aggregate inhomogeneity to be tested under a variety of gradation mixes and

sampling programs. Third, simulation enables the testing to be made without

uncontrolled variation of external factors, which is not always possible in the laboratory.

Fourth, millions of specimens can be created and analyzed in a matter of minutes

(McCuen et al. 2001).

While simulation has numerous advantages, it has a few drawbacks. First, it is

possible that differently formulated models of a system could lead to different decisions.

Second, if the data used in the calibration of the model is limited, then extrapolation out

of range of the measured data could introduce inaccuracy into the results (Ayyub and

McCuen 1997). Third, the simulated models might not satisfactorily include all aspects of

a real system.

### 2.7.3   Generation of Random Numbers

Simulation requires a random number generator to create the sequence of random

numbers to represent the random variables. Random numbers are real numbers that have

a uniform distribution with values of the location and scale parameter of 0 and 1,

respectively. A sequence of random numbers should not be serially correlated. The

uniform numbers can be transformed into real values of any distribution of interest (Ayyub and McCuen 1997).

The generation of the random numbers can be based on analytical models. In these generators, a random number is obtained based on a uniform number (numbers) and a fixed arithmetic equation. Therefore, an initial value that is called the *seed value* is needed to start the generation of the random numbers. From that point a series of random numbers is generated. An important characteristic of an arithmetic random generator is that for a given seed number, the same stream of random values will be generated. The repeatability of the generated values is important for any comparison study of the alternative parameters of a system. Most computer installations provide random number generators for most probability functions. An introduction on methods of generating random numbers is provided by Kennedy and Gentle (1980).

### 2.7.4 Accuracy Assessment

The accuracy of simulation results highly depends on having an accurate definition of the system. Including all of the critical parameters of the system is essential in obtaining accurate results. It is important to have the knowledge of the statistical and probabilistic characteristics such as moments and the distribution types of the input parameters. The accuracy of a simulation result is also dependent on the number of simulation runs. The accuracy is expected to increase with an increasing number of simulations (Ayyub and McCuen 1997).

When distribution theory is available, Monte Carlo testing provides an exact alternative for small samples and is a useful check on the applicability of the underlying theory. If the results of classical and Monte Carlo tests are not in substantial agreement,

the explanation is usually that the classical test uses inappropriate distribution

assumptions (Diggle, 1983).

### 2.7.5  Verification of Simulation

It is essential that the results of simulation be validated with actual responses of

the system to the same input. The objective of the validation process is to ensure that the

simulation model satisfactorily duplicates the real system. The criteria that are to be used

in the validation should be the useful characteristics of the real system that were carefully

selected initially to be included in simulation. All of the details of the system need not to

be modeled and validated. Only those characteristics pertaining to the design and

performance of the system need to be included in the modeling and to be evaluated in the

validation stage (Ayyub and McCuen 1997).

## 2.8  STATISTICAL EVALUATION OF INDEX RELIABILITY

The Statistical method for the analysis of the indices of homogeneity includes use

of statistical hypothesis tests. The application of statistical tests is generally encouraged

because it systematically accounts for the sampling variation of the random variable.

Statistical testing provides a systematic means of identifying a significant result and

indicates the risk involved in making an incorrect decision. Statistical tests require

knowledge of the distribution of the test statistic and the selection of the level of

significance that is appropriate for the physical system being studied (McCuen 2003).

Statistical evaluation involves comparing of the distribution of the test statistics for the

condition of complete homogeneity and condition of inhomogeneity, identifying the

critical values of the test statistics, evaluating probability of type I ($\alpha$) and type II ($\beta$)

errors, and assessing the power of the test (Heltshe and Ritchey 1984).

Statistical analysis of the point pattern starts with the null hypothesis, $H_o$, that the

observed distribution of events is homogeneous (Diggle et al. 1976). In general, the

hypothesis of complete spatial randomness is tested by comparing of the measures of

selected characteristics of the empirical point pattern with those of the hypothesized

pattern (Okabe et al. 1992).

## 2.8.1   Parametric and Nonparametric Methods

In general, a decision-making using hypothesis test on random variables is based

on the assumption of having a known distribution such as the normal distribution with

known distribution parameters (McCuen 1985). A test of hypothesis based on the

assumption of a known distribution and parameters is called a parametric test. In cases

where the distribution of a random variable is not that which is specified in the

underlying theorem, testing a hypothesis using a parametric test might lead to erroneous

results. Therefore, other methods of testing that do not require the random variable to

follow the underlying distribution should be used. These methods are called

nonparametric tests. An example of a nonparametric test on the distribution of a random

variable is the Kolmogorov-Smirnoff one-sample test. A nonparametric test is also used

when the random variable is not measured on continuous scales; For example, values

measured on nominal or ordinal scales require the use of nonparametric tests.

## 2.8.2   Type I and Type II Errors

The first step in performing a statistical analysis is formulating two or more

hypotheses for testing. If the objective is to compare two or more distributions or specific

parameters of the distributions, the hypotheses will be statements formulated to indicate the absence or present of differences. The first hypothesis that is the null hypothesis ($H_o$) and the second hypothesis that is the alternative hypothesis ($H_A$) are formulated as follows:

*$H_o$: The difference does not exist*

*$H_A$: The difference does exist*

When using sample data to draw conclusions about the population, it is quite possible to make an erroneous decision to select one of the above two hypotheses. The task is to choose the decision criteria that minimize the likelihood of error.

The errors associated with the above hypotheses can be expressed in a decision table. Table 2-6 shows a decision table in terms of using sample information to make decisions about populations. Two errors are possible. A type I error occurs when the decision is made that the specimen is inhomogeneous even though the specimen is homogeneous; in this case, the sample information failed to reflect the true condition of the specimen. The probability of making this type of error is typically referred to as the level of significance, which is denoted as $\alpha$.

The second type of error occurs when the sample information leads erroneously to the conclusion that the specimen is homogeneous, when, in fact, it is not. The probability of this type of error is usually denoted as $\beta$.

The two types of errors are not independent. While the best decisions are made when both errors are small, it is unfortunate that, when the decision is made to reduce the probability of one type of error, the probability of the other type is made larger.

**Table 2-6. Decision table for hypothesis testing (McCuen 1985)**

| | | Population | |
|---|---|---|---|
| | | **H$_o$ is true** | **H$_A$ is true** |
| **Sample** | **Accept H$_o$** | Correct | Type II error: Incorrect decision |
| | **Accept H$_A$** | Type I error: Incorrect decision | Correct |

Therefore, the decision criterion should be selected to yield acceptable values of both α and β. The only way to simultaneously reduce both α and β is to increase the sample size, but an increase in both time and cost is associated with increasing the sample size (McCuen 1985).

Heltshe and Ritchey (1984) evaluated various quadrat methods for different population sizes by monitoring the probability of type I errors. They found poor control over the probability of type I error when very large quadrats and consequently small sample sizes are used. Given a fixed total sampling area, they suggest that taking many small quadrats is better than taking a few large ones. For all population sizes, except for the lowest population size, use of many small quadrats resulted in the α-level less than the nominal level of 0.05.

## 2.8.3    Power of a Statistical Test

In making statistical decisions, it is a general practice to select a level of significance α and essentially ignore the magnitude of the type II error. However, the type II error is a measure of the quality of the test. Subtracting the value of β from 1.0 gives the power of the test, i.e., power = 1- β. The power of the test is useful for

comparing alternative tests. The test with the highest power for a given level of significance is generally preferred. Heltshe and Ritchey (1984) have investigated two quadrat sampling procedures by comparing the power of the two test statistics. On the basis of their simulation studies they found that one test is more powerful in detecting regularity and the other test is more powerful in detecting loose clumps. Diggle et al. (1976) have evaluated the power of the various distance methods against extreme aggregated and regular spatial point patterns using the Monte Carlo simulation. He found that T-square test statistic is more powerful than the rest of test statistics. Holgate (1965) considers the power of various distance methods against a lattice of clusters.

## 2.9 MECHANICAL PROPERTIES

The mechanical response of vertically inhomogeneous specimens is hypothesized to be different from the response of homogeneous specimens since each of the coarse-graded and fine-graded portions of the specimen have been shown to behave differently. Khedaywi and White (1994) showed shorter fatigue life of the coarse-graded and higher rutting susceptibility of the fine-graded mixtures compared to the well-graded mixtures. Williams et al., (1996) have shown a 70% decrease in the resistance of the material to failure of both fine-graded and coarse-graded mixtures tested in a wheel-track device. However, one cannot speculate about the performance of an inhomogeneous specimen that consists of both coarse graded and fine graded mixtures based on these findings.

The influence of inhomogeneity on the performance of the material might also be greatly dependent on the type of mechanical testing that is being applied. If the test is sensitive to the distribution of aggregates, it will measure different properties when a

specimen is homogeneous than when it is not. In this case, care should be taken to prepare the specimen to be as homogeneous as possible. On the other hand, a test that is insensitive to the distribution of the mixture components, would measure some overall property that is indifferent to the local flaws.

The main objective of this study is to determine whether a relationship exists between the aggregate distribution and the engineering properties of the laboratory prepared specimens. Therefore, it is essential to select a mechanical test method that is sensitive to the aggregate-asphalt structure. This requires that the test specimens include the type of inhomogeneity that is intended to be measured. For example, the simple performance tester cannot measure the effect of radial inhomogeneity since the test requires a 100-mm core from the middle of the gyratory specimen where the coarser gradation at the periphery of the specimen has been removed. Similarly, the Superpave shear tester cannot measure vertical inhomogeneity since the test specimen is not tall enough to represent vertical inhomogeneity.

In addition to the specimen size and shape requirement, the mechanical test should have several characteristics in order to be recognized as an appropriate test. First, the test should be able to mobilize the aggregates by applying a repetitive load either in the elastic range (modulus tests) or exceeding the elastic tolerance of the material (permanent deformation tests). Second, the test configuration should be such that aggregates exhibit high involvement in resisting the load. For example, in the shearing mode of testing the aggregates are greatly involved in resisting the applied stress. Third, the variability in the produced data should not be related to the test configuration. For example, the high variability in the resilient modulus indirect tensile test has been related

to the test configuration and fixture setup. Therefore, resilient modulus test will not indicate the variability due to various aggregate structures. Based on the above information, the compression mode of loading for measuring the effect of vertical inhomogeneity and the shear mode of loading for measuring the effect of radial inhomogeneity are selected for this research.

The use of both compression and shear mode of loading for the measurement of the effect of aggregate structure can be found in several occasions in the literature. Witczak et al. (1999) subjected fine and coarse graded specimens with different height to diameter ratios to set of simple performance tests to investigate the changes in modulus with the changes in position of aggregates relative to the boundary of the specimens. Masad and Tashman (2001) have used shear mode of loading for detection of the changes in the mechanical responses of hot mix asphalt specimens with the change in their internal structure as a result of the changes in compaction efforts. Romero and Masad (2000) applied shear load to the specimens with different aggregate size to specimen dimension ratio to detect the changes in the variability of the measured shear properties as a result of changes in relative internal positioning of the aggregates. In the following sections the methods and application of the simple performance tests and the Superpave shear tests will be explained.

### 2.9.1   Simple Performance Tests

The common tests for determining the behavior of hot mix asphalt in compression loading are Simple Performance Tests (SPT). The Simple Performance Tests, in addition to characterizing the constitutive behavior of the asphalt-aggregate mixture, evaluates the performance of the material in permanent deformation.

Three types of tests can be conducted using SPT; the dynamic modulus (E*), the repeated shear Flow Number test (FN), and the static flow time test (FT). The first two tests are mostly used in research and are also found applicable in this study. The dynamic modulus determines the relationship between the stress and strain for the asphalt material in the linear visco-elastic range. The Flow Number test is used for determining the performance-based properties of asphalt mix, i.e., permanent deformation estimation and the number of cycles to failure. A schematic diagram of the simple performance tester is shown in Figure 2-7.

### 2.9.1.1    Testing Procedures

**Dynamic Modulus**- The standard method for performing the Dynamic Modulus (E*) test is provided in the AASHTO standard TP 62-03 (2003) test procedure and NCHRP report 465 (2003). The test determines the dynamic modulus and phase angle of asphalt concrete mixtures over a range of temperatures and loading frequencies. A sinusoidal (haversine) axial compressive stress is applied to a specimen of asphalt concrete in the linear viscoelastic range of the material at a given temperature and loading frequency. The applied stress and the resulting recoverable axial strain response of the specimen is measured and used to calculate the dynamic modulus and phase angle. The dynamic modulus is computed by dividing the maximum (peak-to-peak) axial stress by the recoverable (peak-to-peak) axial strain. The phase angle ($\varphi$) is the angle in degrees between a sinusoidal applied (peak-to-peak) stress and the resulting (peak to peak) strain in a controlled-stress test.
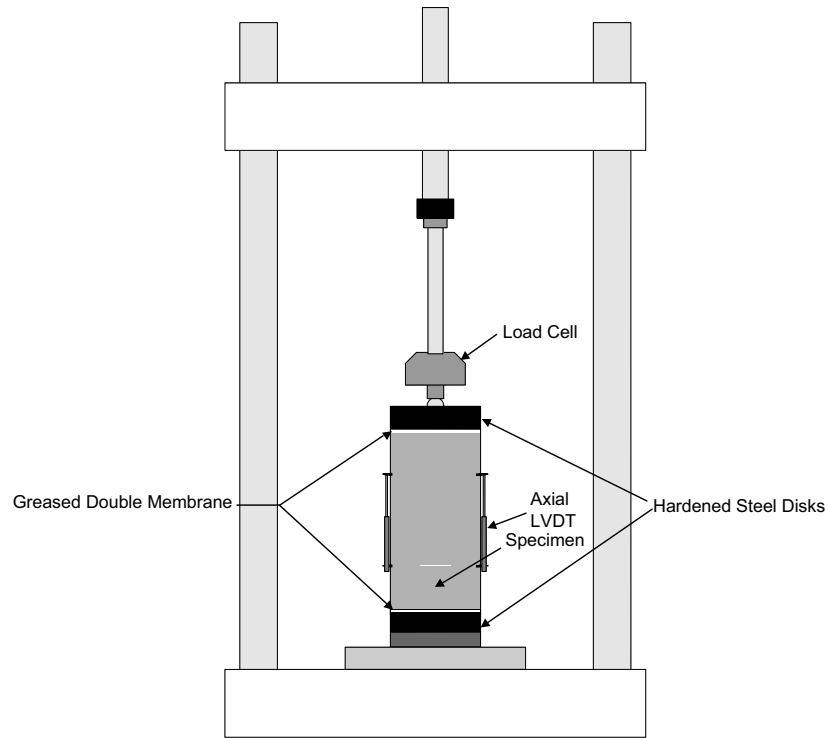
**Figure 2-7. General schematic diagram of the Simple Performance Tester**

The dynamic modulus test system consists of a testing machine, environmental chamber, and measuring system. The testing machine is a servo-hydraulic testing machine, which produces a controlled haversine compressive loading. The testing machine applies a range of frequencies from 0.1 to 25 Hz and stress levels up to 2800 kPa (400 psi). The environmental chamber controls the temperature of the specimen over a temperature range from –10 to 60°C.

The measurement system measures and records the time history of the applied load, and the axial deformations. The load is measured with an electronic load cell in contact with one of the specimen caps. The axial deformations are measured with linear variable differential transformers (LVDT) mounted between gauge points glued to the specimen as shown in Figure 2-8. The deformations are measured at three locations

located 120° apart. The gauge length for measuring axial deformations is 100 mm, which is the distance between the centers of the glued studs for mounting the LVDTs.
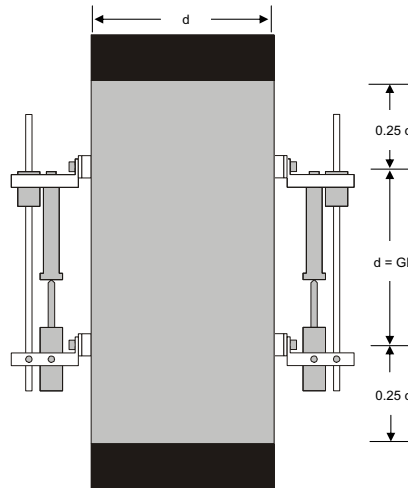


**Figure 2-8. General schematic of gauge points**

Dynamic modulus testing is performed on test specimens cored from the center of gyratory compacted mixtures. The average diameter of the test specimens is 100 mm. The average height of the test specimen is 150 mm, which cut from 170 mm high specimens compacted to the desired air void content.

The recommended test series consists of testing at −10, 4.4, 21.1, 37.8, and 54.4°C at loading frequencies of 0.1, 0.5, 1.0, 5, 10, and 25 Hz at each temperature. The specimen is tested from lowest to highest temperature and at each temperature the load is applied from highest to lowest frequency; that is from 25 Hz to 0.1 Hz. At the beginning of testing, the specimen is precondition with 200 cycles at 25 Hz at stress level corresponding to Table 2-7. Then the specimen is loaded as specified in Table 2-8. A typical rest period between each frequency run is between two to 30 minutes. The dynamic load should be adjusted to obtain axial strains between 50 and 150 microstrain.

**Table 2-7. Typical dynamic stress levels**

| Temperature, °C (°F) | Range, kPa | Range, psi |
|---|---|---|
| −10 (14) | 1400–2800 | 200–400 |
| 4.4 (40) | 700–1400 | 100–200 |
| 21.1 (70) | 350–700 | 50–100 |
| 37.8 (100) | 140–250 | 20–50 |
| 54.4 (130) | 35–70 | 5–10 |

**Table 2-8. Number of cycles for dynamic modulus test sequence**

| Frequency (Hz) | Number of Cycles |
|---|---|
| 25 | 200 |
| 10 | 200 |
| 5 | 100 |
| 1 | 20 |
| 0.5 | 15 |
| 0.1 | 15 |

The dynamic modulus for each test condition is determined using the average amplitude of the sinusoidal load from the load cell and the average deformation measured from each axial LVDT over the last five loading cycles. Over the last five loading cycles and for each test condition, the loading stress, $\sigma_o$, is computed as follows:

$$\sigma_o = \frac{\overline{P}}{A}$$

(2-9)

where $\overline{P}$ is the average peak load, $A$ is the area of specimen, and $\sigma_o$ is the average peak stress.

Over the last five loading cycles and for each test condition, the average recoverable axial strain, $\varepsilon_o$, is computed as follows:

$$\varepsilon_o = \frac{\overline{\Delta}}{GL}$$

(2-10)

where $\overline{\Delta}$ is the average peak deformation, GL is the gage length.

Over the last five loading cycles and for each test condition, the dynamic

modulus, |E*| is computed as follows:

$$|E^*| = \frac{\sigma_o}{\varepsilon_o}$$
(2-11)

Over the last five loading cycles and for each test condition, the phase angle is

calculated as follows:

$$\phi = \frac{t_l}{t_p} * 360$$
(2-12)

where $t_l$ is the average lag time between a cycle of stress and strain (sec), $t_p$ is the average

time for a stress cycle (sec), and $\phi$ is the phase angle (degree). The average dynamic

modulus and phase angle are calculated from the results of three LVDTs.

**Flow Number Test**- This test is a simple performance test for measurement of

permanent deformation based on repeated axial load test on asphalt concrete mixtures.

The standard method for performing the flow number ($F_N$) test is provided in NCHRP

report 465 (2002). The procedure uses a loading cycle of 1.0 second in duration, which

consists of applying 0.1-second haversine load followed by 0.9-second rest period. The

test is conducted at a single effective temperature, $T_{eff}$, and the design stress level. The

test is performed for duration of 10,000 load cycles.

The recorded data during the test are the applied load and the axial deflections

measured from actuator LVDT. To determine the flow number, the plastic deformation is

measured from the LVDT for the specified cycles. The average deformation values are

converted to total axial strain ($\varepsilon_{Ta}$), mm/mm by dividing them by the length of the

specimen, which is 150 mm. The plastic strains are summed to obtain the cumulative

axial permanent strain. The cumulative axial permanent strain is plotted versus number of

loading cycles in log space. The flow number of repetitions is viewed as the lowest point in the curve of rate of change in axial strain versus number of loading cycles. The rate of change of axial strain versus number of loading cycles is plotted and flow number ($F_N$) is estimated where a minimum or a zero slope is observed.

### 2.9.1.2    Accuracy of Tests

The accuracy of the SPT result is measured by the evaluation of the variability of the data from replicate samples. Although, the variability in SPT data has been documented to be in the acceptable range, on occasional basis a high amount of variability has been observed in the results of SPT. The source of the variability is not believed to be from the testing equipment or testing configuration, but from the structural characteristics of the specimen. Therefore, E* and $F_N$ tests might be sensitive to inhomogeneity that is found in the laboratory prepared specimens.

### 2.9.1.3    Effect of Inhomogeneity

The effect of inhomogeneity on compressive properties of hot mix asphalt has not been studied in a systematic manner. However, variability in the measured compressive properties of the laboratory prepared specimen has been traditionally related to the arrangement of the aggregates, specifically arrangement of the coarse aggregates in the direction of the applied load and within the LVDT gage points.

### 2.9.2  Superpave Shear Tests

The common test for determining the shear behavior of hot mix asphalt can be conducted using a simple shear test device (Superpave Shear Tester-SST). The SST

device in addition to characterizing the constitutive behavior of asphalt-aggregate mixture is one of the devices considered as a laboratory test for the evaluation of the mechanical performance of the hot mix asphalt. The description of the components of a shear test device is provided in the AASHTO standard TP7-94 test procedure. A shear test system consists of a loading device, specimen deformation measurement equipment, an environmental chamber, and a data acquisition system. The loading device consists of two hydraulic actuators, which simultaneously apply both vertical and horizontal loads to a specimen. Figure 2-9 shows a Superpave shear tester equipment. Several kinds of shear tests can be conducted using the SST device. The two types of shear tests that are mostly used in research and are found applicable for this research are the frequency sweep test at a constant height (FSCH) and the repeated shear test at a constant height (RSCH).

### 2.9.2.1   Testing Procedures

The standard method for performing the FSCH and RSCH tests is provided in the AASHTO standard TP7-94 test procedure. The standard method requires that the SST specimens be cut into 50mm thickness, 150-mm diameter circular disks after making the bulk specific gravity measurements and determining the air voids of hot mix asphalt specimens. The samples are glued to two parallel aluminum platens. The platen-specimen assembly is equipped with two vertical LVDTs. The axial deformation from platen to platen is measured using a vertical LVDT attached vertically between the two platens. To measure shear deformation, the horizontal LVDT is mounted on the side of the test specimen between two points at least 40mm apart. The assembled system is then placed and kept in an environmental chamber for 2 to 4 hours to reach the required temperature.

**Figure 2-9. Superpave shear tester equipment**

**FSCH Test**- The FSCH test is a strain-controlled test for determining the stress-strain behavior of the asphalt mixture (shear stiffness). During the test the height of the specimen is held constant by controlling the vertical actuator from a LVDT that measures the vertical displacement. The horizontal actuator is controlled from an LVDT that is mounted directly on the specimen that measures the shear deformation. The shear strain should not exceed 0.0001 mm/mm (100 micron) in order for the mixture to behave as a linear elastic material. The test is performed by applying a constant static vertical strain and a sinusoidal shear (horizontal) strain with peak amplitude of approximately 0.5 μm/mm at each of the cycle and frequency specified in Table 2-9. A frequency sweep test is usually conducted at 4, 20, and 40°C. However, to improve the detection of the effect of aggregate distribution, the high temperature will be increased to 50°C for this study. Recorded data for the test is the axial deformation, the shear deformation, the axial load, the shear load, and the phase angle. The phase angle ($\varphi$) is the angle in degrees between a

68

sinusoidal applied shear strain and the resulting shear stress. The axial and shear stress, the shear strain, and the shear modulus are calculated using the data obtained during FSCH test using the following formulas:

$$\sigma = P/A \tag{2-13}$$

$$\tau = V/A \tag{2-14}$$

$$\varepsilon = \delta/2d \tag{2-15}$$

$$G^* = \tau/\varepsilon \tag{2-16}$$

**Table 2-9. Number of cycles for the FSCH test sequence**

| Frequency (Hz) | Number of Cycles |
|---|---|
| 10 | 50 |
| 5 | 50 |
| 2 | 20 |
| 1 | 20 |
| 0.5 | 7 |
| 0.2 | 7 |
| 0.1 | 7 |
| 0.05 | 4 |
| 0.02 | 4 |
| 0.01 | 4 |

where,

$\sigma$ = stress along the vertical axis,

P = load applied along the vertical axis

A = cross-sectional area of the specimen

$\tau$= shear stress

V = shear force

$\varepsilon$ = shear strain

69

δ = displacement in the shear direction

d = distance along which shear deformation is measured

G* = complex shear modulus

**RSCH Test-** The RSCH test is a stress-controlled test and is used for determining the performance-based properties of asphalt mixture, i.e., rut depth estimation and the number of cycles to failure. During the test the height of the specimen is kept constant by controlling the vertical actuator and the magnitude of shear load is controlled by horizontal actuator. The test cycle duration is 0.7 sec consisting of the application of a 0.1 sec haversine load followed by a 0.6 sec rest period. The repeated shear test has a duration of 5000 load cycles or until the permanent accumulated deformation strain reaches a level of 5 percent. The test is conducted at a single effective temperature, $T_{eff}$, and the design stress level. The recorded data from the test are the axial load, the shear load, and the displacement in the shear direction. From the data recorded, the axial stress, shear stress and shear strain are computed using Equations (2-13) through (2-15).

### 2.9.2.2   Accuracy of Tests

The accuracy of the SST tester is measured by the variability of the data from replicate samples. The amount of variability in the shear test data is within acceptable range, with typical CV values of less than 15%; however, on an occasional basis, a high amount of variability has been observed in the results of SST. The source of the variability has not been related to the testing equipment or testing configuration, but to the structural characteristics of the specimens. Therefore, the shear test can be a good

candidate for examining the effect of inhomogeneity of the laboratory prepared specimens.

### 2.9.2.3   *Effect of Inhomogeneity*

The effect of inhomogeneity on shear properties of hot mix asphalt has not been studied in a systematic manner. However, the variability in the measured shear properties of the laboratory prepared specimen has been traditionally related to the arrangements of the aggregates (Romero and Anderson 1999). Tashman and Masad (2001) investigated the relationship between the internal structure of asphalt mixtures and their shear properties. In most parts they found correlations between the results of aggregate distribution analysis and mechanical behavior of the asphalt mixture specimens. Harvey et al. (1994) have also studied the effect of aggregate and air structure, which was caused by various laboratory compaction methods, using the simple shear test.  However, a concluding remark regarding the result of simple shear test could not be made due to the problems with the air-void content measurements.

# CHAPTER 3 -  SIMULATION OF HOMOGENEOUS AND INHOMOGENEOUS SPECIMENS

## 3.1  INTRODUCTION

Assembling hot-mix asphalt specimens in the laboratory is costly, time consuming, and somewhat imprecise, especially when a large number of samples are required. Computer simulation offers the capability to analyze alternative indices of homogeneity without requiring preparation of specimens in the laboratory. Simulation enables the development and analysis of both homogeneously configured specimens and specimens intentionally configured to be inhomogeneous. A large number of specimens can be quickly generated, such that each of the generated specimens will have the design gradation and homogeneity characteristics of actual specimens. The specimens will differ in the specific location of the aggregates. Computer simulated 3-dimensional cylindrical specimens configured with spherical aggregates can be sliced in any way. The exposed 2-dimensional face can then be analyzed for homogeneity by examining the distribution of the circular faces of particles. This provides a more realistic representation of the aggregate cross-section than when two-dimensional slice faces are simulated, which requires deduction of probability distribution of the circular cross-section from the distribution of the spheres (Taylor 1983; Hanisch and Stoyan 1981; Edwards and Wilkinson 1980; Tallis 1970). Figure 3-1 shows schematic diagrams of the simulated homogeneous, vertically inhomogeneous, and radially inhomogeneous specimens.

## 3.2 COMPUTER DEVELOPMENT OF HOMOGENEITY

In order to obtain realistic results, the computer model of a specimen must adhere to realistic volume, weight, and packing constraints. The volume of air voids ($V_a$) and the weight fractions of both asphalt ($f_a$) and aggregate ($f_p$) must be specified. The weight of the specimen ($W_s$) equals the sum of the weights of asphalt ($W_a$) and aggregate ($W_p$). The volume of the specimen ($V_s$) equals the sum of the volumes of aggregate ($V_p$), asphalt ($V_a$), and air voids ($V_v$). Given these constraints, the weight of the specimen was related to the other variables by:

$$W_s = \frac{V_s(1-r_v)}{\left[\dfrac{f_a}{\gamma_a} + \dfrac{f_p}{\gamma_p}\right]} \tag{3-1}$$

in which $\gamma_a$ and $\gamma_p$ are the specific weights of the asphalt and aggregate particles, respectively. Defining the volume packing fraction ($P_v$) as the ratio of the volume of particles to the volume of the specimen yields the following expression:
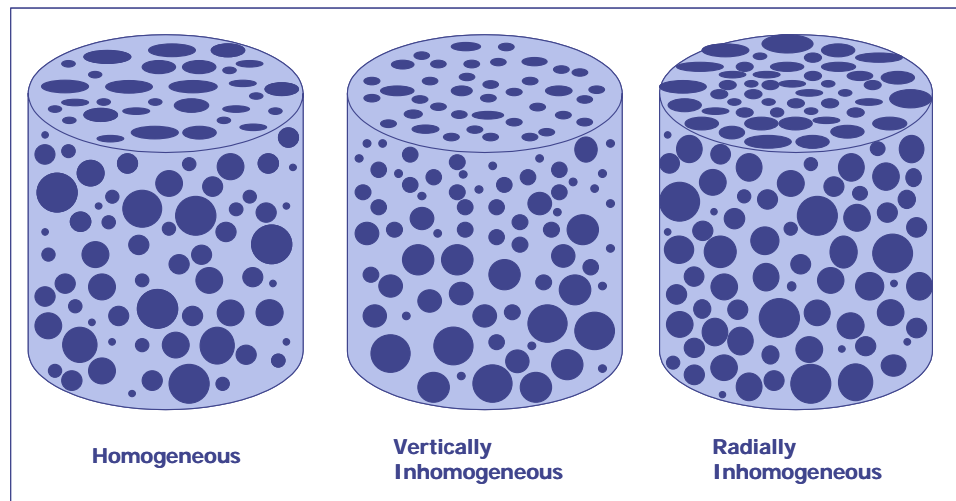


**Figure 3-1. Schematic diagram of simulated homogeneous and inhomogeneous specimens**

$$P_v = \frac{V_p}{V_s} = \frac{W_p/\gamma_p}{V_s} = \frac{f_p\,W_s/\gamma_p}{V_s} = \frac{1 - r_v}{1 + \left(\dfrac{f_a}{f_p}\right)\left(\dfrac{\gamma_p}{\gamma_a}\right)} \qquad (3\text{-}2)$$

Detailed derivations of Equations (3-1) and (3-2) are provided in Appendix A.

### 3.2.1 Number of Particles

To simulate 3-dimensional specimens, it is necessary to determine the number of particles in each gradation level of each specimen. In order to compute the number, particles were assumed to be spherical. In the actual simulation, diameters across the entire range of sieve openings were used. If the number of particles for gradation level $i$ is $n_i$ and is equal to the ratio of the volume of all particles in the gradation level ($V_i$) to the volume of one particle ($v_i$), then the following relationship applied:

$$n_i = \frac{V_i}{v_i} = \frac{W_i/\gamma_p}{\pi d_i^3/6} = \frac{6F_iW_p}{\pi\gamma_p d_i^3} = \frac{6F_i\gamma V_p}{\pi\gamma_p d_i^3} = \frac{6F_i P_v V_s}{\pi d_i^3} = \frac{1.5F_i P_v D_s^2 H_s}{d_i^3} \qquad (3\text{-}3)$$

in which $d_i$ is the average particle diameter for level $i$, $F_i$ is the weight fraction for level $i$ of the weight gradation curve, and $D_s$ and $H_s$ are the diameter and height of the specimen, respectively. A detailed derivation of Equation (3-3) is provided in Appendix A.

As indicated by Equation (3-3) the number of particles in a specimen is determined by the dimensions of the specimen ($D_s$ and $H_s$). Two different specimen sizes that represent the specimens made in the laboratory were simulated. The first set of specimens was simulated with diameters of 100 mm and heights of 150 mm, which is the required size for the Simple Performance Tests, SPT (NCHRP, 2002). Specimens of this size were made homogeneous and vertically inhomogeneous.

Specimens in the second set were simulated to have diameters of 150 mm and heights of 100 mm. Each specimen was then cut in half horizontally to provide two 150-mm diameter by 50-mm thick cylindrical disks, which represent the specimens made in laboratory for the Superpave Shear Tests, SST (AASHTO, 1998). Using Equation (3-3), the number of particles in each class size was determined taking into consideration of the height and diameter of the simulated specimen.

The smallest aggregate diameter used in simulation is 2.36 mm, because this is the minimum diameter used in the computation of a number of the indices of homogeneity. On separate occasions, particles with diameters of 2.36 mm and 4.75 mm were defined as the coarse particles in the literature and their properties were indicated to be effective in the measurement of inhomogeneity (Bryant, 1967; Cross and Brown, 1993). For the gradations that are used in this study, with a maximum aggregate size of 19 mm, four class sizes above 2.36 mm were defined. Spherical aggregates in the range of 2.36 mm to 19 mm in diameter were simulated. The number of particles in each of the four class sizes for the two specimen sizes and the properties of the mixtures are provided in Table 3-1.

### 3.2.2 Diameter of Particles

For homogeneous specimens, the diameter of each particle was generated in such a way that the diameters within each class size were uniformly distributed between the values of the lower and upper sieve openings. Within each class, the diameter ($d_j$) of $j^{th}$ particle was generated randomly according to the equation:

$$d_j = d_i + u_j(d_{i+1} - d_i) \qquad (3\text{-}4)$$

**Table 3-1. Number of particles retained in the class sizes above 2.36 mm sieve**

| Class Size (mm) | $d_i$ Average Diameter (mm) | $P_i$ Percent Passing (%) | $F_i$ Percent Retained (%) | $n_i$ Number of Particles (SST size) 150 mm x 100 mm | $n_i$ Number of Particles (SPT size) 100 mm x 150 mm |
|---|---|---|---|---|---|
| 19-12.5 | 15.8 | 76.0 | 24.0 | 168 | 112 |
| 12.5-9.5 | 11 | 62.0 | 14.0 | 288 | 192 |
| 9.5-4.75 | 7.1 | 44.0 | 17.9 | 1357 | 905 |
| 4.75-2.36 | 3.6 | 30.1 | 14.0 | 8543 | 5695 |
| < 2.36 | | | 30.1 | | |

Percent Air void, $A_V$ = **7 %**
Asphalt Weight Fraction, $f_a$ = **4.85**
Aggregate Weight Fraction, $f_p$ = **95.15**
Aggregate Specific Gravity, $\gamma_p$ = **2.87 g/m³**
Asphalt Binder Specific Gravity, $\gamma_a$ = **1.02**
Packing Fraction, $P_v$ = **0.81**

where $d_i$ is the sieve size on which aggregates are retained (lower class size), $d_{i+1}$ is the

next largest sieve size through which all of the aggregates passed (upper class size), and

$u_j$ is a uniform random number between 0 and 1.

### 3.2.3 Positioning Particles

For homogeneous specimens, the aggregates were randomly placed within the

specimen. The coarse particles were identified first to avoid problems in locating

particles. The random location of the particles in the cylindrical specimen was generated

in polar coordinates. The use of polar coordinates simplified the simulation such that

particles did not reside outside of the cylinder. Once each aggregate particle was located

in the specimen, the polar coordinates were converted to rectangular coordinates to

simplify the assessment of the indices of homogeneity. Figure 3-2 shows the polar and rectangular coordinates of a particle in a cylindrical specimen.

For a homogeneously configured aggregate structure, the individual particles were assigned a random location. Using a constant-slope transformation curve, three random uniform numbers ($u_i$) were transformed to three different parameters: a radial coordinate ($r_i$), an angular coordinate ($\theta_i$), and a vertical coordinate ($h_i$). To randomly assign a radial position to the particle centroid, the following expression was used:

$$ r_i = \left( R_s - \frac{d_i}{2} \right) u_i \qquad\qquad (3\text{-}5) $$

where $r_i$ is the radial distance of the particle centroid from the vertical centroid axis; $R_s$ is the radius of the specimen, which is equal to 75 mm for SST sized specimens and 50 mm for SPT sized specimens; $d_i$ is the diameter of the particle; and $u_i$ is a random number between 0 and 1.
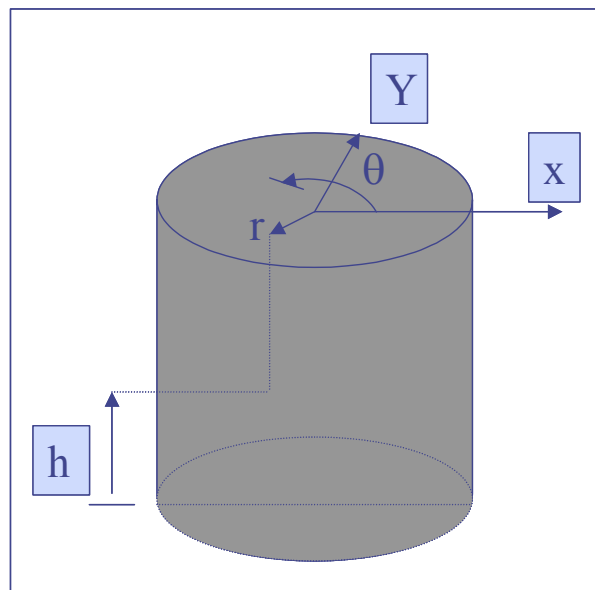


**Figure 3-2. Rectangular ($x, y, h$) and polar ($\theta, r, h$) coordinates of a particle in a three-dimensional cylinder**

To determine the angular position, $\theta_i$, of a centroid between 0° and 360° the following equation was used:

$$\theta_i = 360° u_i \qquad (3\text{-}6)$$

To randomly assign a vertical position to a particle centroid, the following expression was used:

$$h_i = \frac{d_i}{2} + (H_s - d_i) u_i \qquad (3\text{-}7)$$

where $h_i$ is the vertical position of the particle centroid and $H_s$ is the height of the specimen, which is equal to 100 mm for SST specimens and 150 mm for SPT specimens. Equations (3-5) through (3-7) ensured transforming the uniform random numbers to any random radial, angular, and vertical position within the specimen.

The $x$ and $y$ coordinates of the particles were computed from the original polar coordinates $r_i$ and $\theta_i$ (Equations (3-5) and (3-6)) and the $z$ coordinate was the same as the vertical position of the particle, $h_i$ (Equation (3-7)):

$$x_i = r_i \cos \theta_i \qquad (3\text{-}8)$$

$$y_i = r_i \sin \theta_i \qquad (3\text{-}9)$$

$$z_i = h_i \qquad (3\text{-}10)$$

### 3.2.4  Verification of Particle Overlap

Once the coordinates of a particle were determined, it was necessary to show that the new particle did not overlap with any of the particles already parked. The process of locating the particles, which is called "parking", continued until all particles were placed within the boundaries of the specimen. In order to verify the process, the distance between the centroid of the new particle and the centroid of every particle already parked

was computed. The distance between any two centroids must be greater than the summation of the radii of the two particles.

To compute the distance between any two centroids, the rectangular coordinates of the centroids were used. Knowing the rectangular coordinates of the aggregate centroids, the distance between any two centroids ($D$) could be computed and compared with the summation of the two aggregate radii:

$$D = \sqrt{x^2 + y^2 + z^2}$$
(3-11)

where $D$ is the distance between the centroid of a new particle and the centroid of an already parked particle, and the x, y, and z coordinates were defined as follows:

$$x = x_2 - x_1$$
(3-12)

$$y = y_2 - y_1$$
(3-13)

$$z = z_2 - z_1$$
(3-14)

where $x_2$, $y_2$, and $z_2$ are rectangular coordinates of the new particle and $x_1$, $y_1$, and $z_1$ are the rectangular coordinates of the already parked particle, which were computed from Equations (3-8) through (3-10).

## 3.3 COMPUTER DEVELOPMENT OF VERTICAL INHOMOGENEITY

A vertically inhomogeneous specimen is defined as a specimen that has changes in gradation throughout its height; however, the total gradation of the specimen is the same as that of a homogeneous specimen. Depending on the process of mixing and compaction, the vertical change in the gradation could occur in various levels. Two levels of inhomogeneity are defined here. First, a specimen can be inhomogeneous in two

layers: coarser and finer. The two-layer inhomogeneity represents abrupt inhomogeneity. Second, vertical inhomogeneity may be separated into three gradations: coarse, medium, and fine. The three-layer inhomogeneity is intended to reflect gradual inhomogeneity. Both the abrupt and gradual forms of inhomogeneity in two and three layers were computer simulated. The following sections provide the information required for simulating each of these conditions.

### 3.3.1    Abrupt Vertical Inhomogeneity

For abrupt vertical inhomogeneity, the design gradation was used to form two distinct gradations, one for each of the two layers. The specimens had a coarser gradation in the lower portion and a finer gradation in the upper portion. This would represent the situation wherein the coarse aggregates become separated from the fine aggregates in the process of the mixture being transferred into the mold. In order to simulate the vertical inhomogeneity in two layers, the gradations of the layers, the number of particles in each layer, the volume of the layers, and the position of the particles within each layer were determined.

### *3.3.1.1    Gradation of the Layers*

The design gradation was used to create a coarser and a finer gradation, placed in the lower and upper layers of an abrupt vertically inhomogeneous specimen. A sieve that separates the weight of the dry aggregates into about 50% above and 50% below the sieve was identified. This sieve served as the demarcation between the coarse and fine aggregates (Khedaywi and White, 1994). For this study, the #4 sieve, which has a 4.75-mm opening, separated the aggregates by weight into 56% above and 44% below the

sieve. The two gradations were referred to as the "very coarse" and the "very fine" gradations (Figure 3-3).

The next step of the process involves combining different percentages of the very coarse and the very fine gradations to create two gradations that are placed in the lower and the upper portions of the specimen. Blending of 25% of the particles from the very fine gradation with 75% of the particles from the very coarse gradation provided the gradation for the lower portion of the specimen. The gradation at the lower portion is referred to as the "coarser" gradation. To create the gradation for the upper portion of the specimen, 75% of the particles in the very fine gradation were blended with 25% of the particles in the very coarse gradation (Figure 3-4). The gradation at the upper portion is referred to as the "finer" gradation. The percentages were selected based on the workability of the mixtures in each layer, particularly the bottom layer. If the bottom layer were made too coarse, the aggregates would not hold and the mixture would fall apart. Moreover, it was necessary to maximize the difference between gradations in order to ensure that the indices would detect the created inhomogeneity and to enable the selected mechanical test to detect the effect of inhomogeneity on material response. The design, the coarser, and the finer gradations are provided in Table 3-2.

### 3.3.1.2    *Number of Particles in the Layers*

The number of particles in the coarser and finer gradations was obtained by blending the required percentages of the number of aggregates from the very coarse and very fine gradations. The number of particles of the coarser and finer gradations, based on the selected percentages of the very coarse and very fine gradations, is provided in
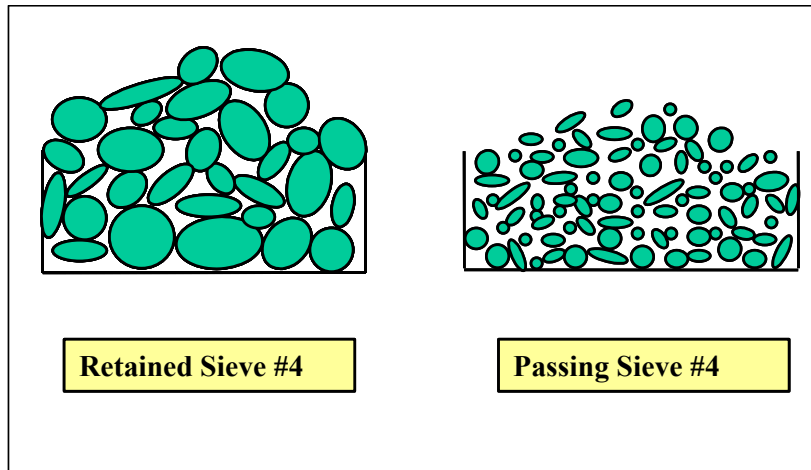
**Figure 3-3. "Very coarse" and "very fine" gradations**
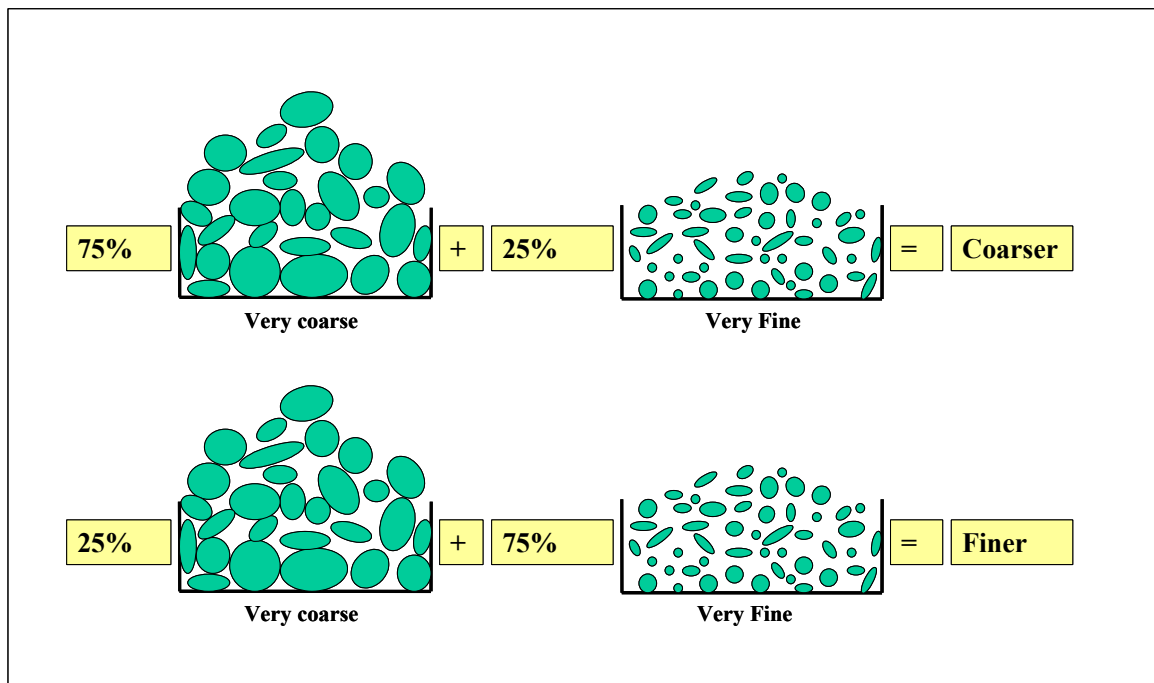


**Figure 3-4. Proportioning of the coarser and finer gradations**

**Table 3-2. The design, coarser, and finer gradations**

| Sieve Size (mm) | % Passing | | |
| --- | --- | --- | --- |
| | Design Aggregate Gradation | Coarser Aggregate Gradations | Finer Aggregate Gradation |
| 19 | 100.0 | 100.0 | 100.0 |
| 12.5 | 76.0 | 66.0 | 87.2 |
| 9.5 | 62.0 | 46.2 | 79.8 |
| 4.75 | 44.1 | 20.8 | 70.3 |
| 2.36 | 30.1 | 14.2 | 48.0 |
| 1.18 | 22.3 | 10.5 | 35.5 |
| 0.6 | 15.7 | 7.4 | 25.0 |
| 0.3 | 10.2 | 4.8 | 16.3 |
| 0.15 | 7.1 | 3.4 | 11.3 |
| 0.075 | 4.9 | 2.3 | 7.8 |

Table 3-3. The number of aggregates in the design gradation (Column 4) that are above sieve #4 represent the very coarse aggregates. The number of aggregates in column 4 that are below sieve #4 represent the very fine aggregates. Multiplying the number of particles in the very coarse gradation by 0.75 and multiplying the number of particles in the very fine gradation by 0.25 provided the aggregate numbers in the coarser gradation (Column 2). Multiplying the number of particles in the very coarse gradation by 0.25 and multiplying the number of particles in the very fine gradation by 0.75 provided the numbers in the finer gradation (Column 3).

### 3.3.1.3   Volume of the Layers

In order to position the particles in the appropriate portion of the specimen, the volumes of coarser and finer mixtures were determined. The volumes of the mixtures in the lower and upper portions were computed using volumes of the aggregates, air voids, and asphalt binder in each portion. The volume of the aggregates in each portion was determined by summing the volume of individual particles in that portion. Table 3-4 shows the calculation of the volume of aggregates in a homogeneous

**Table 3-3. Number of particles in the lower and upper portions of a two-layered vertically inhomogeneous specimen**

| (1)<br>Class Size<br>(mm) | (2)<br>Coarser<br>Gradation<br>(Lower Portion) | (3)<br>Finer Gradation<br>(Upper Portion) | (4)<br>Design Gradation<br>(Homogeneous<br>Specimen) |
|---|---|---|---|
| 19-12.5 | 84 | 28 | 112 |
| 12.5-9.5 | 144 | 48 | 192 |
| 9.4-4.74 | 679 | 226 | 905 |
| 4.75-2.36 | 1424 | 4271 | 5695 |

specimen and the volume of aggregates in the coarser and finer portions of an inhomogeneous specimen. The volume of each particle was based on the assumption that it was spherical. To compute the volume of aggregates in each class size, the number of particles in that class size was multiplied by the volume of an individual particle. The total volume of the aggregates equaled the summation of the volumes of aggregates in all class sizes. The asphalt binder contents were estimated from specific surface area calculations (Kandhal et al. 1997; Christensen 2001). The computational details are provided in Appendix B. The air void content was estimated based on the results of a study by Khedaywi and White (1994) and the measurements made on trial specimens prepared in the laboratory as part of this study. Table 3-5 provides the volume percentages occupied by the aggregates, air voids, and asphalt binder, along with the total volume of the coarser and finer mixtures. The heights of the coarser and finer portions, which are also provided in Table 3-5, were obtained using the ratio of the volume of each portion to the total volume of the specimen. The height of the coarser mixture was computed as follows:

**Table 3-4. Calculation of the ratio of the volume of the specimen occupied by the aggregates where $n_i$ is the number of aggregates in various class sizes**

| Class Size (mm) | Homogeneous | | Coarser | | Finer | |
|---|---|---|---|---|---|---|
| | $n_i$ | Volume (mm³) | $n_i$ | Volume (mm³) | $n_i$ | Volume (mm³) |
| 19-12.5 | 112 | 229668 | 84 | 172251 | 28 | 57417 |
| 12.5-9.5 | 192 | 133973 | 144 | 10048 | 48 | 33493 |
| 9.5-4.74 | 905 | 171294 | 678 | 128470 | 226 | 42824 |
| 4.75-2.36 | 5695 | 133973 | 1424 | 33493 | 4271 | 10048 |
| 2.36-1.18 | 25708 | 74642 | 6427 | 18661 | 19281 | 55982 |
| 1.18-0.6 | 171105 | 63159 | 42776 | 15790 | 128329 | 47370 |
| 0.6-0.3 | 1103101 | 52632 | 275775 | 13158 | 827326 | 39474 |
| 0.3-0.15 | 4973981 | 29665 | 1243495 | 7416 | 3730486 | 22249 |
| 0.15-0.075 | 28239378 | 21053 | 7059845 | 5263 | 21179534 | 15790 |
| <0.075 | 212276689 | 46891 | 53069172 | 11723 | 159207517 | 35168 |
| Total | 246796866 | 956949 | 61699821 | 506704 | 185097045 | 450244 |
| Packing Fraction ($P_v$) | | 0.812 | | 0.430 | | 0.382 |

$$\frac{V_c}{V_s} = \frac{\pi R_s^2 H_c}{\pi R_s^2 H_s} = 0.528 \qquad (3\text{-}15)$$

where $V_c$ is the volume of the coarser mixture, $V_s$ is the volume of the specimen, $R_s$ is the radius of the specimen, $H_c$ is the height of the coarser mixture, and $H_s$ is the height of the specimen. Removing the like terms and rearranging yields:

$$H_c = 0.528 H_s \qquad (3\text{-}16)$$

Substituting for $H_s$, which is 150 mm, determined the height of the coarse mixture:

$$H_c = 79.2 mm \qquad (3\text{-}17)$$

Subtracting the height of the coarser mixture from the total height of the specimen yielded the height of the finer mixture, $H_f$, which is 70.8 mm. Therefore, in simulating a two-layer vertically inhomogeneous specimen, the separation line between the two gradations was located at a height of 79.2 mm from the bottom of the specimen.

**Table 3-5. Percent volume of the specimen occupied by the mixture components**

| Mixtures | Percent Aggregates | Percent Air Void | Percent Asphalt Binder | Percent Volume | Height (mm) |
|---|---|---|---|---|---|
| Coarser | 43.0 | 5.5 | 4.3 | 52.8 | 79.2 |
| Finer | 38.2 | 1.5 | 7.5 | 47.2 | 70.8 |
| Homogeneous | 81.2 | 7.0 | 11.8 | 100 | 150 |

### 3.3.1.4   *Positioning the Particles*

In a homogeneous specimen, each particle has an equal chance of being in any portion of the specimen. On the other hand, in specimens with two-layer vertical inhomogeneity, the large particles have a higher probability of being located in the bottom portion and the smaller particles have a higher probability of being located in the top portion of a specimen.

In simulating homogeneous specimens, the coarse particles were placed first, with the same probability of being at any point of the specimen. Fine particles were then randomly positioned to fill up the empty spaces between the coarse particles.

In simulating abrupt inhomogeneity, coarse particles were placed first. Coarse particles could reside anywhere in the specimen but had a 75% probability of being within 79.2 mm from the bottom and a 25% probability of being within 70.8 mm from the top of the bottom layer. The fine particles were then placed in the spaces that were available between the coarse particles with a 25% probability of being within 79.2 mm from the bottom of the specimen and a 75% probability of being within 70.8 mm from the top of the bottom layer.

To place particles of the coarser and finer gradations in the bottom and in the top portions of a specimen, a series of transformation curves were used to transform a random number between 0 and 1 to the vertical, radial, and angular coordinates of a random position. Equations (3-5) and (3-6) made placement of particles of the coarser and finer gradations possible anywhere along a radius of the specimen and at any angular position between 0° and 360°.

In developing the transformation curves for the vertical positioning of the particles, two conditions were satisfied. First, the particles were allowed to occupy any vertical position, with different probabilities associated to each layer of the specimen. Second, the aggregates were not forced to reside entirely within the boundary of the two mixtures and as much as half of the volume of each particle was allowed to reside in the adjacent mixture. These were intended to mimic the condition in a laboratory compacted specimen. In the laboratory coarser and finer gradations were placed in different lifts into the gyratory mold and the compaction process blended the two gradations in the vicinity of the borderline between the two layers. Therefore, a clear separation line between the gradations was not enforced in the simulated specimens, as seen in the laboratory.

Considering the two conditions above, a second-order transformation curve was used to convert the uniform random numbers associated with the coarse aggregates to a random location along the height of the specimen in such a way that 25% of the particles were located in the top 47.2% and 75% were located in the bottom 52.8% of the specimen volume. Likewise, a second-order transformation curve was used to convert the uniform random numbers associated with fine particles to a location along the height of the specimen in such a way that 75% of the particles were placed in the top 47.2% and

25% were placed in the bottom 52.8% of the volume of the specimen. Table 3-6 provides the transformation equations for determining the location of particles with respect to the height of the specimen. Figure 3-5 shows the plot of the transformation curves for positioning of the coarse and the fine particles in homogeneous and inhomogeneous specimens. The detailed derivation of Equations (3-18) through (3-20) is provided in Appendix C.

### 3.3.2    Gradual Vertical Inhomogeneity

Simulated specimens are separated into three layers to reflect gradual inhomogeneity, with the coarse particles near the bottom and the fine particles near the top of the specimen. The design gradation is used to form three distinct gradations, one for each layer. To simulate gradual vertical inhomogeneity, the gradations of the layers, the number of particles in each layer, the volume of the layers, and the position of the particles within each layer were determined.

#### 3.3.2.1    *Gradation of the Layers*

The design gradation of the homogeneous specimens was used to create the coarse, fine, and the average gradations that were placed in the bottom, top, and the middle layers of a gradual vertically inhomogeneous specimen, respectively. The procedure included the separation of the original gradation into the very coarse and very fine gradations, followed by blending of various percentages of very coarse and the very fine gradations to create the gradations of the three layers.

**Table 3-6. Transformation equations for assigning a vertical position ($h_i$) to the particles in a homogeneous and in an abrupt two-layered vertically inhomogeneous specimen**

| Particles | Transformation Equation | Equation Number |
|---|---|---|
| Homogeneous | $h_i = (150 - d_i)u_i + {d_i}/{2}$ | (3-18) |
| Inhomogeneous (Coarse Particles) | $h_i = (177.6 - 1.33d_i)u_i^2 - (27.6 - 0.33d_i)u_i + d_i/2$ | (3-19) |
| Inhomogeneous (Fine Particles) | $h_i = (-222.4 + 1.33d_i)u_i^2 + (372.4 - 2.33d_i)u_i + d_i/2$ | (3-20) |

To separate the design gradation into very coarse and very fine gradations, the procedure in Section 3.3.1.1 was followed. Varying proportions of the very coarse and very fine gradations were used to create the gradations for the three layers. Table 3-7 provides the percentages of the very coarse and very fine gradations that were blended to create the gradations of the three layers. The coarse gradation that was used in the bottom portion of the specimen was made by blending 15% from the very fine and 52% from the
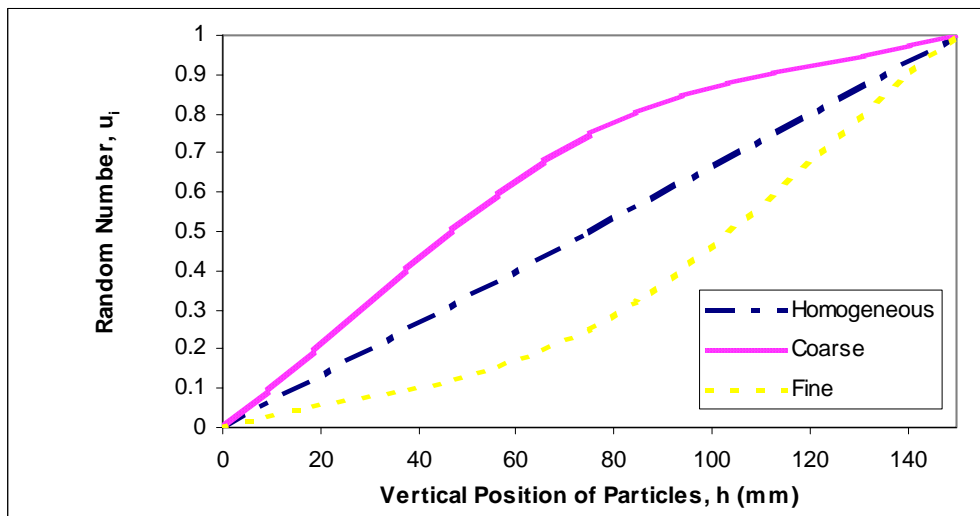


**Figure 3-5. Transformation curves for vertical positioning of particles in a homogeneous and in an abrupt two-layered vertically inhomogeneous specimen**

**Table 3-7. Percentages of the very coarse and the very fine gradations to make gradations of the layers in a three-layer vertically inhomogeneous specimen**

| Layer | Percent of Gradations | |
|---|---|---|
| | Very Fine | Very Coarse |
| Top (fine) | 52 | 15 |
| Middle (average) | 33 | 33 |
| Bottom (bottom) | 15 | 52 |

very coarse gradation. To create the fine gradation for the top portion of the specimen, 52% from the very fine was blended with 15% from the very coarse gradation. The average gradation for the middle layer was made by blending of 33% from the very fine and 33% from the very coarse gradations, which resulted in the same gradation as the design gradation. The selection of the percentage blends was based on creating the maximum difference between the three gradations that ensured detection of the created inhomogeneity using the suggested indices, and at the same time, not creating too coarse a mixture at the bottom that is not realistic in preparation of actual specimens. The coarse, fine, and the average gradations are provided in Table 3-8.

### 3.3.2.2    Number of Particles in the Layers

The number of particles in each of the three mixtures is required to compute the volume of the mixtures. The number of particles in the bottom, middle, and the top layers was obtained by applying the percentages of Table 3-7 to the number of aggregates in the very coarse and very fine gradations. Table 3-9 provides the computed number of aggregates in the design gradation and in each layer of the gradual vertically inhomogeneous specimen. The numbers in Column 5 (design gradation) that are above sieve #4 represent the number of aggregates in a very coarse gradation and the numbers

**Table 3-8. The design, coarse, fine, and average gradations for three-layer vertically inhomogeneous specimens**

| Sieve Size (mm) | % Passing | | | |
|---|---|---|---|---|
| | Design Aggregate Gradation | Coarse Aggregate Gradations | Fine Aggregates Gradation | Average Aggregates Gradation |
| 19 | 100.0 | 100.0 | 100.0 | 100.0 |
| 12.5 | 76.0 | 62.9 | 88.5 | 76.0 |
| 9.5 | 62.0 | 41.3 | 81.8 | 62.0 |
| 4.75 | 44.1 | 13.6 | 73.2 | 44.1 |
| 2.36 | 30.1 | 9.3 | 50.0 | 30.1 |
| 1.18 | 22.3 | 6.9 | 37.0 | 22.3 |
| 0.6 | 15.7 | 4.9 | 26.1 | 15.7 |
| 0.3 | 10.2 | 3.2 | 17.0 | 10.2 |
| 0.15 | 7.1 | 2.2 | 11.8 | 7.1 |
| 0.075 | 4.9 | 1.5 | 8.1 | 4.9 |

in Column 5 that are below sieve #4 represent the number of aggregates in the very fine gradation. The numbers in the coarse gradation (Column 2) were obtained by multiplying the number of particles in the very coarse gradation by 0.52 and in the very fine gradation by 0.15. The numbers in the fine gradation (Column 3) were obtained by multiplying the number of particles in the very coarse gradation by 0.15 and in the very fine gradation by 0.52. The number of aggregates in the average gradation (Column 4) was obtained by multiplying the aggregate numbers in the design gradation, both above and below the #4 sieve, by 0.33.

### 3.3.2.3 *Volume of the Layers*

To position the particles in the appropriate portion of the specimen, the volume of each layer was determined. The volumes of the layers were computed using the volume of the aggregates, volume of the air voids, and volume of the asphalt binder in each layer. The volume of aggregates in each portion was determined by summing the volume of the individual particles in that portion. Table 3-10 shows the calculation of the volume of

**Table 3-9. Number of particles in a three-layer vertically inhomogeneous specimen**

| (1) Class Size (mm) | (2) Coarse Gradation (Lower Portion) | (3) Fine Gradation (Upper Portion) | (4) Average Gradation (Middle Portion) | (5) Design Gradation (Homogeneous Specimens) |
|---|---|---|---|---|
| 19-12.5 | 58 | 17 | 37 | 112 |
| 12.5-9.5 | 100 | 29 | 63 | 192 |
| 9.4-4.74 | 470 | 136 | 298 | 905 |
| 4.75-2.36 | 854 | 2961 | 1879 | 5695 |

aggregates in a homogeneous specimen and the volume of aggregates in the three layers of a vertically inhomogeneous specimen. The volume of each particle was computed based on the assumption that the particles were spherical. To compute the volume of the aggregates in each class size, the number of particles was multiplied by the average volume of an individual particle in that class size. The total volume of the aggregates equaled sum of the volumes of the aggregates in all class sizes.

The asphalt binder contents were estimated from the specific surface area calculations (Kandhal et al., 1997; Christensen, 2001). The air void content was estimated based on the results of a study by Khedaywi and White (1994) and the air void measurements made on the trial specimens prepared in the laboratory. Table 3-11 provides the estimated volume percentages occupied by the aggregates, air voids, and asphalt binder, as well as the estimated volume percentages of the total volume of the specimen that is occupied by the three mixtures. The heights of the coarse and fine portions, which are also provided in Table 3-11, were obtained using the ratio of the

**Table 3-10. Calculation of the ratio of the volume of each layer of a three-layer vertically inhomogeneous specimen occupied by the aggregates where $n_i$ is the number of aggregates in various class sizes**

| Class size (mm) | Coarse | | Fine | | Average | |
|---|---|---|---|---|---|---|
| | $n_i$ | Volume (mm³) | $n_i$ | Volume (mm³) | $n_i$ | Volume (mm³) |
| 19-12.5 | 58 | 119427 | 17 | 34450 | 37 | 75790 |
| 12.5-9.5 | 100 | 69666 | 29 | 20096 | 63 | 44211 |
| 9.5-4.74 | 470 | 89073 | 136 | 25694 | 298 | 56527 |
| 4.75-2.36 | 854 | 20096 | 2961 | 69666 | 1879 | 44211 |
| 2.36-1.18 | 3856 | 11196 | 13368 | 38814 | 8484 | 24632 |
| 1.18-0.6 | 25666 | 9474 | 88975 | 32842 | 56465 | 20842 |
| 0.6-0.3 | 165465 | 7895 | 573612 | 27369 | 364023 | 17369 |
| 0.3-0.15 | 746097 | 4450 | 2586470 | 15426 | 1641414 | 9790 |
| 0.15-0.075 | 4235907 | 3158 | 14684477 | 10947 | 9318995 | 6947 |
| <0.075 | 31841503 | 7034 | 110383878 | 24383 | 70051307 | 15474 |
| Total | 37019977 | 341468 | 128333923 | 299688 | 81442966 | 315793 |
| Packing Fraction ($P_v$) | | 0.290 | | 0.254 | | 0.268 |

volume of each portion to the total volume of the specimen. The height of the coarse mixture was computed as follows:

$$\frac{V_c}{V_s} = \frac{\pi R_s{}^2 H_c}{\pi R_s{}^2 H_s} = 0.345 \tag{3-21}$$

where $V_c$ is the volume of the coarse mixture, $V_s$ is the volume of the specimen, $R_s$ is the radius of the specimen, $H_c$ is the height of the coarse mixture, and $H_s$ is the height of the specimen. Removing the like terms and rearranging yields:

$$H_c = 0.345 H_s \tag{3-22}$$

The height of the coarse mixture is determined by substituting for $H_s$, which is 150 mm:

$$H_c = 51.7mm \tag{3-23}$$

Similarly the height of the average and fine gradations were computed as 49.6 mm and 48.7 mm, respectively. Therefore in simulating a three-layer vertically inhomogeneous

**Table 3-11. Percent volume of the homogeneous specimen and each portion of three-layer vertically inhomogeneous specimen occupied by the mixture components (Columns 2, 3, 4), percent volume of the specimen occupied by each layer (Column 5), and height of each layer of three-layer vertically inhomogeneous specimen (Column 6)**

| (1) Mixtures | (2) Aggregates | (3) Air Void | (4) Asphalt Binder | (5) Percent Volume | (6) Height (mm) |
|---|---|---|---|---|---|
| Coarse | 29.0 | 3.50 | 1.96 | 34.5 | 51.7 |
| Average | 26.8 | 2.33 | 3.90 | 33.0 | 49.6 |
| Fine | 25.4 | 1.17 | 5.91 | 32.5 | 48.7 |
| Homogeneous | 81.2 | 7.0 | 11.8 | 100 | 150 |

specimen, the separation lines between the three gradations were located at the heights of 51.7 mm and 101.3 mm from the bottom of the specimen.

### 3.3.2.4   Positioning the Particles

In simulating the homogeneous specimens, each particle has an equal chance of being at any point of the specimen. The coarse particles were placed first and the fine particles were randomly positioned to fill up the empty spaces between the coarse particles. In simulating gradual inhomogeneity, the coarse particles were placed first. While coarse particles were positioned throughout the specimen, they had a higher probability of being located in the bottom portion than in the middle or upper portions. The coarse particles had a 52% probability of being within 51.7 mm from the bottom, 33% probability of being within 49.6 mm from the top of the bottom layer, and 15% probability of being within 48.7 mm from the top of the middle layer. The fine particles were then placed in the spaces that were available between the coarse particles with a 15% probability of being within 51.7 mm from the bottom, a 33% probability of being

within 49.6 mm from the top of the bottom layer, and 52% probability of being within 48.7 mm from the top of the middle layer.

In order to place the particles of the coarse, average, and fine gradations in the three portions of a specimen, a series of transformation curves were used to transform three random numbers between 0 and 1 to the vertical, radial, and angular coordinates of a random position. Equations (3-5) and (3-6) were used to place the particles along a radius and at any angular position within the specimen.

In developing the transformation curves for the vertical positioning of the particles, two conditions were satisfied. First, particles were allowed to occupy any vertical position, with different probabilities associated with the various portions of the specimen. Second, the aggregates were not forced to reside entirely within the boundaries of the three mixtures and as much as half of the volume of each particle was allowed to reside in the adjacent mixture. These were intended to mimic the condition in the laboratory compacted specimen, where a defined borderline between the three gradations would not be expected. Therefore, clear separation lines between the gradations were not enforced in the simulated specimens, as in the laboratory.

Considering the two conditions above, a second-order transformation curve was used to convert the uniform random numbers associated with the coarse aggregates to a random location along the height of the specimen in such a way that 15% of the particles locate in the top 32.5%, 33% of the particles locate in the middle 33%, and 52% locate in the bottom 34.5% of the specimen volume. Likewise, a second-order transformation curve was used to convert the random numbers associated with the fine aggregates to a random location along the height of the specimen in such a way that 52% of the particles

were placed in the top 32.5%, 33% of the particles were placed in the middle 33%, and

15% were placed in the bottom 34.5% of the specimen volume. Figure 3-6 shows the plot

of the transformation curves for positioning the coarse and fine particles in homogeneous

and inhomogeneous specimens. Table 3-12 provides the transformation equations for

determining the location of the particles along the height of the three-layer vertically

inhomogeneous specimen. A detailed derivation of Equations (3-24) through (3-26) is

provided in Appendix C.

## 3.4 COMPUTER DEVELOPMENT OF RADIAL INHOMOGENEITY

A radially inhomogeneous specimen is defined as a specimen that has changes in

gradation in the lateral extent; however, the total gradation of the specimen is the same as

that of a homogeneous specimen. Comparable to the preparation of the shear test

specimens in the laboratory, the simulated specimens were made 150-mm in diameter by
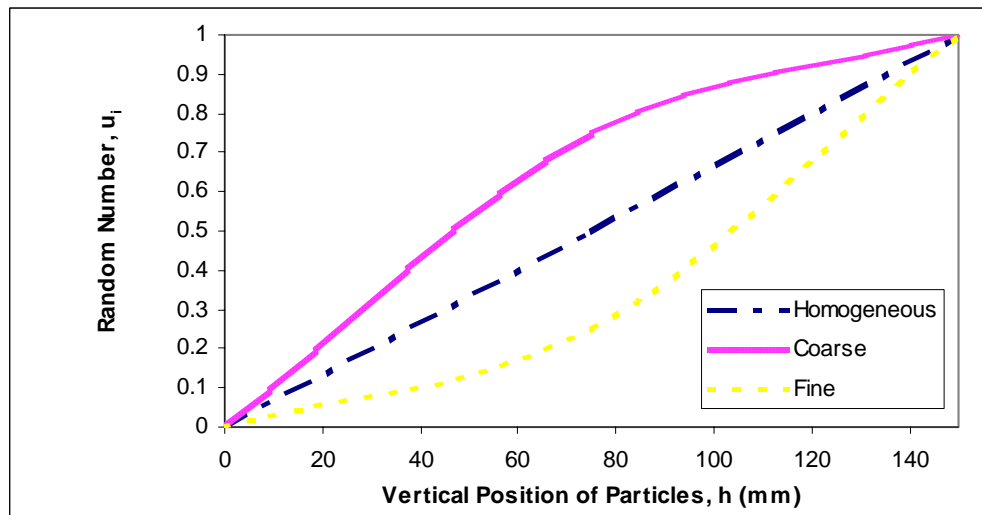


**Figure 3-6. Transformation curves for vertical positioning of particles in a homogeneous and in a gradual three-layer vertically inhomogeneous specimen**

**Table 3-12. Transformation equations for assigning a vertical position ($h_i$) to the particles in a homogeneous and in a gradual three-layer vertically inhomogeneous specimen**

| Particles | Transformation Equation | Equation Number |
|---|---|---|
| Homogeneous | $$h_i = (150 - d_i)u_i + \frac{d_i}{2}$$ | (3-24) |
| Inhomogeneous (Coarse Particles) | $$h_i = (2.75d_i)u_i^2 + (150.0 - 3.75d_i)u_i + \frac{d_i}{2}$$ | (3-25) |
| Inhomogeneous (Fine Particles) | $$h_i = (-2.75d_i)u_i^2 + (150 + 1.75d_i)u_i + \frac{d_i}{2}$$ | (3-26) |

100-mm in height and then cut in half along the height of the specimen to provide two 150-mm diameter by 50-mm thick cylindrical disks for homogeneity testing.

Radial inhomogeneity was created in two layers: a core and a ring. The specimens are inhomogeneously coarser near the periphery of the specimen. Similar to the simulation of the abrupt two-layer vertical inhomogeneity, simulation of two-layered radial inhomogeneity involved four steps: First, from the design gradation a coarser and a finer gradation were created. Second, the number of particles in each class size of each gradation was determined. Third, the volumes of the two gradations were computed. Fourth, the particles were assigned to the positions within each volume.

### 3.4.1 Gradation of the Mixtures

A coarser and a finer gradation that were assigned to two radial portions of the specimen were the same as the coarser and the finer gradations that were introduced in Section 3.3.1.1 for making of vertical inhomogeneity. The coarser and the finer gradations were placed at the periphery and the core of the specimen, respectively, to mimic the effect of gyration on the mixtures compacted in Superpave gyratory compactor and also to mimic the effect of a boundary condition imposed by the gyratory mold.

Mixing the coarser and finer gradations would result in the design gradation of the homogeneous specimen. As explained earlier, the selection of the two gradations was based on creating a high level of inhomogeneity that was detectable by both the inhomogeneity and mechanical testing, and at the same time creating a manageable specimen that did not crumble in the process of preparation and testing.

### 3.4.2   Number of Particles

The number of particles of the coarser and finer gradations was determined by blending the required percentages of the aggregate numbers from the very coarse and the very fine gradations. Table 3-13 provides the number of particles in the core and the ring of the radially inhomogeneous specimen having a 150-mm diameter and a 100-mm height. The numbers in Column 4 (design gradation) that are above sieve #4 represent the number of aggregates in very coarse gradation and the numbers in Column 4 that are below sieve #4 represent the number of aggregates in very fine gradation. Multiplying the number of particles in very coarse gradation by 0.75 and the number of particles in very fine gradation by 0.25 provided the number of aggregates in the coarser gradation (Column 2). Multiplying the number of particles in very coarse gradation by 0.25 and the number of particles in very fine gradation by 0.75 provided the number of aggregates in the finer gradation (Column 3).

### 3.4.3   Volume of the Mixtures

The volumes of the core and the ring were determined from the percent volume of the specimen that was occupied by the aggregates, asphalt binder, and the air voids. The volume of the aggregates in the ring and the core portions were determined by

**Table 3-13. Number of particles in the core and ring of a radially inhomogeneous specimen**

| (1)<br>Class Size (mm) | (2)<br>Coarser Gradation (Ring) | (3)<br>Finer Gradation (Core) | (4)<br>Design Gradation (Homogeneous Specimen) |
|---|---|---|---|
| 19-12.5 | 126 | 42 | 168 |
| 12.5-9.5 | 216 | 72 | 288 |
| 9.4-4.74 | 1018 | 339 | 1357 |
| 4.75-2.36 | 2136 | 6407 | 8543 |

summing the volumes of the individual particles in each portion. Table 3-14 provides total volumes of particles in the coarser and finer portions. It is noticeable that the volume percentage of the aggregates in the ring and the core are the same as in the bottom and top portions of the vertically inhomogeneous specimens. Using the same percent air void and the same binder content as provided in Table 3-5 resulted in the same total volume proportions of the coarser and finer mixtures as of the vertical inhomogeneity, which are provided in Table 3-15. Using the ratio of the volume of the finer gradation in the core to the total volume of the specimen, the diameter of the core and the thickness of the ring were determined:

$$\frac{V_c}{V_s} = \frac{\pi R_c^2 H_s}{\pi R_s^2 H_s} = 0.472 \qquad (3\text{-}27)$$

where $V_c$ is the volume of the core, $V_s$ is the volume of the specimen, $R_c$ is the radius of the core, $R_s$ is the radius of the specimen, and $H_s$ is the height of the specimen. Removing the like terms and rearranging yields:

$$R_c = 0.687 R_s \qquad (3\text{-}28)$$

Substituting for $R_s$, which is 75 mm, the radius of the core mixture was determined:

**Table 3-14. Calculation of the percent volume of a radially inhomogeneous specimen occupied by the aggregates**

| Class Size (mm) | Homogeneous | | Coarser | | Finer | |
|---|---|---|---|---|---|---|
| | $n_i$ | Volume (mm³) | $n_i$ | Volume (mm³) | $n_i$ | Volume (mm³) |
| 19-12.5 | 168 | 344502 | 126 | 258376 | 42 | 86125 |
| 12.5-9.5 | 288 | 200959 | 216 | 150719 | 72 | 50240 |
| 9.5-4.74 | 1357 | 256941 | 1018 | 192706 | 339 | 64235 |
| 4.75-2.36 | 8543 | 200959 | 2136 | 50240 | 6407 | 150719 |
| 2.36-1.18 | 38562 | 111963 | 9640 | 27991 | 28921 | 83972 |
| 1.18-0.6 | 256658 | 94738 | 64165 | 23684 | 192494 | 71053 |
| 0.6-0.3 | 1654651 | 78948 | 413663 | 19737 | 1240988 | 59211 |
| 0.3-0.15 | 7460972 | 44498 | 1865243 | 11125 | 5595729 | 33374 |
| 0.15-0.075 | 42359067 | 31579 | 10589767 | 7895 | 31769300 | 23684 |
| <0.075 | 318415033 | 70336 | 79603758 | 17584 | 238811275 | 52752 |
| Total | 370195300 | 1435423 | 277645568 | 675367 | 92549732 | 760056 |
| Packing Fraction ($P_v$) | | 0.812 | | 0.382 | | 0.430 |

$$R_c = 51.5mm \qquad (3\text{-}29)$$

Subtracting the radius of the core mixture from the radius of the specimen yielded the thickness of the ring mixture, $T_r$, which is 23.5 mm. Therefore in simulating the radial inhomogeneity, the separation line between the two gradations was located at a radius of 51.5 mm from the center of the specimen. The radius of the core and the thickness of the ring that were computed based on the percent volume of the specimen occupied by the coarser and finer mixtures are also provided in Table 3-15.

### 3.4.4 Positioning the Particles

In a homogeneous specimen, each particle has an equal chance of being in the ring or in the core of the specimen. In a radially inhomogeneous specimen, the coarse particles have a higher probability of being located in the ring portion and the fine

**Table 3-15. Percent volume of a specimen occupied by mixture components**

| Mixtures | Percent Aggregates | Percent Air Void | Percent Asphalt Binder | Percent Volume | Radius /Width (mm) |
|---|---|---|---|---|---|
| Coarser (Ring) | 43.0 | 5.5 | 4.3 | 52.8 | 23.5 |
| Finer (core) | 38.2 | 1.5 | 7.5 | 47.2 | 51.5 |
| Homogeneous | 81.2 | 7.0 | 11.8 | 100 | 75 |

particles had a higher probability of being located in the core of the specimen. The coarse particles were placed first with a 75% probability of being in the ring and a 25% probability of being in the core. The fine particles were then placed in the spaces available between the coarse particles with a 75% probability of being in the core and a 25% probability of being in the ring portions of the specimen.

In order to place the particles of the finer and the coarser gradations in the core and the ring of a specimen, a series of transformation curves were used to transform three random numbers between 0 and 1 to the vertical, radial, and angular coordinate of a random position. Equations (3-6) and (3-7) made possible placement of the particles of the finer and the coarser gradations anywhere along the height of the specimen and at any angular position between 0 and 360°.

In developing the transformation curves for radial positioning of the particles, two conditions were satisfied. First, the particles were allowed to occupy any radial position, with different probabilities associated with the two radial portions. Second, the aggregates were not forced to reside entirely within the boundary of the two mixtures and as much as half of the volume of each particle was allowed to reside in the adjacent mixture. These were intended to mimic the condition in the laboratory compacted

specimen. While the coarser and the finer gradations were placed in different positions of the gyratory mold, the compaction process in the laboratory blended the two gradations in the vicinity of the borderline between the two radial layers. Therefore, a clear separation line between the gradations was not enforced in the simulated specimens as occurs in the laboratory.

Considering the two conditions above, a second-order transformation curve was used to convert the uniform random numbers associated with the coarse aggregates to a random location along a radius of the specimen in such a way that 25% of the particles were located in the core portion of the specimen and 75% were located in the ring portion of the specimen. Likewise, a second-order transformation curve was used to convert the uniform random numbers associated with the fine particles to a random location along the radius of the specimen in such a way that 75% of the particles were placed in the core portion and 25% were placed in the ring portion of the specimen. Figure 3-7 shows the plot of the transformation curves for positioning the coarse and fine particles in
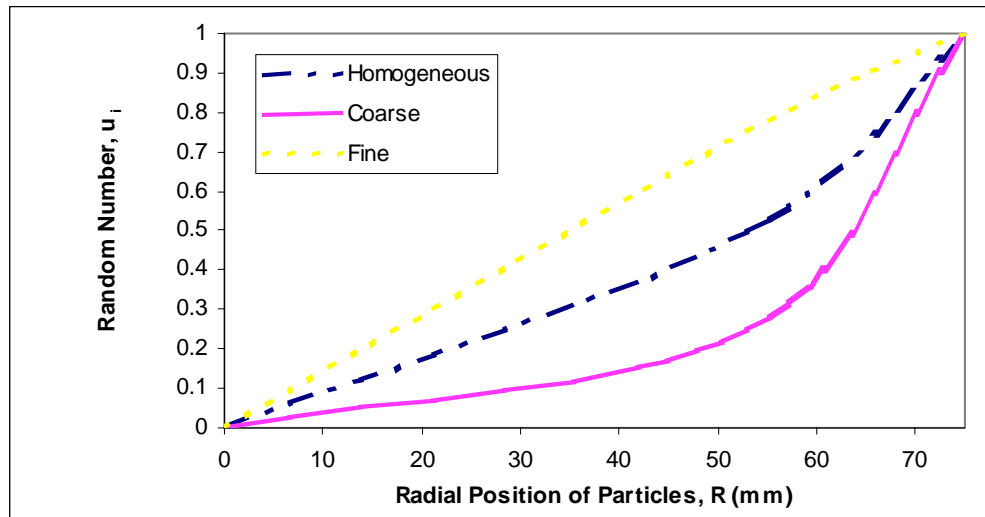


**Figure 3-7. Transformation curves for radial positioning of particles in a homogeneous and in a two-layered radially inhomogeneous specimen**

homogeneous and radially inhomogeneous specimens. Table 3-16 provides the

transformation equations for determining the location of the particles along the radius of

the specimen. The detailed derivation of Equations (3-30) through (3-32) is provided in

Appendix C.

**Table 3-16. Transformation equations for assigning a radial position ($r_i$) to the particles in a homogeneous and in a radially inhomogeneous specimen**

| Particles | Transformation Equation | Equation Number |
|---|---|---|
| Homogeneous | $r_i = (75 - \frac{d_i}{2})u_i$ | (3-30) |
| Inhomogeneous (Coarse Particles) | $r_i = (-174.64 - 0.67d_i)u_i^2 + (249.67 + 0.17d_i)u_i$ | (3-31) |
| Inhomogeneous (Fine Particles) | $r_i = (25.33 - 2d_i)u_i^2 + (49.67 + 1.5d_i)u_i$ | (3-32) |

# CHAPTER 4 - DEVELOPMENT OF INDICES OF VERTICAL HOMOGENEITY

## 4.1 INTRODUCTION

To test simulated and actual specimens for vertical homogeneity, several statistical tests are being introduced. The statistical tests involve the six steps of hypothesis testing. The basis of a hypothesis test is the comparison of the sample value of the test statistic with the population value for the condition of complete homogeneity. This requires knowledge of the distributions of the test statistic for conditions of both homogeneity and inhomogeneity. Although, some statistical tests were derived from standard tests, such as chi-square, t, and z tests, their distributions differ from those of the standard tests. This is because the properties that are being tested (geometric properties of the aggregates) are not the same as the properties on which the statistical tests were developed. Therefore, the distributions need to be identified either analytically or by simulation before decisions can be made with the homogeneity tests.

The first step in hypothesis testing is to formulate the null hypothesis and two or more hypotheses that reflect the alternative lines of action. The null and the alternative hypotheses are formulated based on the differences between specific properties of the aggregates in different portions of the specimens or the differences between specific properties of the specimens with the expected values of the same properties for the state of homogeneity. The null hypothesis always reflects homogeneity while the alternative hypothesis reflects inhomogeneity:

$H_o$ : *The specimen is homogeneous.* (4-1)

$H_A$ : *The specimen is inhomogeneous.* (4-2)

104

The second step of a hypothesis test is to identify the method of computing a value of the test statistic and its distribution. The test statistic should distinguish between the conditions of homogeneity and inhomogeneity.

The third step is to specify the level of significance. It is necessary to select a level of significance that is appropriate for the physical property that is being tested. The level of significance is an indicator of the probability of a certain type of statistical error, namely the probability of rejecting the null hypothesis when, in fact, it is true.

The fourth step of a hypothesis test involves collecting a sample of data and computing an estimate of the test statistic. The collected data include the geometric properties such as the area, frequency, and location of the aggregates that are measured from various slice faces. Using the collected data, the sample value of the test statistic for a specimen is computed.

In the fifth step, the region of rejection of the test statistic is defined, whether in the lower, in the upper, or in both tails of the distribution function. The region of rejection, in one tail or two tails and in the lower tail or upper tail, is based on the knowledge on the expected locations of the coarser and the finer gradations.

The decision to accept or reject the null hypothesis is made in the sixth step when the sample value of the test statistic is compared with the critical value of the test statistic. If the null hypothesis is rejected, then inhomogeneity is assumed.

Vertical inhomogeneity can be either abrupt or gradual. For abrupt inhomogeneity, the changes occur over a relatively short length while for gradual inhomogeneity the changes occur gradually over a longer length through the height of a specimen. Therefore, vertical inhomogeneity is assumed to occur in either two or

three-layers, with the two-layer analyses used to test for abrupt inhomogeneity and three-layer analyses used to test for gradual inhomogeneity. Two separate sets of indices were defined for abrupt and gradual forms of vertical inhomogeneity (Sections 4.3 and 4.4). In addition, a third set of indices was described that can be used to measure both forms of abrupt and gradual vertical inhomogeneity (Section 4.5). It is important to identify the test statistic that is specific to the form of vertical inhomogeneity that the user suspects being present.

The tests are also described for horizontal or vertical slice faces. Several of the tests are defined for both vertical and horizontal slice faces, while others are specific to only one slice face direction. For example, the chi-square test is defined for both slice face directions, while the Spearman-Conley test is defined specifically for horizontal slice faces.

The size of the specimens for testing vertical homogeneity is 100 mm in diameter and 150 mm in height, which is the size requirement for the axial compression testing of asphalt mixture specimens. Use of 100-mm tall specimens allows the evaluation of vertical homogeneity of the specimens as they are compacted in the Superpave gyratory compactor. In addition, the specimens can be tested in compression and the measured compressive properties can be correlated with the computed vertical homogeneity indices.

## 4.2  TWO-LAYER VERTICAL INHOMOGENEITY: HORIZONTAL SLICE FACES

A number of statistical tests are suggested for the detection and measurement of two-layer vertical inhomogeneity using horizontal slice faces. The suggested tests are

adopted from the chi-square and the two sample t-tests. The tests include the chi-square test on aggregate frequencies and the t-test on total aggregate areas, aggregate frequencies, and mean nearest neighbor distances. The test statistics are computed based on comparison of the geometric properties of coarse aggregates in the lower and the upper portions of the specimens. The statistical tests examine the significance of the difference between the aggregate properties in the two portions.

### 4.2.1 Selection of Specimen Sampling

Application of the statistical tests requires specifying the slices of the specimen from which the measurements would be made. The level of vertical inhomogeneity that was created resulted in unequal volumes of the coarser and the finer mixtures. The volume of the coarser mixture was 1.125 times the volume of the finer mixture (Section 3.3.1.3). Thus, in a 150-mm high specimen, the coarser portion would have a height of 79.2 mm and the finer portion would have a height of 70.8 mm. However, to eliminate the bias in statistical sampling from the coarser and the finer gradations, an equal number of horizontal slices were sampled from the lower and the upper portions of the specimens.

The location and the number of the slices in the coarser and finer portions were determined with two considerations: First, the slices should be independent; second, the slices within each portion should be from the same population. To ensure independency of the slices, McCuen and Azari (2001) showed that 10-mm spacing was required between the slices. To ensure that the slices are from the same population, the top and bottom slices are located 15 mm away from the ends of the specimen to allow for large particles to be fully contained within the specimen. In addition, a 20 mm thick cylindrical

volume, between the lower and the upper sampling portions, was considered the

transition zone and the aggregates whose centers lied in that volume were disregarded.

The reason is that the process of compaction blends the two mixtures around the

borderline between the layers, which results in a gradation that does not distinctively

follow either the coarser or the finer gradation. By selecting the sampling portions away

from the blended mixture, the materials in each portion should follow a distinct statistical

population.

The number and location of the slices were then determined based on the above

factors. Six horizontal slices in the lower and six horizontal slices in the upper portions of

the specimen were made. The first bottom slice was taken 15 mm from the bottom of the

specimen. The other five slices were taken at 10-mm intervals starting from the first

bottom slice. The first top slice was taken 15 mm from the top of the specimen. The other

five slices were taken at 10-mm intervals below the first top slice (Figure 4-1).
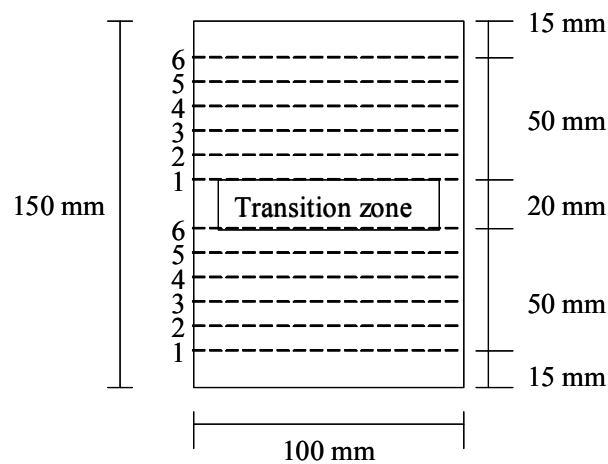


**Figure 4-1. Locations of the horizontal slice faces on a specimen to be evaluated for two-layer vertical inhomogeneity**

108

### 4.2.2 Computation of Parameters of Test Statistics

The computation of the test statistics requires measurement of geometric properties of coarse aggregates and computation of the selected statistical parameters. The steps of the procedure are as follows:

a.  The area of one horizontal slice face ($A_{hv}$) is computed as:

$$A_{hv} = 0.25\pi D_v^{\,2} \qquad\qquad (4\text{-}3)$$

where $D_v$ is the diameter of a horizontal slice face of a specimen evaluated for vertical homogeneity, which is 100 mm.

b.  The total area of six slice faces in the lower ($A_{hl}$) and upper ($A_{hl}$) portions are computed as:

$$A_{hl} = A_{hu} = 6A_{hv} \qquad\qquad (4\text{-}4)$$

c.  On each slice face that is located in the lower or the upper portion of the specimen, the frequency ($f_{hli}$, $f_{hui}$), the total area ($a_{hli}$, $a_{hui}$), and the mean nearest neighbor distance ($\overline{d}_{hli}$, $\overline{d}_{hui}$) of the coarse aggregates that have a diameter equal to or greater than 4.75 mm are measured. The nearest neighbor distance of each aggregate is the distance between each aggregate centroid and its nearest neighbor centroid.

d.  The coarse aggregate frequencies from the slice faces in the lower and the upper portions of the specimen are summed:

$$f_{hl} = \sum_{i=1}^{n_{hl}} f_{hli} \qquad\qquad (4\text{-}5)$$

$$f_{hu} = \sum_{i=1}^{n_{hu}} f_{hui} \qquad\qquad (4\text{-}6)$$

where $f_{hl}$ and $f_{hu}$ are the total coarse aggregate frequencies in the lower and the upper portions; $n_{hl}$ and $n_{hu}$ are the number of slice faces in the lower and the upper portions, which are six; and $f_{hli}$ and $f_{hui}$ are the aggregate frequencies in the $i^{th}$ horizontal slice face in the lower and the upper portions of the specimen, respectively (see Step c).

e.  The total frequency from the 12 slice faces is computed by:

$$f_{hv} = f_{hl} + f_{hu} \tag{4-7}$$

where $f_h$, $f_{hl}$, and $f_{hu}$ will be used in chi-square test (see Section 4.2.3.2).

f.  The means and standard deviations of the aggregate frequencies observed on the six slice faces in the lower portion ($\overline{f}_l$, $s_{fl}$) and six slice faces in the upper portion ($\overline{f}_u$, $s_{fu}$) are computed as:

$$\overline{f}_l = \frac{1}{n_{hl}} \sum_{i=1}^{n_{hl}} f_{hli} \tag{4-8}$$

$$s_{fl} = \left[ \frac{1}{n_{hl}-1} \sum_{i=1}^{n_{hl}} (f_{hli} - \overline{f}_l)^2 \right]^{0.5} \tag{4-9}$$

$$\overline{f}_u = \frac{1}{n_{hu}} \sum_{i=1}^{n_{hu}} f_{hui} \tag{4-10}$$

$$s_{fu} = \left[ \frac{1}{n_{hu}-1} \sum_{i=1}^{n_{hu}} (f_{hui} - \overline{f}_u)^2 \right]^{0.5} \tag{4-11}$$

where $n_{hl}$ and $n_{hu}$ are the number of slice faces in the lower and the upper portions, which are six; and $f_{hli}$ and $f_{hui}$ are the aggregate frequencies in the $i^{th}$ horizontal slice face in the lower and the upper portions of the specimen, respectively (see

Step c). The computed means and standard deviations are used for the t-test on

frequencies (see Section 4.2.3.4).

g.  The total aggregate areas in the lower ($a_{hl}$) and the upper ($a_{hu}$) portions are

computed by:

$$a_{hl} = \sum_{i=1}^{n_{hl}} a_{hli} \qquad (4\text{-}12)$$

$$a_{hu} = \sum_{i=1}^{n_{hu}} a_{hui} \qquad (4\text{-}13)$$

where $n_{hl}$ and $n_{hu}$ are the number of slice faces in the lower and the upper portions,

which are six; $a_{hli}$ and $a_{hui}$ are the total aggregate areas in the $i^{th}$ slice face in the

lower and the upper portions of the specimen, respectively (see Step c).

h.  The mean and the standard deviation of the total aggregate areas on the slice faces

in the lower portion ($\overline{a}_l$, $s_{al}$) and in the upper portion ($\overline{a}_u$, $s_{au}$) of the specimen are

computed as:

$$\overline{a}_l = \frac{1}{n_{hl}} \sum_{i=1}^{n_{hl}} a_{hli} \qquad (4\text{-}14)$$

$$s_{al} = \left[ \frac{1}{n_{hl}-1} \sum_{i=1}^{n_{hl}} (a_{hli} - \overline{a}_l)^2 \right]^{0.5} \qquad (4\text{-}15)$$

$$\overline{a}_u = \frac{1}{n_{hu}} \sum_{i=1}^{n_{hu}} a_{hui} \qquad (4\text{-}16)$$

$$s_{au} = \left[ \frac{1}{n_{hu}-1} \sum_{i=1}^{n_{hu}} (a_{hui} - \overline{a}_u)^2 \right]^{0.5} \qquad (4\text{-}17)$$

where $n_{hl}$ and $n_{hu}$ are the number of slice faces in the lower and the upper portions,

which are six; $a_{hli}$ and $a_{hui}$ are the total aggregate areas in the $i^{th}$ slice face in the

lower and the upper portions of the specimen, respectively (see Step c), the computed means and standard deviations are used for the t-test on total areas (see Section 4.2.3.3).

i.  The mean and the standard deviation of the nearest neighbor distances in six slices in the lower ($\overline{d}_l$, $s_{dl}$) and six slices in the upper ($\overline{d}_u$, $s_{du}$) portions are computed as:

$$\overline{d}_l = \frac{1}{n_{hl}} \sum_{i=1}^{n_{hl}} \overline{d}_{hli} \tag{4-18}$$

$$s_{dl} = \left[ \frac{1}{n_{hl}-1} \sum_{i=1}^{n_{hl}} (\overline{d}_{hli} - \overline{d}_l)^2 \right]^{0.5} \tag{4-19}$$

$$\overline{d}_u = \frac{1}{n_{hu}} \sum_{i=1}^{n_{hu}} \overline{d}_{hui} \tag{4-20}$$

$$s_{du} = \left[ \frac{1}{n_{hu}-1} \sum_{i=1}^{n_{hu}} (\overline{d}_{hui} - \overline{d}_u)^2 \right]^{0.5} \tag{4-21}$$

where $\overline{d}_{hli}$ and $\overline{d}_{hui}$ were defined in Step c. The means and standard deviations on the mean nearest neighbor distances are used in the t-test on mean nearest neighbor distances (see Section 4.2.3.5).

## 4.2.3 Hypothesis Testing using Suggested Test Statistics

The six steps of hypothesis testing are followed in order to evaluate the homogeneity of a specimen. The following sections explain the steps for evaluation of two-layered vertical inhomogeneity using various statistical tests on horizontal slice faces.

### 4.2.3.1  Two-Sample chi-Square Test on Frequencies

The two-sample chi-square test on frequencies is used to measure the two-layer vertical inhomogeneity by comparing the frequencies of the aggregates in the coarser and the finer portions of the specimen with the expected frequency of a homogeneous specimen. It is hypothesized that the frequencies of the coarse particles in both the top and bottom portions of a vertically inhomogeneous specimen are significantly different from the expected frequency of the particles in a homogeneous specimens. The difference between this method and the t-test is that the chi-square test is indifferent to the direction of the coarser-to-finer gradation. Regardless of the location of the coarser and the finer gradations, the critical value is always in the upper tail of the distribution. The exceedance of the test statistic over the critical value will indicate that the aggregate frequencies of either top, bottom, or both portions of the specimen are different from the expected frequencies of the portions of a homogeneous specimen. However, from the value of the test statistic, it is not indicated whether the observed aggregate frequency is lower or higher than the expected frequency. The steps of a hypothesis test using the two-sample chi-square test as applied to the horizontal slice faces are as follows:

1. The following hypotheses for the aggregate frequency, which are implications of the hypotheses of Equations (4-1) and (4-2), are tested:

    $H_o$ : *The observed frequencies of the portions are equal to the mean frequency.*

    (4-22)

    $H_A$ : *The observed frequency of at least one portion is different from the mean*

    *frequency.*                                                                                      (4-23)

    A specimen is considered homogeneous if the null hypothesis is accepted.

2. To test the hypotheses in step 1, the chi-square test statistic, as the index of homogeneity of the specimen, is used:

$$\chi_{hv}^2 = \frac{(f_{hl} - f_{hv}r_{hl})^2}{f_{hv}r_{hl}(1 - r_{hl})} + \frac{(f_{hu} - f_{hv}r_{hu})^2}{f_{hv}r_{hu}(1 - r_{hu})} \qquad (4\text{-}24)$$

in which $\chi_{hv}^2$ is the index of homogeneity and is a random variable that has a $\chi^2$ distribution with the degree of freedom of $(N_l\text{-}1)$ where $N_l$ is the number of layers in specimens that are evaluated for two-layer vertical inhomogeneity, which is two; $f_{hl}, f_{hu}, f_{hv}$ are the coarse aggregate frequencies (Equations (4-5), (4-6), and (4-7), respectively); $r_{hl}$ and $r_{hu}$ are the ratios of the slice face areas in the lower and the upper portions to the slice face areas in both the lower and upper portions:

$$r_{hl} = r_{hu} = \frac{A_{hl}}{A_{hT}} = \frac{A_{hu}}{A_{hT}} = 0.5 \qquad (4\text{-}25)$$

where $A_{hl}$ is the total area of the six slice faces in the lower portion, $A_{hu}$ is total area of six slice faces in the upper portions, and $A_{hT}$ is the total area of the twelve slice faces.

3. The level of significance is selected. The selection of the level of significance should be based on the physical significance of homogeneity and the impact of rejecting the null hypothesis of Equation (4-22) on design and performance decisions.

4. The measured and computed data on the geometric properties of the coarse aggregates (Equations (4-5) through (4-7)) are used to compute an estimate of the test statistic of Equation (4-24).

5. The critical chi-square value ($\chi_{hv\alpha}^2$) is determined from the distribution of $\chi_{hv}^2$ statistic for the selected level of significance. For an inhomogeneous specimen the

differences between the observed aggregate frequencies and the expected

aggregate frequencies in the lower and upper portions are significant. Therefore,

the critical value would be represented by the upper tail of the distribution.

6.   The decision on homogeneity or inhomogeneity of a specimen depends on a

comparison of the computed value of the test statistic and the critical value. Any

chi-square value greater than the critical value suggests an inhomogeneous

specimen.

### *4.2.3.2   Two-Sample t-Test on Total Aggregate Areas*

The assessment of a difference in the total coarse aggregate area on horizontal

slice faces in the lower portion and upper portions of a specimen will indicate

inhomogeneity. The mean of coarse aggregate total areas on the slices in the coarser

portion is hypothesized to be greater than the mean of coarse aggregate total areas on the

slices in the finer portion of a specimen. A two-sample t-test is used to assess the

significance of the difference between the two means. The procedure for hypothesis

testing using a t-statistic of total coarse aggregate area is as follows:

1.   The following null hypothesis for the aggregate total area, which is an implication

of the null hypothesis of Equation (4-1), is tested:

$$H_o : \overline{A}_l = \overline{A}_u \qquad\qquad\qquad (4\text{-}26)$$

where $\overline{A}_l$ and $\overline{A}_u$ are the population values of the mean total coarse aggregate

areas from the slice faces in the lower and the upper portions, respectively. A

specimen is considered homogeneous if the null hypothesis is accepted. The

possible alternative hypotheses for the mean total aggregate areas are provided in

Table 4-1. In the case where the coarser gradation is expected at the bottom of the specimen, the alternative hypothesis of Equation (4-29) would be tested. If the coarser gradation were expected at the top of the specimen, the alternative hypothesis of Equation (4-30) would be tested. If the expected direction of the coarser-to-finer gradation were not known *a priori*, the alternative hypothesis of Equation (4-31) would then be used.

2.  The t statistic, which is the index of homogeneity of the specimen, is selected:

$$t_{av} = \frac{\bar{a}_l - \bar{a}_u}{s_{av}(\frac{1}{n_{hl}} + \frac{1}{n_{hu}})^{0.5}}$$

(4-27)

in which $t_{av}$ is the index of homogeneity and is a random variable that has a $t$ distribution with degrees of freedom of $(n_{hl} + n_{hu} - 2)$; $n_{hl}$ and $n_{hu}$ are the number of slice faces in the coarser and the finer gradations, respectively; $\bar{a}_l$ and $\bar{a}_u$ are the means of total aggregate areas (Equations (4-14) and (4-16)); and $s_{av}$ is the square root of the pooled variance given by:

$$s_{av}^2 = \frac{(n_{hl} - 1)s_{al}^2 + (n_{hu} - 1)s_{au}^2}{n_{hl} + n_{hu} - 2}$$

(4-28)

in which $s_{al}^2$ and $s_{au}^2$ are the variances of total area values in the lower and the upper portions (Equations (4-15) and (4-17)).

3.  The level of significance is selected. This selection should be based on the impact of rejecting the null hypothesis on design and performance decisions.

**Table 4-1. The alternative hypotheses and the corresponding critical regions for the t-test on mean total areas**

| Test for: | $H_A$ | Equation Number | Test | Critical Region |
|---|---|---|---|---|
| Coarse Material on Bottom | $\overline{A}_l > \overline{A}_u$ | (4-29) | One-tailed upper | $t_{av} > t_{av\alpha}$ |
| Coarse Material on Top | $\overline{A}_l < \overline{A}_u$ | (4-30) | One-tailed lower | $t_{av} < -t_{av\alpha}$ |
| Coarse Material on Top or Bottom | $\overline{A}_l \neq \overline{A}_u$ | (4-31) | Two-tailed | $t_{av} < -t_{av\alpha/2}$ or $t_{av} > t_{av\alpha/2}$ |

4. The measured and computed data on the coarse aggregate total area are used to compute both an estimate of the test statistic of Equation (4-27) and a statistical parameter that is required to define the sampling distribution of the test statistic (Equation (4-28)).

5. The region of rejection, which consists of those values of test statistic that would be unlikely to occur when a specimen is homogeneous, is represented by one or both tails of the distribution. The critical $t_{av\alpha}$ values, which separate the region of rejection from the region of acceptance, are obtained from the distribution of the $t_{av}$ statistic for the selected level of significance. Table 4-1 provides the regions of rejection that correspond to the possible alternative hypotheses. If the expected locations of the coarser and the finer gradations are known *a priori*, a one-way t-test is utilized. In the case where the coarser gradation is expected to be in the lower portion of the specimen, the region of rejection would be represented by the upper-tail of the distribution. In the case where the coarser gradation is expected to be in the upper portion of the specimen, the region of rejection would be represented by the lower tail of the distribution. If the expected locations of the coarser and the finer gradations are not known *a priori*, the region of rejection

would be represented by both the lower and the upper tails of the distribution but with half of the level of significance in each tail.

6. The decision on homogeneity of a specimen depends on a comparison of the computed value of the test statistic with the critical value. In the case where region of rejection is in the upper tail of the distribution, any $t_{av}$ value greater than the critical value ($t_{av\alpha}$) is assumed to indicate an inhomogeneous specimen. In the case where the region of rejection is in the lower tail of the distribution, any $t_{av}$ value more negative than the critical value ($-t_{av\alpha}$) is assumed to indicate an inhomogeneous specimen. In the case where the region of rejection is in both tails of the distribution, any $t_{av}$ value greater than upper tail critical value ($t_{av\alpha/2}$) or more negative than the lower tail critical value ($-t_{av\alpha/2}$) is assumed to indicate an inhomogeneous specimen.

### 4.2.3.3   Two-Sample t-Test on Frequencies

A two-sample t-test can also be used to compare the mean frequency of the coarse particles in the lower and upper portions to assess vertical inhomogeneity. The coarse particle frequency in the portion with the coarser gradation is hypothesized to be significantly greater than the coarse particle frequency in the portion with the finer gradation. The procedure for hypothesis testing using a t-statistic of the aggregate frequencies is as follows:

1. The following null hypothesis for the aggregate frequency, which is an implication of the null hypothesis of Equation (4-1), is tested:

$$H_o : \overline{F}_b = \overline{F}_t \tag{4-32}$$

where $\overline{F}_b$ and $\overline{F}_t$ are the population values of the mean coarse aggregate frequencies in the bottom and the top portions, respectively. A specimen is considered homogeneous if the null hypothesis is accepted. The possible alternative hypotheses for the mean aggregate frequencies are provided in Table 4-2. In the case where the coarser gradation is expected at the bottom of the specimen, the alternative hypothesis of Equation (4-35) would be tested. If the coarser gradation was expected at the top of the specimen, the alternative hypothesis of Equation (4-36) would be tested. If the expected direction of the coarser-to-finer gradation were not known *a priori*, the alternative hypothesis of Equation (4-37) would then be used.

2.   The test statistic is:

$$t_{fv} = \frac{\overline{f}_l - \overline{f}_u}{s_{fv}(\frac{1}{n_{hl}} + \frac{1}{n_{hu}})^{0.5}}$$
(4-33)

in which $t_{fv}$ is the index of homogeneity that is a random variable having a $t$ distribution with degrees of freedom of $(n_{hl} + n_{hu} - 2)$; $\overline{f}_l$ and $\overline{f}_u$ are the mean coarse aggregate frequencies (Equations (4-8) and (4-10)); $n_{hl}$ and $n_{hu}$ are the number of slice faces in the coarser and finer gradations, which are six; and $s_{fv}$ is the square root of the pooled variance given by:

$$s_{fv}^{2} = \frac{(n_{hl} - 1)s_{fl}^2 + (n_{hu} - 1)s_{fu}^2}{n_{hl} + n_{hu} - 2}$$
(4-34)

in which $s_{fl}^2$ and $s_{fu}^2$ are the variances of the total aggregate frequencies in the lower and the upper portions (Equations (4-9) and (4-11)).

**Table 4-2. The alternative hypotheses and the corresponding critical regions for the t-test on frequencies**

| Test for: | $H_A$ | Equation Number | Test | Critical Region |
|---|---|---|---|---|
| Coarse Material on Bottom | $\overline{F}_l > \overline{F}_u$ | (4-35) | One-tailed upper | $t_{fv} > t_{fv\alpha}$ |
| Coarse Material on Top | $\overline{F}_l < \overline{F}_u$ | (4-36) | One-tailed lower | $t_{fv} < -t_{fv\alpha}$ |
| Coarse Material on Top or Bottom | $\overline{F}_l \neq \overline{F}_u$ | (4-37) | Two-tailed | $t_{fv} < -t_{fv\alpha/2}$ or $t_{fv} > t_{fv\alpha/2}$ |

3. The level of significance is selected. The selection of the level of significance should be based on the physical significance of homogeneity and the impact of rejecting the null hypothesis of Equation (4-32) on design and performance decisions.

4. The measured and computed data on the geometric properties of the coarse aggregates are used to compute both an estimate of the test statistic of Equation (4-33) and the statistical parameter that is required to define the sampling distribution of the test statistic (Equation (4-34)).

5. The region of rejection, which consists of those values of the test statistic that would be unlikely to occur if the specimen was homogeneous, is represented by one or both tails of the distribution, depending on the alternative hypothesis. The critical $t_{fv}$ values, which separate the region of rejection from the region of acceptance, are obtained from the distribution of $t_{fv}$ statistic for the selected level of significance. Table 4-2 provides the regions of rejection that correspond to the possible alternative hypotheses. If the expected locations of the coarser and the finer gradations are known *a priori*, a one-way t-test is utilized. In the case where the coarser gradation is expected at the bottom of the specimen, the critical region

would be represented by the upper-tail of the distribution. In the case where the coarser gradation is expected at the top of the specimen, the critical region would be represented by the lower tail of the distribution. If the expected locations of the coarser and the finer gradations are not known *a priori*, the critical region would be represented by both the lower and the upper tails of the distribution but with half of the level of significance in each tail.

6. The decision on homogeneity of a specimen depends on comparison of the computed value of the test statistic and the critical value. In the case where the region of rejection is in the upper tail of the distribution, any $t_{fv}$ value greater than the critical value ($t_{fv\alpha}$) is assumed to indicate an inhomogeneous specimen. In the case where the region of rejection is in the lower tail of the distribution, any $t_{fv}$ value more negative than the critical value ($-t_{fv\alpha}$) is assumed to indicate an inhomogeneous specimen. In the case where the region of rejection is in both tails of the distribution, any $t_f$ value greater than critical value ($t_{fv\alpha/2}$) or more negative than the critical value ($-t_{fv\alpha/2}$) is assumed to indicate an inhomogeneous specimen.

### *4.2.3.4   Two-Sample t-Test on Nearest Neighbor Distances*

The two-sample t-test is used to compare the mean distances between the nearest neighbor aggregates in the lower and upper portions of a vertically inhomogeneous specimen. It is hypothesized that the mean distance between the nearest neighbor particles in the coarser portion of the specimen is significantly smaller than the mean distance between the nearest neighbor particles in the finer portion since a greater concentration of the coarse particles is in the coarser portion of the specimens. The

procedure for computing the t-statistic using the mean nearest neighbor distances from the horizontal slice faces is as follows:

1.  The following null hypothesis for the nearest neighbor distances, which is an implication of the null hypothesis of Equation (4-1), is tested:

$$H_o : \overline{D_l} = \overline{D_u} \tag{4-38}$$

where $\overline{D_l}$ and $\overline{D_u}$ are the population values of the mean coarse aggregate nearest neighbor distance for the lower and the upper portions, respectively. A specimen is considered homogeneous if the null hypothesis is accepted. The possible alternative hypotheses for the mean nearest neighbor distances of the aggregate are provided in Table 4-3. In the case where the coarser gradation being expected in the lower portion of the specimen, the alternative hypothesis of Equation (4-40) would be tested. If the coarser gradation is expected in the upper portion of the specimen, the alternative hypothesis of Equation (4-41) would be tested. If the direction of the coarser-to-finer gradation is not known *a priori*, the alternative hypothesis of Equation (4-42) would then be used.

2.  The t statistic, which is the index of homogeneity of the specimen, is:

$$t_{dv} = \frac{\overline{d}_u - \overline{d}_l}{s_{dv}(\dfrac{1}{n_{hl}} + \dfrac{1}{n_{hu}})^{0.5}} \tag{4-39}$$

in which $t_{dv}$ is the index of homogeneity that is a random variable having a $t$ distribution with degrees of freedom of $(n_{hl} + n_{hu} - 2)$; $\overline{d}_l$ and $\overline{d}_u$ are the mean nearest neighbor distances (Equations (4-18) and (4-20)); $n_{hl}$ and $n_{hu}$ are the

**Table 4-3. The alternative hypotheses and the corresponding critical regions for the t-test on means of the nearest neighbor distances**

| Test for: | H$_A$ | Equation Number | Test | Critical Region |
|---|---|---|---|---|
| Coarse Material on Bottom | $\overline{D}_u > \overline{D}_l$ | (4-40) | One-tailed upper | $t_{dv} > t_{dv\alpha}$ |
| Coarse Material on Top | $\overline{D}_u < \overline{D}_l$ | (4-41) | One-tailed lower | $t_{dv} < -t_{dv\alpha}$ |
| Coarse Material on Top or Bottom | $\overline{D}_l \neq \overline{D}_u$ | (4-42) | Two-tailed | $t_{dv} < -t_{dv\alpha/2}$ or $t_{dv} > t_{dv\alpha/2}$ |

number of slice faces in the coarser and the finer gradations, which are six; and $s_{dv}$

is the square root of the pooled variance given by:

$$s_{dv}{}^2 = \frac{(n_{hl}-1)s_{dl}{}^2 + (n_{hu}-1)s_{du}{}^2}{n_{hl}+n_{hu}-2} \qquad (4\text{-}43)$$

in which $s_{dl}{}^2$ and $s_{du}{}^2$ are the variances of the mean nearest neighbor distances in

the lower and the upper portions (Equations (4-19) and (4-21)).

3.  The level of significance is selected. The selection of the level of significance

    should be based on the physical significance of homogeneity and the impact of

    rejecting the null hypothesis of Equation (4-38) on design and performance

    decisions.

4.  The measured and computed data on the geometric properties of the coarse

    aggregates are used to compute both an estimate of the test statistic of Equation

    (4-39) and the statistical parameter that is required to define the sampling

    distribution of the test statistic (Equation (4-43)).

5.  The region of rejection, which consists of those values of the test statistic that

    would be unlikely to occur when the specimen is homogeneous, is represented by

    one or both tails of the distribution, depending on the alternative hypothesis. The

critical $t_{dv}$ value, which separates the region of rejection from the region of acceptance, is obtained from the distribution of the $t_{dv}$ statistic for the selected level of significance. Table 4-3 provides the regions of rejection that correspond to the possible alternative hypotheses. If the expected locations of the coarser and the finer gradations are known a priori, a one-way t-test is utilized. In the case where the coarser gradation is expected to be in the lower portion of the specimen, the critical value would be represented by the upper tail of the distribution. In the case where the coarser gradation is expected to be in the upper portion of the specimen, the region of rejection would then be represented by the lower tail of the distribution. If the expected locations of the coarser and the finer gradations are not known a priori, the critical region would be represented by both the lower and the upper tails of the distribution with half of the level of significance in each tail.

6.  The decision on homogeneity or inhomogeneity of a specimen depends on the comparison of the computed value of the test statistic with the critical value. In the case of the region of rejection in the upper tail of the distribution, any $t_{dv\alpha}$ value greater than the critical value $(t_{dv\alpha})$ is assumed to indicate an inhomogeneous specimen. In the case of the region of rejection in the lower tail of the distribution, any $t_{dv}$ value smaller than the critical value $(-t_{dv\alpha})$ is assumed to indicate an inhomogeneous specimen. In the case of the region of rejection in both tails of the distribution, any $t_{dv}$ value greater than the upper tail critical value $(t_{dv\alpha/2})$ or more negative than the lower tail critical value $(-t_{dv\alpha/2})$ is assumed to indicate an inhomogeneous specimen.

Table 4-4 provides a summary of the test statistics for the measurement of vertical inhomogeneity in two layers using horizontal slice faces, the statistical tests, the corresponding geometric properties, the equation numbers, and the section numbers where the tests are described. The tests will be applied to both simulated and actual specimens and their accuracy will be tested in Chapters 6 and 7.

**Table 4-4. Indices of two-layer vertical inhomogeneity using horizontal slice faces**

| Statistical Test | Property | Statistical Index | Section Number | Equation Number |
|---|---|---|---|---|
| Two-Sample Chi-Square | Frequencies | $\chi_{hv}^2 = \dfrac{(f_{hl} - f_{hv}r_{hl})^2}{f_{hv}r_{hl}(1-r_{hl})} + \dfrac{(f_{hu} - f_{hv}r_{hu})^2}{f_{hv}r_{hu}(1-r_{hu})}$ | 4.2.3.1 | 4-24 |
| Two-Sample t-Test | Total Aggregate Areas | $t_{av} = \dfrac{\overline{a}_{hl} - \overline{a}_{hu}}{s_{av}(\dfrac{1}{n_{hl}} + \dfrac{1}{n_{hu}})^{0.5}}$ | 4.2.3.2 | 4-27 |
| Two-Sample t-Test | Frequencies | $t_{fv} = \dfrac{\overline{f}_{hl} - \overline{f}_{hu}}{s_{fv}(\dfrac{1}{n_{hl}} + \dfrac{1}{n_{hu}})^{0.5}}$ | 4.2.3.3 | 4-36 |
| Two-Sample t-Test | Nearest Neighbor Distances | $t_{dv} = \dfrac{\overline{d}_{hl} - \overline{d}_{hu}}{s_{dv}(\dfrac{1}{n_{hl}} + \dfrac{1}{n_{hu}})^{0.5}}$ | 4.2.3.4 | 4-42 |

## 4.3 TWO-LAYER VERTICAL INHOMOGENEITY: VERTICAL SLICE FACES

A number of statistical tests are suggested for the detection and measurement of two-layer vertical inhomogeneity using horizontal slice faces. The suggested tests are adopted from the normal standard z, chi-square, and two sample t-tests. The tests include the normal z test on aggregate frequency proportions, the chi-square test on aggregate frequencies, and the t-test on total aggregate areas, aggregate frequencies, and mean nearest neighbor distances. The test statistics are computed based on comparison of the

geometric properties of coarse aggregates in the lower and the upper portions of vertical slice faces of specimens. The statistical tests examine the significance of the difference between the aggregate properties in the two portions.

### 4.3.1 Selection of Vertical Slices

To determine the location and the number of vertical slice faces, two factors were considered: First, independency of the slices and second, adequacy of the sampling areas on each slice face. To ensure independency of the vertical slices, McCuen and Azari (2001) showed that 10-mm spacing was required between the slices. To ensure adequacy of the sampling areas, the smallest cross-section that is used for the homogeneity sampling should have a width equal to the diameter of the largest size aggregate. The distance of the smallest slice face from the center of the specimen can then be determined based on the geometry of the circular cross-section of the specimen (Figure 4-2). If the maximum aggregate size were 19 mm, then the minimum width of the slice face should



w = width of the furthest slice face
d = distance of the furthest slice face from the middle slice face
R= 50 mm
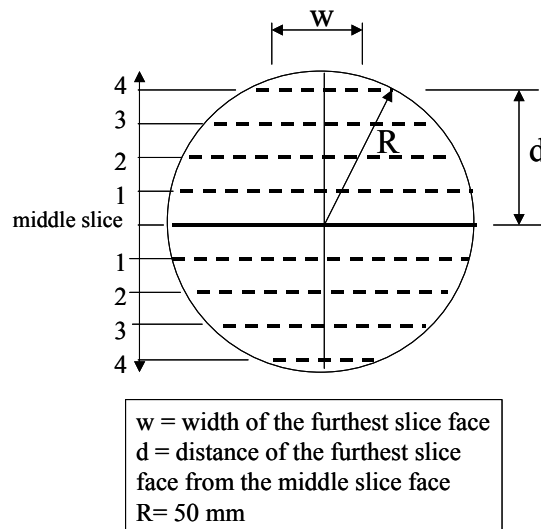
**Figure 4-2. Location of vertical slice faces for the analysis of vertically inhomogeneous and corresponding homogeneous specimen**

be equal to 19 mm, which is located 49 mm from the middle slice face. Allowing 10-mm spacing between the slices results in the furthest slice face to be taken at 40 mm from the middle slice face. Therefore, nine vertical slices were made on each 100-mm diameter specimen. One slice face was made in the middle, two slices were made at 40 mm from the middle slice face, and six additional slices were taken in between the middle slice and the outermost slices at the distances of 10 mm, 20 mm, and 30 mm from the middle slice.

### 4.3.2 Selection of Sampling Areas

Measurement of the aggregate properties in the lower and the upper portions of the vertical slices require determination of the sampling areas. The level of vertical inhomogeneity that was created resulted in unequal areas of the lower and the upper portions. The volume of the coarser mixture was 1.125 times the volume of the finer mixture. Thus, in a 150-mm high specimen, the coarser portion would have an approximate height of 79.2 mm and the finer portion would have an approximate height of 70.8 mm. However, to avoid a bias in statistical sampling from the coarser and finer portions, sampling was conducted on two equal lower and upper areas. Two rectangular areas with the height of 60 mm were selected at the top and bottom, 5 mm away from the ends of each slice face to avoid uneven ends of the specimen. A rectangular area between the lower and the upper sampling portions, which is 20-mm high, was considered the transition zone and the aggregate properties in that area were disregarded (Figure 4-3).

### 4.3.3 Computation of Parameters of Test Statistics

The parameters of test statistics are computed using the geometric properties of the coarse aggregates. However, several of the properties need to be modified to account for unequal cross-sections of the vertical faces. The properties that are mainly affected by
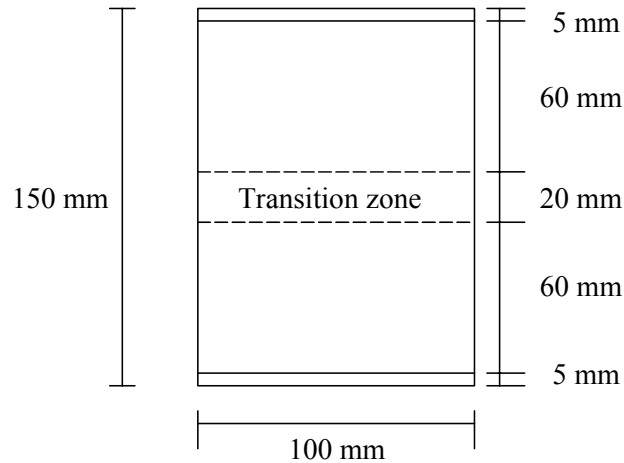
**Figure 4-3. Location of the lower and upper sampling areas on vertical slice faces of vertically inhomogeneous specimens**

the changing sampling area are the properties that are used by the t-test. This is because

the t-test uses the means of the properties, which should not be biased by the size of the

sampling area. The t-tests are defined for three geometric properties of the total aggregate

area, the frequency, and the mean nearest neighbor distance, which would be divided by

the area of the cross-sections, where the properties were measured. The computed

properties referred to as frequency density, area proportion, and mean nearest neighbor

distant density are then compared from the lower and upper portions of vertical slice

faces using the t-statistic. The steps for the measurement of the geometric properties and

computation of the parameters of the test statistics using vertical slice faces are as

follows:

  a.  The width of the slice face $i$ is computed by:

$$w_{vi} = 2\sqrt{R_v^2 - d_i^2}$$
(4-44)

128

where $w_{vi}$ is the width of the $i^{th}$ vertical slice face, $R_v$ is the radius of the specimen, which is 50 mm, and $d_i$ is the distance between the slice face $i$ and the middle slice face measured along a radius that is perpendicular to the slice face.

b.  The areas of the lower and the upper portions of the $i^{th}$ slice face are computed as:

$$A_{lvi} = A_{uvi} = h_v w_{vi} \qquad (4\text{-}45)$$

where $h_v$ is the height of the sampling area, which is 60 mm, and $w_{vi}$ is the width of each slice face that changes according to its distance from the middle slice face (Step a).

c.  The Total areas of the lower and upper portions of nine vertical slice faces are computed as:

$$A_{lv=} = \sum_{i=1}^{n_{lv}} A_{lvi} \qquad (4\text{-}46)$$

$$A_{uv=} = \sum_{i=1}^{n_{uv}} A_{uvi} \qquad (4\text{-}47)$$

where $A_{lvi}$ and $A_{uvi}$ are the areas of the lower and the upper portions of the $i^{th}$ slice face, respectively.

d.  On the lower portion and upper portion of each slice face, the frequency ($f_{lvi}, f_{uvi}$), the total area ($a_{lvi}, a_{uvi}$), and the mean nearest neighbor distance ($\bar{d}_{lvi}, \bar{d}_{uvi}$) of the coarse aggregates that have a diameter equal to or greater than 4.75 mm are measured. The nearest neighbor distance of each aggregate is the distance between each aggregate centroid and its nearest neighbor centroid.

e.  The coarse aggregate frequencies from the nine lower portions and nine upper portions of the slice faces are summed:

$$f_{lv} = \sum_{i=1}^{n_{lv}} f_{lvi} \qquad (4\text{-}48)$$

$$f_{uv} = \sum_{i=1}^{n_{uv}} f_{uvi} \qquad (4\text{-}49)$$

where $f_{lv}$ and $f_{uv}$ are the total coarse aggregate frequency in the lower and the upper portions; $n_{lv}$ and $n_{uv}$ are equal to the number of slices, which is nine; and $f_{lvi}$ and $f_{uvi}$ are the aggregate frequencies in the lower and the upper portions of the $i^{th}$ slice face, which were measured in Step d.

f.  The total frequency from the nine slice faces is computed by:

$$f_{vv} = f_{lv} + f_{uv} \qquad (4\text{-}50)$$

where $f_{lv}$, $f_{uv}$, and $f_{vv}$ are used for chi-square test.

g.  The aggregate frequency densities in the lower portion ($f_{dli}$) and upper portion ($f_{dui}$) of the $i^{th}$ slice face are computed as follows:

$$f_{dli} = \frac{f_{lvi}}{A_{lvi}} \qquad (4\text{-}51)$$

$$f_{dui} = \frac{f_{uvi}}{A_{uvi}} \qquad (4\text{-}52)$$

where $f_{lvi}$ and $f_{uvi}$ are the aggregate frequencies in the lower and upper portions of the $i^{th}$ slice face, which were measured in Step d; $A_{lvi}$ and $A_{uvi}$ are the areas of the lower and the upper portions of the $i^{th}$ slice face, which were computed using Equation (4-44).

h.  The means and standard deviations of the aggregate frequency densities in the lower portions ($\overline{f}_{dl}$, $s_{fdl}$) and upper portions ($\overline{f}_{du}$, $s_{fdu}$) of nine slice faces are computed as follows:

$$\overline{f}_{dl} = \frac{1}{n_{lv}} \sum_{i=1}^{n_{lv}} f_{dli} \qquad (4\text{-}53)$$

$$s_{fdl} = \left[ \frac{1}{n_{lv}-1} \sum_{i=1}^{n_{lv}} (f_{dli} - \overline{f}_{dl})^2 \right]^{0.5} \qquad (4\text{-}54)$$

$$\overline{f}_{du} = \frac{1}{n_{uv}} \sum_{i=1}^{n_{uv}} f_{dui} \qquad (4\text{-}55)$$

$$s_{fdu} = \left[ \frac{1}{n_{uv}-1} \sum_{i=1}^{n_{uv}} (f_{dui} - \overline{f}_{du})^2 \right]^{0.5} \qquad (4\text{-}56)$$

where $f_{dli}$ and $f_{dui}$ were computed using Equations (4-51) and (4-52); $n_{lv}$ and $n_{uv}$ are the number of lower and upper portions of the slice faces, which are nine. The computed means and standard deviations are used in the t-test on frequency density.

i. The aggregate area proportions in the lower portion ($a_{pli}$) and the upper portion ($a_{pui}$) of the $i^{th}$ slice face are computed as follows:

$$a_{pli} = \frac{a_{lvi}}{A_{lvi}} \qquad (4\text{-}57)$$

$$a_{pui} = \frac{a_{uvi}}{A_{uvi}} \qquad (4\text{-}58)$$

where $a_{lvi}$ and $a_{uvi}$ are the total aggregate areas in the lower and the upper portions of the $i^{th}$ slice face, which were measured in Step d, $A_{lvi}$ and $A_{uvi}$ are the areas of the lower and the upper portions of the $i^{th}$ slice face, which were computed using Equation (4-45).

131

j.  The means and standard deviations of the total aggregate proportions in the lower portions ($\bar{a}_{pl}$, $s_{apl}$) and in the upper portions ($\bar{a}_{pu}$, $s_{apu}$) of the slice faces are computed as follows:

$$\bar{a}_{pl} = \frac{1}{n_{lv}} \sum_{i=1}^{n_{lv}} a_{pli} \qquad (4\text{-}59)$$

$$s_{apl} = \left[ \frac{1}{n_{lv}-1} \sum_{i=1}^{n_{lv}} (a_{pli} - \bar{a}_{pl})^2 \right]^{0.5} \qquad (4\text{-}60)$$

$$\bar{a}_{pu} = \frac{1}{n_{uv}} \sum_{i=1}^{n_{u}v} a_{pui} \qquad (4\text{-}61)$$

$$s_{apu} = \left[ \frac{1}{n_{uv}-1} \sum_{i=1}^{n_{uv}} (a_{pui} - \bar{a}_{pu})^2 \right]^{0.5} \qquad (4\text{-}62)$$

where $a_{pli}$ and $a_{pui}$ are the aggregate area proportions in the lower portion and the upper portions of the $i^{th}$ slice face (Equations ((4-57) and (4-58)), respectively; and $n_{lv}$ and $n_{uv}$ are the number of lower and upper portions, which is nine. The means and standard deviations of Equations (4-59) through (4-62) are used in the t-test on total area proportions.

k.  The total aggregate areas on the lower ($a_{lv}$) and the upper ($a_{uv}$) portions of the slice faces are computed:

$$a_{lv} = \sum_{i=1}^{n_{lv}} a_{lvi} \qquad (4\text{-}63)$$

$$a_{uv} = \sum_{i=1}^{n_{lv}} a_{lvi} \qquad (4\text{-}64)$$

132

where $a_{lvi}$ and $a_{uvi}$ are the total aggregate areas on the lower or the upper portions of the $i^{th}$ slice face, which were defined in Step d; $n_{lv}$ and $n_{uv}$ are the number of lower and the upper portions, which are 9.

l.  The total area of the coarse aggregates from the nine slice faces is computed by:

$$a_{vv} = a_{lv} + a_{uv} \qquad (4\text{-}65)$$

m.  The mean area of the coarse aggregates, $\bar{a}_{vv}$, is computed as:

$$\bar{a}_{vv} = \frac{a_{vv}}{f_{vv}} \qquad (4\text{-}66)$$

where $a_{vv}$ is the total area and $f_{vv}$ is the total frequency of the coarse aggregates on both the lower and upper portions of nine slices (Equations (4-65) and (4-50), respectively).

n.  The expected maximum frequencies on the lower and the upper portions ($x_{lv}$ and $x_{uv}$) are computed as:

$$x_{lv} = x_{uv} = \frac{A_{lv}}{\bar{a}_{vv}} = \frac{A_{uv}}{\bar{a}_{vv}} \qquad (4\text{-}67)$$

where $A_{lv}$ and $A_{uv}$ are the total area of nine lower and nine upper portions, respectively (Equations (4-46) and (4-47)); and $\bar{a}_{vv}$ is the mean area of the coarse aggregates (Equation (4-66)).

o.  The frequency proportions of the coarse aggregates in the lower, upper, and both portions of the slices are computed as follows:

$$\hat{p}_{lv} = \frac{f_{lv}}{x_{lv}} \qquad (4\text{-}68)$$

$$\hat{p}_{uv} = \frac{f_{uv}}{x_{uv}} \qquad (4\text{-}69)$$

133

$$\hat{p}_{vv} = \frac{f_{lv} + f_{uv}}{x_{lv} + x_{uv}} \qquad (4\text{-}70)$$

where $f_{lv}$ and $f_{uv}$ are the total frequency of the coarse aggregates on the lower and the upper portions (Equations (4-48) and (4-49)), $x_{lv}$ and $x_{uv}$ are the expected maximum frequencies on the lower and the upper portions. The values of $\hat{p}_{lv}$, $\hat{p}_{uv}$, $\hat{p}_{vv}$, $x_{lv}$, and $x_{uv}$ are used in the frequency proportion test.

p.  The mean nearest neighbor distance density in the lower portion ($\overline{d}_{dli}$) and in the upper portion ($\overline{d}_{dui}$) of each of nine slice faces are computed as follows:

$$\overline{d}_{dli} = \frac{\overline{d}_{lvi}}{A_{lvi}} \qquad (4\text{-}71)$$

$$\overline{d}_{dui} = \frac{\overline{d}_{uvi}}{A_{uvi}} \qquad (4\text{-}72)$$

where $\overline{d}_{lvi}$ and $\overline{d}_{uvi}$ are the mean nearest neighbor distances in the lower and the upper portions of the $i^{th}$ slice face, which were measured in Step d, $A_{lvi}$ and $A_{uvi}$ are the areas of the lower and the upper portions of the $i^{th}$ slice face.

q.  The means and standard deviations of the mean nearest neighbor distance densities in the lower ($\overline{d}_{dl}$, $s_{ddl}$) and the upper ($\overline{d}_{du}$, $s_{ddu}$) portions of nine slice faces are computed.

$$\overline{d}_{dl} = \frac{1}{n_{lv}} \sum_{i=1}^{n_{lv}} \overline{d}_{dli} \qquad (4\text{-}73)$$

$$s_{ddl} = \left[ \frac{1}{n_{lv}-1} \sum_{i=1}^{n_{lv}} (\overline{d}_{dli} - \overline{d}_{dl})^2 \right]^{0.5} \qquad (4\text{-}74)$$

$$\overline{d}_{du} = \frac{1}{n_{uv}} \sum_{i=1}^{n_{uv}} \overline{d}_{dui} \qquad (4\text{-}75)$$

134

$$s_{ddu} = \left[ \frac{1}{n_{uv} - 1} \sum_{i=1}^{n_{uv}} (\overline{d}_{dui} - \overline{d}_{du})^2 \right]^{0.5} \qquad (4\text{-}76)$$

where $\overline{d}_{dli}$ and $\overline{d}_{dui}$ are the mean nearest neighbor distance densities, which were computed using Equations (4-71) and (4-72). The means and standard deviations of Equations (4-73) through (4-76) are used in the t-test on nearest neighbor distance densities.

### 4.3.4 Hypothesis Testing using Suggested Test Statistics

The statistical hypothesis tests are made using the z-test on frequency proportions, the chi-square test on aggregate frequencies, and the t-tests on total area proportion, frequency density, and mean nearest neighbor distance density using vertical slice faces. The hypothesis tests using the chi-square and the t-tests follow the procedures explained in Section 4.2.3. The hypothesis test using standard normal z test on frequency proportions is explained in this section. The test is adapted from the standard normal test and compares the proportion of the coarse aggregate frequency to the maximum expected coarse aggregate frequency of the lower and the upper portions of a specimen. The procedure for making a decision on homogeneity of a specimen using normal frequency proportion $z$ statistic is as follows:

1. The following null hypothesis for the aggregate frequency proportions, which is an implication of the null hypothesis of Equation (4-1), is tested:

$$H_o : \overline{P}_l = \overline{P}_u \qquad (4\text{-}77)$$

where $\overline{P}_l$ and $\overline{P}_u$ are the population values of the coarse aggregate frequency proportions for the lower and the upper portions, respectively. A specimen is considered homogeneous if the null hypothesis is accepted. The possible

alternative hypotheses for the aggregate frequency proportions for inhomogeneous

specimens are provided in Table 4-5. If the coarser gradation is expected to be in

the lower portion of the specimen, the alternative hypothesis of Equation (4-78)

would be tested. If the coarser gradation is expected to be in the upper portion of

the specimen, the alternative hypothesis of Equation (4-79) would be tested. If *a*

*priori* knowledge of the expected location of the coarser gradation is not specified,

the alternative hypothesis of Equation (4-80) would then be tested.

**Table 4-5. The alternative hypotheses and the corresponding critical regions for the frequency proportion z test**

| Test for: | $H_A$ | Equation | Test | Critical Region |
|---|---|---|---|---|
| Coarse Material on Bottom | $\overline{P_l} > \overline{P_u}$ | (4-78) | One-tailed upper | $z_{hv} > z_{hv\alpha}$ |
| Coarse Material on Top | $\overline{P_l} < \overline{P_u}$ | (4-79) | One-tailed lower | $z_{hv} < -z_{hv\alpha}$ |
| Coarse Material on Top or Bottom | $\overline{P_l} \neq \overline{P_u}$ | (4-80) | Two-tailed | $z_{hv} < -z_{hv\alpha/2}$ or $z_{hv} > z_{hv\alpha/2}$ |

2. To test the hypotheses in Step 1, the standard proportion *z* statistic is used:

$$z_{vv} = \frac{\hat{p}_{lv} - \hat{p}_{uv}}{s_{pvv}}$$  (4-81)

where $z_{vv}$ is the value of a random variable having a standard normal distribution;

$\hat{p}_{lv}$ and $\hat{p}_{uv}$ are the coarse aggregate frequency proportions (Equations (4-68) and

(4-69)); and $s_{pvv}$ is the pooled sample standard deviation, which is defined as

follows:

$$s_{pvv} = \left[ \hat{p}_v(1 - \hat{p}_v)(\frac{1}{x_{lv}} + \frac{1}{x_{uv}}) \right]^{0.5}$$  (4-82)

where $\hat{p}_v$ is the proportion of coarse aggregate frequency in both lower and upper portions (Equation (4-70)); $x_{lv}$ and $x_{uv}$ are the maximum expected frequencies of coarse aggregates in the lower and the upper portions (Equation (4-67)).

3.  The level of significance is selected. The selection of the level of significance should be based on the physical significance of homogeneity and the impact of rejecting the null hypothesis of Equation (4-77) on design and performance decisions.

4.  The measured and computed data on the geometric properties of the coarse aggregates (Equations (4-67) through (4-70)), are used to compute both an estimate of the test statistic of Equation (4-81) and the statistical parameters that are required to define the sampling distribution of the test statistic (Equations (4-82)).

5.  The region of rejection, which consists of those values of the test statistic that would be unlikely to occur when a specimen is homogeneous, is represented by one or both tails of the distribution, depending on the alternative hypothesis. The critical $z_{vv}$ values, which separate the region of rejection from the region of acceptance, are obtained from the probability distribution of $z_{vv}$ for the selected level of significance. Table 4-5 provides the critical regions that correspond to the possible alternative hypotheses. If the expected locations of the coarser and the finer gradations are known *a priori*, a one-way z-test is utilized. In the case where the coarser gradation is expected to be in the lower portion of the specimen, the critical region would be represented by the upper-tail of the distribution. In the case where the coarser gradation is expected to be in the upper portion of the

specimen, the critical region would be represented by the lower tail of the distribution. If expected locations of the coarser and finer gradations are not known *a priori*, the critical region would be represented by both the lower and the upper tails of the distribution but with half of the level of significance in each tail.

6. The decision on homogeneity of a specimen depends on a comparison of the computed value of the test statistic and the critical value. In the case where the region of rejection is in the upper tail of the distribution, any sample $z_{vv}$ value greater than the critical value ($z_{vv\alpha}$) suggests an inhomogeneous specimen. In the case where the region of rejection is in the lower tail of the distribution, any sample $z_{vv}$ value more negative than the critical value (-$z_{vv\alpha}$) suggests an inhomogeneous specimen. In case where regions of rejection in both tails of the distribution, any sample $z_{hv}$ value more negative than the lower tail critical value (-$z_{vv\alpha/2}$) and greater than the upper tail critical value ($z_{vv\alpha/2}$) suggest an inhomogeneous specimen.

Table 4-6 provides a summary of the test statistics for evaluation of vertical inhomogeneity in two layers using vertical slice faces. The statistical tests and the corresponding geometric properties are also provided in the table. The proposed tests would be applied to both simulated and actual specimens and their accuracy will be tested in Chapters 6 and 7.

## 4.4 THREE-LAYER VERTICAL INHOMOGENEITY: HORIZONTAL SLICE FACES

Vertical inhomogeneity may be gradual rather than abrupt. The abrupt vertical inhomogeneity was simulated by two layers, while gradual vertical inhomogeneity was

**Table 4-6. Indices of two-layer vertical inhomogeneity using vertical slice faces**

| Statistical Test | Property | Statistical Index | Equation Number |
|---|---|---|---|
| Standard Normal z | Frequency Proportions | $$z_{vv} = \frac{\hat{p}_{lv} - \hat{p}_{uv}}{s_{pvv}}$$ | (4-81) |
| | | $$s_{pvv} = \left[ \hat{p}_v (1 - \hat{p}_v)(\frac{1}{x_{lv}} + \frac{1}{x_{uv}}) \right]^{0.5}$$ | (4-82) |
| Two-Sample Chi-Square | Frequencies | $$\chi_{vv}^2 = \frac{(f_{lv} - f_{vv}r_{lv})^2}{f_{vv}r_{lv}(1 - r_{lv})} + \frac{(f_{uv} - f_{vv}r_{uv})^2}{f_{vv}r_{uv}(1 - r_{uv})}$$ | (4-83) |
| | | $$r_{lv} = r_{uv} = \frac{A_{lv}}{A_{uv} + A_{lv}} = \frac{A_{uv}}{A_{uv} + A_{lv}} = 0.5$$ | (4-84) |
| Two-Sample t-Test | Area Proportions | $$t_{apv} = \frac{\overline{a}_{pl} - \overline{a}_{pu}}{s_{apv}(\frac{1}{n_{lv}} + \frac{1}{n_{uv}})^{0.5}}$$ | (4-85) |
| | | $$s_{apv}^{\;2} = \frac{(n_{lv} - 1)s_{apl}^{\;2} + (n_{uv} - 1)s_{apu}^{\;2}}{n_{lv} + n_{uv} - 2}$$ | (4-86) |
| Two-Sample t-Test | Frequency Density | $$t_{fdv} = \frac{\overline{f}_{dl} - \overline{f}_{du}}{s_{fdv}(\frac{1}{n_{lv}} + \frac{1}{n_{uv}})^{0.5}}$$ | (4-87) |
| | | $$s_{fdv}^{\;2} = \frac{(n_{lv} - 1)s_{fdl}^{\;2} + (n_{uv} - 1)s_{fdu}^{\;2}}{n_{lv} + n_{uv} - 2}$$ | (4-88) |
| Two-Sample t-Test | Nearest Neighbor Distance Density | $$t_{ddv} = \frac{\overline{d}_{dl} - \overline{d}_{du}}{s_{ddv}(\frac{1}{n_{lv}} + \frac{1}{n_{uv}})^{0.5}}$$ | (4-89) |
| | | $$s_{ddv}^{\;2} = \frac{(n_{lv} - 1)s_{ddl}^{\;2} + (n_{uv} - 1)s_{ddu}^{\;2}}{n_{lv} + n_{uv} - 2}$$ | (4-90) |

modeled using specimens made with three layers. In such a case, the selected tests should involve comparison of the properties of the coarse aggregates in three horizontal layers. A number of statistical tests are suggested for the detection and measurement of three-layer vertical inhomogeneity using horizontal slice faces. The tests include the chi-square test on aggregate frequencies and the F-test on total aggregate areas, aggregate frequencies, and mean nearest neighbor distances. The test statistics are computed based on comparison of the aggregate properties observed in the lower, middle, and the upper portions of the specimens. The statistical tests examine the significance of the difference between the aggregate properties in the three layers.

### 4.4.1    Selection of Specimen Sampling

Application of the statistical tests requires selection of the sampling spaces, in which the measurements of the geometric properties of the coarse aggregates need to be conducted. Although, the level of gradual vertical inhomogeneity that was created resulted in three unequal volumes of the coarse, medium, and fine portions (Section 3.3.2.3), equal number of the slices was taken in each portion to avoid a bias in statistical sampling.

The selection of the slices in each of the three portions was determined with two considerations: First, the slices should be independent; second, the slices within each portion should be from the same population. To ensure independency of the slices, McCuen and Azari (2001) showed that a 10-mm spacing was required between the slices. To ensure that the slices are from the same population, the top and bottom slices are located 15 mm away from the ends of the specimen to allow for the large particles to be fully contained within the specimen. In addition, a 15 mm gap between the last and the

first slices of any two adjacent portions was considered as a transition zone. The reason is that the process of compaction blends the two mixtures around the borderline between the portions, which results in a gradation that does not distinctively follow either the coarse, medium, or the fine gradation. By selecting the sampling portions away from the blended mixture, the materials in each portion should follow a distinct statistical population.

Therefore, four horizontal slices in each of the three portions of the specimen were made. The first slice of the lower portion was taken 15 mm from the bottom of the specimen (bottom slice). The other three slices were taken at 10-mm intervals starting from the bottom slice. The first slice in the middle portion was taken 15 mm from the last slice of the lower portion. The other three slices were taken at 10-mm intervals starting from the first slice of the middle portion. The last slice of the upper portion was taken 15 mm from the top of the specimen (top slice). The other three slices were taken at 10-mm intervals below the top slice (Figure 4-4).
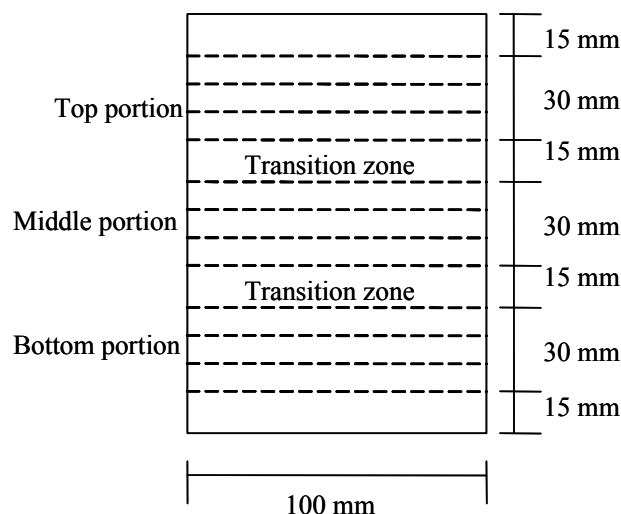


**Figure 4-4. Location of the horizontal slice faces on a specimen to be evaluated for three-layer vertical inhomogeneity**

### 4.4.2 Computation of Parameters of Test Statistics

The computation of the test statistics requires measurement of geometric properties of coarse aggregates and computation of the selected statistical parameters. The steps of the procedure are as follows:

a. On each slice face that is located in the $j^{th}$ sampling portion (lower, middle, and upper portions) of the specimen, the frequency ($f_{hji}$), the total area ($a_{hji}$), and the mean nearest neighbor distance ($\overline{d}_{hji}$) of the coarse aggregates that have a diameter equal to or greater than 4.75 mm are measured; $j$ indicates the sampling portion and $i$ indicates the slice face in each portion.

b. The coarse aggregate frequencies from the slice faces in each of the three portions are summed:

$$f_{hj} = \sum_{i=1}^{n_s} f_{hji} \qquad (4\text{-}91)$$

where $f_{hj}$ is the total coarse aggregate frequency in the $j^{th}$ portion; $n_s$ is the number of slices in each portion, which is four; and $f_{hji}$ is the aggregate frequency in the $i^{th}$ slice face of the $j^{th}$ portion, which was measured in Step a.

c. The total frequency ($f_h$) from the three sampling portions is computed by:

$$f_h = \sum_{j=1}^{n_p} f_{hj} \qquad (4\text{-}92)$$

where $n_p$ is the number of portions, which is three and $f_{hj}$ is the total coarse aggregate frequency in the $j^{th}$ portion.

d. The area ratio of the slices ($r_{hj}$) in the $j^{th}$ portion to total number of slices is:

$$r_{hj} = \frac{A_{hj}}{A_{hT}} = \frac{1}{3} \qquad (4\text{-}93)$$

where $A_{hj}$ is the total area of four slice faces in the $j^{th}$ portion and $A_{hT}$ is the total area of twelve slices in the three sampling portions. The variables computed in Equations (4-91) through (4-93) are used in the chi-square test on frequencies.

e.  The mean aggregate frequency in each portion is computed:

$$\overline{f}_{hj} = \frac{1}{n_s} \sum_{i=1}^{n_s} f_{hji} \qquad (4\text{-}94)$$

where $n_s$ is the number of slices in the $j^{th}$ portion, which is four and $f_{hji}$ is the aggregate frequency in the $i^{th}$ slice face of the $j^{th}$ portion of the specimen, which was measured in Step a.

f.  The grand mean ($\overline{f}_h$) of the aggregate frequencies of the three portions is computed by:

$$\overline{f}_h = \frac{1}{n_p} \sum_{j=1}^{n_p} \overline{f}_{hj} \qquad (4\text{-}95)$$

where $\overline{f}_{hj}$ is the mean aggregate frequency in portion $j$ and $n_p$ is the number of sampling portions, which is three. The mean frequency values computed using Equations (4-94) and (4-95) are used in the F-test on frequencies.

g.  The mean total aggregate area ($\overline{a}_{hj}$) in each sampling portion of the specimen is computed:

$$\overline{a}_{hj} = \frac{1}{n_s} \sum_{i=1}^{n_s} a_{hji} \qquad (4\text{-}96)$$

where $n_s$ is the number of slices in the $j^{th}$ portion, which is four and $a_{hji}$ is the total coarse aggregate area in the $i^{th}$ slice face of the $j^{th}$ portion of the specimen, which was measured in Step a.

h.  The grand mean ($\bar{a}_h$) of the total coarse aggregate areas from all portions are

computed:

$$\bar{a}_h = \frac{1}{n_p} \sum_{j=1}^{n_p} \bar{a}_{hj} \qquad (4\text{-}97)$$

where $\bar{a}_{hj}$ is the mean of total coarse aggregate areas in portion j and $n_p$ is the

number of sampling portions, which is three. The mean values computed using

Equations (4-96) and (4-97) are used in the F-test on total areas.

i.  The mean of the nearest neighbor distances in any of the three sampling portions is

computed:

$$\bar{d}_{hj} = \frac{1}{n_s} \sum_{i=1}^{n_s} \bar{d}_{hji} \qquad (4\text{-}98)$$

where $n_s$ is the number of slices in the $j^{th}$ portion, which is four and $\bar{d}_{hji}$ is the

mean nearest neighbor distance of the coarse aggregates on the $i^{th}$ slice face of the

$j^{th}$ portion of the specimen, which was measured in Step a.

j.  The grand mean ($\bar{d}_h$) of the mean nearest neighbor distances in the three sampling

portions is computed by:

$$\bar{d}_h = \frac{1}{n_p} \sum_{j=1}^{n_p} \bar{d}_{hj} \qquad (4\text{-}99)$$

where $\bar{d}_{hj}$ is the mean nearest neighbor distance in portion j and $n_p$ is the number

of sampling portions, which is three. The mean values computed using Equations

(4-98) and (4-99) are used in the F-test on mean nearest neighbor distances.

**4.4.3    Hypothesis Testing using Suggested Test Statistics**

The six steps of hypothesis testing are followed in order to test homogeneity of a specimen. In the following sections the steps for testing the three-layer vertical inhomogeneity using the proposed statistical tests on the horizontal slice faces are explained:

*4.4.3.1    Three-Sample chi-Square Test on Frequencies*

The chi-square test can be applied to aggregate frequencies to test gradual vertical inhomogeneity. The test compares the frequencies of the coarse aggregates in the lower, middle, and the upper portions of a specimen. The objective is to examine whether the aggregate frequencies of the portions vary from the expected aggregate frequency for a homogeneous specimen. It is hypothesized that for an inhomogeneous specimen, the frequency of the coarse particles in at least one of the three sampling portions is significantly different from the expected frequency. The procedure for testing the homogeneity of a specimen using three-sample chi-square test on frequencies is as follows:

1.   The following hypotheses for the aggregate frequencies, which are implications of the hypotheses of Equations (4-1) and (4-2), are tested:

$H_o$ : *The observed frequency of each portion is equal to the mean.*

(4-100)

$H_A$ : *At least one observed frequency is different from the mean.*

(4-101)

A specimen is considered homogeneous if the null hypothesis is accepted.

2.   To test the hypotheses, the chi-square test statistic is used:

$$\chi_{3h}^2 = \sum_{j=1}^{n_p} \frac{(f_{hj} - r_{hj} f_h)^2}{r_{hj} f_h (1 - r_{hj})}$$

(4-102)

where $\chi_{3h}^2$ is the value of a random variable having a chi-square distribution with

the degree of freedom of $\nu_{3\chi}$:

$$\nu_{3\chi} = n_p - 1$$

(4-103)

where $n_p$ is the number of layers, which is three; $f_{hj}$ is the total frequency of the

coarse aggregates in the $j^{th}$ portion (Equation (4-91)); $r_{hj}$ is the area ratio of the

slices in the $j^{th}$ portion to all 12 slices (Equation (4-93)); and $f_h$ is the total

aggregate frequency on 12 slices in the three sampling portions (Equation (4-92)).

3.  The level of significance is selected. The selection of the level of significance
    should be based on the physical significance of homogeneity and the impact of
    rejecting the null hypothesis of Equation (4-100) on design and performance
    decisions.

4.  The measured and computed data on the geometric properties of the coarse
    aggregates are used to compute an estimate of the test statistic of Equation (4-102).

5.  The region of rejection, which consists of those values of test statistic that would
    be unlikely to occur when a specimen is homogeneous, is represented by upper tail
    of the distribution. The critical $\chi_{3h}^2$ value ($\chi_{3h\alpha}^2$) value, which separates the region
    of rejection from the region of acceptance, is obtained from the distribution of $\chi_{3h}^2$
    statistic for the selected level of significance.

6.  The decision on homogeneity of a specimen depends on comparison of the
    computed value of the test statistic and the critical value. Any chi-square value
    greater than the critical value suggests an inhomogeneous specimen.

### 4.4.3.2  F-Test on Total Aggregate Areas

The assessment of a difference in the total area of the coarse aggregates observed on the horizontal slice faces in the upper, middle, and the lower portions of a specimen will indicate inhomogeneity. The mean of the total coarse aggregate areas in the coarse portion is hypothesized to be greater than the mean of the total coarse aggregate areas in the medium or fine portions of the specimen. An F-test is used to assess the difference between the three means. The procedure for testing homogeneity of a specimen using an F-test on total coarse aggregate areas is as follows:

1. The following hypotheses for the aggregate total areas, which are implications of the hypotheses of Equations (4-1) and (4-2), are tested:

$$H_o : \overline{A}_b = \overline{A}_m = \overline{A}_t \tag{4-104}$$

$$H_A : At\ least\ one\ pair\ of\ the\ means\ is\ not\ equal. \tag{4-105}$$

where $\overline{A}_b$, $\overline{A}_m$, and $\overline{A}_t$ are the population values of the total coarse aggregate areas in the bottom, middle, and top portions of a specimen, respectively. A specimen is considered homogeneous if the null hypothesis is accepted.

2. To test the hypothesis, the F statistic is used:

$$F_a = \frac{MS_{ba}}{MS_{wa}} \tag{4-106}$$

where $F_a$ is the index of homogeneity that is a random variable that has an $F$ distribution with degrees of freedom of $(n_p - 1, n - n_p)$, where $n_p$ is the number of sampling portions, which is three and $n$ is the total number of slice faces in the three sampling portions, which is 12. $MS_{ba}$ and $MS_{wa}$ are the between and within total area mean squares (McCuen, 1985), which are computed as follows:

$$MS_{ba} = \left.\sum_{j=1}^{n_p} n_s (\bar{a}_{hj} - \bar{a}_h)^2 \middle/ (n_p - 1)\right. \tag{4-107}$$

$$MS_{wa} = \left.\sum_{j=1}^{n_p}\sum_{i=1}^{n_s} (a_{hij} - \bar{a}_{hj})^2 \middle/ (n - n_p)\right. \tag{4-108}$$

where $n_s$ is the number of slice faces in the $j^{th}$ layer, which is 4; $\bar{a}_{hj}$ is the mean of total coarse aggregate areas on the slices in the $j^{th}$ layer (Equation (4-96)); $\bar{a}_h$ is the grand mean of the total coarse aggregate areas of 12 slice faces in the three sampling portions (Equation (4-97)); and $a_{hij}$ is the total coarse aggregate area on the $i^{th}$ slice face in the $j^{th}$ sampling portion (Section 4.4.2, Step a).

3. The level of significance is selected. The selection of the level of significance should be based on the physical significance of homogeneity and the impact of rejecting the null hypothesis of Equation (4-112) on design and performance decisions.

4. The measured and the computed data on the geometric properties of the coarse aggregates are used to compute an estimate of the test statistic of Equation (4-106) and its components (Equations (4-107) and (4-108)).

5. The region of rejection, which consists of those values of test statistic that would be unlikely to occur when a specimen is homogeneous, is represented by the upper tail of the distribution. The critical F value ($F_{a\alpha}$), which separates the region of rejection from the region of acceptance, is obtained from the distribution of $F_a$ statistic for the selected level of significance.

6. The decision on homogeneity of a specimen depends on comparison of the computed value of the test statistic and the critical value. Any $F_a$ value greater than the critical value suggests an inhomogeneous specimen.

### 4.4.3.3  F-Test on Aggregate Frequencies

An F-test can also be utilized to compare the mean frequencies of the coarse particles in the lower, middle, and upper sampling portions of a specimen. The mean of coarse aggregate frequencies in the coarse portion is hypothesized to be greater than the mean of coarse aggregate frequencies in the medium or fine portions of the specimen. An F-test is used to assess the difference between the three means. The procedure to test the homogeneity of a specimen using F-test on mean frequencies is as follows:

1. The following hypotheses for the aggregate frequencies, which are implications of the hypotheses of Equations (4-1) and (4-2), are tested:

$$H_o : \overline{F}_b = \overline{F}_m = \overline{F}_t \qquad\qquad (4\text{-}109)$$

$$H_A : \textit{At least one pair of frequency means is not equal.} \qquad (4\text{-}110)$$

where $\overline{F}_b$, $\overline{F}_m$, and $\overline{F}_t$ are the population values of the coarse aggregate frequencies in the bottom, middle, and top portions of a specimen, respectively. A specimen is considered homogeneous if the null hypothesis is accepted.

2. To test the hypothesis, the F statistic is used:

$$F_f = \frac{MS_{bf}}{MS_{wf}} \qquad\qquad (4\text{-}111)$$

where $F_f$ is the index of homogeneity that is a random variable that has an $F$ distribution with degrees of freedom of $(n_p - 1, n - n_p)$, where $n_p$ is the number of

149

sampling portions, which is three and $n$ is the total number of slice faces in the three sampling portions which is 12. $MS_{bf}$ and $MS_{wf}$ are the between and within mean squares, which are computed as follows:

$$MS_{bf} = \sum_{j=1}^{n_p} n_s (\overline{f}_{hj} - \overline{f}_h)^2 \bigg/ (n_p - 1)$$

(4-112)

$$MS_{wf} = \sum_{j=1}^{n_p} \sum_{i=1}^{n_s} (f_{hij} - \overline{f}_{hj})^2 \bigg/ (n - n_p)$$

(4-113)

where $n_s$ is the number of slice faces in the $j^{th}$ layer, which is four; $\overline{f}_{hj}$ is the mean of coarse aggregate frequencies on the slices in the $j^{th}$ layer (Equation (4-94)); $\overline{f}_h$ is the grand mean of the coarse aggregate frequencies of 12 slice faces in the three sampling portions (Equation (4-95)); and $f_{hji}$ is the aggregate frequency on the $i^{th}$ slice face in the $j^{th}$ layer.

3. The level of significance is selected. The selection of the level of significance should be based on the physical significance of homogeneity and the impact of rejecting the null hypothesis of Equation (4-117) on design and performance decisions.

4. The measured and the computed data on the geometric properties of the coarse aggregates are used to compute an estimate of the test statistic of Equation (4-111) and its components (Equations (4-112) and (4-113)).

5. The region of rejection, which consists of those values of test statistic that would be unlikely to occur when a specimen is homogeneous, is represented by the upper tail of the distribution. The critical $F_f$ value ($F_{f\alpha}$), which separates the regions of

rejection from the region of acceptance, is obtained from the distribution of $F_f$ statistic for the selected level of significance.

6. The decision on homogeneity or inhomogeneity of a specimen depends on comparison of the computed value of the test statistic and the critical value. Any $F_f$ value greater than the critical value suggests an inhomogeneous specimen.

#### 4.4.3.4   F-Test on Nearest Neighbor Distances

The F-test is utilized to compare the mean distances between the nearest neighbor aggregates in the lower, middle, and upper portions of a specimen. It is hypothesized that the mean distance between the nearest neighbor particles in the coarse portion is significantly smaller than the mean distance in the medium or the fine portion of an inhomogeneous specimen. This is because of a greater concentration of the coarse aggregates in the coarser portion of the specimen. The procedure for testing homogeneity of a specimen using F-test on mean nearest neighbor distances is as follows:

1. The following hypotheses for the aggregate nearest neighbor distances, which are implications of the hypotheses of Equations (4-1) and (4-2), are tested:

$$H_o : \overline{D}_b = \overline{D}_m = \overline{D}_t \tag{4-114}$$

$H_A$ : *At least one pair of mean nearest neighbor distances is not equal.*

$$\tag{4-115}$$

where $\overline{D}_b$, $\overline{D}_m$, and $\overline{D}_t$ are the population values of the mean coarse aggregate nearest neighbor distances in the bottom, middle, and top portions of a specimen, respectively. A specimen is considered homogeneous if the null hypothesis is accepted.

151

2. To test the hypothesis, the F statistics is used:

$$F_d = \frac{MS_{bd}}{MS_{wd}}$$

(4-116)

where $F_d$ is the index of homogeneity that is a random variable and has an $F$ distribution with degrees of freedom of $(n_p - 1, n - n_p)$, where $n_p$ is the number of sampling portions, which is three and $n$ is the total number of slice faces in the three sampling portions, which is 12. $MS_{bd}$ and $MS_{wd}$ are the between and within nearest neighbor distance mean squares, which are computed as follows:

$$MS_{bd} = \frac{\sum_{j=1}^{n_p} n_s (\overline{d}_{hj} - \overline{d}_h)^2}{(n_p - 1)}$$

(4-117)

$$MS_{wd} = \frac{\sum_{j=1}^{n_p} \sum_{i=1}^{n_s} (\overline{d}_{hji} - \overline{d}_{hj})^2}{(n - n_p)}$$

(4-118)

where $n_s$ is the number of slice faces in the $j^{th}$ layer, which is four; $\overline{d}_{hj}$ is the average of the mean nearest neighbor distances on the slices of the $j^{th}$ layer (Equations (4-98)); $\overline{d}_h$ is the grand mean of the mean nearest neighbor distances on 12 slice faces in the three sampling portions (Equation (4-99)); and $\overline{d}_{hji}$ is the mean nearest neighbor distance on the $i^{th}$ slice face in the $j^{th}$ layer (Section 4.4.2, Step a).

3. The level of significance is selected. The selection of the level of significance should be based on the physical significance of homogeneity and the impact of rejecting the null hypothesis of Equation (4-122) on design and performance decisions.

4. The measured and computed data on the geometric properties of the coarse aggregates are used to compute an estimate of the test statistic of Equation (4-116) and its components (Equations (4-117) and (4-118)).

5. The region of rejection, which consists of those values of test statistic that would be unlikely to occur when a specimen is homogeneous, is represented by the upper tail of the distribution. The critical $F_d$ value ($F_{d\alpha}$), which separates the region of rejection from the region of acceptance, is obtained from the distribution of $F_d$ statistic for the selected level of significance.

6. The decision on homogeneity of a specimen depends on the comparison of the computed value of the test statistic and the critical value. Any $F_d$ value greater than the critical value suggests an inhomogeneous specimen.

Table 4-7 provides a summary of the test statistics for the measurement of vertical inhomogeneity in three layers using horizontal slice faces, the statistical tests, the corresponding geometric properties, the equation numbers, and the section numbers where the tests are described. The tests of Table 4-7 would be applied to simulated specimens and their accuracy will be tested in Chapter 6.

## 4.5 TESTS FOR ALL FORMS OF VERTICAL INHOMOGENEITY

When the nature of vertical inhomogeneity, whether in two or three layers, is not known, a test that is specific to one form of vertical inhomogeneity would not be powerful enough for the detection of the other form of vertical inhomogeneity. Number of tests is proposed for the cases where the nature of vertical inhomogeneity, abrupt or

**Table 4-7. Indices of three-layer vertical inhomogeneity using horizontal slice faces**

| Statistical Test | Property | Statistical Index | Section Number | Equation Number |
|---|---|---|---|---|
| Three-Sample Chi-Square | Frequencies | $$\chi^2 = \sum_{j=1}^{n_p} \frac{(f_{hj} - r_{hj} f_h)^2}{r_{hj} f_{hj}(1 - r_{hj})}$$ | 4.4.3.1 | (4-102) |
| F-Test | Total Areas | $$F_a = \frac{\displaystyle\sum_{j=1}^{n_p} n_s (\bar{a}_{hj} - \bar{a}_h)^2 \Big/ (n_p - 1)}{\displaystyle\sum_{j=1}^{n_p}\sum_{i=1}^{n_s} (\bar{a}_{hji} - \bar{a}_{hj})^2 \Big/ (n - n_p)}$$ | 4.4.3.2 | (4-106) (4-107) (4-108) |
| F-Test | Frequencies | $$F_f = \frac{\displaystyle\sum_{j=1}^{n_p} n_s (\bar{f}_{hj} - \bar{f}_h)^2 \Big/ (n_p - 1)}{\displaystyle\sum_{j=1}^{n_p}\sum_{i=1}^{n_s} (f_{hij} - \bar{f}_{hj})^2 \Big/ (n - n_p)}$$ | 4.4.3.3 | (4-111) (4-112) (4-113) |
| F-Test | Neighbor Distances | $$F_d = \frac{\displaystyle\sum_{j=1}^{n_p} n_s (\bar{d}_{hj} - \bar{d}_h)^2 \Big/ (n_p - 1)}{\displaystyle\sum_{j=1}^{n_p}\sum_{i=1}^{n_s} (\bar{d}_{hij} - \bar{d}_{hj})^2 \Big/ (n - n_p)}$$ | 4.4.3.4 | (4-116) (4-117) (4-118) |

gradual, is not known. The tests are the Spearman-Conley, the runs, and the average depth. The six steps of hypothesis testing are followed in order to evaluate vertical homogeneity of a specimen using the proposed tests.

### 4.5.1 Spearman-Conley Test (Horizontal Slice Faces)

The Spearman-Conley test (Conley and McCuen, 1997) can be used to measure the change in the frequency of the coarse aggregates through depth of a specimen by evaluating the serial correlation of the coarse aggregate frequency in the adjacent

horizontal slice faces. Prior to the application of the test, the parameters of test statistic are computed based on the frequency of the coarse aggregates. The steps for the measurement of the frequencies and the computation of the parameters of the test statistic are as follows:

a.   Twelve horizontal slices are made at 10-mm spacing. The first and the last slices are taken 15 mm from the ends of the specimen to allow the large size aggregates to be fully contained within the specimen.

b.   On each slice face, the frequency ($f_i$) of the coarse aggregates that have a diameter equal to or greater than 4.75 mm is measured.

c.   Two data series from the aggregate frequency of the slice faces are formed. The first sequence includes aggregate frequencies of all slices excluding the frequency of the first slice face. The second sequence includes the aggregate frequencies of the slice faces excluding the value of the last slice face.

d.   While keeping the values in each series in chronological order, the rank of each frequency value in each series is determined.

e.   The difference in the ranks ($\Delta_i$) of the frequencies of the two series is computed.

     The six steps of hypothesis testing are then followed in order to evaluate the homogeneity of a specimen. Using the information obtained above, the steps of hypothesis test using the Spearman-Conley test statistic are as follows:

1.   The following hypotheses for the aggregate frequencies, which are the implications of the hypotheses of Equations (4-1) and (4-2), are tested:

     $H_o$ : *The aggregate frequencies of the consecutive slices are independent.*

(4-119)

$H_A$ : *The aggregate frequencies of the consecutive slices are correlated.*

(4-120)

A specimen is homogeneous if the null hypothesis is accepted.

2.  To test the hypotheses, the test statistic, which is Spearman–Conley correlation coefficient is specified as follows:

$$R_{sc} = 1 - \frac{6\sum_{i=1}^{n-1} \Delta_i^2}{(n-1)^3 - (n-1)}$$

(4-121)

where $n$ is the number of slice faces, which is 12; and $\Delta_i$ is the $i^{th}$ difference in the ranks of the two series (see Step e).

3.  The level of significance is selected. The selection of the level of significance should be based on the physical significance of homogeneity and the impact of rejecting the null hypothesis of Equation (4-127) on design and performance decisions.

4.  An estimate of the test statistic of Equation (4-121) is computed.

5.  The critical $R_{sc}$ value, which separates the region of rejection from the region of acceptance, is obtained from the table of Spearman-Conley critical values. The critical $R_{sc}$ is obtained by entering the table with the number of pairs of data ($n$-$1$) for the selected level of significance. For an inhomogeneous specimen, the aggregate frequencies of the consecutive slices would be correlated. As the result, $R_{sc}$ would be large and the region of rejection would be represented by the upper tail of the distribution.

6.  The decision on homogeneity of a specimen depends on the comparison of the computed value of the test statistic and the critical value. Any sample $R_{sc}$ value greater than the critical $R_{sc}$ suggests an inhomogeneous specimen.

### 4.5.2   Average Depth Test (Vertical Slice Faces)

The average depth test was suggested by McCuen and Azari (2001) for the measurement of vertical inhomogeneity. The details of the test are provided in Section 2.3.2.7. For that test, the particles larger than 2.35 mm in diameter were sampled on the middle slice face. The particles were then grouped into different area-gradation classes. The distance from the top of the specimen to the center point of each particle was measured, and the average distance for each sieve size was computed. For a homogeneous specimen, the means were expected to be equal to one-half of the specimen height. For an inhomogeneous specimen with the large particles in the lower portion of the specimen, the mean distances for the large sieve sizes was expected to be larger than the mean distances for the smaller sieve sizes. A one-way analysis of variance on the means was used to test for equality of the mean distances. Here, the test is modified for multiple vertical slices and for aggregates larger than 4.75 mm in diameter. The average distance of the centroids of all sampled aggregates to the top of the specimen is computed and compared to the mid-height of the specimen. The one sample t-test is used to measure the significance of the difference between the average depth of the coarse aggregate centroids and the mid-height of the specimen. Prior to applying the test, the required parameters of the t-statistic are computed as follows:

a.  Nine vertical slices at 10-mm spacing are made on each 100-mm diameter specimen. The primary slice face passes through the geometric center of the core.

The slice face at the middle of the specimen provides the largest cross-sectional area; four additional equally spaced slices are made on each side of the middle slice face (see Section 4.3.1).

b.  On each slice face, the centroid of each particle that has a diameter equal to or greater than 4.75 mm is identified.

c.  The distance ($d_{ij}$) of aggregate centroid $j$ to the top of slice face $i$ is measured.

d.  The average distance ($\overline{d}_i$) of the aggregate centroids on slice face $i$ to the top of the slice face is computed as:

$$\overline{d}_i = \frac{1}{n_a} \sum_{j=1}^{n_a} d_{ij} \tag{4-122}$$

where $n_a$ is the number of aggregates on slice face $i$ and $d_{ij}$ is the distance of aggregate centroid $j$ to top of slice face $i$.

e.  The mean ($\overline{d}$) and standard deviation ($s_d$) of the average centroid distances is computed as:

$$\overline{d} = \frac{\sum_{i=1}^{n_{vv}} \overline{d}_i}{n_{vv}} \tag{4-123}$$

$$s_d = \left[ \frac{1}{n_{vv}-1} \sum_{i=1}^{n_{vv}} (\overline{d}_i - \overline{d})^2 \right]^{0.5} \tag{4-124}$$

where $\overline{d}_i$ is the average centroid distance of the aggregates on slice face $i$ and $n_{vv}$ is the number of vertical slice faces.

The six steps of hypothesis testing are followed in order to evaluate homogeneity of a specimen. Using the information obtained above, the steps of hypothesis test using the t-statistic on average centroid distances are as follows:

1. The following hypothesis for the aggregate frequencies, which is an implication of the hypothesis of Equation (4-1) are tested:

$$H_o : \overline{D} = H/2$$  (4-125)

where $\overline{D}$ is the population value of the coarse aggregate centroid distance to top of a specimen and $H$ is the height of the specimen. The specimen is homogeneous if the null hypothesis is accepted. The possible alternative hypotheses for the aggregate locations are provided in Table 4-8. If the coarser gradation is expected to be in the lower portion of the specimen, the alternative hypothesis of Equation (4-127) would be tested. If the coarser gradation is expected to be in the upper portion of the specimen, the alternative hypothesis of Equation (4-128) would be tested. If *a priori* knowledge of the expected location of the coarser gradation were not known, the alternative hypothesis of Equation (4-129) would then be tested.

2. The test statistic is specified as follows:

$$t = \frac{\overline{d} - h_v/2}{s_d / \sqrt{n_{vv}}}$$  (4-126)

**Table 4-8. The alternative hypotheses and the corresponding critical regions for the t-test on mean distance to the top**

| Test for: | $H_A$ | Equation Number | Test | Critical Region |
|---|---|---|---|---|
| **Coarse Material on Bottom** | $\overline{D} > H/2$ | (4-127) | One-tailed upper | $t > t_\alpha$ |
| **Coarse Material on Top** | $\overline{D} < H/2$ | (4-128) | One-tailed lower | $t < -t_\alpha$ |
| **Coarse Material on Top or Bottom** | $\overline{D} \neq H/2$ | (4-129) | Two-tailed | $t < -t_{\alpha/2}$ or $t > t_{\alpha/2}$ |

where $n_{vv}$ is the number of slice faces, which is nine, $h_v$ is the height of specimen, $\overline{d}$ and $s_d$ are the mean and standard deviation of average centroid distances, respectively.

3. The level of significance is selected. The selection of the level of significance should be based on the physical significance of homogeneity and the impact of rejecting the null hypothesis of Equation (4-134) on design and performance decisions.

4. The computed statistical parameters of Equations (4-123) and (4-124) are used to compute an estimate of the test statistic of Equation (4-126).

5. The region of rejection, which consists of those values of the test statistic that would be unlikely to occur when the specimen is homogeneous, is represented by one or both tails of the distribution. The critical $t$ value ($t_\alpha$), which separates the region of rejection from the region of acceptance, is obtained from the t distribution, for the selected level of significance. Table 4-8 provides the regions of rejection that correspond to the possible alternative hypotheses. If the expected locations of the coarser and the finer gradations are known *a priori*, a one-way t-test is utilized. In the case where the coarser gradation expected at the bottom of the specimen, the critical value would be represented by the upper-tail of the distribution. In the case where the coarser gradation expected at the top of the specimen, the critical region would then be represented by the lower tail of the distribution. If the expected locations of the coarser and the finer gradations are not known *a priori*, the critical region would be represented by both the lower and

the upper tails of the distribution but with half of the level of significance in each

tail.

6.  The decision on homogeneity or inhomogeneity of a specimen depends on the

    comparison of the computed value of the test statistic and the critical value. In the

    case of the region of rejection in the upper tail of the distribution, any sample $t$

    value greater than the critical $t$ $(t_\alpha)$ suggests an inhomogeneous specimen. In the

    case of the region of rejection in the lower tail of the distribution, any sample $t$

    value smaller than the critical $t$ $(-t_\alpha)$ suggests an inhomogeneous specimen. In the

    case of the region of rejection in both tails of the distribution, any sample $t$ value

    lower than the lower tail critical $t$ $(-t_{\alpha/2})$ and greater than the upper tail critical $t$

    $(t_{\alpha/2})$ suggest an inhomogeneous specimen.

### 4.5.3   Runs Test (Horizontal Slice Faces)

The runs test on the aggregate frequencies has been suggested by McCuen and

Azari (2001) for evaluation of randomness of the aggregate distribution observed on the

vertical slice face that goes through the diameter of a specimen (the middle slice face).

The slice face was divided into a number of horizontal layers of equal thickness from top

to bottom and the number of particles in each layer was computed. The basis of the test is

the number of times (runs) the aggregate frequency in the layers oscillates between above

and below the median aggregate frequency of all layers. The detailed explanation of the

runs test is provided in Section 2.3.2.6. Here, the test is modified to be applied to multiple

horizontal slice faces. The frequency of aggregates on each slice face is measured and

compared with the median aggregate frequency of all slice faces. Each layer is assigned a

"+" sign if the aggregate frequency of the slice face is greater than the median frequency.

161

A "-" sign is assigned if the measured frequency is smaller than the median frequency. For each specimen, the number of runs ($n_r$), as the index of homogeneity, is defined as the number of times that the signs associated to the slice faces change direction, i.e., from positive to negative and vice versa. For a selected level of significance, the measured number of runs is then compared with the critical number of runs ($n_{r\alpha}$) from the table of runs for complete randomness. Prior to the application of the test, the statistical parameters for computing the runs test statistics are obtained as follows:

a.  Twelve horizontal slices at 10-mm spacing are made on each specimen. The first and the last slice of each portion are taken 15 mm away from the ends of the specimen to allow the large size aggregates to be fully contained within the specimen.

b.  On each slice face, the centroid of each particle that has a diameter greater than 4.75 mm is identified.

c.  The frequency of the coarse aggregate centroids ($f_i$) on each slice face is measured.

d.  The median of the particle frequencies of all slice faces ($f_m$) is obtained. The median is the frequency that half of the slices have frequencies above and half of the slices have frequencies below that.

e.  The frequency of the centroids on each slice face ($f_i$) is compared with the median frequency ($f_m$). A "+" sign is devoted to a slice in which $f_i$ exceeds the median frequency ($f_m$) and a "-" sign is devoted to a slice in which $f_i$ does not exceed $f_m$.

f.  The number of runs ($n_r$) is then computed as the number of times that the signs devoted to the slice faces change direction.

g.  The exceedance ($x_1$) and nonexceedance ($x_2$) frequencies are computed where $x_1$ is

the number of times the slice face frequencies exceed the median and $x_2$ is the

number of times the slice face frequencies do not exceed the median.

The six steps of hypothesis testing are then followed in order to evaluate the

homogeneity of a specimen. Using the information obtained above, the steps of

hypothesis test using the runs statistic are as follows:

1.  The following hypotheses on the randomness of the coarse aggregates in vertical

    direction, which are the implications of the hypotheses of Equations (4-1) and

    (4-2), are tested:

    $H_o$ : *Aggregates are distributed randomly in vertical direction.*          (4-130)

    $H_A$ : *Aggregates are not distributed randomly in vertical direction.*          (4-131)

    A specimen is considered homogeneous if the null hypothesis is accepted.

2.  The test statistic as the number of runs ($n_r$) is specified. The number of runs is the

    number of times the aggregate frequencies oscillates above and below the median

    frequency.

3.  The level of significance is selected. The selection of the level of significance

    should be based on the physical significance of homogeneity and the impact of

    rejecting the null hypothesis of Equation (4-138) on design and performance

    decisions.

4.  An estimate of the test statistic ($n_r$) is obtained (see steps c through f).

5.  The region of rejection, which consists of those values of the test statistic that

    would be unlikely to occur when a specimen is homogeneous, is represented by

    the lower tail of the distribution. In a homogeneous specimen the number of

particles in each slice face is either slightly below or slightly above the median

particle frequency. Therefore, there are frequent shift between "+" and "-" signs.

In a vertically inhomogeneous specimen, where the coarser gradation is vertically

separated from the finer gradation, the number of centroids is significantly below

the median frequency for the slice faces that are placed in the fine graded portion

and significantly above the median in the slice faces placed in the coarse graded

portion. Therefore, there is less number of changes in the direction of signs from

the slice faces. As a result, the critical region would be represented by the lower

tail of the distribution. For the selected level of significance, the exceedance ($x_1$)

and nonexceedance ($x_2$) frequencies (see Step g) are used to determine the critical

runs value from the table of critical runs.

6. The decision on homogeneity of a specimen depends on the comparison of the
computed value of the runs statistic and the critical value. Any sample runs value,
$n_r$, smaller than the critical runs ($n_{r\alpha}$) suggests an inhomogeneous specimen.

Table 4-9 provides a summary of the test statistics for the measurement of all

forms of vertical inhomogeneity, the statistical tests, the corresponding geometric

properties, the equation numbers, and the section numbers where the tests are described.

The tests of  Table 4-9 would be applied to actual specimens only and their accuracy will

be tested in Chapter 6.

**Table 4-9. Indices of all forms of vertical inhomogeneity**

| Slice Face Direction | Statistical Test | Property | Statistical Index | Section Number | Equation |
|---|---|---|---|---|---|
| Horizontal | Spearman Conley | Frequency | $R_{sc} = 1 - \dfrac{6\sum\limits_{i=1}^{n} d_i^2}{n^3 - n}$ | 4.5.1 | (4-121) |
| Vertical | t-test | Centroid Distance to the Top | $t_d = \dfrac{\overline{d} - H/2}{s_d/\sqrt{n}}$ | 4.5.2 | (4-126) |
| Horizontal | Runs | Frequency | $n_r$ (Number of runs) | 4.5.3 | - |

# CHAPTER 5 - DEVELOPMENT OF INDICES OF RADIAL HOMOGENEITY

## 5.1 INTRODUCTION

To test simulated and actual specimens for radial homogeneity, several statistical tests are being introduced. The statistical tests use the six steps of hypothesis testing. The basis of a hypothesis test is the comparison of the sample value of the test statistic with the population value for the condition of complete homogeneity.

The first step in hypothesis testing is to formulate the null hypothesis and one or more hypotheses that reflect the alternative lines of action. The null and the alternative hypotheses are formulated based on the differences between the specific geometric properties of the aggregates in two radial portions of a specimen or based on the differences between specific geometric properties of the entire specimen with the expected values of the same properties for the state of homogeneity. The null hypothesis always reflects homogeneity while the alternative hypothesis reflects inhomogeneity:

$H_o$ : *The specimen is homogeneous.* (5-1)

$H_A$ : *The specimen is inhomogeneous.* (5-2)

The second step of a hypothesis test is the selection of the appropriate theorem that identifies the test statistic. The test statistic should distinguish between the conditions of homogeneity and inhomogeneity.

The third step is to specify the level of significance. It is necessary to select a level of significance that is appropriate for the physical property that is being tested. The level of significance is an indicator of the probability of a certain type of statistical error, namely the probability of rejecting the null hypothesis when, in fact, it is true.

The fourth step of a hypothesis test involves collecting a sample of data and computing an estimate of the test statistic. The collected data include the geometric properties such as the area, frequency, or the location of coarse aggregates measured from slice faces of a specimen.

In the fifth step, the region of rejection of the test statistic, whether in the lower or the upper tail of the distribution function, is defined. The region of rejection is selected based on the test statistic and the nature of property that is measured.

The decision on accepting or rejecting the null hypothesis is made in the sixth step when the sample value of the test statistic is compared with the population test statistic. If the null hypothesis is rejected, then inhomogeneity is assumed.

Several statistical tests are offered for the detection and measurement of radial inhomogeneity. The proposed tests are adopted from the standard tests such as the z, chi-square, and the t-tests. The proposed tests are defined for both horizontal and vertical slice faces. It is important to evaluate the level of agreement between computed test statistics using vertical and horizontal slice faces and to assess the slice face direction that results in a more accurate test statistic.

In addition to the statistical tests mentioned above, three other tests are presented at the end of this chapter that have been defined based on the tests found in literature. The tests will be applied exactly the way they have been proposed by the authors (the inner-outer average diameter test) or they have been specifically modified for test of radial homogeneity (the eccentricity and the moment of inertia tests. Since the critical values of these statistics are not known, the accuracy of the tests would be examined by

comparison of the values of statistics computed from laboratory fabricated homogeneous and inhomogeneous specimens (Chapter 7).

The size of the specimens for testing radial inhomogeneity is 150-mm in diameter and 50-mm in thickness, which is the size requirement for the Superpave shear tester (SST). Use of 150-mm diameter specimens allows evaluation of radial homogeneity of the specimens as they are compacted in the Superpave gyratory compactor. In addition, the specimens can be tested in shear tester and the measured shear properties can be correlated with the computed radial homogeneity indices (Chapter 9).

## 5.2  STATISTICAL TESTS OF RADIAL HOMOGENEITY: HORIZONTAL SLICES

A number of statistical tests are proposed for the detection and measurement of radial inhomogeneity using horizontal slice faces. The tests are adapted from the normal standard z, the chi-square, and the two sample t-tests. The tests include normal z test on aggregate frequency proportions, the chi-square test on aggregate frequencies, the t-test on total aggregate areas, and the t test on aggregate frequencies. The test statistics are computed based on comparison of the geometric properties of coarse aggregates in two radial sampling portions on horizontal slice faces: the ring and the core. The statistical tests examine the significance of the difference between properties of the two portions.

### 5.2.1   Selection of the Horizontal Slices

The selection of the slices for the test of homogeneity was determined with two considerations: First, the slices should be independent; second, the slices should be from the same population. To ensure independency of the slices, McCuen and Azari (2001) showed that 10-mm spacing was required between the slices. To ensure that the slices are

from the same population, the top and bottom slices are located 15 mm away from the

ends of the specimen to allow for large particles to be fully contained within the

specimen. Five mm from the top and 5 mm from the bottom of each gyratory specimen is

trimmed to prepare the specimens for mechanical shear testing. The cutting process

would cause the properties of the slices that are within 14 mm (the diameter of the

maximum aggregate size, which is 19 mm minus the 5 mm that was trimmed) of the

specimen ends to be different from those slices that are located within the specimen. To

resolve this problem, the slices within 15 mm from the ends of the specimens were

disregarded. As a result, three horizontal slices were taken on each 50-mm thick

specimen. The first and the last slices were made 15 mm from the ends of the specimen

and one more slice was taken in the middle of the two slices with 10-mm spacing in

between the slices (Figure 5-1).
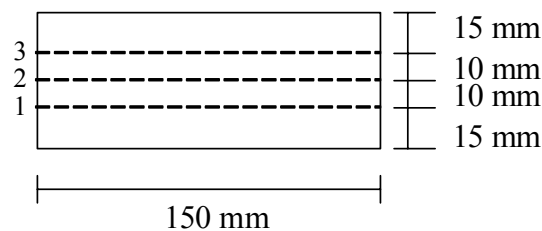


**Figure 5-1. Location of the horizontal slices for evaluation of radial homogeneity**

## 5.2.2    Selection of the Sampling Portions

Statistical testing of radial homogeneity is based on comparison of the geometric

properties of coarse aggregates in the ring and core portions of a cylindrical specimen. To

make this comparison, separate measurements of the aggregate properties in the two

portions are required. Therefore, the boundaries of the ring and core in which the

sampling would take place need to be known. The volume of the coarser and the finer

169

asphalt mixtures in a radially inhomogeneous specimen was used to determine the approximate limits of the ring and the core. The level of radial inhomogeneity that was created resulted in the volume of the coarser mixture to be 1.125 times the volume of the finer mixture (Section 3.4.3). Consequently, the area of the ring was 1.125 times the area of the core on each horizontal slice face. However, to eliminate the bias in statistical sampling from the coarser and the finer gradations the sampling areas were selected to be equal in area. In addition, a transition zone with a thickness of 4.95 mm was located between the core and the ring sampling portions, which was not included in the sampling. This was to ensure distinct statistical population in each sampling area since the coarser and the finer gradations might have been blended during the gyration process. The equal areas of the ring and the core with a consideration of a 4.95-mm transition zone resulted in a core of 101-mm in diameter and a ring of 19.55-mm in thickness (Figure 5-2).

### 5.2.3 Computation of Components of Test Statistics

The computation of test statistics, as the indices of homogeneity, requires measurement of geometric properties of coarse aggregates and computation of their statistical parameters. The steps are explained as follows:

a. The area of the core ($A_{chi}$) and the area of the ring ($A_{rhi}$) on the $i^{th}$ horizontal slice face, which are equal to each other are computed as follows:

$$A_{chi} = A_{rhi} = \pi D_c^2 \Big/ 4$$

(5-3)

where $D_c$ is the diameter of the core, which is 101 mm.

b. The total area of the cores or rings of the three slice faces are computed:

$$A_{ch} = A_{rh} = 3 * A_{chi} = 3 * A_{rhi}$$

(5-4)

170

where $A_{chi}$ and $A_{chi}$ are the areas of the core and ring of the $i^{th}$ slice face.

c.  On the core and ring of horizontal slice $i$, the frequency $(f_{chi}, f_{rhi})$ and total area $(a_{chi}, a_{rhi})$ of the coarse aggregates that have a diameter equal to or greater than 4.75 mm are measured.



$D_c$ = Diameter of the core, 101 mm
$w_R$ = width of the ring, 19.55 mm
$w_T$ = width of the transition zone, 4.95 mm
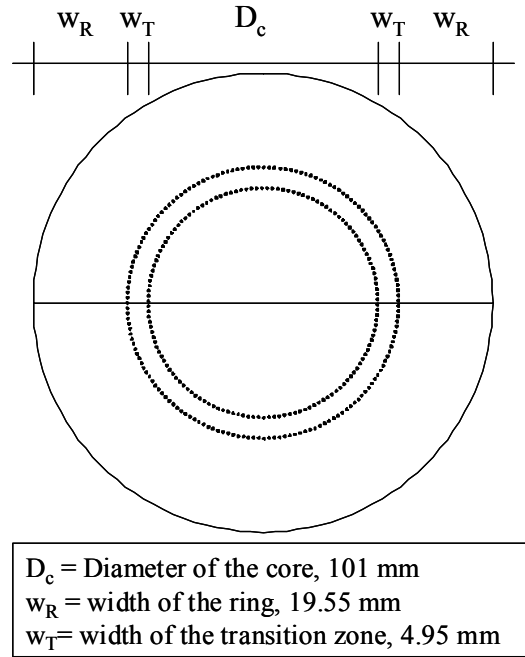
**Figure 5-2. Position of ring, core, and the transition zone**

d.  Total area of the sampling portions on the three slice faces is computed:

$$A_{hh} = A_{ch} + A_{rh} \qquad (5\text{-}5)$$

e.  The ratio of the area of the core or the ring portions to the entire sampling portions of the three slices is as follows:

$$r_{ch} = r_{rh} = \frac{A_{ch}}{A_{hh}} = \frac{A_{rh}}{A_{hh}} = 0.5 \qquad (5\text{-}6)$$

f.  The total frequency of the coarse aggregates on cores of the three slices are computed:

171

$$f_{ch} = \sum_{i=1}^{3} f_{chi}$$

(5-7)

where $f_{chi}$ is the coarse aggregate frequency on the core of the $i^{th}$ slice face, Step c.

g.  The total frequency of the coarse aggregates on the rings of the three slices are computed:

$$f_{rh} = \sum_{i=1}^{3} f_{rhi}$$

(5-8)

where $f_{rhi}$ is the coarse aggregate frequency on the ring of the $i^{th}$ slice, Step c.

h.  The total frequency of the coarse aggregates on entire sampling areas of the three slices are computed:

$$f_{hh} = f_{ch} + f_{rh}$$

(5-9)

where $f_{ch}$ and $f_{rh}$ are the coarse aggregate frequency on the core and ring portions of the three slices (Equations (5-7) and (5-8)). The computed frequency parameters in Steps e through h are utilized by the chi-square test on frequencies.

i.  The total coarse aggregate area on both core and ring of the $i^{th}$ slice face is computed:

$$a_{hhi} = a_{chi} + a_{rhi}$$

(5-10)

where $a_{chi}$ and $a_{rhi}$ were measured in Step c.

j.  The total area of the coarse aggregates on the entire sampling areas of the three slices are computed:

$$a_{hh} = \sum_{i=1}^{3} a_{hhi}$$

(5-11)

where $a_{hhi}$ is the total coarse aggregate area on both core and ring of the $i^{th}$ slice (Equation (5-10)).

k.  The mean area of coarse aggregate ($\bar{a}_{hh}$) is computed as follows:

$$\bar{a}_{hh} = \frac{a_{hh}}{f_{hh}}$$

(5-12)

where $a_{hh}$ and $f_{hh}$ are the total area and total frequency of the coarse aggregates on the entire sampling areas of the three slices (Equations (5-11) and (5-9), respectively).

l.  The expected maximum frequencies on the core and ring portions ($x_{ch}$, $x_{rh}$) are computed as follows:

$$x_{ch} = x_{rh} = \frac{A_{ch}}{\bar{a}_{hh}} = \frac{A_{rh}}{\bar{a}_{hh}}$$

(5-13)

where $A_{ch}$ and $A_{rh}$ are the total area of three cores or three rings (Equation (5-4)), and $\bar{a}_{hh}$ is the mean area of coarse aggregate (Equation (5-12)).

m.  The frequency proportions of the coarse aggregates in the core, ring, and both portions of slice faces are computed as follows:

$$\hat{p}_{ch} = \frac{f_{ch}}{x_{ch}}$$

(5-14)

$$\hat{p}_{rh} = \frac{f_{rh}}{x_{rh}}$$

(5-15)

$$\hat{p}_{hh} = \frac{f_{rh} + f_{ch}}{x_{rh} + x_{ch}}$$

(5-16)

where $f_{ch}$ and $f_{rh}$ are total frequency of the coarse aggregates on the core and on the ring portions of three slice faces (Equations (5-7) and (5-8)); $x_{ch}$ and $x_{rh}$ are the expected maximum frequencies in the core and ring portions (Equation (5-13)).

The computed parameters in Steps (5-13) through (5-16) are used in the z test on frequency proportions.

n.  The mean and the standard deviation of the coarse aggregate frequencies observed on the three rings ($\overline{f}_r$, $s_{fr}$) and the three cores ($\overline{f}_c$, $s_{fc}$) are computed:

$$\overline{f}_r = \frac{1}{n_{rh}} \sum_{i=1}^{n_{rh}} f_{rhi} \tag{5-17}$$

$$s_{fr} = \left[ \frac{1}{n_{rh} - 1} \sum_{i=1}^{n_{rh}} (f_{rhi} - \overline{f}_r)^2 \right]^{0.5} \tag{5-18}$$

$$\overline{f}_c = \frac{1}{n_{ch}} \sum_{i=1}^{n_{ch}} f_{chi} \tag{5-19}$$

$$s_{fc} = \left[ \frac{1}{n_{ch} - 1} \sum_{i=1}^{n_{ch}} (f_{chi} - \overline{f}_c)^2 \right]^{0.5} \tag{5-20}$$

where $f_{rhi}$ and $f_{chi}$ are the coarse aggregate frequencies on the core and ring areas of the $i^{th}$ slice face (Step c); $n_{rh}$ and $n_{ch}$ are the number of rings and core portions, which are three. The computed statistics are utilized by the t-test on frequency.

o.  The mean and standard deviation of total aggregate areas on the rings ($\overline{a}_r$, $s_{ar}$) and on the cores ($\overline{a}_c$, $s_{ac}$) of the three slice faces are computed:

$$\overline{a}_r = \frac{1}{n_{rh}} \sum_{i=1}^{n_{rh}} a_{rhi} \tag{5-21}$$

$$s_{ar} = \left[ \frac{1}{n_{rh} - 1} \sum_{i=1}^{n_{rh}} (a_{rhi} - \overline{a}_r)^2 \right]^{0.5} \tag{5-22}$$

$$\overline{a}_c = \frac{1}{n_{ch}} \sum_{i=1}^{n_{ch}} a_{chi} \tag{5-23}$$

174

$$S_{ac} = \left[ \frac{1}{n_{ch} - 1} \sum_{i=1}^{n_{ch}} (a_{chi} - \bar{a}_c)^2 \right]^{0.5}$$

(5-24)

where $a_{rhi}$ and $a_{chi}$ are the total coarse aggregate areas on the ring and on the core areas of the $i^{th}$ slice face (Step c); and $n_{rh}$ and $n_{ch}$ are the number of rings and core portions, which are three. The computed statistics are utilized by the t-test on total aggregate area.

### 5.2.4 Hypothesis Testing Using Suggested Test Statistics

The statistical hypothesis testing are conducted using the z-test on aggregate frequency proportions, the chi-square test on aggregate frequencies, the t-tests on total aggregate areas, and the t-tests on frequencies using horizontal slice faces. The six steps of hypothesis testing are followed in order to measure homogeneity of a specimen. In the following sections the steps of hypothesis tests for testing radial inhomogeneity using horizontal slice faces are explained:

#### 5.2.4.1 Standard Normal Proportion Test

The standard normal proportion test is adapted for the measurement of radial homogeneity. The test is used for comparison of the frequency proportions of coarse aggregates on the ring and on the core of the horizontal slice faces. The procedure for making the decision on homogeneity of a specimen using standard normal proportion statistic ($z$) follows the six steps of hypothesis test:

1. The following hypotheses for the aggregate frequency proportions, which are the implications of the hypotheses of Equations (5-1) and (5-2) are tested:

$$H_o : \bar{P}_r = \bar{P}_c$$

(5-25)

175

$$H_o : \overline{P_r} > \overline{P_c} \tag{5-26}$$

where $\overline{P_r}$ and $\overline{P_c}$ are the population values of the coarse aggregate frequency proportion on the ring and on the core of a specimen, respectively. A specimen is considered homogeneous if the null hypothesis is accepted.

2.  The proportion test statistic, z, is computed:

$$z_{hh} = \frac{\hat{P}_{rh-} \hat{P}_{ch}}{S_{phh}} \tag{5-27}$$

where $z_{hh}$ is the value of a random variable having a standard normal distribution; $\hat{p}_{rh}$ and $\hat{p}_{ch}$ are the coarse aggregate frequency proportions (Equations (5-15) and (5-14)); and $s_{phh}$ is the pooled sample standard deviation, which is defined as follows:

$$S_{phh} = \left[ \hat{p}_{hh}(1 - \hat{p}_{hh})(\frac{1}{x_{rh}} + \frac{1}{x_{ch}}) \right]^{0.5} \tag{5-28}$$

where $\hat{p}_{hh}$ is the proportion of coarse aggregate frequency in the ring and core, (Equation (5-16)); $x_{rh}$ and $x_{ch}$ are the maximum expected frequency of the coarse aggregates on the rings and on the cores (Equation (5-13)).

3.  The level of significance is selected. The selection of the level of significance should be based on the physical significance of homogeneity and the impact of rejecting the null hypothesis of Equation (5-25) on design and performance decisions.

4.  The measured and computed geometric properties of the coarse aggregates (Equations (5-13) through (5-16)) are used to compute both an estimate of the test

statistic of Equation (5-27) and the statistical parameter that is required to define the sampling distribution of the test statistic (Equation (5-28)).

5. The region of rejection, which consists of those values of the test statistic that would be unlikely to occur when the specimen is homogeneous, is determined by the alternative hypothesis of Equation (5-26). For the radially inhomogeneous specimens the coarser gradation is located in the ring of the specimen therefore, the region of rejection is represented by the upper-tail of the distribution. The critical $z_{hh}$ value, at the upper tail of the distribution, separates the region of rejection from the region of acceptance and is obtained from the distribution of $z_{hh}$ statistic for the selected level of significance.

6. The decision on homogeneity of a specimen depends on comparison of the computed value of the test statistic and the critical value. With the region of rejection in the upper tail of the distribution, any sample $z_{hh}$ value greater than the critical value ($z_{hh\alpha}$) suggests an inhomogeneous specimen.

### 5.2.4.2   *Two-Sample chi-Square Test on Frequencies*

The two-sample chi-square test on frequencies is used to test the radial homogeneity by comparing the frequencies of the aggregates in the coarser and the finer portions of the specimen with the expected frequency of a homogeneous specimen. It is hypothesized that the frequency of the coarse aggregates in the ring and in the core portions of the radially inhomogeneous specimen is significantly different from the expected frequency of the aggregates for those portions. The procedure for the two-sample chi-square test on frequencies is as follows:

1. The following null and alternative hypotheses, which are the implications of the hypotheses of Equations (5-1) and (5-2) are tested:

   $H_o$ : *The observed frequencies on the ring and on the core are equal to the mean*

   *frequency.* (5-29)

   $H_A$ : *The observed frequency of at least the ring or the core is different from the*

   *mean frequency.* (5-30)

   A specimen is considered homogeneous if the null hypothesis is accepted.

2. The chi-square test statistic, as the index of homogeneity of the specimen, is computed:

$$\chi^2_{hh} = \frac{(f_{rh} - f_{hh}r_{rh})^2}{f_{hh}r_{rh}(1 - r_{rh})} + \frac{(f_{ch} - f_{hh}r_{ch})^2}{f_{hh}r_{ch}(1 - r_{ch})}$$

(5-31)

   in which $f_{ch}, f_{rh}, f_{hh}$ are the total coarse aggregate frequencies on the cores, rings, and on the entire sampling areas of all three slices (Equations (5-7) through (5-9)); $r_{ch}$ and $r_{hh}$ are the ratios of the core and ring areas to the entire sampling areas (Equation (5-6)).

3. The level of significance is selected. The selection of the level of significance should be based on the physical significance of homogeneity and the impact of rejecting the null hypothesis of Equation (5-29) on mechanical performance of asphalt mixtures.

4. The measured and computed data on the geometric properties of the coarse aggregates (Equations (5-7) through (5-9)), are used to compute an estimate of the test statistic of Equation (5-31).

5. From the distribution of the chi-square statistic, for the selected level of significance, the critical chi-square value ($\chi^2_{hh\alpha}$) is determined. For an inhomogeneous specimen the difference between the observed aggregate frequency and the expected aggregate frequency in the coarser and the finer portions is significant. Therefore, the region of rejection would be represented by the upper tail of the distribution.

6. The decision on homogeneity of a specimen depends on the comparison of the computed value of the test statistic and the critical value. Any chi-square value greater than the critical value suggests an inhomogeneous specimen.

### 5.2.4.3  Two-Sample t-Test on Total Aggregate Areas

The assessment of the difference in total area of the coarse aggregates observed on the ring and on the core portions of the horizontal slice faces of a specimen will indicate homogeneity. It is hypothesized that the mean of the total coarse aggregate areas on the rings of an inhomogeneous specimen is greater than the mean of the total coarse aggregate areas on the cores. A two-sample t-test is used to assess the difference between the two means. The procedure for making a decision on radial homogeneity of a specimen using the t-statistic on total coarse aggregate area follows the six steps of hypothesis test:

1. The following hypotheses for the coarse aggregate total area, which are the implications of the hypotheses of Equations (5-1) and (5-2) are tested:

$$H_o : \overline{A}_r = \overline{A}_c \tag{5-32}$$

$$H_A : \overline{A}_r > \overline{A}_c \tag{5-33}$$

where $\overline{A}_r$ and $\overline{A}_c$ are the population values of the total coarse aggregate areas from the ring and the core, respectively. A specimen is considered homogeneous if the null hypothesis is accepted.

2. The t statistics is:

$$t_{ah} = \frac{\overline{a}_r - \overline{a}_c}{s_{ah}(\frac{1}{n_{rh}} + \frac{1}{n_{ch}})^{0.5}}$$

(5-34)

in which $t_{ah}$ is the index of homogeneity that is a random variable having a $t$ distribution with degrees of freedom of $(n_{rh} + n_{ch} - 2)$; $n_{rh}$ and $n_{ch}$ are the number of the rings and the cores, which are equal to three; $\overline{a}_r$ and $\overline{a}_c$ are the means of the total coarse aggregate areas on the rings and on the cores (Equations (5-21) and (5-23), respectively); and $s_{ah}$ is the square root of the pooled variance given by:

$$s_{ah}^2 = \frac{(n_{rh} - 1)s_{ar}^2 + (n_{ch} - 1)s_{ac}^2}{n_{rh} + n_{ch} - 2}$$

(5-35)

in which $s_{ar}^2$ and $s_{ac}^2$ are the variances of the total coarse aggregate areas in the rings and in the cores (Equations (5-22) and (5-24)).

3. The level of significance is selected. The selection of the level of significance should be based on the physical significance of homogeneity and the impact of rejecting the null hypothesis of Equation (5-32) on the design and performance decisions.

4. The measured and computed data on the geometric properties of the coarse aggregates (Equations (5-21) through (5-24)) are used to compute both an estimate of the test statistic of Equation (5-34) and the statistical parameter that is required to define the sampling distribution of the test statistic (Equation (5-35)).

5. For a radially inhomogeneous specimen, the total area of the coarse aggregates in the ring is greater than the total area of the coarse aggregates in the core. Therefore, the region of rejection that corresponds to the alternative hypothesis of Equation (5-33) is represented by the upper tail of the distribution. The critical $t_{ah}$ value ($t_{ah\alpha}$), which separates the region of rejection from the region of acceptance, is obtained from the distribution of $t_{ah}$ statistic for the selected level of significance.

6. The decision on homogeneity of a specimen depends on the comparison of the computed value of the test statistic with the critical value. For the region of rejection in the upper tail of the distribution, any $t_{ah}$ value greater than the critical value ($t_{ah\alpha}$) is assumed to indicate an inhomogeneous specimen.

### 5.2.4.4 *Two-Sample t-Test on Frequencies*

A two-sample t-test is utilized to compare the mean frequency of the coarse particles in the ring and in the core of the horizontal slice faces. It is hypothesized that the coarse particle frequency in the ring portion of an inhomogeneous specimen is significantly greater than the coarse particle frequency in the core portion. The procedure for measuring radial inhomogeneity using t-statistic on aggregate frequencies follows the six steps of hypothesis test:

1. The following hypotheses for the coarse aggregate frequency, which are the implications of the hypotheses of Equations (5-1) and (5-2) are tested:

$$H_o : \overline{F}_r = \overline{F}_c \qquad\qquad (5\text{-}36)$$

$$H_A : \overline{F}_r > \overline{F}_c \qquad\qquad (5\text{-}37)$$

where $\overline{F}_r$ and $\overline{F}_c$ are the population values of the mean coarse aggregate frequencies in the rings and the in cores, respectively. A specimen is considered homogeneous if the null hypothesis is accepted.

2.  The t statistics is:

$$t_{fh} = \frac{\overline{f}_r - \overline{f}_c}{s_{fh}(\frac{1}{n_{rh}} + \frac{1}{n_{ch}})^{0.5}}$$

(5-38)

in which $t_{fh}$ is the index of homogeneity which is a random variable having a $t$ distribution with degrees of freedom of $(n_{rh} + n_{ch} - 2)$; $\overline{f}_r$ and $\overline{f}_c$ are the mean coarse aggregate frequencies in the ring and in the core (Equations (5-17) and (5-19)); $n_{rh}$ and $n_{ch}$ are the number of rings and cores, which are equal to three; and $s_{fh}$ is the square root of the pooled variance given by:

$$s_{fh}^2 = \frac{(n_{rh} - 1)s_{fr}^2 + (n_{ch} - 1)s_{fc}^2}{n_{rh} + n_{ch} - 2}$$

(5-39)

in which $s_{fr}^2$ and $s_{fc}^2$ are the variances of the coarse aggregate frequencies on the rings and on the cores (Equations (5-18) and (5-20)).

3.  The level of significance is selected. The selection of the level of significance should be based on the physical significance of homogeneity and the impact of rejecting the null hypothesis of Equation (5-36) on the design and performance decisions.

4.  The measured and computed geometric properties of the coarse aggregates, Equations (5-17) through (5-20), are used to compute both an estimate of the test

statistic of Equation (5-38) and the statistical parameter that is required to define the sampling distribution of the test statistic (Equation (5-39)).

5. The region of rejection that corresponds to the alternative hypotheses of Equation (5-37) is represented by the upper tail of the distribution. The critical $t_{fh}$ value ($t_{fh\alpha}$), which separates the region of rejection from the region of acceptance, is obtained from the distribution of $t_{fh}$ statistic for the selected level of significance.

6. The decision on homogeneity of a specimen depends on the comparison of the computed value of the test statistic with the critical value. For the region of rejection in the upper tail of the distribution, any $t_{fh}$ value greater than the critical value ($t_{fh\alpha}$) is assumed to indicate an inhomogeneous specimen.

Table 5-1 provides a summary of the test statistics for the measurement of radial inhomogeneity using horizontal slice faces, the statistical tests, the corresponding geometric properties, the equation numbers, and the section numbers where the tests are described. The tests will be applied to both simulated and actual specimens and their accuracy will be tested in Chapters 6 and 7.

## 5.3 STATISTICAL TESTS OF RADIAL HOMOGENEITY: VERTICAL SLICES

The tests of radial inhomogeneity using horizontal slice faces are also applied to vertical slice faces. The standard normal z test, the chi-square test, and the t-tests are used to examine the significance of the difference between the aggregate properties in the ring and core portions of vertical slice faces of the specimens.

**Table 5-1. Standard tests of radial inhomogeneity using horizontal slice faces**

| Statistical Test | Property | Statistical Index | Section Number | Equation Number |
|---|---|---|---|---|
| Standard Normal z | Frequency Proportions | $z_{hh} = \dfrac{\hat{p}_{rh-}\hat{p}_{ch}}{s_{phh}}$ | 5.2.4.1 | (5-27) |
| | | $s_{phh} = \left[ \hat{p}_{hh}(1-\hat{p}_{hh})(\dfrac{1}{x_{rh}} + \dfrac{1}{x_{ch}}) \right]^{0.5}$ | | (5-28) |
| Two-Sample Chi-Square | Frequencies | $\chi_{hh}^2 = \dfrac{(f_{rh} - f_{hh}r_{rh})^2}{f_{hh}r_{rh}(1-r_{rh})} + \dfrac{(f_{ch} - f_{hh}r_{ch})^2}{f_{hh}r_{ch}(1-r_{ch})}$ | 5.2.4.2 | (5-31) |
| Two-Sample t-Test | Total Aggregate Areas | $t_{ah} = \dfrac{\bar{a}_r - \bar{a}_c}{s_{ah}(\dfrac{1}{n_{rh}} + \dfrac{1}{n_{ch}})^{0.5}}$ | 5.2.4.3 | (5-34) |
| | | $s_{ah}^{\;2} = \dfrac{(n_{rh}-1)s_{ar}^2 + (n_{ch}-1)s_{ac}^2}{n_{rh} + n_{ch} - 2}$ | | (5-35) |
| Two-Sample t-Test | Frequencies | $t_{fh} = \dfrac{\bar{f}_r - \bar{f}_c}{s_{fh}(\dfrac{1}{n_{rh}} + \dfrac{1}{n_{ch}})^{0.5}}$ | 5.2.4.4 | (5-38) |
| | | $s_{fh}^{\;2} = \dfrac{(n_{rh}-1)s_{fr}^2 + (n_{ch}-1)s_{fc}^2}{n_{rh} + n_{ch} - 2}$ | | (5-39) |

The application of the tests to the vertical slice faces requires the adjustment of several of the measured geometric properties relative to the cross-sections of the vertical slice faces that vary with the location of the slices. The unequal area of slice faces mainly affects the t-test, which uses the mean and standard deviation of the measured properties. The changing cross-sectional area does not affect the z and the chi-square statistics, since they use the summation of the measured properties.

To account for the unequal slice face areas, the geometric properties that are used by the t-test are divided by the area from which they are sampled. The computed properties are then referred to as the frequency density and the area proportion.  The t-test on the two adjusted properties, the standard normal z test on aggregate frequency proportions, and the chi-square test on aggregate frequencies are used to examine the significance of the difference between the aggregate properties in the ring and core portions of vertical slice faces of specimens.

## 5.3.1    Selection of Sampling Areas

On each vertical slice face three vertical strips representing the core and the ring of a specimen were selected. The height of the strips is equal to the height of the specimen, which is 50 mm. The widths of the strips on the middle slice face are determined by the width of the ring and the diameter of the core. Based on the discussion in Section 5.2.2, on the slice face that goes through the diameter of a specimen, the width of each ring strip would be 19.55 mm and the width of the core strip would be 101 mm. Two 4.95-mm strips were allowed between the core and the ring strips as the transition zone (Figure 5-3).

For the other slices, the width of a slice face along with the widths of the ring and core strips change according to the distance of the slice face from the middle of specimen. The following general relationships are used to determine the width of the $i^{th}$ slice face ($w_{hi}$), the middle strip ($w_{ci}$) that represents the core and the width of each side strip ($w_{ri}$) that represents the ring on the $i^{th}$ slice face:

$$w_{hi} = 2\sqrt{R_h^2 - d_i^2}$$

(5-40)

$$w_{ci} = 2\sqrt{R_c^2 - d_i^2}$$ (5-41)

$$w_{ri} = \sqrt{R_h^2 - d_i^2} - \sqrt{R_t^2 - d_i^2}$$ (5-42)

$$w_{ti} = \sqrt{R_t^2 - d_i^2} - \sqrt{R_c^2 - d_i^2}$$ (5-43)

where $R_h$ is the radius of the specimen, which is 75 mm; $R_c$ is the radius of the core, which is 50.5 mm; $d_i$ is the distance between the $i^{th}$ slice face and the middle slice face measured along a radii that is perpendicular to the slice faces; $R_t$ is the radius of a circle limited by the outer boundary of the transition zone, which is 55.45 mm; and $w_{ti}$ is the width of the transition zone (see Figure 5-4).
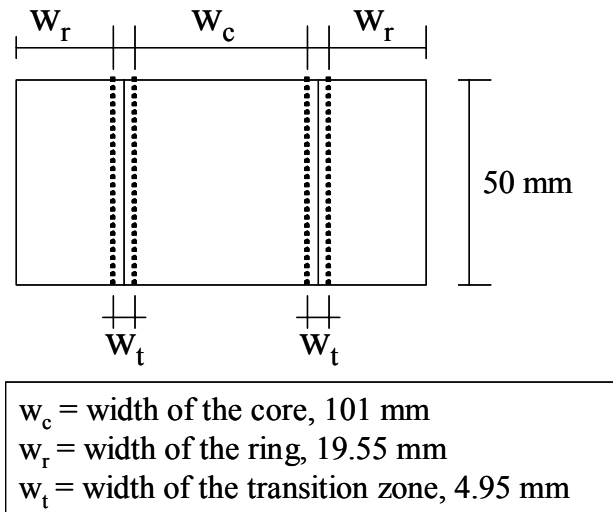


Figure 5-3. **The widths of the sampling areas over the core and the ring portions on the middle slice face**

## 5.3.2 Selection of the Vertical Slices

To determine the location and the number of vertical slice faces, two factors were considered: First, independency of the slices and second, adequacy of the sampling areas on each slice face. To ensure independency of the vertical slices, McCuen and Azari

186

(2001) showed that 10-mm spacing was required between the slices. To ensure adequacy of the sampling areas, the smallest cross-section that is used for the homogeneity sampling should have a core width not smaller than the diameter of the largest size aggregate. The middle slice face that has the largest cross-section includes 19.55-mm ring strip at each side and a 101-mm core strip in the middle of the cross-section (Figure 5-3).



$w_{hi}$ = width of the slice i
$w_{ci}$ = width of the core i
$w_{ri}$ =width of the ring i
$w_{ti}$= width of the transition zone i
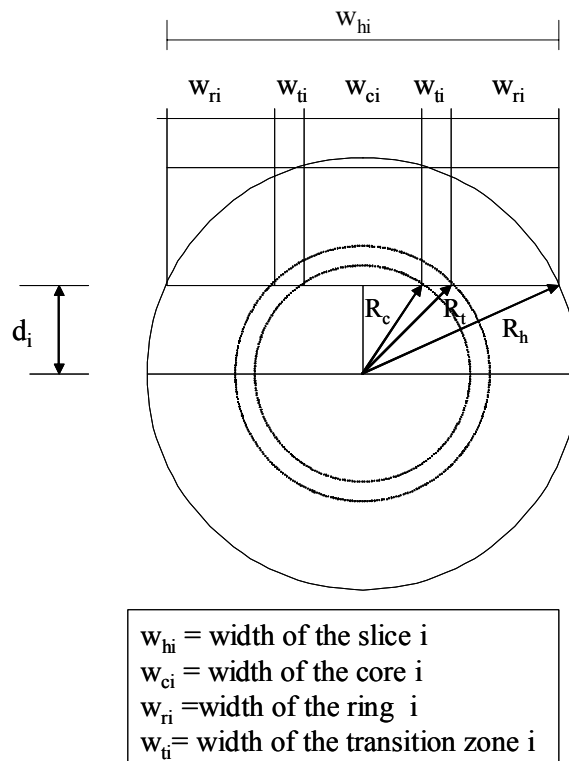
**Figure 5-4. Schematic top view of the width of the core, transition zone, and the ring of an arbitrary slice**

The largest aggregate with a 19 mm diameter can fit in either of the rings or the core portions of this slice face. As the distance of a slice face from the middle of the specimen increases, the width of the ring strips slightly increase allowing better accommodation of the aggregates in the ring portions. Simultaneously, the width of the core strip decreases; which would eventually make it impossible to fit a coarse aggregate in the core strip.

Therefore, the location of the furthest slice face should be controlled by the width of the core strip. In order for the core to hold the largest size aggregate, the width of the core should not be smaller than the diameter of the largest aggregate, which is 19 mm. Based on the geometry of the circular cross-section (see Figure 5-4), a core width of 19 mm would correspond to the distance of 49 mm from the middle slice face. Therefore, considering 10-mm spacing between the slices would result in nine vertical slices at a 10-mm spacing on a 150-mm diameter specimen. The primary slice face passes through the geometric center of the specimen. The eight additional slices are made at both sides of the middle slice face at 10, 20, 30, and 40 mm from the middle slice face (Figure 5-5).

### 5.3.3    Computation of Components of Test Statistics

The computation of test statistics, as the indices of homogeneity, requires measurement of geometric properties of coarse aggregates and computation of selected statistical parameters. The steps are explained as follows:

a.  The area of the ring and the core strips on each slice face is computed as:

$$A_{rvi} = 2h_h w_{ri}$$
(5-44)

$$A_{cvi} = h_h w_{ci}$$
(5-45)

where $h_h$ is the height of the slice face, which is 50 mm; $w_{ri}$ is the width of each ring strip on the $i^{th}$ slice face and $w_{ci}$ is the width of the core strip on the $i^{th}$ slice face (Equations (5-42) and (5-41)), respectively.

b.  The total area of the ring and core portions on nine slice faces are computed as:

$$A_{rv} = 2h_h \sum_{i=1}^{n_{rv}} w_{ri}$$
(5-46)

188

$$A_{cv} = h_h \sum_{i=1}^{n_{cv}} w_{ci} \qquad (5\text{-}47)$$

where $h_h$ is the height of the slice faces, which is 50 mm; $w_{ri}$ and $w_{ci}$ are the widths of the ring and core strips (Equations (5-42) and (5-41), respectively); and $n_{rv}$ and $n_{cv}$ are the number of rings and cores, which are nine.
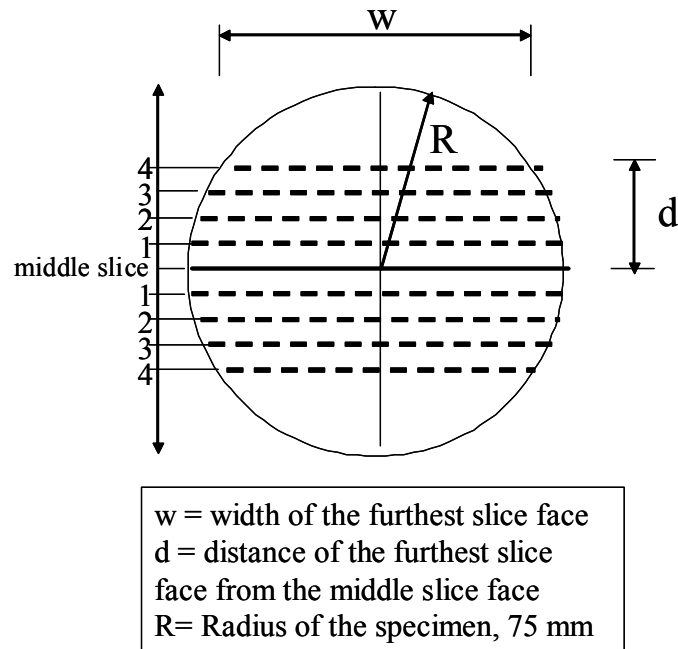


**Figure 5-5. Location of the slice faces within the allowable distance "d" from the middle slice face.**

c.  The total area of the sampling portions on all nine slices is computed as:

$$A_{vh} = A_{rv} + A_{cv} \qquad (5\text{-}48)$$

where $A_{rv}$ and $A_{cv}$ are the areas of the ring and core portions on nine slice faces (Equations (5-46) and (5-47)).

d.  On the two rings and the core strips (see Figure 5-3), the frequency ($f_{r1i}, f_{r2i}, f_{cvi}$) and the total areas ($a_{r1i}, a_{r2i}, a_{cvi}$) of the coarse aggregates that have a diameter

189

equal to or greater than 4.75 mm are measured, where the subscripts *1*, *2* represent ring 1 strip and ring 2 strip.

e.   The aggregate properties measured on the two ring strips ($f_{r1i}, f_{r2i}$ and $a_{r1i}, a_{r2i}$) are summed to obtain the aggregate properties in the ring:

$$f_{rvi} = f_{r1i} + f_{r2i} \tag{5-49}$$

$$a_{rvi} = a_{r1i} + a_{r2i} \tag{5-50}$$

f.   The total frequency of the coarse aggregates on the ring strips and core strips of the nine slices are computed by:

$$f_{rv} = \sum_{i=1}^{n_{rv}} f_{rvi} \tag{5-51}$$

$$f_{cv} = \sum_{i=1}^{n_{cv}} f_{cvi} \tag{5-52}$$

where $f_{rvi}, f_{cvi}$ are the frequencies of the coarse aggregates on the ring and core portions of the $i^{th}$ slice (Steps e and d); and $n_{rv}$ and $n_{cv}$ are the number of rings and cores, which are nine.

g.   The total frequency of the coarse aggregates on entire sampling portions of the nine slices are computed as:

$$f_{vh} = f_{rv} + f_{cv} \tag{5-53}$$

where $f_{rv}$ and $f_{cv}$ are the frequencies of the coarse aggregates on the ring and core portions of the nine slice faces (Equations (5-51) and (5-52)).

h.   The ratios of the ring and core areas to the area of the entire sampling portions of the nine vertical slices are computed as:

$$r_{rv} = \frac{A_{rv}}{A_{vh}} \tag{5-54}$$

$$r_{cv} = \frac{A_{cv}}{A_{vh}} \tag{5-55}$$

where $A_{rv}$, $A_{rc}$, and $A_{vh}$ are the total areas of the rings, cores, and entire sampling

portions of the nine slices (Equations (5-46) through (5-48)). The parameters of

Steps f through h are used for the computation of the chi-square statistics.

i.   The total area of the coarse aggregates on the ring strips and on the core strips of

the nine slices are computed:

$$a_{rv} = \sum_{i=1}^{n_{rv}} a_{rvi} \tag{5-56}$$

$$a_{cv} = \sum_{i=1}^{n_{cv}} a_{cvi} \tag{5-57}$$

where $a_{rvi}$ and $a_{cvi}$ are the total areas of the coarse aggregates on the ring and core

portions of the $i^{th}$ slice (Steps e and d); and $n_{rv}$ and $n_{cv}$ are the number of rings and

cores, which are nine.

j.   The total area of coarse aggregates from the entire sampling portions of the nine

slices is computed by:

$$a_{vh} = a_{rv} + a_{cv} \tag{5-58}$$

where $a_{rv}$ and $a_{cv}$ are the total areas of coarse aggregates on the ring and core

portions of the nine vertical slice faces (Equations (5-56) and (5-57)).

k.   The mean area of coarse aggregate ($\bar{a}_{vh}$) is computed as follows:

$$\bar{a}_{vh} = \frac{a_{vh}}{f_{vh}} \tag{5-59}$$

where $a_{vh}$ and $f_{vh}$ are the total area and total frequency of the coarse aggregates on both ring and core sampling portions of nine vertical slices (Equations (5-58) and (5-53)).

l. The expected maximum frequencies ($x_{rv}$, $x_{cv}$) on the ring and the core portions are computed as follows:

$$x_{rv} = \frac{A_{rv}}{\overline{a}_{vh}}$$ 

(5-60)

$$x_{cv} = \frac{A_{cv}}{\overline{a}_{vh}}$$

(5-61)

where $A_{rv}$ and $A_{cv}$ are the total area of ring and core portions of nine slices (Equations (5-46) and (5-47)); $\overline{a}_{vh}$ is the mean area of the coarse aggregates (Equation (5-59)).

m. The frequency proportions of the coarse aggregates in the ring, core, and both portions of the slices are computed as follows:

$$\hat{p}_{rv} = \frac{f_{rv}}{x_{rv}}$$

(5-62)

$$\hat{p}_{cv} = \frac{f_{cv}}{x_{cv}}$$

(5-63)

$$\hat{p}_{vh} = \frac{f_{rv} + f_{cv}}{x_{rv} + x_{cv}}$$

(5-64)

where $f_{rv}$ and $f_{cv}$ are the total frequency of the coarse aggregates in the ring and the core portions (Equations (5-51) and (5-52)); $x_{rv}$ and $x_{cv}$ are the expected maximum frequencies on the ring and the core portions (Equation (5-60) and (5-61)). The computed parameters are used in the normal frequency proportion test.

n. The aggregate frequency densities in the ring portion ($f_{dri}$) and core portion ($f_{dci}$) of the $i^{th}$ slice face are computed as follows:

$$f_{dri} = \frac{f_{rvi}}{A_{rvi}}$$

(5-65)

$$f_{dci} = \frac{f_{cvi}}{A_{cvi}}$$

(5-66)

where $f_{rvi}$ and $f_{cvi}$ are the aggregate frequencies in the ring and core portions of the $i^{th}$ slice face, which were measured in Steps e and d, respectively; $A_{rvi}$ and $A_{cvi}$ are the areas of the ring and the core portions of the $i^{th}$ vertical slice face (Equations (5-44) and (5-45)).

o. The means and standard deviations of the aggregate frequency densities in the ring ($\overline{f}_{dr}$, $s_{fdr}$) and core portions ($\overline{f}_{dc}$, $s_{fdc}$) of nine slice faces are computed as follows:

$$\overline{f}_{dr} = \frac{1}{n_{rv}} \sum_{i=1}^{n_{rv}} f_{dri}$$

(5-67)

$$s_{fdr} = \left[ \frac{1}{n_{rv}-1} \sum_{i=1}^{n_{rv}} (f_{dri} - \overline{f}_{dr})^2 \right]^{0.5}$$

(5-68)

$$\overline{f}_{dc} = \frac{1}{n_{cv}} \sum_{i=1}^{n_{cv}} f_{dci}$$

(5-69)

$$s_{fdc} = \left[ \frac{1}{n_{cv}-1} \sum_{i=1}^{n_{cv}} (f_{dci} - \overline{f}_{dc})^2 \right]^{0.5}$$

(5-70)

where $f_{dri}$ and $f_{dci}$ are computed using Equations (5-65) and (5-66); $n_{rv}$ and $n_{cv}$ are the number of rings and cores, which are nine. The computed means and standard deviations are used in t-test on frequency density.

p.  The aggregate area proportions in the ring portion ($a_{pri}$) and in the core portion ($a_{pci}$) of the $i^{th}$ slice face are computed as follows:

$$a_{pri} = \frac{a_{rvi}}{A_{rvi}}$$  (5-71)

$$a_{pci} = \frac{a_{cvi}}{A_{cvi}}$$  (5-72)

where $a_{rvi}$ and $a_{cvi}$ are the total aggregate areas in the ring and the core portions of the $i^{th}$ slice face (Steps e and d), $A_{rvi}$ and $A_{cvi}$ are the areas of the ring and the core portions of the $i^{th}$ vertical slice face (Equations (5-44) and (5-45)).

q.  The means and standard deviations of total aggregate area proportions in the ring ($\bar{a}_{pr}$, $s_{apr}$) and in the core portions ($\bar{a}_{pc}$, $s_{apc}$) of the slice faces are computed as follows:

$$\bar{a}_{pr} = \frac{1}{n_{rv}} \sum_{i=1}^{n_{rv}} a_{pri}$$  (5-73)

$$s_{apr} = \left[ \frac{1}{n_{rv}-1} \sum_{i=1}^{n_{rv}} (a_{pri} - \bar{a}_{pr})^2 \right]^{0.5}$$  (5-74)

$$\bar{a}_{pc} = \frac{1}{n_{cv}} \sum_{i=1}^{n_{cv}} a_{pci}$$  (5-75)

$$s_{apc} = \left[ \frac{1}{n_{cv}-1} \sum_{i=1}^{n_{cv}} (a_{pci} - \bar{a}_{pc})^2 \right]^{0.5}$$  (5-76)

where $a_{pri}$ and $a_{pci}$ are the aggregate area proportions in the ring portion and in the core portion of the $i^{th}$ slice face (Equations (5-71) and (5-72)), respectively; and $n_{rv}$ and $n_{cv}$ are the number of ring and core portions, which are nine. The computed means and standard deviations are used in t-test on total area proportion.

### 5.3.4 Hypothesis Testing Using Suggested Test Statistics

The statistical hypothesis tests are made using the z-test on frequency proportions, the chi-square test on aggregate frequencies, the t-tests on total area proportion, and the t-tests on frequency density using vertical slice faces. Table 5-2 provides a summary of the test statistics for evaluation of radial inhomogeneity using vertical slice faces, the statistical tests, and the corresponding geometric properties. The hypothesis tests using the test statistics of Table 5-2 follow the procedures explained in Sections 5.2.4.1 through 5.2.4.4. The proposed tests will be applied to both simulated and actual specimens and their accuracy will be tested in Chapters 6 and 7.

## 5.4 APPLICATION OF EXISTING INDICES TO TEST RADIAL HOMOGENEITY

A number of tests are available in literature that are either specifically suggested or can be modified to test radial homogeneity. The tests include inner-outer average diameter (Tashman et al. 2001), the eccentricity, and the moment of inertia tests (Yue et al. 1995). The sampling distributions of these tests are not defined and therefore the critical values, which distinguish between the state of homogeneity and inhomogeneity, are not available. As explained in Chapter 2, the decisions on homogeneity of specimens are based on comparison of the computed indices with conceptual decision criteria. In the following sections the geometric properties that are required by each test and application of the tests to actual specimen are explained.

## 5.4.1.1  Inner-Outer Average Diameter

A test that has been specifically suggested for test of radial homogeneity is the inner-outer average diameter test (Tashman et al. 2001). As described in Chapter 2, the test is based on the comparison of the aggregate diameters in the inner and outer portions of the vertical slice faces. The test uses three vertical slice faces of a specimen, which are made 37.5 mm apart on each specimen (Figure 2-2). One slice face is made in the middle

**Table 5-2. Proposed tests of radial inhomogeneity using vertical slice faces**

| Statistical Test | Property | Statistical Index | Equation Number |
|---|---|---|---|
| Standard Normal z | Area Proportions | $$z_{vh} = \frac{\hat{p}_{rv-}\hat{p}_{cv}}{s_{pvh}}$$ | (5-77) |
| | | $$s_{pvh} = \left[ \hat{p}_{vh}(1-\hat{p}_{vh})(\frac{1}{x_{rv}}+\frac{1}{x_{cv}}) \right]^{0.5}$$ | (5-78) |
| Two-Sample Chi-Square | Frequencies | $$\chi^2_{vh} = \frac{(f_{rv} - f_{vh}r_{rv})^2}{f_{vh}r_{rv}(1-r_{rv})} + \frac{(f_{cv} - f_{vh}r_{cv})^2}{f_{vh}r_{cv}(1-r_{cv})}$$ | (5-79) |
| Two-Sample t-Test | Total Aggregate Area Proportions | $$t_{aph} = \frac{\bar{a}_{pr} - \bar{a}_{pc}}{s_{aph}(\frac{1}{n_{rv}}+\frac{1}{n_{cv}})^{0.5}}$$ | (5-80) |
| | | $$s_{aph}{}^2 = \frac{(n_{rv}-1)s^2_{apr} + (n_{cv}-1)s^2_{apc}}{n_{rv}+n_{cv}-2}$$ | (5-81) |
| Two-Sample t-Test | Frequency Densities | $$t_{fdh} = \frac{\bar{f}_{dr} - \bar{f}_{dc}}{s_{fdh}(\frac{1}{n_{rv}}+\frac{1}{n_{cv}})^{0.5}}$$ | (5-82) |
| | | $$s_{fdh}{}^2 = \frac{(n_{rv}-1)s^2_{fdr} + (n_{cv}-1)s^2_{fdc}}{n_{rv}+n_{cv}-2}$$ | (5-83) |

of the specimen and two additional equally spaced slices are made, one on each side of the middle slice face. The required measurements of the aggregates in the inner and outer portions of the slices and the computation of the inner-outer test statistic have been explained in Section 2.3.2.9. Appendix D provides the information on the coordinates of the inner rectangle with respect to the coordinates of the outer rectangle. For the purpose of evaluating the inner-outer test, the test would be applied to the actual homogeneous and inhomogeneous specimens and the ability of the test in distinguishing between homogeneity and inhomogeneity would be examined. The steps for applying the inner-outer test are as follows:

1. The following hypotheses for the aggregate area proportions is tested:

$$H_o : \overline{D}_{outer} = \overline{D}_{inner}$$ (5-84)

$$H_o : \overline{D}_{outer} > \overline{D}_{inner}$$ (5-85)

   where $\overline{D}_{inner}$ and $\overline{D}_{outer}$ are the population values of the average diameter of the aggregates that have a diameter equal to or greater than 2.35 mm in the inner and in the outer portions of the specimen, respectively. A specimen is considered homogeneous if the null hypothesis is accepted.

2. From each slice face, the inner-outer lateral segregation parameter is computed:

$$S_{li} = (\frac{\overline{d}_{oi}}{\overline{d}_{ni}} - 1) \times 100$$ (5-86)

   in which $\overline{d}_{oi}$ and $\overline{d}_{ni}$ are the average diameters of the aggregates that have a diameter equal to or greater than 2.35 mm in the outer and in the inner portions of a slice face, respectively (Section 2.3.2.9).

3. The test statistic, $S_l$, is the mean of the three lateral segregation parameters computed from the three slice faces:

$$S_l = \tfrac{1}{3} \sum_{i=1}^{3} S_{li} \qquad (5\text{-}87)$$

where $S_{li}$ is the lateral segregation parameter computed from the $i^{th}$ slice face.

4. The measured data on the diameter of the aggregates in the outer and in the inner portions ($\overline{d}_{oi}$ and $\overline{d}_{ni}$) are used to compute an estimate of the test statistics using Equations of (5-86) and (5-87).

5. For a homogeneous specimen the mean diameter of the aggregates in the inner and outer portions are the same, therefore the ratio of the mean diameters in the outer and inner portions ($\dfrac{\overline{d}_{oi}}{\overline{d}_{ni}}$) would be 1 and as a result the lateral segregation index would zero. For an inhomogeneous specimen the mean diameter ratio ($\dfrac{\overline{d}_{oi}}{\overline{d}_{ni}}$) would be greater than 1 and as a result the lateral segregation index would be greater than zero. Therefore, the decision on homogeneity of a specimen will be made by comparison of the computed index values with zero. Index values close to zero would indicate radial homogeneity.

### 5.4.1.2 Eccentricity Index

The use of eccentricity concept was originally suggested by Zhong et al. (1995) to examine the vertical uniformity of asphalt mixture specimens (Section 2.3.2.4); however, the test can be modified for the measurement of radial inhomogeneity. The test assesses the equilibrium of the coarse aggregates in the radial plane by computing coarse

aggregate eccentricity. An eccentricity ratio, as the index of homogeneity, is the ratio of the mean of the distances between the coarse aggregate centroids and the geometric center of the horizontal slice faces to the radius of the slice face. The measurement of the geometric properties of the coarse aggregates from horizontal slice faces and the application of the test for the measurement of radial inhomogeneity of actual specimens are explained as follows:

a. Three horizontal slices are taken on each 50-mm thick specimen (Figure 5-1).

b. On entire face of the slices, the x-y coordinates of the coarse aggregate centroids $(x_{ij}, y_{ij})$ and the x-y coordinates of the geometric center of the slice face $(x_o, y_o)$ are measured.

c. Using the coordinates of the aggregate centroids and the coordinates of the geometric center of the slice face, the distance of each particle to the geometric center of the slice face is computed:

$$d_{ij} = [(x_o - x_{ij})^2 + (y_o - y_{ij})^2]^{0.5}$$
(5-88)

where $d_{ij}$ is the distance between the $j^{th}$ particle of the $i^{th}$ slice face and the center of the $i^{th}$ slice face; $x_o$ and $y_o$ are the coordinates of the geometric center of the $i^{th}$ slice face; and $x_{ij}$ and $y_{ij}$ are the coordinates of the centroids of the $j^{th}$ particle on the $i^{th}$ slice face.

d. For each slice face, the average of the distances of the coarse particles from the geometric center of the slice face is computed:

$$\overline{d_i} = \frac{1}{n_{pi}} \sum_{j=1}^{n_{pi}} d_{ij}$$
(5-89)

where $\overline{d}_i$ is the average of the distances of coarse aggregate centroids to the center

of the $i^{th}$ slice face; $n_{pi}$ is the number of coarse aggregates on the $i^{th}$ slice face.

e.  For each specimen, the mean coarse aggregate centroid distance ($\overline{d}$) to the center

of specimen is represented by the average of the $\overline{d}_i$ distances obtained from three

slice faces of the specimen:

$$\overline{d} = \frac{1}{n_{hh}} \sum_{i=1}^{n_{hh}} \overline{d}_i \qquad (5\text{-}90)$$

where $n_{hh}$ is the number of horizontal slice faces, which is three.

Subsequent to the computation of the parameters of eccentricity test, radial

homogeneity of a specimen is tested using the following steps:

1.  The following null and alternative hypotheses are defined for this comparison:

    $H_o$ : *The specimen is not eccentric in coarse aggregates.* $\qquad$ (5-91)

    $H_A$ : *The specimen is eccentric in coarse aggregates.* $\qquad$ (5-92)

    A specimen is considered homogeneous if the null hypothesis is accepted.

2.  The eccentricity ratio, as the radial homogeneity index, is defined:

    $$E = \frac{\overline{d}}{R_h} \qquad (5\text{-}93)$$

    where $\overline{d}$ is the mean distance between the coarse aggregate centroids and the

    center of the slice face (Equation (5-90)); and $R_h$ is the radius of the specimen,

    which is 75 mm.

3.  Using the collected data, radial homogeneity index ($E$) is computed.

4.  The decision on homogeneity of specimens is made by comparing the computed

    test statistic (E) with the E value for the state of homogeneity. For a homogeneous

specimen, coarse aggregates are distributed randomly in radial direction therefore, the average distance between the aggregate centroids and the center of the slice face is about one half the radius of the slice face. As a result, eccentricity ($E$) of 0.5 would be expected for a radially homogeneous specimen. For an inhomogeneous specimen, with the concentration of coarse aggregates in the periphery of the specimen, the eccentricity ($E$) should be close to the limit value of 1.0. The decision on homogeneity of a specimen will then depend on the comparison of the computed value of the test statistic with the E value that represents homogeneity. An eccentricity of greater than 0.5 is assumed to indicate inhomogeneity.

### 5.4.1.3   *Moment of Inertia Method*

The use of moment of inertia concept was also suggested by Zhong et al. (1995) to examine vertical uniformity of asphalt mixture specimens (Section 2.3.2.5); however, the test can be redefined for the measurement of radial homogeneity. The test utilizes the size of aggregates and the distances between aggregate centroids and the geometric center of the slice face to examine the area equilibrium of the coarse aggregates on horizontal slice faces. The test statistic is defined as the ratio of the mean moment of inertia of the coarse aggregates computed from horizontal slice faces to the moment of inertia of a solid circle with respect to the center of the circle. The required geometric properties of the coarse aggregates and the application of the test for measurement of radial inhomogeneity from horizontal slice faces of actual specimens are explained as follows:

a.   Three horizontal slices are taken on each 50-mm thick specimen (Figure 5-1).

b.  On entire face of the five horizontal slices of the specimen, the x-y coordinates of the coarse aggregate centroids ($x_{ij}$, $y_{ij}$) and the x-y coordinates of the geometric center of the slice face ($x_o$, $y_o$) are measured.

c.  On entire face of the slices, the area of each coarse aggregate ($a_{ij}$) is measured.

d.  Using the coordinates of the aggregate centroids and the coordinates of the geometric center of the slice face, the distance of each particle from the geometric center of the slice face is computed:

$$d_{ij} = [(x_o - x_{ij})^2 + (y_o - y_{ij})^2]^{0.5}$$

(5-94)

where $d_{ij}$ is the distance of $j^{th}$ particle on the $i^{th}$ slice face to the center of the slice face; $x_o$ and $y_o$ are the coordinates of the geometric center of the $i^{th}$ slice face; and $x_{ij}$ and $y_{ij}$ are the coordinates of the centroids of the $j^{th}$ particle on the $i^{th}$ slice face.

e.  On each slice face, moment of inertia of the coarse aggregates with respect to the center of the slice face is computed:

$$I_{ai} = \sum_{j=1}^{n_{pi}} a_{ij} d_{ij}$$

(5-95)

in which $a_{ij}$ is the area of the $j^{th}$ coarse aggregate on the $i^{th}$ slice face, $d_{ij}$ is obtained using Equation (5-94), and $n_{pi}$ is the number of coarse particles on the $i^{th}$ slice face.

f.  For each specimen, the moment of inertia of the coarse aggregates with respect to the center of the specimen is computed as the mean of the moments of inertia of the coarse aggregates from the three slice faces:

$$I_a = \frac{1}{n_{hh}} \sum_{i=1}^{n_{hh}} I_{ai}$$

(5-96)

where $n_{hh}$ is the number of horizontal slice faces, which is three.

g.    The moment of inertia of the entire slice face ($I_s$), as a solid circular disk, with

respect to its center axis, is computed as follows:

$$I_s = \frac{1}{2} A_h R_h{}^2$$

(5-97)

where $A_h$ is the area of the circular cross-section of the specimen and $R_h$ is the

radius of the specimen, which is 75 mm.

Subsequent to the computation of the parameters of the moment of inertia test,

radial homogeneity of a specimen is tested using the following steps:

1.    The following null and alternative hypotheses are defined for this comparison:

$H_o$ : *The moment of inertia of coarse aggregates is equal to the moment of inertia*

*of a solid circle.*                                                                              (5-98)

$H_A$ : *The moment of inertia of coarse aggregates is not equal to the moment of*

*inertia of a solid circle.*                                                                      (5-99)

A specimen is considered homogeneous if the null hypothesis is accepted.

2.    The moment of inertia ratio, as the index of radial inhomogeneity, is:

$$R_I = \frac{I_a}{I_s}$$

(5-100)

where $I_a$ is the moment of inertia of coarse aggregates (Equation (5-96)) and $I_s$ is

the moment of inertia of a solid circular slice face (Equation (5-97)).

3.    Radial inhomogeneity ($R_I$) is computed.

4.    The decision on homogeneity of specimens is made by comparing the computed

test statistic with the value of the statistic for the state of homogeneity. For a

homogeneous specimen, coarse aggregates are distributed randomly in radial

direction; therefore, the moment of inertia of the coarse aggregates with respect to

the central axis would not be significantly different from the moment of inertia of a solid circle. As a result, for a homogenous specimen a moment of inertia ratio ($R_I$) of 1.0 would be expected. For an inhomogeneous specimen, with the concentration of coarse aggregates in the periphery of the specimen, the moment of inertia of the coarse aggregates should not be significantly different from the moment of inertia of a solid ring with respect to its central axis. Knowing that the moment of inertia of a solid ring is twice as much as the moment of inertia of a solid circle, the test statistic ($R_I$) of an inhomogeneous specimen would be greater than 1.0 and smaller than 2.0. The decision on homogeneity or inhomogeneity of a specimen will then depend on the comparison of the computed value of the test statistic with the critical value. Any $R_I$ value greater than 1 is assumed to indicate inhomogeneity.

Table 5-3 provides a summary of the test statistics for the measurement of radial homogeneity adapted from the existing tests in literature. The statistical tests, the corresponding geometric properties, the equation numbers, and the section numbers where the tests are described are also provided in the Table. The tests will be applied to the actual specimens and their accuracy will be tested in Chapters 7.

**Table 5-3. Suggested tests of radial inhomogeneity**

| Slice Face Direction | Test | Tested Property | Statistical Index | Section Number | Equation Number |
|---|---|---|---|---|---|
| Vertical | Inner-Outer Average Diameter | Diameter | $S_{li} = (\dfrac{\overline{d}_{oi}}{\overline{d}_{ni}} - 1) \times 100$ | 5.4.1.1 | (5-86) |
| | | | $S_l = \dfrac{1}{3} \sum_{i=1}^{3} S_{li}$ | | (5-87) |
| Horizontal | Eccentricity | Frequency & Distance | $E = \dfrac{\overline{d}}{R_h}$ | 5.4.1.2 | (5-93) |
| Horizontal | Moment of Inertia | Area & Distance | $R_I = \dfrac{I_a}{I_s}$ | 5.4.1.3 | (5-100) |

# CHAPTER 6 - ANALYSIS OF SIMULATION RESULTS

## 6.1  INTRODUCTION

Inhomogeneity of laboratory prepared specimens can be assessed if accurate indices and reliable reference values for the comparison of the measured indices are available. Several indices have been proposed as part of this study (Chapters 4 and 5); however, the accuracy of the tests and the values of the critical statistics that could distinguish between homogeneous and inhomogeneous specimens are not known. To determine the critical values and the accuracy of the proposed indices, knowledge of their sampling distributions for both states of homogeneity and inhomogeneity are required. Monte Carlo simulation was used to generate thousands of virtual specimens and to subject them to the statistical tests suggested in Chapters 4 and 5 in order to determine the distribution functions of the test statistics.

## 6.2  HOMOGENEITY DECISION

In making statistical decisions regarding homogeneity of specimens, several parameters are used.  The first parameter is the sample size (n), which is determined by economics and the resources. The second parameter is the probability of type I error ($\alpha$), which is referred to as the level of significance. The third parameter is the probability of type II error ( $\beta$), which is the measure of accuracy of the tests. The values of $\alpha$ and $\beta$ are determined by the amount of tolerance for making incorrect decisions. The fourth parameter is the criterion for rejection (C), which is determined based on engineering. It is a common practice to set C and n and to determine $\alpha$ and $\beta$. However, for homogeneity

decisions, the criterion C is unknown and needs to be determined. Computer simulation was used to compute the critical test statistics for the selected sample sizes (n) and the typical levels of significance ($\alpha$). The probability of type II error ($\beta$), from which the statistical power of test is determined, uses the computed critical test statistic. If critical statistics other than those computed from simulation (e.g., from standard tables) or $\alpha$ values other than those in simulation are used, the probability of a type II error and consequently the power of the test would be different. Therefore, to ensure the accuracy of decisions about homogeneity, the parameters used to make a decision should be the same as of those from simulation.

## 6.3  SIMULATION MODELS

To obtain the probability distribution functions (pdf) of the suggested test statistics, the simulation models introduced in Chapter 3 were used to create virtual homogeneous and inhomogeneous specimens. Computer simulation was used to generate three-dimensional, randomly packed cylindrical specimens (homogeneous) and specimens intentionally packed to be inhomogeneous. The virtual specimens were then sliced both horizontally and vertically and the exposed two-dimensional faces were analyzed for homogeneity using the statistical tests of Chapters 4 and 5.

## 6.4  SIMULATION RUNS

The simulation programs require the input of several parameters such as the percent air voids, the packing fraction, and the number of simulation runs. Based on the values of the input parameters, the values of the test statistics were computed. The computed statistics are then compiled and the probability distribution function (pdf) and

cumulative probability density function of the statistics were calculated. From the cumulative pdfs of homogeneous and inhomogeneous specimens, the critical statistics, the probabilities of a type II error, and the statistical power of the tests were determined. In the following sections, the parameters of the simulation program (simulation input) and the computed properties from the simulation output are explained.

### 6.4.1    Input Parameters for Simulation Program

#### 6.4.1.1    Packing Parameters of the Simulated Specimens

Since only aggregates that have a diameter larger than 4.75 mm are used to assess homogeneity, the aggregates in the three largest sieve sizes of 4.75-9.0, 9.0-12.5, and 12.5-19 mm were placed within the simulated specimens. The number of aggregates was determined with respect to the design gradation, air void content, and the binder content. The packing parameters of the simulated specimens include the volume fraction of the air voids and the weight fraction of the aggregates, which was determined using the weight fraction of the binder. In this study, an air void fraction of 0.07 was used. The binder weight fraction was 0.0485, which results in an aggregate weight fraction of 0.9515.

#### 6.4.1.2    Parameters of Probability Distribution Function

In order to determine the critical value of each test statistic, a portion of the homogeneous probability distribution function (pdf) that includes the three rejection probabilities of 10%, 5%, and 1% needed to be formed. For each pdf, the bounds of the histogram ordinates were determined from the cumulative probabilities of occurrence in the range of 0.90 to 0.99. The optimum values of the width of the interval and the end of the first interval were obtained using the simulation program.

### 6.4.1.3   Number of Simulation Runs

Accurate determination of the critical statistics and the power of the tests require simulation of a large number of specimens. In general, the accuracy of the simulation increases with the number of virtual specimens. However, at some point, the improvement in accuracy is negligible and the values of the critical statistics stabilize. To ensure that the computed critical statistics and the power of the tests are reliable, simulation sets of 1000, 5000, 10000, and 15000 simulations were run and the values of the statistics from each set were compared.

### 6.4.1.4   Sample Size (Number of Slices)

To quantify homogeneity of a specimen, a number of independent slices (n) at 10-mm spacing are required (McCuen and Azari 2001). When sliced horizontally, the slice faces have equal areas and if taken in the right position, the slices would be from the same population. Therefore, each selected slice face is equally important in the computation of the statistics. Since a greater number of slices will provide more reliable statistics, the maximum number of independent slices would then be used in analyses that involve horizontal slice faces. The maximum number of independent horizontal slices was 12 for the evaluation of vertical inhomogeneity (Chapter 4) and 3 for the evaluation of radial inhomogeneity (Chapter 5).

When sliced vertically, the cross sections of the slices are not the same. The middle slice face provides the largest cross-sectional area, while slices not in the middle provide smaller cross sections. The maximum number of vertical slices for evaluation of both vertical and radial homogeneity was determined to be nine (Chapters 4 and 5).

However, the decrease in the size of the slice faces raised the question, are all nine slices necessary for reliable determination of the statistics? This can be determined by comparing the computed values of the statistics using a different numbers of slices. The indices were computed using sets of five, seven, and nine vertical slices for simulated specimens.

### 6.4.2    Computed Properties from the Simulation

#### 6.4.2.1    Critical Statistics

Critical statistics are necessary for distinguishing the state of homogeneity from inhomogeneity. To obtain values of the critical statistic for a test, the distribution of the test statistic for the state of homogeneity is required. The critical statistic was determined for three levels of significance since the importance of inhomogeneity might be different from one project to another. The three levels of significance considered were: 10%, 5%, and 1%. The critical statistics for the levels of significance were obtained from the cumulative probability distribution functions of homogeneous specimens corresponding to cumulative probabilities of occurrence of 0.90, 0.95, and 0.99.

#### 6.4.2.2    Type I Error

The probability of a type I error ($\alpha$), which is also referred to as the level of significance, is the probability that sample information leads erroneously to the conclusion that the specimen is not homogeneous, when, in fact, it is. The critical statistics of the existing indices are usually determined based on 5% probability of this type of error. However, to ensure accurate decisions, the probability of type II error should also be considered.

### 6.4.2.3 Type II Error

The type II error ($\beta$) is a measure of the quality of the test. Sample information can lead to erroneous decisions, specifically that the specimen is homogeneous when, in fact, it is not (McCuen et al. 2001). To obtain the probabilities of the type II error ($\beta$), the cumulative probability distribution function (pdf) of the test statistic for the state of inhomogeneity is required. From the cumulative pdf of inhomogeneous specimens, the cumulative probabilities of occurrence that correspond to the critical statistics for 10%, 5%, and 1% levels of significance were determined. This is the area under the inhomogeneous probability density function below the critical statistic. The smaller the $\beta$ values are, the more accurate are the homogeneity tests.

### 6.4.2.4 Power of the Tests

The statistical power of a test is a measure of its accuracy. The power is computed by subtracting the probability of a type II error ($\beta$) from 1.0, i.e., power = 1- $\beta$. The higher the statistical power of a test, the more accurate the test is in the measurement of homogeneity. For the two types of inhomogeneity, vertical and radial, the power of each statistical test was computed for the three levels of significance.

## 6.5 ANALYSIS OF THE SIMULATION RESULTS

The computed statistics were obtained for four sets of simulation runs (1000, 5000, 10,000, 15,000). Comparisons of the computed statistics were made for three sets of vertical slice faces (five, seven, and nine). The results of the analysis for two-layer and

three-layer vertical inhomogeneity and radial inhomogeneity using horizontal and vertical slice faces are summarized in the following sections.

### 6.5.1    Two- Layer Vertical Inhomogeneity, Horizontal Slice Faces

Table 6-1 thorough Table 6-3 provide the critical statistics, probabilities of type II errors, and the power of the tests for evaluation of vertical inhomogeneity using horizontal slice faces. The values are presented for each statistic, for three levels of significance and four different sets of simulation runs.

A comparison of the statistics from 1000, 5000, 10000, and 15000 simulation runs indicates the variation of the critical statistics with the increase in the number of runs. As indicated from Table 6-1 through Table 6-3, the critical statistics and the probability values stabilize after 10,000 simulations. This is shown by the small difference between the parameters obtained after 10,000 and 15,000 of runs. Therefore, 15,000 runs of simulation were adequate for reliable determination of critical statistics, the probabilities of type II errors, and the power of the tests.

A comparison of the power of the tests after 15,000 of simulation runs (Table 6-3) indicates that the test on frequencies provided a very high statistical power. For a 5% level of significance, the chi-square test and the t-test on frequency each have 90% and 99.9% power in the detection of the created level of inhomogeneity, respectively. The t-test on nearest neighbor distances provided fair power of 75%, and the t-test on total area provided the lowest power of 18% in detection of inhomogeneity.

As observed, some tests are more accurate in measurement of homogeneity than the others. The frequency-based indices indicated very high power compared to the area-based indices. This is because the frequency of the aggregates is less affected by the

**Table 6-1. Values of the critical statistics for evaluation of two-layer vertical inhomogeneity using horizontal slice faces for three levels of significance and four sets of simulation runs**

| Level of Significance | Simulation Runs | Test Statistics | | | |
|---|---|---|---|---|---|
| | | Chi-Square on Frequency | t-Test on Total Area | t-test on Frequency | t-Test on Nearest Neighbor |
| $\alpha = 0.10$ | 1000 | 2.384 | 1.725 | 1.763 | 1.732 |
| | 5000 | 2.406 | 1.784 | 1.795 | 1.625 |
| | 10000 | 2.406 | 1.792 | 1.795 | 1.624 |
| | 15000 | 2.405 | 1.795 | 1.795 | 1.616 |
| $\alpha = 0.05$ | 1000 | 3.396 | 2.243 | 2.210 | 2.03 |
| | 5000 | 3.404 | 2.286 | 2.236 | 1.949 |
| | 10000 | 3.403 | 2.308 | 2.248 | 1.939 |
| | 15000 | 3.403 | 2.309 | 2.244 | 1.929 |
| $\alpha = 0.01$ | 1000 | 5.540 | 3.575 | 3.133 | 2.640 |
| | 5000 | 5.828 | 3.350 | 3.460 | 2.595 |
| | 10000 | 5.840 | 3.368 | 3.522 | 2.577 |
| | 15000 | 5.829 | 3.361 | 3.511 | 2.581 |

**Table 6-2. Probabilities of type two errors ($\beta$) of the tests for measurement of two-layer vertical inhomogeneity using horizontal slice faces for three levels of significance and four sets of simulation runs**

| Level of Significance | Simulation Runs | Test Statistics | | | |
|---|---|---|---|---|---|
| | | Chi-Square on Frequency | t-Test on Total Area | t-test on Frequency | t-Test on Nearest Neighbor |
| $\alpha = 0.10$ | 1000 | 0.055 | 0.697 | 0.000 | 0.138 |
| | 5000 | 0.053 | 0.694 | 0.000 | 0.165 |
| | 10000 | 0.052 | 0.696 | 0.000 | 0.163 |
| | 15000 | 0.052 | 0.696 | 0.000 | 0.160 |
| $\alpha = 0.05$ | 1000 | 0.100 | 0.826 | 0.001 | 0.220 |
| | 5000 | 0.094 | 0.817 | 0.001 | 0.254 |
| | 10000 | 0.097 | 0.821 | 0.001 | 0.248 |
| | 15000 | 0.097 | 0.820 | 0.001 | 0.245 |
| $\alpha = 0.01$ | 1000 | 0.217 | 0.956 | 0.013 | 0.251 |
| | 5000 | 0.238 | 0.951 | 0.036 | 0.485 |
| | 10000 | 0.239 | 0.954 | 0.040 | 0.476 |
| | 15000 | 0.237 | 0.954 | 0.040 | 0.476 |

**Table 6-3. Statistical power of the tests for the measurement of two-layer vertical inhomogeneity using horizontal slice faces for three levels of significance and four sets of simulation runs**

| Level of Significance | Simulation Runs | Test Statistics | | | |
|---|---|---|---|---|---|
| | | Chi-Square on Frequency | t-Test on Total Area | t-test on Frequency | t-Test on Nearest Neighbor |
| $\alpha = 0.10$ | 1000 | 0.945 | 0.303 | 1.000 | 0.862 |
| | 5000 | 0.947 | 0.306 | 1.000 | 0.835 |
| | 10000 | 0.948 | 0.304 | 1.000 | 0.837 |
| | 15000 | 0.948 | 0.304 | 1.000 | 0.840 |
| $\alpha = 0.05$ | 1000 | 0.900 | 0.174 | 0.999 | 0.780 |
| | 5000 | 0.906 | 0.183 | 0.999 | 0.746 |
| | 10000 | 0.903 | 0.179 | 0.999 | 0.752 |
| | 15000 | 0.903 | 0.180 | 0.999 | 0.755 |
| $\alpha = 0.01$ | 1000 | 0.783 | 0.044 | 0.987 | 0.749 |
| | 5000 | 0.762 | 0.049 | 0.964 | 0.515 |
| | 10000 | 0.761 | 0.046 | 0.960 | 0.524 |
| | 15000 | 0.763 | 0.046 | 0.960 | 0.524 |

location at which the aggregates are sliced. On each slice face, frequencies of the particles that have a diameter equal to or larger than 4.75 mm are captured with the same weight. Therefore, the variability in frequency measurements between the slice faces would be small and the computed statistics would be large. This would result in a large power of the test. However, the area-based test (t-test on total area) is significantly affected by the locations at which the aggregates are sliced. The slicing would result in a wide range of cross-sectional areas, which would cause high variability of the area measurements between the slice faces. Therefore, the computed t statistic on total area would be small and the power of the test would be low.

The power provided by the nearest neighbor index was higher than that of the area-based index. This is because the distances between the aggregate are less affected by the location at which the aggregates are sliced than the areas of the aggregates. A smaller range of the values is then measured for the distances than the areas. The outcome is less

variation in the distance measurements than in the area measurements between the slice faces, which is indicated by the higher power of the nearest neighbor distance test than the total area test.

In other words, the variability that is associated with the frequency measurements is a function of the number of coarse aggregates that appear as particles larger than 4.75 mm in diameter. However, the variability that is associated with the area and distance measurements is a function of both the number of particles larger than 4.75 mm in diameter and the variation in the measured area and distance values.

The power of the tests is also obtained from the plots of the distribution functions. The plots of the tails of probability distributions for several of the statistics are provided in Figure 6-1 through Figure 6-4. The amount of overlap between the distribution plots for the state of homogeneity and inhomogeneity is an indication of the power of the tests. Distinct homogeneous and inhomogeneous distributions with the least amount of overlap indicate that the test is powerful for measurement of homogeneity. On the other hand, major overlap of the tails of distributions indicates that the test is not powerful in distinguishing between states of homogeneity and inhomogeneity. As shown in the plots, the overlap of the homogeneous and inhomogeneous distributions is minimum for the frequency-based statistics and maximum for the total area t-statistic.

Although each test of homogeneity was structured based on the standard t and chi-square tests, the critical values needed to be obtained through simulation. The computed critical statistics were compared with the values provided in the table of critical values for the standard tests of t and chi-square by comparing the exceedance probabilities of the computed statistics and the corresponding levels of significance. If the
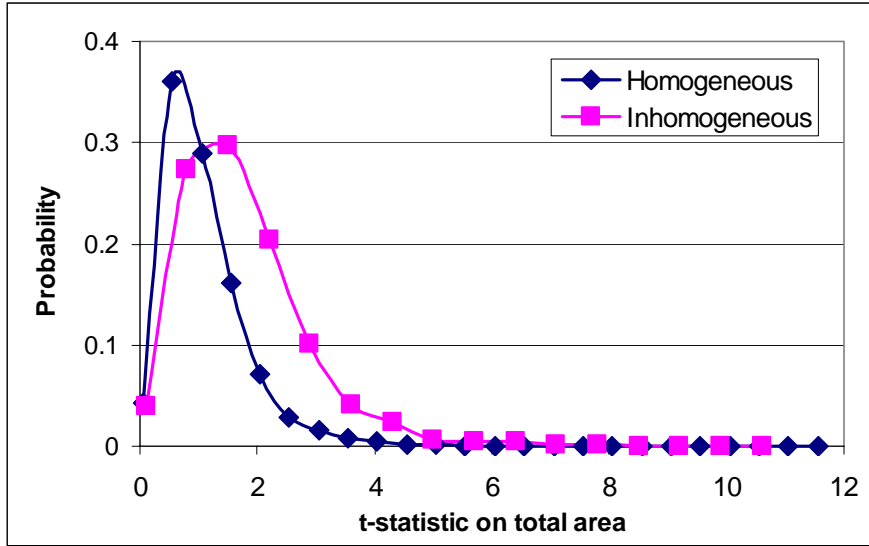
**Figure 6-1. Tails of the probability density functions (pdf) of total area t-statistic for homogeneous and two-layer vertically inhomogeneous specimens**
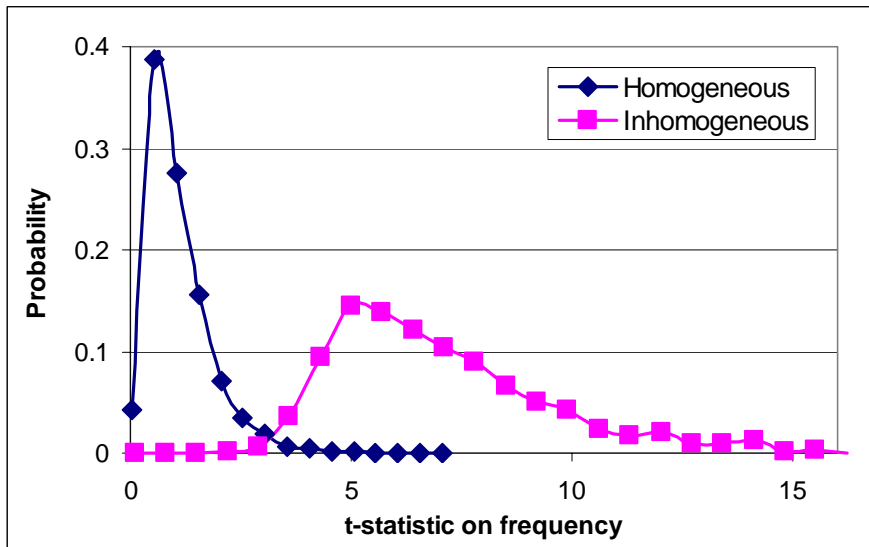


**Figure 6-2. Tails of the probability density functions (pdf) of frequency t-statistic for homogeneous and two-layer vertically inhomogeneous specimens**
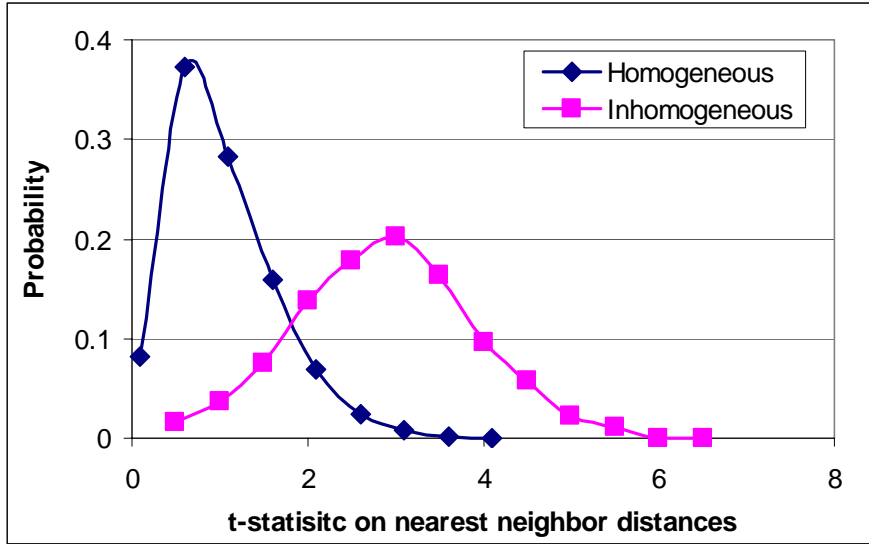
**Figure 6-3. Tails of the probability density functions (pdf) of the nearest neighbor t statistic for homogeneous and two-layer vertically inhomogeneous specimens**
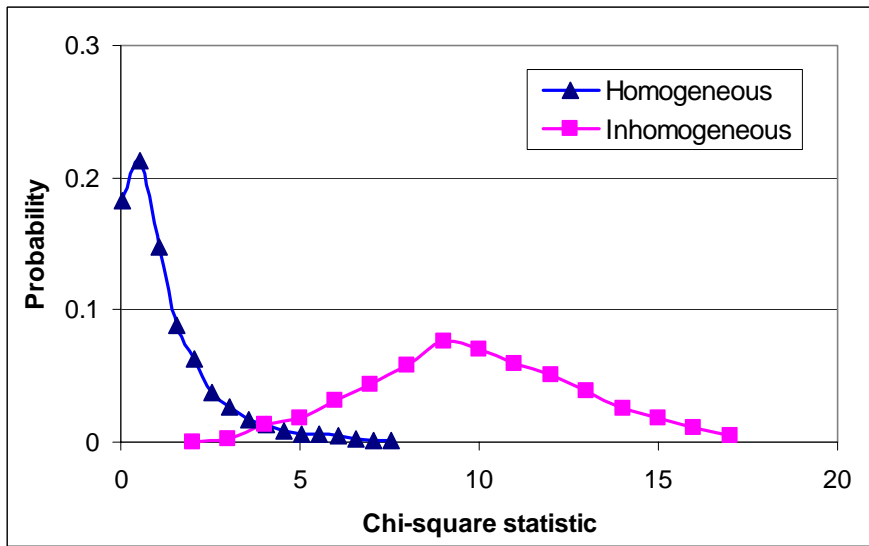


**Figure 6-4. Tails of the probability density functions (pdf) of chi-square statistic for homogeneous and two-layer vertically inhomogeneous specimens**

217

exceedance probabilities are not significantly different from the corresponding levels of

significance, then standard tables can be used for the critical values. The simulated and

table values are included in Table 6-4. As observed from the table, the exceedance

probability values are different from the levels of significance. For example, for a 5%

level of significance, the exceedance probability for the t-statistic on frequencies is 2.9%.

The difference in the simulated and table values is caused by the difference between the

properties that are being tested (aggregate area, frequency, and distance) and the

properties on which the statistical tests were developed.

### 6.5.2   Two-Layer Vertical Inhomogeneity, Vertical Slice Faces

Simulated vertically inhomogeneous and corresponding homogeneous specimens

were sliced vertically along the diameter and along additional planes parallel to the

diametral plane. Sets of five, seven, and nine slices were made equidistance from each

other on each simulated specimen. Table 6-5 through Table 6-7 provide the critical

statistics, the probabilities of type II error, and the powers of the tests of vertical

inhomogeneity using nine vertical slice faces for the three levels of significance. A

comparison of the computed statistics from 1000, 5000, 10000, and 15000 simulation

runs indicates the variation of the critical statistics with increase in the number of runs.

As shown from Table 6-5, the difference between the critical values obtained from each

two successive sets of simulations is small; particularly, the difference between 10,000

and 15,000 runs is insignificant, which leads to the conclusion that 15,000 simulation

runs is adequate for reliable determination of the critical statistics.

Table 6-6 provides the probabilities of type II errors. As indicated from the table,

the probability of this error is zero for all of the tests. Therefore, it can be concluded that

the power of the tests in the detection of vertical inhomogeneity using vertical slices are

all equal to 100%, as indicated in Table 6-7.

**Table 6-4. Comparison of the critical statistics computed from computer simulation and from the standard tables (two-layer vertical inhomogeneity, horizontal slice faces)**

| Level of Significance | | Test statistic | | | |
|---|---|---|---|---|---|
| | | Chi-Square on Frequency | t-Test on Total Area | t-test on Frequency | t-test on Nearest Neighbor |
| $\alpha = 0.10$ | Standard | 2.706 | 1.356 | 1.356 | 1.356 |
| | Simulation | 2.405 | 1.795 | 1.795 | 1.616 |
| | Exceedance Probability | 0.128 | 0.049 | 0.049 | 0.069 |
| $\alpha = 0.05$ | Standard | 3.842 | 1.782 | 1.782 | 1.782 |
| | Simulation | 3.403 | 2.309 | 2.244 | 1.929 |
| | Exceedance Probability | 0.069 | 0.015 | 0.029 | 0.043 |
| $\alpha = 0.01$ | Standard | 6.637 | 2.681 | 2.681 | 2.681 |
| | Simulation | 5.829 | 3.361 | 3.511 | 2.581 |
| | Exceedance Probability | 0.022 | 0.003 | 0.002 | 0.014 |

**Table 6-5. Values of the critical statistics of two-layer vertical inhomogeneity using nine vertical slice faces for three levels of significance and four sets of simulation runs**

| Level of Significance | Simulation Runs | Test Statistics | | | |
|---|---|---|---|---|---|
| | | Chi-Square on Frequency | t-Test on Total Area | t-Test on Frequency | Proportion z |
| $\alpha = 0.10$ | 1000 | 3.100 | 1.305 | 1.247 | 1.133 |
| | 5000 | 3.275 | 1.329 | 1.305 | 1.184 |
| | 10000 | 3.263 | 1.312 | 1.337 | 1.193 |
| | 15000 | 3.328 | 1.333 | 1.349 | 1.206 |
| $\alpha = 0.05$ | 1000 | 4.782 | 1.681 | 1.69 | 1.525 |
| | 5000 | 4.805 | 1.726 | 1.744 | 1.562 |
| | 10000 | 4.685 | 1.716 | 1.762 | 1.578 |
| | 15000 | 4.712 | 1.739 | 1.767 | 1.590 |
| $\alpha = 0.01$ | 1000 | 8.900 | 2.54 | 2.402 | 2.162 |
| | 5000 | 8.425 | 2.546 | 2.545 | 2.267 |
| | 10000 | 8.278 | 2.553 | 2.609 | 2.309 |
| | 15000 | 8.233 | 2.579 | 2.600 | 2.341 |

**Table 6-6. Probabilities of type two errors (β) of statistics for measurement of two-layer vertical inhomogeneity using nine vertical slice faces for three levels of significance and four sets of simulation runs**

| Level of Significance | Simulation Runs | Test Statistics | | | |
|---|---|---|---|---|---|
| | | Chi-Square on Frequency | t-Test on Total Area | t-Test on Frequency | Proportion z |
| $\alpha = 0.10$ | 1000 | 0.000 | 0.000 | 0.000 | 0.000 |
| | 5000 | 0.000 | 0.000 | 0.000 | 0.000 |
| | 10000 | 0.000 | 0.000 | 0.000 | 0.000 |
| | 15000 | 0.000 | 0.000 | 0.000 | 0.000 |
| $\alpha = 0.05$ | 1000 | 0.000 | 0.000 | 0.000 | 0.000 |
| | 5000 | 0.000 | 0.000 | 0.000 | 0.000 |
| | 10000 | 0.000 | 0.000 | 0.000 | 0.000 |
| | 15000 | 0.000 | 0.000 | 0.000 | 0.000 |
| $\alpha = 0.01$ | 1000 | 0.000 | 0.000 | 0.000 | 0.000 |
| | 5000 | 0.000 | 0.000 | 0.000 | 0.000 |
| | 10000 | 0.000 | 0.000 | 0.000 | 0.000 |
| | 15000 | 0.000 | 0.000 | 0.000 | 0.000 |


**Table 6-7. Statistical power of the tests for measurement of two-layered vertical inhomogeneity using nine vertical slice faces for three levels of significance and four sets of simulation runs**

| Level of Significance | Simulation Runs | Test Statistics | | | |
|---|---|---|---|---|---|
| | | Chi-Square on Frequency | t-Test on Total Area | t-Test on Frequency | Proportion z |
| $\alpha = 0.10$ | 1000 | 1.000 | 1.000 | 1.000 | 1.000 |
| | 5000 | 1.000 | 1.000 | 1.000 | 1.000 |
| | 10000 | 1.000 | 1.000 | 1.000 | 1.000 |
| | 15000 | 1.000 | 1.000 | 1.000 | 1.000 |
| $\alpha = 0.05$ | 1000 | 1.000 | 1.000 | 1.000 | 1.000 |
| | 5000 | 1.000 | 1.000 | 1.000 | 1.000 |
| | 10000 | 1.000 | 1.000 | 1.000 | 1.000 |
| | 15000 | 1.000 | 1.000 | 1.000 | 1.000 |
| $\alpha = 0.01$ | 1000 | 1.000 | 1.000 | 1.000 | 1.000 |
| | 5000 | 1.000 | 1.000 | 1.000 | 1.000 |
| | 10000 | 1.000 | 1.000 | 1.000 | 1.000 |
| | 15000 | 1.000 | 1.000 | 1.000 | 1.000 |

The reason for the 100% power of the t-tests when applied to vertical slice faces can be explained based on the rationale of the statistic and the trend of the coarse aggregate distribution in vertical and lateral directions. Vertically inhomogeneous specimens were simulated in such a way that coarse aggregates are distributed with varying probability in vertical direction and equal probability in lateral directions. This would yield a large difference in the means and small sampling variation in the coarse aggregate property measurements in the lower and upper portions of vertical slice faces. The small sampling variation along with the large difference in the means would result in a large t value and consequently a high power of the t-test when computed from vertical slice faces.

A comparison of the computed statistics from sets of five, seven, and nine slices reveals the change in the values of the statistics with the change in the number of slices. A comparison also indicates if the power of the tests is greatly affected by the number of slices being analyzed. If the differences between the powers were not significant, then it would be more efficient to analyze using a smaller number of slices. Table 6-8 provides the critical values for 5% level of significance computed from sets of five, seven, and nine slices of 1000, 5000, 10000, and 15000 simulated specimens. The table shows that the critical values, to different degrees, change with the change in the number of slices. For the chi-square test the critical values changed in the range of 4.59 to 4.71, which represents a very small difference in probability. Therefore, only five slices are needed for this test. For the t-test on total area the critical values changed in the range of 1.74 to 1.84. This is also a small difference. The critical values for the t-test on frequency changed in the range of 1.77 to 1.86. This is also a small difference and indicates that 5

slices are adequate. The largest difference between the critical values corresponded to the z proportion test, which changed in the range of 1.59 to 2.24. Therefore, all nine slices are needed for this test.

Table 6-9 indicates that computing any of the test statistics using five slice faces would result in zero probability of type II error. This would show that the statistical tests when applied to vertical slices are powerful in the measurement of homogeneity even if the maximum sampling capacity of a specimen is not utilized. Despite the high power of test when using even the least number of slices, use of nine slice faces is recommended to ensure the accuracy of the homogeneity measurement of actual specimens. Although each test of homogeneity was structured based on the standard z, t, and chi-square test, the critical values needed to be obtained through simulation. The computed critical statistics were compared with the values provided in the standard tables of t, z, and chi-square statistics by comparison of the exceedance probability of each test statistic with the corresponding level of significance. The values are provided in Table 6-10. As observed from the table, the values are the same in some occasions and different in others. For example, for a 5% level of significance, the t-test on total area has exceedance probability of 5.1% while the chi-square test has exceedance probability of 3.8%. The difference in the simulated and table values is caused by the difference between the properties that are being tested (aggregate area, frequency, and distance) and the properties on which the statistical tests were developed.

### 6.5.3   Three-Layer Vertical Inhomogeneity, Horizontal Slice Faces

Table 6-11 thorough Table 6-13 provide the critical statistics, the probabilities of type II errors, and the powers of the tests for three-layer vertical inhomogeneity using

**Table 6-8. Values of the critical statistics of two-layer vertical inhomogeneity using five, seven, and nine vertical slice faces for 5% level of significance and for four sets of simulation runs**

| Simulation Runs | Number of Slices | Test Statistics | | | |
|---|---|---|---|---|---|
| | | Chi-Square on Frequency | t-Test on Total Area | t-Test on Frequency | Proportion z |
| 1000 | 5 | 4.813 | 1.670 | 1.839 | 2.120 |
| | 7 | 4.650 | 1.670 | 1.713 | 1.780 |
| | 9 | 4.782 | 1.681 | 1.690 | 1.525 |
| 5000 | 5 | 4.750 | 1.820 | 1.867 | 2.238 |
| | 7 | 4.622 | 1.745 | 1.758 | 1.779 |
| | 9 | 4.805 | 1.726 | 1.744 | 1.562 |
| 10000 | 5 | 4.726 | 1.809 | 1.877 | 2.226 |
| | 7 | 4.575 | 1.758 | 1.801 | 1.812 |
| | 9 | 4.685 | 1.716 | 1.762 | 1.578 |
| 15000 | 5 | 4.671 | 1.842 | 1.861 | 2.238 |
| | 7 | 4.598 | 1.777 | 1.790 | 1.831 |
| | 9 | 4.712 | 1.739 | 1.767 | 1.590 |

**Table 6-9. Probabilities of type two errors ($\beta$) of statistics for measurement of two-layer vertical inhomogeneity using five, seven, and nine vertical slice faces for 5% level of significance and four sets of simulation runs**

| Simulation Runs | Number of Slices | Test Statistics | | | |
|---|---|---|---|---|---|
| | | Chi-Square on Frequency | t-Test on Total Area | t-Test on Frequency | Proportion z |
| 1000 | 5 | 0.000 | 0.001 | 0.000 | 0.003 |
| | 7 | 0.000 | 0.000 | 0.000 | 0.000 |
| | 9 | 0.000 | 0.000 | 0.000 | 0.000 |
| 5000 | 5 | 0.000 | 0.001 | 0.000 | 0.007 |
| | 7 | 0.000 | 0.000 | 0.000 | 0.000 |
| | 9 | 0.000 | 0.000 | 0.000 | 0.000 |
| 10000 | 5 | 0.000 | 0.001 | 0.000 | 0.006 |
| | 7 | 0.000 | 0.000 | 0.000 | 0.000 |
| | 9 | 0.000 | 0.000 | 0.000 | 0.000 |
| 15000 | 5 | 0.000 | 0.000 | 0.000 | 0.005 |
| | 7 | 0.000 | 0.000 | 0.000 | 0.000 |
| | 9 | 0.000 | 0.000 | 0.000 | 0.000 |

**Table 6-10. Comparison of the critical statistics computed from simulation and from the standard tables of the test statistics (two-layer vertical inhomogeneity, vertical slice faces)**

| Level of Significance | | Test statistics | | | |
|---|---|---|---|---|---|
| | | Chi-Square on Frequency | t-Test on Total Area | t-Test on Frequency | Proportion z |
| $\alpha = 0.10$ | Standard | 2.706 | 1.337 | 1.337 | 1.282 |
| | Simulation | 3.328 | 1.333 | 1.349 | 1.206 |
| | Exceedance Probability | 0.113 | 0.101 | 0.097 | 0.117 |
| $\alpha = 0.05$ | Standard | 3.842 | 1.746 | 1.746 | 1.645 |
| | Simulation | 4.712 | 1.739 | 1.767 | 1.590 |
| | Exceedance Probability | 0.038 | 0.051 | 0.049 | 0.058 |
| $\alpha = 0.01$ | Standard | 6.637 | 2.583 | 2.583 | 2.328 |
| | Simulation | 8.233 | 2.579 | 2.60 | 2.341 |
| | Exceedance Probability | 0.005 | 0.010 | 0.010 | 0.010 |

horizontal slice faces. The values are presented for each statistic, for the three levels of significance and for four different number of simulation runs. The comparison of the statistics for the four sets of simulation runs indicated that the values of the statistics stabilize after 10,000 simulations. This is indicated by the small difference between the parameters obtained after 10,000 and 15,000 runs. Therefore, 15,000 runs of simulation were adequate for reliable determination of the critical statistics, the probabilities of type II errors, and the powers of the tests.

A comparison of the powers of the tests after 15,000 simulation runs (Table 6-13) indicates that the tests on frequency provide the highest statistical power. For 95% reliability, the chi-square test and the F test on frequency have 85% and 99.8% power in the detection of the created level of inhomogeneity, respectively. The F test on nearest neighbor distances provided power of 66% and the F test on total area provided the lowest power (18%) for the detection of inhomogeneity. The reason for the difference in

the statistical power of various tests was explained earlier based on the characteristics of the area, frequency, and distance properties (Section 6.4.1).

Although each test of homogeneity was structured based on the standard F and chi-square test, the critical values needed to be obtained through simulation. The computed critical statistics were compared with the values provided in the standard tables of chi-square and F statistics by comparing the exceedance probabilities of the statistics with the corresponding levels of significance. The values are included in Table 6-14. As observed from the table, the exceedance probabilities and the corresponding levels of significance are the same in some instances and different in other instances. For example, for a 5% level of significance, the F test on frequency has an exceedance probability of 4.8%, while chi-square test has an exceedance probability of 14.5%. The difference in the simulated and table values is caused by the difference between the properties that are being tested and the properties on which the statistical tests were developed.

**Table 6-11. Values of the critical statistics of three-layer vertical inhomogeneity using horizontal slice faces for three levels of significance and four sets of simulation runs**

| Level of Significance | Simulation Runs | Chi-Square on frequency | F-Test on Total Area | F-Test on Frequency | F-test on Nearest Neighbor |
|---|---|---|---|---|---|
| $\alpha = 0.10$ | 1000 | 3.087 | 2.917 | 3.032 | 2.440 |
| | 5000 | 3.083 | 3.097 | 3.028 | 2.265 |
| | 10000 | 3.077 | 3.126 | 3.042 | 2.241 |
| | 15000 | 3.082 | 3.128 | 3.04 | 2.24 |
| $\alpha = 0.05$ | 1000 | 3.917 | 3.993 | 4.183 | 3.110 |
| | 5000 | 3.978 | 4.346 | 4.346 | 3.004 |
| | 10000 | 3.978 | 4.424 | 4.402 | 2.984 |
| | 15000 | 3.988 | 4.415 | 4.385 | 2.972 |
| $\alpha = 0.01$ | 1000 | 5.470 | 7.350 | 7.150 | 4.420 |
| | 5000 | 6.104 | 7.866 | 7.816 | 4.593 |
| | 10000 | 6.094 | 7.888 | 7.837 | 4.579 |
| | 15000 | 6.085 | 7.889 | 7.807 | 4.569 |

**Table 6-12. Probabilities of type two errors (β) of statistics for measurement of three-layer vertical inhomogeneity using horizontal slice faces for three levels of significance and four sets of simulation runs**

| Level of Significance | Simulation Runs | Test Statistics | | | |
| --- | --- | --- | --- | --- | --- |
| | | Chi-Square on frequency | F-Test on Total Area | F-Test on Frequency | F-test on Nearest Neighbor |
| $\alpha = 0.10$ | 1000 | 0.084 | 0.658 | 0.001 | 0.242 |
| | 5000 | 0.093 | 0.697 | 0.000 | 0.237 |
| | 10000 | 0.093 | 0.704 | 0.000 | 0.235 |
| | 15000 | 0.094 | 0.704 | 0.000 | 0.235 |
| $\alpha = 0.05$ | 1000 | 0.137 | 0.769 | 0.001 | 0.347 |
| | 5000 | 0.152 | 0.806 | 0.002 | 0.342 |
| | 10000 | 0.154 | 0.815 | 0.002 | 0.342 |
| | 15000 | 0.155 | 0.816 | 0.002 | 0.34 |
| $\alpha = 0.01$ | 1000 | 0.269 | 0.853 | 0.019 | 0.561 |
| | 5000 | 0.325 | 0.94 | 0.024 | 0.584 |
| | 10000 | 0.325 | 0.94 | 0.023 | 0.583 |
| | 15000 | 0.325 | 0.94 | 0.023 | 0.582 |

**Table 6-13. The statistical power of the tests for the measurement of three-layer vertical inhomogeneity using horizontal slice faces for three levels of significance and four sets of simulation runs**

| Level of Significance | Simulation Runs | Test Statistics | | | |
| --- | --- | --- | --- | --- | --- |
| | | Chi-Square on frequency | F-Test on Total Area | F-Test on Frequency | F-test on Nearest Neighbor |
| $\alpha = 0.10$ | 1000 | 0.916 | 0.342 | 0.999 | 0.758 |
| | 5000 | 0.907 | 0.303 | 1.000 | 0.763 |
| | 10000 | 0.907 | 0.296 | 1.000 | 0.765 |
| | 15000 | 0.906 | 0.296 | 1.000 | 0.765 |
| $\alpha = 0.05$ | 1000 | 0.863 | 0.231 | 0.999 | 0.653 |
| | 5000 | 0.848 | 0.194 | 0.998 | 0.658 |
| | 10000 | 0.846 | 0.185 | 0.998 | 0.658 |
| | 15000 | 0.845 | 0.184 | 0.998 | 0.660 |
| $\alpha = 0.01$ | 1000 | 0.731 | 0.147 | 0.981 | 0.439 |
| | 5000 | 0.675 | 0.060 | 0.976 | 0.416 |
| | 10000 | 0.675 | 0.060 | 0.977 | 0.417 |
| | 15000 | 0.675 | 0.060 | 0.977 | 0.418 |

**Table 6-14. Comparison of the critical statistics computed from computer simulation and from the standard tables (three-layer vertical inhomogeneity, horizontal slice faces)**

| Level of Significance | | Test statistics | | | |
|---|---|---|---|---|---|
| | | Chi-Square on Frequency | F-Test on Total Area | F-Test on Frequency | F-Test on Nearest Neighbor |
| $\alpha = 0.10$ | Standard | 4.604 | * | * | * |
| | Simulation | 3.082 | 3.128 | 3.040 | 2.240 |
| | Exceedance Probability | 0.222 | * | * | * |
| $\alpha = 0.05$ | Standard | 5.995 | 4.26 | 4.26 | 4.26 |
| | Simulation | 3.978 | 4.424 | 4.402 | 2.984 |
| | Exceedance Probability | 0.145 | 0.048 | 0.048 | >>0.05** |
| $\alpha = 0.01$ | Standard | 9.221 | 8.02 | 8.02 | 8.02 |
| | Simulation | 6.085 | 7.889 | 7.807 | 4.569 |
| | Exceedance Probability | 0.049 | 0.011 | 0.012 | 0.047 |

*The critical F for 10% level of significance is not available in the standard F table. **The exact value of the exceedance probability can not be computed since the level of significance greater than 5% is not available in the table of critical F.

## 6.5.4  Radial Inhomogeneity, Horizontal Slice Faces

Table 6-15 thorough Table 6-17 provide the critical statistics, the probabilities of type II errors, and the powers of the tests of radial inhomogeneity using horizontal slice faces. The values are presented for each statistic, for three levels of significance (10%, 5%, and 1%), and for four different numbers of simulation runs (1000, 5000, 10000, and 15000). The comparison of the statistics for various sets of simulation runs indicates that the differences in the critical values are very small. Therefore, 15,000 runs of simulation were adequate. The comparison of the power of the tests in Table 6-17 indicates that all of the tests have a statistical power of 100% for the detection of radial inhomogeneity at all levels of significance. Although each test of homogeneity was structured based on the t, z, and chi-square test, the critical values needed to be obtained through simulation. The computed critical statistics were compared with the values provided in the standard tables

**Table 6-15. Values of the critical statistics for measurement of radial homogeneity using horizontal slice faces for three levels of significance and four sets of simulation runs**

| Level of Significance | Simulation Runs | Chi-Square on Frequency | t-Test on Total Area | t-Test on Frequency | Proportion z |
|---|---|---|---|---|---|
| | | **Test Statistics** | | | |
| $\alpha = 0.10$ | 1000 | 2.805 | 0.973 | 1.077 | 1.256 |
| | 5000 | 2.600 | 0.998 | 1.094 | 1.248 |
| | 10000 | 2.635 | 1.018 | 1.100 | 1.264 |
| | 15000 | 2.731 | 1.012 | 1.089 | 1.275 |
| $\alpha = 0.05$ | 1000 | 3.826 | 1.326 | 1.552 | 1.643 |
| | 5000 | 3.678 | 1.390 | 1.525 | 1.599 |
| | 10000 | 3.724 | 1.439 | 1.543 | 1.620 |
| | 15000 | 3.827 | 1.426 | 1.514 | 1.640 |
| $\alpha = 0.01$ | 1000 | 6.340 | 2.570 | 2.620 | 2.370 |
| | 5000 | 6.560 | 2.480 | 2.710 | 2.310 |
| | 10000 | 6.740 | 2.570 | 2.750 | 2.310 |
| | 15000 | 6.740 | 2.480 | 2.650 | 2.310 |

**Table 6-16. Probabilities of type two error ($\beta$) of statistics for measurement of radial homogeneity using horizontal slice faces for three levels of significance and four sets of simulation runs**

| Level of Significance | Simulation Runs | Chi-Square on Frequency | t-Test on Total Area | t-Test on Frequency | Proportion z |
|---|---|---|---|---|---|
| | | **Test Statistics** | | | |
| $\alpha = 0.10$ | 1000 | 0.000 | 0.000 | 0.000 | 0.000 |
| | 5000 | 0.000 | 0.000 | 0.000 | 0.000 |
| | 10000 | 0.000 | 0.000 | 0.000 | 0.000 |
| | 15000 | 0.000 | 0.000 | 0.000 | 0.000 |
| $\alpha = 0.05$ | 1000 | 0.000 | 0.000 | 0.000 | 0.000 |
| | 5000 | 0.000 | 0.000 | 0.000 | 0.000 |
| | 10000 | 0.000 | 0.000 | 0.000 | 0.000 |
| | 15000 | 0.000 | 0.000 | 0.000 | 0.000 |
| $\alpha = 0.01$ | 1000 | 0.000 | 0.000 | 0.000 | 0.000 |
| | 5000 | 0.000 | 0.000 | 0.000 | 0.000 |
| | 10000 | 0.000 | 0.000 | 0.000 | 0.000 |
| | 15000 | 0.000 | 0.000 | 0.000 | 0.000 |

**Table 6-17. Statistical power of the tests for the measurement of radial homogeneity using horizontal slice faces for three levels of significance and four sets of simulation runs**

| Level of Significance | Simulation Runs | Chi-Square on Frequency | t-Test on Total Area | t-Test on Frequency | Proportion z |
|---|---|---|---|---|---|
| | | | Test Statistics | | |
| α = 0.10 | 1000 | 1.000 | 1.000 | 1.000 | 1.000 |
| | 5000 | 1.000 | 1.000 | 1.000 | 1.000 |
| | 10000 | 1.000 | 1.000 | 1.000 | 1.000 |
| | 15000 | 1.000 | 1.000 | 1.000 | 1.000 |
| α = 0.05 | 1000 | 1.000 | 1.000 | 1.000 | 1.000 |
| | 5000 | 1.000 | 1.000 | 1.000 | 1.000 |
| | 10000 | 1.000 | 1.000 | 1.000 | 1.000 |
| | 15000 | 1.000 | 1.000 | 1.000 | 1.000 |
| α = 0.01 | 1000 | 1.000 | 1.000 | 1.000 | 1.000 |
| | 5000 | 1.000 | 1.000 | 1.000 | 1.000 |
| | 10000 | 1.000 | 1.000 | 1.000 | 1.000 |
| | 15000 | 1.000 | 1.000 | 1.000 | 1.000 |

**Table 6-18. Comparison of the critical statistics computed from computer simulation and from the standard tables (radial inhomogeneity, horizontal slice face)**

| Level of Significance | | Chi-Square on Frequency | t-Test on Total Area | t-Test on Frequency | Proportion z |
|---|---|---|---|---|---|
| | | | Test statistics | | |
| α = 0.10 | Standard | 2.706 | 1.533 | 1.533 | 1.282 |
| | Simulation | 2.731 | 1.012 | 1.089 | 1.275 |
| | Exceedance Probability | 0.099 | 0.143 | 0.184 | 0.102 |
| α = 0.05 | Standard | 3.842 | 2.132 | 2.132 | 1.645 |
| | Simulation | 3.827 | 1.426 | 1.514 | 1.640 |
| | Exceedance Probability | 0.051 | 0.109 | 0.104 | 0.051 |
| α = 0.01 | Standard | 6.637 | 3.747 | 3.747 | 2.328 |
| | Simulation | 6.740 | 2.480 | 2.650 | 2.310 |
| | Exceedance Probability | 0.010 | 0.041 | 0.037 | 0.011 |

of t, z, and chi-square statistics by comparison of the exceedance probabilities with the corresponding levels of significance. The values are included in Table 6-18. As observed from the table, the exceedance probabilities of the chi-square and the z statistics are the same and those of the t-tests are significantly different from the corresponding levels of significance. The difference in the simulated and table values is caused by the difference between the properties that are being tested (aggregate area, frequency, and distance) and the properties on which the statistical tests were developed.

### 6.5.5   Radial Inhomogeneity, Vertical Slice Faces

Simulated radially inhomogeneous and corresponding homogeneous specimens were sliced vertically along the diameter and along additional planes parallel to the diametral plane. Sets of five, seven, and nine slices were made equidistance from each other on each simulated specimen. Table 6-19 thorough Table 6-21 include the critical statistics, the probabilities of type II errors, and the powers of the tests of radial homogeneity using nine vertical slice faces for three levels of significance of 10%, 5%, and 1%.

A comparison of the computed statistics for 1000, 5000, 10000, and 15000 simulation runs indicates the variation of the critical statistics with the change in the sample size. As it is shown from Table 6-19, the difference between the critical values obtained from either set of simulation runs is not significant, which leads to the conclusion that 15,000 simulation runs is adequate to provide reliable values of the critical statistics. Table 6-20 includes the probabilities of type II errors. As indicated from the table, the probability of this error is zero for any of the test statistics. Therefore, it can

be concluded that the power of the tests in the detection of radial inhomogeneity are all

100% (Table 6-21).

A comparison between the computed statistics from the sets of five, seven, and

nine slices indicates the variation of the values of the statistics with the change in the

number of slices. Table 6-22 provides the values of the critical statistics. Other than the z

statistic on frequency proportion, all other test statistics provided similar values when

computed from either sets of slices. For the chi-square test the critical values changed in

the range of 4.01 to 4.16, which represents a very small difference in probability.

Therefore, only five slices is needed for this test. For the t-test on total area the critical

values changed in the range of 1.75 to 1.85. This is also small. The critical values for the

t-test on frequency changed in the range of 1.76 to 1.86. This is also a small difference

**Table 6-19. Values of the critical statistics for measurement of radial homogeneity using nine vertical slice faces for three levels of significance and four sets of simulation runs**

| Level of Significance | Simulation Runs | Test Statistics | | | |
|---|---|---|---|---|---|
| | | Chi-Square on Frequency | t-Test on Total Area | t-Test on Frequency | Proportion z |
| $\alpha = 0.10$ | 1000 | 2.847 | 1.371 | 1.384 | 1.971 |
| | 5000 | 2.936 | 1.361 | 1.371 | 1.904 |
| | 10000 | 2.839 | 1.330 | 1.320 | 1.877 |
| | 15000 | 2.858 | 1.340 | 1.323 | 1.890 |
| $\alpha = 0.05$ | 1000 | 4.186 | 1.791 | 1.858 | 2.607 |
| | 5000 | 4.166 | 1.765 | 1.787 | 2.511 |
| | 10000 | 4.099 | 1.730 | 1.737 | 2.472 |
| | 15000 | 4.079 | 1.752 | 1.755 | 2.480 |
| $\alpha = 0.01$ | 1000 | 7.600 | 2.513 | 2.920 | 3.920 |
| | 5000 | 7.211 | 2.522 | 2.618 | 3.853 |
| | 10000 | 7.162 | 2.489 | 2.574 | 3.720 |
| | 15000 | 7.120 | 2.536 | 2.566 | 3.733 |

**Table 6-20. Probabilities of type two errors (β) of statistics for the measurement of radial homogeneity using nine vertical slice faces for three levels of significance and four sets of simulation runs**

| Level of Significance | Simulation Runs | Test Statistics | | | |
|---|---|---|---|---|---|
| | | Chi-Square on Frequency | t-Test on Total Area | t-Test on Frequency | Proportion z |
| α = 0.10 | 1000 | 0.000 | 0.000 | 0.000 | 0.000 |
| | 5000 | 0.000 | 0.000 | 0.000 | 0.000 |
| | 10000 | 0.000 | 0.000 | 0.000 | 0.000 |
| | 15000 | 0.000 | 0.000 | 0.000 | 0.000 |
| α = 0.05 | 1000 | 0.000 | 0.000 | 0.000 | 0.000 |
| | 5000 | 0.000 | 0.000 | 0.000 | 0.000 |
| | 10000 | 0.000 | 0.000 | 0.000 | 0.000 |
| | 15000 | 0.000 | 0.000 | 0.000 | 0.000 |
| α = 0.01 | 1000 | 0.000 | 0.000 | 0.000 | 0.000 |
| | 5000 | 0.000 | 0.000 | 0.000 | 0.000 |
| | 10000 | 0.000 | 0.000 | 0.000 | 0.000 |
| | 15000 | 0.000 | 0.000 | 0.000 | 0.000 |

**Table 6-21. Statistical power of the tests for the measurement of radial homogeneity using nine vertical slice faces for three levels of significance and four sets of simulation runs**

| Level of Significance | Simulation Runs | Test Statistics | | | |
|---|---|---|---|---|---|
| | | Chi-Square on Frequency | t-Test on Total Area | t-Test on Frequency | Proportion z |
| α = 0.10 | 1000 | 1.000 | 1.000 | 1.000 | 1.000 |
| | 5000 | 1.000 | 1.000 | 1.000 | 1.000 |
| | 10000 | 1.000 | 1.000 | 1.000 | 1.000 |
| | 15000 | 1.000 | 1.000 | 1.000 | 1.000 |
| α = 0.05 | 1000 | 1.000 | 1.000 | 1.000 | 1.000 |
| | 5000 | 1.000 | 1.000 | 1.000 | 1.000 |
| | 10000 | 1.000 | 1.000 | 1.000 | 1.000 |
| | 15000 | 1.000 | 1.000 | 1.000 | 1.000 |
| α = 0.01 | 1000 | 1.000 | 1.000 | 1.000 | 1.000 |
| | 5000 | 1.000 | 1.000 | 1.000 | 1.000 |
| | 10000 | 1.000 | 1.000 | 1.000 | 1.000 |
| | 15000 | 1.000 | 1.000 | 1.000 | 1.000 |

**Table 6-22. Values of the critical statistics for measurement of radial homogeneity using sets of five, seven, and nine vertical slice faces for four sets of simulation run (N)**

| Simulation Runs (N) | Number of Slices | Test Statistics | | | |
|---|---|---|---|---|---|
| | | Chi-Square on Frequency | t-Test on Total Area | t-Test on Frequency | Proportion z |
| **1000** | 5 | 3.964 | 1.800 | 1.874 | 3.690 |
| | 7 | 3.875 | 1.815 | 1.758 | 2.820 |
| | 9 | 4.186 | 1.791 | 1.858 | 2.607 |
| **5000** | 5 | 4.049 | 1.886 | 1.901 | 3.594 |
| | 7 | 4.254 | 1.802 | 1.812 | 2.846 |
| | 9 | 4.166 | 1.765 | 1.787 | 2.511 |
| **10000** | 5 | 3.988 | 1.815 | 1.861 | 3.513 |
| | 7 | 4.198 | 1.780 | 1.791 | 2.814 |
| | 9 | 4.099 | 1.730 | 1.737 | 2.472 |
| **15000** | 5 | 4.013 | 1.848 | 1.854 | 3.541 |
| | 7 | 4.158 | 1.788 | 1.787 | 2.846 |
| | 9 | 4.079 | 1.752 | 1.755 | 2.480 |

**Table 6-23. Probabilities of type two errors ($\beta$) of statistics for measurement of radial homogeneity using sets of five, seven, and nine vertical slice faces and four sets of simulation runs**

| Simulation Runs | Number of Slices | Test Statistics | | | |
|---|---|---|---|---|---|
| | | Chi-Square on Frequency | t-Test on Total Area | t-Test on Frequency | Proportion z |
| **1000** | **5** | 0.000 | 0.001 | 0.000 | 0.004 |
| | **7** | 0.000 | 0.000 | 0.000 | 0.000 |
| | **9** | 0.000 | 0.000 | 0.000 | 0.000 |
| **5000** | **5** | 0.000 | 0.001 | 0.000 | 0.002 |
| | **7** | 0.000 | 0.000 | 0.000 | 0.000 |
| | **9** | 0.000 | 0.000 | 0.000 | 0.000 |
| **10000** | **5** | 0.000 | 0.001 | 0.000 | 0.005 |
| | **7** | 0.000 | 0.000 | 0.000 | 0.000 |
| | **9** | 0.000 | 0.000 | 0.000 | 0.000 |
| **15000** | **5** | 0.000 | 0.000 | 0.000 | 0.003 |
| | **7** | 0.000 | 0.000 | 0.000 | 0.000 |
| | **9** | 0.000 | 0.000 | 0.000 | 0.000 |

and indicates that five slices are adequate. The largest difference between the critical values corresponded to the z proportion test. The critical values for the z statistic changed in the range of 2.48 to 3.54. This is a significant difference and indicates that all nine slices are required for this test. Table 6-23 indicates that computing any of the test statistics even using five slice faces would result in zero probability of type II error. This would show that the statistical tests when applied to vertical slices are powerful in detection of radial inhomogeneity even if the maximum sampling capacity of a specimen is not utilized. However, despite the high power of the tests with even the least number of slices, use of nine slice faces is recommended to ensure the accuracy of the statistics.

Although each test of homogeneity was structured based on the standard z, t, and chi-square test, the critical values needed to be obtained through simulation. The computed critical statistics were compared with the values provided in the standard tables of t, z, and chi-square statistics by comparison of the exceedance probabilities of the statistics and the corresponding levels of significance. The values are included in Table 6-24. As observed from the table, the exceedance probabilities and the corresponding levels of significance are similar for the chi-square and the t-tests; however, the values are significantly different for the z test. For example, for a 5% level of significance, the exceedance probabilities are 4.7% and 5% for the chi-square and t statistics, respectively, while the exceedance probability of the z statistic is 0.07%. The difference in the simulated and table values is caused by the difference between the properties that are being tested (aggregate area, frequency, and distance) and the properties on which the statistical tests were developed.

**Table 6-24. Comparison of the critical statistics computed from simulation and from the standard tables (radial inhomogeneity, vertical slices)**

| Level of Significance | | Test statistics | | | |
|---|---|---|---|---|---|
| | | Chi-Square on Frequency | t-Test on Total Area | t-Test on Frequency | Proportion z |
| $\alpha$ = 0.10 | Standard | 2.706 | 1.337 | 1.337 | 1.282 |
| | Simulation | 2.858 | 1.340 | 1.323 | 1.890 |
| | Exceedance Probability | 0.093 | 0.100 | 0.103 | 0.036 |
| $\alpha$ = 0.05 | Standard | 3.842 | 1.746 | 1.746 | 1.645 |
| | Simulation | 4.079 | 1.752 | 1.755 | 2.480 |
| | Exceedance Probability | 0.047 | 0.050 | 0.050 | 0.007 |
| $\alpha$ = 0.01 | Standard | 6.637 | 2.583 | 2.583 | 2.328 |
| | Simulation | 7.120 | 2.536 | 2.566 | 3.733 |
| | Exceedance Probability | 0.008 | 0.009 | 0.011 | 0.000 |

# CHAPTER 7 - LABORATORY WORK TO SUPPORT SIMULATION

## 7.1 INTRODUCTION

Homogeneous and inhomogeneous specimens were fabricated in the laboratory to validate the results of simulation regarding the level of accuracy of the statistical indices in the measurement of homogeneity. The proposed statistical tests of Chapters 4 and 5 were applied to thousands of simulated specimens (Chapter 6) and the power of the tests in the measurement of the intended inhomogeneity was evaluated. It is necessary to validate the accuracy of the statistical tests by applying them to similarly graded and structured actual laboratory specimens and to observe if the same decisions with the same level of accuracy would be made. The rejection probability of a test statistic with respect to the decision criterion that was obtained from the simulation would reveal the accuracy of the tests when applied to the actual specimens. A robust test of inhomogeneity would result in a high rejection probability when applied to homogeneous specimens and a low rejection probability when applied to inhomogeneous specimens.

The validation process involves several tasks: first, the fabrication of homogeneous and inhomogeneous specimens; second, obtaining the scanned images of specimen using computed x-ray tomography; third, image analysis of the slice faces to measure the geometric properties of the aggregate faces; and finally, the statistical analysis of the measured geometric properties, which includes computation of the indices and their rejection probabilities.

## 7.2  LABORATORY FABRICATION OF SPECIMENS

Laboratory fabrication of the specimens included the selection of the aggregate and the asphalt binder and the selection of the mixture design. The asphalt mixture consisted of one aggregate gradation and one asphalt binder. The aggregates were blended from the diabase stockpiles to meet the 19-mm nominal maximum aggregate size surface gradation of the accelerated loading facility (ALF) test sections of the Federal Highway Administration (FHWA). The satisfactory performance, high abundance, and low absorbency of diabase aggregates have led to extensive use of this aggregate in ALF test sections (Stuart et al., 1999). The asphalt binder was PG 64-28, which is unmodified asphalt from Venezuelan crude. The reason for the selection of a conventional versus modified binder was to emphasis on the role of aggregates in resisting the applied load.

### 7.2.1  Fabrication of Vertically Inhomogeneous and Homogeneous Specimens

To evaluate vertical inhomogeneity two sets of homogeneous and inhomogeneous specimens were fabricated. The size of the specimens was determined based on the size requirement of the Simple Performance Tests, SPT (NCHRP 2002), which would be performed on the specimens (Chapter 8). Eight homogeneous and eight inhomogeneous specimens were compacted in each set using a Superpave gyratory compactor. The homogeneous specimens are referred to as the H-SPT and inhomogeneous specimens are referred to as I-SPT. The specimens were prepared with the optimum asphalt content of 4.85% at a $7 \pm 0.5\%$ air void content. The design parameters were selected based on the mixture design parameters of the ALF test sections of FHWA (Stuart and Mogawer, 2001). To produce the required air void content, the specimens were compacted to the height of 165 mm using approximately 50 gyrations of the gyratory compactor. The

as-compacted gyratory specimens were then sawed and cored into 150-mm tall, 100-mm diameter specimens to meet the specimen size requirements for the SPT.

While effort was made to prepare the first set of specimens to be as homogeneous as possible, the second set of specimens was purposely fabricated to reflect an extreme level of vertical inhomogeneity. The lower portion of these specimens was made to have a significantly coarser gradation than the upper portion even though the overall mix characteristics of the specimen were identical to the homogeneous specimens. The inhomogeneous specimens would mimic extreme case of poor mixture handling at the time of specimen preparation.

The procedure that was used to make the coarser and finer gradations was adapted from Khedaywi and White (1994). The design gradation was separated over sieve #4, which is documented as the demarcation between the coarse and fine gradations (Cross and Brown, 1993). About 56% of the aggregates were retained on the sieve, and 44% were passed through the sieve. The gradation retained on the sieve is called the *very coarse* gradation, and the gradation passed through the sieve is called the *very fine* gradations. To create the gradation in the lower portion, which is called the *coarser* gradation, 75% of the very coarse and 25% of the very fine gradations were blended. The gradation of the upper portion, which is called the *finer* gradation, was made by blending 25% of the very coarse and 75% of very fine gradations. Combining the gradations of the lower and the upper portions would result in the original design gradation. The design gradation and the gradations of the two portions of inhomogeneous specimens are given in Table 7-1 and the gradation curves are shown in Figure 7-1.

The optimum binder content of the coarser and the finer gradations were determined based on theoretical calculations, experimental laboratory results, and the workability of the mixtures. Theoretical calculation of the binder content based on specific surface area method (Kandhal et al., 1997; Christensen, 2001) is explained in Appendix B. While the overall binder content of inhomogeneous specimens should be equal to the optimum binder content of the homogeneous specimens, the portion with the coarser gradation has a lower percentage and the portion with the finer gradation has a higher percentage of the total asphalt binder content. The specific surface computation and the results of past studies on coarse and fine graded specimens (Williams et al., 1996) were the basis for the selection of the binder contents for the coarser and the finer portions of the trial specimens that were initially made in the laboratory. The workability of the coarser and the finer mixtures were then utilized to optimize the selected values of the binder content. The workability was ensured by observations that all aggregates were coated and the mixing process was manageable. The desired workability of the coarser and the finer mixtures were achieved at the optimum binder contents of 3.5% and 6.3%, respectively.

### 7.2.2 Fabrication of Radially Inhomogeneous and Homogeneous Specimens

To evaluate radial inhomogeneity, three sets of eight specimens were compacted: two sets of homogeneous and one set of radially inhomogeneous. The first set of homogeneous specimens was compacted using linear kneading compactor and is referred to as L-SST. The second set of homogeneous specimens was compacted using Superpave gyratory compactor and is referred to as H-SST. An effort was made to fabricate the homogeneous sets as homogeneous as possible. However, some radial inhomogeneity

**Table 7-1. The finer and the coarser gradations**

| Sieve Size (mm) | % Passing | | |
|---|---|---|---|
| | Design Aggregate Gradation | Coarser Aggregate Gradations | Finer Aggregate Gradation |
| **19** | 100.00 | 100.00 | 100.00 |
| **12.5** | 76.00 | 69.90 | 86.19 |
| **9.5** | 63.00 | 52.10 | 78.03 |
| **4.75** | 43.90 | 27.40 | 66.70 |
| **2.36** | 30.40 | 20.80 | 43.67 |
| **1.18** | 22.10 | 15.90 | 30.54 |
| **0.6** | 16.30 | 12.10 | 22.15 |
| **0.3** | 11.00 | 8.20 | 14.78 |
| **0.15** | 7.60 | 5.70 | 10.25 |
| **0.075** | 5.20 | 3.90 | 7.00 |

is hypothesized to be formed during the gyration process in the homogeneous gyratory compacted specimens. The third set of specimens that represents the extreme level of inhomogeneity by design was compacted using Superpave gyratory compactor. The outer portion of these specimens was made to have significantly coarser gradation than the inner portion. This set of specimens is referred to as I-SST.
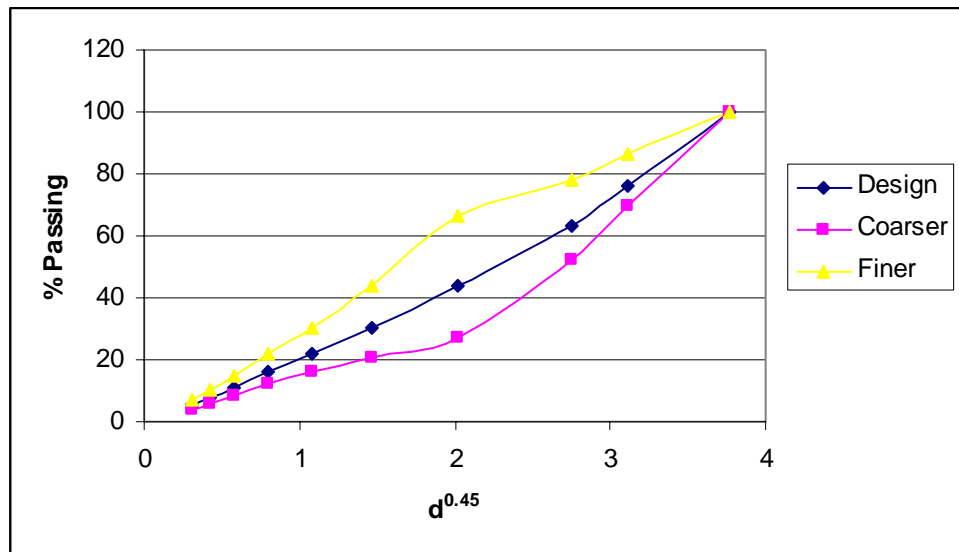


**Figure 7-1. Gradations of homogenous (design) and the coarser and the finer portions of inhomogeneous specimens**

Similar to the specimens for the evaluation of vertical inhomogeneity, the specimens for evaluation of radial inhomogeneity were prepared with the optimum asphalt content of 4.85% at a 7 ± 0.5% air void content. The gradation of the homogeneous SST specimens were the same as that of homogeneous SPT specimens and the gradations of the ring and core of the radially inhomogeneous specimens were the coarser and the finer gradations that were used in the lower and upper portions of vertically inhomogeneous specimens (Table 7-1).

The homogeneous linear kneading compacted specimens were cored out of 180-mm by 480-mm linearly kneaded French slabs. To avoid the vertical inhomogeneity that is commonly experienced with the slab specimens, the specimens were compacted to the minimum possible height of 68 mm. The compacted height was sufficient to allow easy sawing of the top and the bottom of the specimens to achieve the 50-mm depth requirement of the Superpave Shear Tester (SST).

The homogeneous gyratory compacted specimens were compacted to the height of 118 mm, which required approximately 50 gyrations of the gyratory compactor. The as-compacted gyratory specimens were then sawed into two 50-mm thick, 150-mm diameter specimens to meet the specimen size requirement of SST.

The radially inhomogeneous gyratory compacted specimens were fabricated to have the coarser gradation along the periphery (ring) and the finer gradation in the middle (core) of the specimen to mimic the hypothesized effects of gyration and boundary condition on the arrangement of the aggregates. The gyration process of the Superpave gyratory compactor is hypothesized to force the coarse aggregates to the outer edge of the specimen, and the boundary of the gyratory mold is hypothesized to limit the movement

of the coarser aggregates along the periphery of the specimen. Both of these phenomena are assumed to result in the concentration of a coarser mixture in the outer ring, leaving a finer mixture in the middle core of the specimen. Specimens were compacted to the same height as of the homogeneous specimens, which were 118 mm. However, compacting inhomogeneous specimens to 118 mm required approximately 200 gyrations compared to 50 gyrations for homogeneous specimens. Achieving the same height ensured the same overall air void content for both homogeneous and inhomogeneous specimens. The as-compacted gyratory specimens were then sawed into two 50-mm thick, 150-mm diameter specimens to meet the specimen size requirement of SST.

## 7.3  X-RAY COMPUTED TOMOGRAPHY SCAN OF THE SPECIMENS

Following the fabrication, specimens were scanned using x-ray computed tomography (XCT) to access to the specimens internal structure, nondestructively. The specimens were scanned in horizontal and vertical positions to make available vertical and horizontal cross-sectional images of the specimens. Later, it will be determined if slice face direction would make a difference in the accuracy of the homogeneity measurements. The CT scanning of the specimens was done continuously in 0.8 mm intervals. Scanning in horizontal directions was relatively straightforward. The specimens were positioned in upward position (Figure 7-2) and the x-ray beams going through the specimens resulted in reconstruction of circular images of horizontal cross-sections. Figure 7-3 shows a typical horizontal scan of a specimen.

To make available vertical images, which have rectangular cross-sections, specimens were positioned with their main axes parallel to the x-ray beams (Figure 7-4).

Two challenges were faced when scanning the specimens in prone position. The first challenge was that the width dimension of the specimen exceeded the diameter of the x-ray field of view and therefore, the slices in the middle portion of the specimens did not fit in the scanned images. To include the largest width of a specimen in the image, a field of view equal to the diagonal of the specimen was required. For the SPT specimens that are 150 mm tall and 100 mm in diameter, a field of view of 200 mm in diameter was required. A larger field of view was obtained by passing the specimen through the CT scanner at different angles. Through this process, which is called the translate-rotate, the x-ray beams are transmitted with an offset angle while the specimen is being rotated. The translate-rotate mode of scan resulted in a field of reconstruction that was 160% larger than that in the rotate only mode.

The second difficulty with the scanning in the prone position was the shape of the specimen with respect to the x-ray beams. The x-ray system best provides images of the objects that are solid cylinders with consistent density within the limits of the x-ray fan. When the specimen is laid flat, it is no longer considered a solid cylinder with respect to
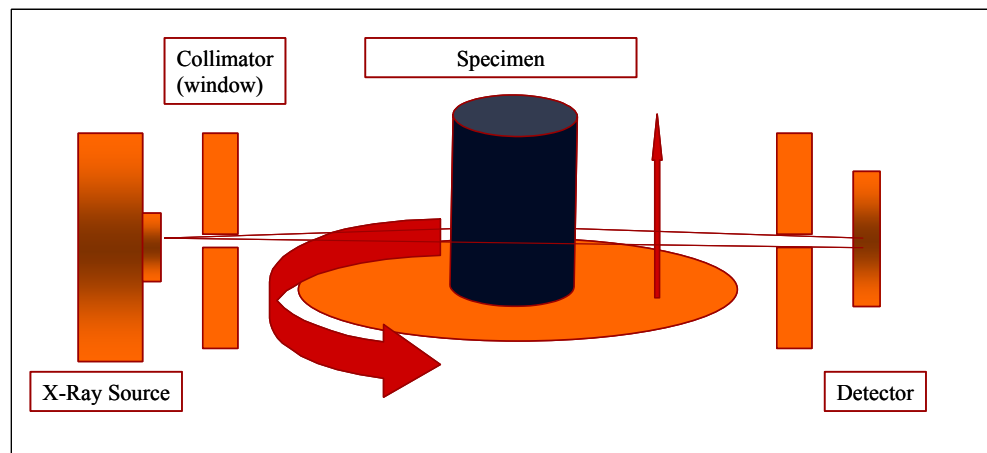


**Figure 7-2. Scanning of the specimens in upright position**

the x-ray fan but a solid object within an imaginary air filled cylinder. This would cause

high contrast in material densities (solid and air) and a large difference between x-ray

attenuation properties of the materials within the imaginary cylinder. As a result, the net

x-ray attenuation that would be computed by the system, which is based on the averaging

of the x-ray attenuations of different phases within the cylinder, would be far different

from the attenuation of the asphalt mixture. Therefore, the images would be highly

affected by blurring. To solve this problem, the specimen in prone position was placed

within a cylindrical container with a diameter slightly greater than the diagonal of the

specimen. The surrounding of the specimen was packed by cement powder, which has

comparable x-ray attenuation property as of the asphalt mixture. This provided relatively

consistent density within the cylindrical container, which resulted in the net x-ray

attenuation of the material within the cylinder not being far from the attenuation of the

asphalt mixture. Following of this procedure removed the blurring and resulted in

satisfactory scanned images. To make the images ready for the analysis, they were

preprocessed by cropping the cement portion and rotating the rectangular asphalt mixture

image to make the top of the image to be the top of the specimen (Figure 7-5).
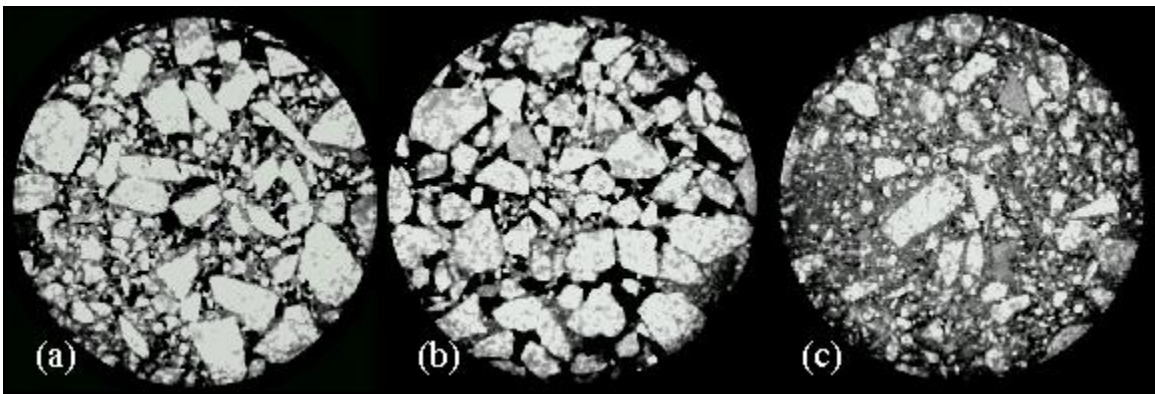


**Figure 7-3. Horizontal slice faces of (a) a homogeneous, (b) the bottom portion of a
vertically inhomogeneous, and (c) the top portion of a vertically inhomogeneous specimen**
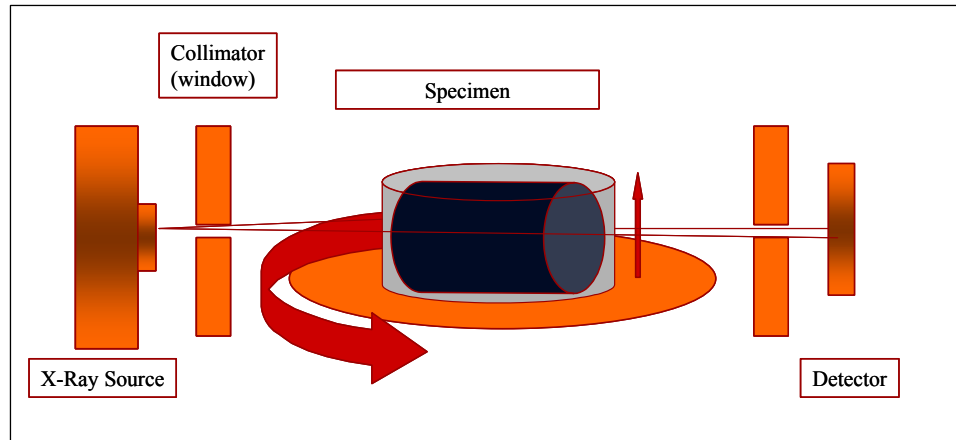
**Figure 7-4. Scanning of the specimens in prone position**

## 7.4 SELECTION OF THE SAMPLING PORTIONS

Although specimens were continuously scanned every 0.8 mm in both horizontal and vertical directions, not all the slices were used for the evaluation of homogeneity. A number of conventions were agreed for the selection of the slices for both radial and vertical homogeneity measurement, which were also followed for the simulated specimens: (1) a 10-mm spacing is required between the slices to ensure independency of the slices. (2) Only vertical slices that are located within 40 mm of the diameter of the specimen are used to ensure adequacy of the sampling areas. (3) The first and last horizontal slices are taken 15 mm away from the ends of the specimen to allow for large particles to be fully contained within the specimen. (4) A transition zone between the coarser and the finer portions is assumed to ensure sampling from distinct populations. Based on the above conventions, the following sampling portions were determined for the measurement of vertical and radial homogeneity using horizontal and vertical slices.
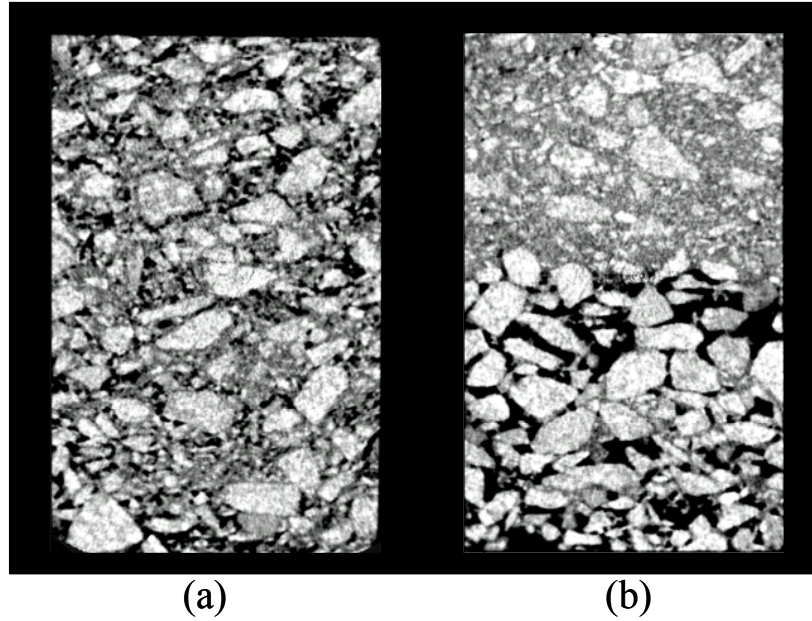
**Figure 7-5. Sections from vertical slices of (a) homogeneous and (b) inhomogeneous specimens**

### 7.4.1 Sampling for Evaluation of Vertical Inhomogeneity, Horizontal Slices

To evaluate vertical homogeneity using horizontal slice faces; total of 12 slices, 6 slices in the lower and 6 slices in the upper portions, were used. The first slice in the lower portion is 15 mm away from the bottom of specimen. The remaining five slices were taken above the first slice with 10-mm spacing between the slices. The last slice of the upper portion is 15 mm away from the top of the specimen. The other five slices are taken below the top slice with 10-mm spacing between the slices. A gap of 20-mm, as a transition zone, was allowed between the last slice of the lower portion and the first slice of the upper portion (Figure 4-1).

### 7.4.2 Sampling for Evaluation of Vertical Inhomogeneity, Vertical Slices

To evaluate vertical homogeneity using vertical slice faces, 9 slices were used. Two sampling areas were positioned on the lower and upper portions of the slice faces.

The width of each sampling area is equal to the width of each slice face, which changes with the location of the slice (Section 4.3.1), and the height of each sampling area is 65 mm. The bottom of the lower sampling area is at the bottom of the specimen and the top of the upper sampling area is at the top of the specimen. A rectangular transition area, 20-mm in height between the upper and the lower portions, was excluded from the sampling (Figure 4-3).

### 7.4.3   Sampling for Evaluation of Radial Inhomogeneity, Horizontal Slices

Separate measurements of the geometric properties from the ring and core portions of each slice required the determination of the ring and core sampling areas. Based on the volume of the coarser and the finer mixtures, the core was determined to be 101 mm in diameter at the center of each slice face. The ring was determined to be 19.55 mm wide at the periphery of each slice face. A transition zone with a thickness of 4.95-mm wide between the ring and the core portions was excluded from sampling (Figure 5-1 and Figure 5-2).

### 7.4.4   Sampling for Evaluation of Radial Inhomogeneity, Vertical Slices

To evaluate radial homogeneity using vertical slice faces, 9 slice faces were used. On each slice face, the sampling areas included two vertical side strips representing the two ring portions and one vertical middle strip representing the core portion of each slice face. The height of the sampling areas is 50 mm and the widths of the sampling areas change with the location of the slices faces (Equation 5.48 through 5.51). For the cross-section that goes through the diameter of the specimen, the width of the core strip is equal to 101 mm and the width of each ring strip is 19.55 mm (Figure 5-3). A transition zone of 4.95-mm wide was considered between a ring and the core strips. The widths of the

sampling areas for the remaining slice faces were computed according to Equation 5.48 through 5.51.

## 7.5  IMAGE ANALYSIS OF X-RAY COMPUTED TOMOGRAPHY SCANS

The selected XCT scanned images were analyzed using a customized computer program, developed under Image-Pro image analysis software (Image-Pro Plus 4.5, 2002). The program opens a sequence of the slice face images of a specimen one at a time and conducts several image processing operations on each image. The image processing of the images includes the selection of the area of interest (AOI) and conducting spatial calibration, thresholding, subject recognition, and geometric measurements.

The AOI of an image is the area from which the sampling takes place. On the XCT images of each slice face direction, the AOI was coincided with the selected sampling areas described in Section 7.4.

The spatial calibration process corresponds the number of image pixels to the unit length of the measurement, i.e., mm. In the processed images, 1 mm of length corresponded to an average number of 4 pixels. This would indicate the nominal spatial resolution of 0.25 mm of the XCT images.

The process of thresholding is used to separate the objects of interest from the rest of the image. In the AOI (sampling areas) of the images, the threshold value that matched the gray intensity of the aggregates were used to highlight the aggregates that had a diameter equal to or greater than 4.75 mm. Similarly, the threshold value that matched the gray intensity of the air voids were used to highlight the voids.

The geometric measurements of the aggregates and the voids were conducted within the AOI of the images. For the aggregates, various geometric properties such as the area, diameter, frequency, the centroid coordinates, and the nearest neighbor distances were measured. For the voids, the total area of the voids was measured, from which the percent air void of the coarser portion, the finer portion, and the entire specimens were computed. The air void content of the specimens and the air void content of the coarser and finer portions of the specimens computed from the XCT images are provided in Appendix E.

## 7.6 STATISTICAL ANALYSIS OF IMAGING MEASUREMENTS

The measured geometric properties of the aggregates from the horizontal and vertical slice face images were used to compute the statistical indices of vertical and radial homogeneity. The homogeneity of the specimens was evaluated by comparing the computed test statistics with the population values for the condition of homogeneity. The procedures for computing the statistical indices are provided in Chapters 4 and 5 and the critical values of the statistics were obtained from computer simulation and are tabulated in Chapter 6.

Several comparisons were made on the computed index values to determine: (a) the tests that provide accurate measurement of both homogeneity and inhomogeneity and (b) the slice face direction that provides the more accurate statistics, horizontal or vertical. Since the tests use different statistics, the values of the statistics could not be compared directly. The computed test statistics were used with the underlying probability distribution to obtain the rejection probabilities, which is the area in the tail of the probability distribution beyond the computed value of the test statistic. It is valid then to

compare the rejection probabilities. The following sections provide the discussion of the results of various statistical tests for the measurement of vertical and radial homogeneity.

## 7.6.1    Comparison of Tests of Vertical Homogeneity

The statistical tests can be compared in terms of their accuracy in detecting both homogeneity and inhomogeneity. Homogeneous specimens are not expected to show a statistical difference, so the rejection probabilities should be greater than 5%, while the rejection probabilities should be less than 5% for inhomogeneous specimens. Therefore, a test is more accurate if the rejection probability is large for homogeneous specimens and small for inhomogeneous specimens.

### 7.6.1.1    *Comparison of the Tests on Horizontal Slice Faces*

The computed test statistics and the corresponding rejection probabilities for the measurement of homogeneity and vertical inhomogeneity using horizontal slice faces are given in Table 7-2 through Table 7-5. Six tests were applied to horizontal faces: the chi-square test on frequency, the t-test on total area, the t-test on frequency, the t-test on nearest neighbor, the runs test, and the Spearman-Conley test. The critical values for the runs and Spearman-Conley tests were obtained from the tables of critical values since these two tests were not tested by computer simulation. The following discussions are made based on the computed test statistics and the rejection probabilities.

For the homogeneous specimens (H-SPT), the computed statistics for the tests from the horizontal slice faces are given in Table 7-2. While the computed test statistics for some individual tests suggested inhomogeneity, on average all of the tests identified the homogeneous specimens to be homogeneous. The t-tests on total area and nearest

**Table 7-2. Computed indices of vertical homogeneity, the means, standard deviations (Sd), and the critical statistics (CS) using the horizontal slice faces of homogeneous (H-SPT) specimens**

| Sample ID | $\chi^2$ test on Frequency | t-Test on Total Area | t-Test on Frequency | t-Test on Nearest Neighbor | No. of Runs* | Spearman-Conley Test $\hat{r}$ |
|---|---|---|---|---|---|---|
| H-SPT1 | 0.032 | 0.635 | 0.330 | 1.784 | 8 | -0.198 |
| H-SPT2 | 0.332 | 2.515 | 1.221 | 0.320 | 7 | -0.371 |
| H-SPT3 | 0.002 | 2.189 | 0.086 | 1.301 | 7 | -0.305 |
| H-SPT4 | 0.037 | 2.105 | 0.413 | 1.038 | 11 | -0.599 |
| H-SPT5 | 1.257 | 0.967 | 1.988 | 3.693 | 9 | 0.000 |
| H-SPT6 | 0.217 | 1.257 | 1.063 | 1.073 | 8 | -0.091 |
| H-SPT7 | 0.072 | 2.039 | 0.555 | 1.150 | 7 | -0.291 |
| H-SPT8 | 0.022 | 0.945 | 0.307 | 1.237 | 8 | -0.230 |
| Mean | 0.246 | 1.581 | 0.745 | 1.450 | 8.2 | -0.261 |
| Sd | 0.424 | 0.708 | 0.635 | 0.990 | 1.3 | 0.182 |
| CS | 3.403 | 2.309 | 2.244 | 1.929 | 3 | 0.385 |

*The critical values for the Runs test are for a 2.5% level of significance.

**Table 7-3. Rejection probabilities, the means, and the standard deviations (Sd) computed from the horizontal slice faces of homogeneous (H-SPT) specimens**

| Sample ID | $\chi^2$ test on Frequency | t-Test on Total Area | t-Test on Frequency | t-Test on Nearest Neighbor | No. of Runs* | Spearman-Conley Test $\hat{r}$ |
|---|---|---|---|---|---|---|
| H-SPT1 | 0.883 | 0.533 | 0.741 | 0.077 | 0.960 | >0.1 |
| H-SPT2 | 0.597 | 0.034 | 0.242 | 0.753 | 0.608 | >0.1 |
| H-SPT3 | 0.990 | 0.052 | 0.930 | 0.198 | 0.738 | >0.1 |
| H-SPT4 | 0.865 | 0.057 | 0.677 | 0.297 | 0.998 | >0.1 |
| H-SPT5 | 0.243 | 0.341 | 0.077 | 0.000 | 0.791 | >0.1 |
| H-SPT6 | 0.687 | 0.226 | 0.291 | 0.277 | 0.911 | >0.1 |
| H-SPT7 | 0.568 | 0.062 | 0.568 | 0.246 | 0.738 | >0.1 |
| H-SPT8 | 0.920 | 0.354 | 0.759 | 0.218 | 0.825 | >0.1 |
| Mean | 0.719 | 0.207 | 0.536 | 0.258 | 0.821 | >0.1 |
| Sd | 0.247 | 0.187 | 0.299 | 0.224 | 0.130 | - |

neighbor distance each misidentified one specimen. All other tests identified eight homogeneous specimens correctly.

The rejection probabilities provide additional insight to the accuracy of the tests. For the homogeneous specimens the rejection probabilities from horizontal slice faces are provided in Table 7-3. Other than one case of t-test on total areas and one case of t-test on nearest neighbor distances, all other individual rejection probabilities were above 5%. In agreement to simulation results, the frequency based tests provided the highest rejection probabilities. The runs test, the chi-square test, and the t-test on frequency had the mean rejection probabilities of 82%, 72%, and 54%, respectively. The rejection probabilities of the Spearman-Conley test could not be computed since the rejection probabilities above 10% cannot be obtained from the table of Spearman-Conley critical values.

For the inhomogeneous specimens (I-SPT), the computed test statistics from the horizontal slice faces are given in Table 7-4. The nearest neighbor t-test, the runs test, and the Spearman-Conley test each misidentified one specimen. The other tests identified all inhomogeneous specimens to be inhomogeneous.

For the inhomogeneous specimens, the rejection probabilities for the tests from the horizontal slice faces are given in Table 7-5. In agreement with the critical values, one individual rejection probability for each of the t-test on nearest neighbor, the runs test, and the Spearman-Conley test were above 5%. All other rejection probabilities were below 5%, which indicates inhomogeneity. Based on the identification of both homogeneity and inhomogeneity, it seems that the chi-square test and the t-test on frequencies are the most accurate tests using horizontal faces. They were the only tests to identify all sixteen-laboratory specimens correctly.

**Table 7-4. Computed indices of vertical homogeneity, the means, standard deviations (Sd), and the critical statistics (CS) using the horizontal slice faces of vertically inhomogeneous (I-SPT) specimens**

| Sample ID | $\chi^2$ test on Frequency | t-Test on Total Area | t-Test on Frequency | t-Test on Nearest Neighbor | No. of Runs* | Spearman-Conley Test $\hat{r}$ |
|---|---|---|---|---|---|---|
| I-SPT1 | 13.938 | 8.468 | 4.899 | 4.274 | 6 | 0.379 |
| I-SPT2 | 8.321 | 4.437 | 5.190 | 1.936 | 4 | 0.720 |
| I-SPT3 | 5.528 | 4.927 | 5.431 | 5.797 | 2 | 0.495 |
| I-SPT4 | 9.632 | 4.004 | 4.040 | 2.125 | 2 | 0.514 |
| I-SPT5 | 8.741 | 5.870 | 4.065 | 2.159 | 4 | 0.714 |
| I-SPT6 | 5.112 | 4.546 | 4.170 | 0.969 | 4 | 0.687 |
| I-SPT7 | 8.696 | 8.441 | 4.382 | 2.443 | 4 | 0.786 |
| I-SPT8 | 4.092 | 3.087 | 2.857 | 2.418 | 4 | 0.445 |
| Mean | 8.007 | 5.473 | 4.379 | 2.765 | 3.8 | 0.592 |
| Sd | 3.135 | 2.001 | 0.812 | 1.530 | 1.3 | 0.151 |
| CS | 3.403 | 2.309 | 2.244 | 1.929 | 3 | 0.385 |

*The critical values for the Runs test are for a 2.5% level of significance

**Table 7-5. Rejection probabilities, the means, and standard deviations (Sd) computed from the horizontal slice faces of vertically inhomogeneous (I-SST) specimens**

| Sample ID | $\chi^2$ test on Frequency | t-Test on Total Area | t-Test on Frequency | t-Test on Nearest Neighbor | No. of Runs* | Spearman-Conley Test $\hat{r}$ |
|---|---|---|---|---|---|---|
| I-SPT1 | 0.000 | 0.000 | 0.002 | 0.000 | 0.209 | 0.053 |
| I-SPT2 | 0.002 | 0.002 | 0.001 | 0.046 | 0.025 | <0.001 |
| I-SPT3 | 0.013 | 0.000 | 0.000 | 0.000 | 0.004 | 0.024 |
| I-SPT4 | 0.001 | 0.004 | 0.004 | 0.032 | 0.001 | 0.019 |
| I-SPT5 | 0.002 | 0.000 | 0.004 | 0.030 | 0.025 | <0.001 |
| I-SPT6 | 0.017 | 0.002 | 0.004 | 0.336 | 0.025 | 0.002 |
| I-SPT7 | 0.002 | 0.000 | 0.003 | 0.017 | 0.025 | <0.001 |
| I-SPT8 | 0.032 | 0.001 | 0.020 | 0.018 | 0.025 | 0.036 |
| Mean | 0.009 | 0.001 | 0.005 | 0.061 | 0.042 | - |
| Sd | 0.011 | 0.001 | 0.006 | 0.113 | 0.068 | - |

### 7.6.1.2  *Comparison of the Tests on Vertical Slice Faces*

The computed test statistics and the corresponding rejection probabilities for the measurement of homogeneity and vertical inhomogeneity using vertical slice faces are given in Table 7-6 through Table 7-9. Six tests were applied to vertical faces: the z-test on frequency proportion, the chi-square test on frequency, the t-test on total area proportion, the t-test on frequency density, the t-test on nearest neighbor density, and the t-test on average depth density. The following discussions are made based on the computed test statistics and the rejection probabilities.

For the homogeneous specimens, the computed statistics for the tests from the vertical slice faces are given in Table 7-6. Other than the t-test on average depth, which misidentified one specimen, all other tests identified individual specimens correctly.

The rejection probabilities provide additional information on the accuracy of the tests. For the homogeneous specimens the rejection probabilities from the vertical slice faces are provided in Table 7-7. It is indicated that the highest rejection probability of 74.7% is provided by the $\chi^2$ test and the lowest rejection probability of 24.7% is provided by the t-test on average depth. The z-test on area proportion provides the second highest rejection probability of 42.5%.

For the inhomogeneous specimens, the computed statistics from the vertical slice fasces are given in Table 7-8. It is indicated from the table that in average all statistics indicated inhomogeneity, correctly. However, three cases of $\chi^2$ statistics were below the

**Table 7-6. Computed indices of vertical homogeneity, the means, coefficients of variations (CV), and the critical statistics (CS) using vertical slice faces of homogeneous (H-SPT) specimens**

| Sample ID | z-Test on Frequency Proportion | $\chi^2$ Test on Frequency | t-Test on Total Area Density | t-Test on Frequency Density | t-Test on Nearest Neighbor Density | t-Test on Average Depth Density |
|---|---|---|---|---|---|---|
| H-SPT1 | 0.147 | 0.352 | 1.266 | 0.383 | 1.328 | 1.268 |
| H-SPT2 | 0.126 | 0.086 | 0.067 | 0.554 | 0.428 | 0.413 |
| H-SPT3 | 0.459 | 0.047 | 0.828 | 0.269 | 0.108 | 0.161 |
| H-SPT4 | 0.071 | 0.222 | 0.066 | 1.016 | 1.477 | 1.931 |
| H-SPT5 | 0.012 | 0.022 | 0.701 | 0.465 | 0.360 | 0.741 |
| H-SPT6 | 0.262 | 0.118 | 0.424 | 0.684 | 0.509 | 0.745 |
| H-SPT7 | 0.150 | 0.033 | 0.679 | 0.086 | 0.631 | 0.522 |
| H-SPT8 | 0.098 | 0.146 | 0.432 | 0.283 | 0.864 | 0.746 |
| Mean | 0.166 | 0.128 | 0.558 | 0.468 | 0.713 | 0.816 |
| Sd | 0.139 | 0.112 | 0.401 | 0.288 | 0.479 | 0.553 |
| CS | 1.59 | 4.712 | 1.739 | 1.767 | 1.746 | 1.860 |

**Table 7-7. Rejection probabilities, the means, and standard deviations (Sd) computed from vertical slice faces of homogeneous (H-SPT) specimens**

| Sample ID | z-Test on Frequency Proportion | $\chi^2$ Test on Frequency | t-Test on Total Area Density | t-Test on Frequency Density | t-Test on Nearest Neighbor Density | t-Test on Average Depth Density |
|---|---|---|---|---|---|---|
| H-SPT1 | 0.428 | 0.553 | 0.112 | 0.353 | 0.101 | 0.120 |
| H-SPT2 | 0.437 | 0.769 | 0.473 | 0.294 | 0.337 | 0.345 |
| H-SPT3 | 0.308 | 0.826 | 0.210 | 0.396 | 0.458 | 0.438 |
| H-SPT4 | 0.469 | 0.638 | 0.474 | 0.162 | 0.080 | 0.045 |
| H-SPT5 | 0.496 | 0.875 | 0.247 | 0.324 | 0.362 | 0.240 |
| H-SPT6 | 0.375 | 0.739 | 0.339 | 0.252 | 0.309 | 0.239 |
| H-SPT7 | 0.426 | 0.848 | 0.253 | 0.466 | 0.268 | 0.308 |
| H-SPT8 | 0.458 | 0.724 | 0.336 | 0.390 | 0.200 | 0.239 |
| Mean | 0.425 | 0.747 | 0.305 | 0.330 | 0.264 | 0.247 |
| Sd | 0.059 | 0.109 | 0.126 | 0.095 | 0.130 | 0.124 |

critical statistic, indicating homogeneity. For the inhomogeneous specimens, the rejection probabilities from vertical slice fasces are given in Table 7-9. In average, all the rejection probabilities were below 5%, which indicate inhomogeneity. However, three individual rejection probabilities of the chi-square statistic were greater than 5%, which indicates homogeneity. All other tests identified individual inhomogeneous specimens correctly.

Based on the identification of both homogeneity and inhomogeneity using vertical faces, it seems that in average all of the proposed tests are reliable in measurement of homogeneity. Among the tests that identified all sixteen specimens correctly, the z test best differentiated between homogeneous and inhomogeneous sets, which are indicated from the difference between the rejection probabilities of the z statistic for the two sets.

It seems that horizontal and vertical slice faces are equally reliable in measurement of homogeneity. However, if it were necessary to decide whether to use vertical or horizontal slice faces, the results of the test indices suggest that vertical slice faces yield the most consistent results. A greater proportion of the tests provided zero incorrect decisions when using vertical slice faces rather than horizontal slice faces. The horizontal slice faces led to incorrect decisions using three tests, while vertical slices yielded incorrect decision using only one test. In addition, the distinction between the computed statistics of homogeneous and inhomogeneous specimens was greater when computed from vertical slice faces than when computed from horizontal slice faces.

Homogeneous statistics of linearly kneaded specimens (L-SST) should show no significant difference; therefore the computed statistics for homogeneous specimens should not exceed the critical statistic for a 5% level of significant. As a result, the rejection probabilities of the computed statistics should be greater than 5%.

**Table 7-8. Computed indices of vertical homogeneity, the means, standard deviations (Sd), and the critical statistics (CS) using the vertical slice faces of vertically inhomogeneous (I-SPT) specimens**

| Sample ID | z-Test on Frequency Proportion | $\chi^2$ Test on Frequency | t-Test on Total Area Density | t-Test on Frequency Density | t-Test on Nearest Neighbor Density | t-Test on Average Depth Density |
|---|---|---|---|---|---|---|
| I-SPT1 | 2.026 | 4.666 | 3.051 | 4.788 | 3.698 | 6.196 |
| I-SPT2 | 2.680 | 8.320 | 2.674 | 2.868 | 4.255 | 6.151 |
| I-SPT3 | 2.529 | 6.650 | 5.019 | 4.318 | 2.264 | 4.590 |
| I-SPT4 | 3.199 | 5.922 | 7.661 | 4.176 | 2.854 | 4.403 |
| I-SPT5 | 2.190 | 6.964 | 5.718 | 2.695 | 3.758 | 4.212 |
| I-SPT6 | 2.508 | 3.491 | 7.133 | 4.375 | 3.127 | 5.255 |
| I-SPT7 | 2.926 | 3.817 | 6.378 | 4.546 | 3.171 | 9.410 |
| I-SPT8 | 2.725 | 7.143 | 5.403 | 4.217 | 4.674 | 6.481 |
| Mean | 2.598 | 5.872 | 5.380 | 3.998 | 3.475 | 5.837 |
| Sd | 0.378 | 1.722 | 1.783 | 0.777 | 0.778 | 1.690 |
| CS | 1.59 | 4.712 | 1.739 | 1.767 | 1.746 | 1.860 |

**Table 7-9. Rejection probabilities, the means, and standard deviations (Sd) computed from vertical slice faces of vertically inhomogeneous (I-SPT) specimens**

| Sample ID | z-Test on Frequency Proportion | $\chi^2$ Test on Frequency | t-Test on Total Area Density | t-Test on Frequency Density | t-Test on Nearest Neighbor Density | t-Test on Average Depth Density |
|---|---|---|---|---|---|---|
| I-SPT1 | 0.017 | 0.051 | 0.004 | 0.000 | 0.001 | 0.000 |
| I-SPT2 | 0.003 | 0.010 | 0.008 | 0.006 | 0.000 | 0.000 |
| I-SPT3 | 0.005 | 0.020 | 0.000 | 0.000 | 0.019 | 0.001 |
| I-SPT4 | 0.001 | 0.029 | 0.000 | 0.000 | 0.006 | 0.001 |
| I-SPT5 | 0.010 | 0.018 | 0.000 | 0.008 | 0.001 | 0.001 |
| I-SPT6 | 0.005 | 0.092 | 0.000 | 0.000 | 0.003 | 0.000 |
| I-SPT7 | 0.001 | 0.078 | 0.000 | 0.000 | 0.003 | 0.000 |
| I-SPT8 | 0.003 | 0.016 | 0.000 | 0.000 | 0.000 | 0.000 |
| Mean | 0.006 | 0.039 | 0.002 | 0.002 | 0.004 | 0.001 |
| Sd | 0.005 | 0.031 | 0.003 | 0.003 | 0.006 | 0.001 |

257

Homogeneous gyratory compacted specimens (H-SST) are hypothesized to show some radial inhomogeneity based on the effect of gyration and boundary condition. Therefore, the computed statistic for H-SST specimens is expected to be larger than those of L-SST specimens and as a result the rejection probability should be smaller than those of L-SST specimens. On the other hand, the statistics of inhomogeneous gyratory compacted specimens (I-SST) should show a significant difference; therefore, the computed statistic should exceed the critical value of the statistic for a 5% level of significance. As a result, the rejection probability should be smaller than 5%. The computed statistics and the rejection probabilities computed from the horizontal slice faces of L-SST, H-SST, and I-SST specimens are examined to make decisions regarding the accuracy of the tests.

### 7.6.1.3    *Comparison of the Tests on Horizontal Slice Faces*

The computed test statistics and the corresponding rejection probabilities for the measurement of radial homogeneity from the horizontal slice faces are given in Table 7-10 through Table 7-15. Six tests were used for the measurements of radial homogeneity using horizontal slice faces: the z-test on frequency proportion, the chi-square test on frequency, the t-tests on total area and frequency, and tests on eccentricity and moment of inertia. As observed from the tables of computed statistic, the computed values of the eccentricity and moment of inertia index did not show sensitivity to the three levels of inhomogeneity and were excluded from the discussion. All other statistics provided reasonable values. The following discussions are made based on the computed test statistics and the rejection probabilities.

The computed test statistics of the L-SST specimens using the horizontal slice faces are provided in Table 7-10, whereas the critical statistics are provided at the bottom of the table. As it is observed from the table two individual values of the t statistics on frequencies are above the critical value. However, in average all computed statistics are below the critical values indicating that the proposed indices are reliable for the detection of homogeneity.

The rejection probabilities provide additional insight to the accuracy of the tests. Table 7-11 indicates that the mean rejection probabilities of all tests are greater than 5%. However, two individual rejection probabilities of the t-test on frequencies are below 5%, resulting in the smallest rejection probability among the tests. This means that the t-test on frequency was the least accurate in measuring homogeneity. The z-test on frequency proportion and the $\chi^2$ test on frequency provide the first and the second highest rejection probabilities, indicating the two most reliable tests in detection of homogeneity.

The computed test statistics of the homogeneous gyratory compacted (H-SST) specimens using horizontal slice faces are provided in Table 7-12, whereas the critical statistics are provided at the bottom of the table. The table shows that 6 out of 8 and 2 out of 8 computed t-statistics on total area and frequency, respectively, are greater than the critical statistics, indicating inhomogeneity. This might be because of slight radial inhomogeneity in H-SST specimens. All other tests provided statistics that were below the critical statistics, indicating homogeneity. It is also observed from the table that the computed average statistics of the z-test on frequency proportion and the t-test on total area are significantly greater than those of the L-SST specimens, indicating presence of slight radial inhomogeneity in the H-SST specimens.

**Table 7-10. Computed indices of radial homogeneity, the means, standard deviations (Sd), and the critical statistics (CS) using the horizontal slice faces of homogeneous linear kneading compacted (L-SST) specimens**

| Sample ID | z-Test on Frequency Proportion | $\chi^2$ Test on Frequency | t-Test on Total Area | t-Test on Frequency | Eccentricity | Moment of Inertia |
|---|---|---|---|---|---|---|
| L-SST1 | 0.58 | 2.41 | 0.13 | 1.76 | 0.71 | 0.36 |
| L-SST2 | 0.02 | 0.56 | 1.00 | 0.23 | 0.67 | 0.33 |
| L-SST3 | 0.09 | 0.97 | 1.37 | 1.05 | 0.67 | 0.42 |
| L-SST4 | 0.82 | 1.07 | -0.35 | 0.65 | 0.70 | 0.32 |
| L-SST5 | 0.39 | 1.34 | -0.99 | 1.00 | 0.69 | 0.35 |
| L-SST6 | 0.3 | 0.21 | 0.68 | 1.41 | 0.70 | 0.35 |
| L-SST7 | 0.01 | 0.50 | 0.12 | 1.07 | 0.69 | 0.29 |
| L-SST8 | 0.77 | 0.34 | 1.11 | 1.69 | 0.67 | 0.39 |
| Mean | 0.19 | 0.92 | 0.39 | 1.11 | 0.69 | 0.35 |
| Sd | 0.66 | 0.71 | 0.80 | 0.51 | 0.01 | 0.04 |
| CS | 1.64 | 3.827 | 1.427 | 1.514 | - | - |

**Table 7-11. Rejection probabilities, means, and standard deviations (Sd) of indices of radial homogeneity computed from horizontal slice faces of (L-SST) specimens**

| Sample ID | z-Test on Frequency Proportion | $\chi^2$ Test on Frequency | t-Test on Total Area | t-Test on Frequency |
|---|---|---|---|---|
| L-SST1 | 0.242 | 0.121 | 0.428 | 0.035 |
| L-SST2 | 0.262 | 0.452 | 0.102 | 0.379 |
| L-SST3 | 0.556 | 0.321 | 0.055 | 0.108 |
| L-SST4 | 0.180 | 0.300 | 0.688 | 0.198 |
| L-SST5 | 0.686 | 0.246 | 0.896 | 0.117 |
| L-SST6 | 0.433 | 0.648 | 0.182 | 0.059 |
| L-SST7 | 0.828 | 0.475 | 0.434 | 0.104 |
| L-SST8 | 0.249 | 0.570 | 0.085 | 0.039 |
| Mean | 0.430 | 0.392 | 0.359 | 0.130 |
| Sd | 0.239 | 0.176 | 0.310 | 0.114 |

**Table 7-12. Computed indices of radial homogeneity, the means, standard deviations (Sd), and the critical statistics (CS) using horizontal slice faces of homogeneous gyratory compacted (H-SST) specimens**

| Sample ID | z-Test on Frequency Proportion | $\chi^2$ Test on Frequency | t-Test on Total Area | t-Test on Frequency | Eccentricity | Moment of Inertia |
|---|---|---|---|---|---|---|
| H-SST1 | 1.22 | 1.82 | 1.76 | 0.46 | 0.70 | 0.29 |
| H-SST2 | 1.45 | 0.82 | 4.25 | 1.05 | 0.69 | 0.29 |
| H-SST3 | 1.33 | 0.54 | 2.81 | 0.96 | 0.66 | 0.37 |
| H-SST4 | 1.50 | 1.17 | 1.53 | 1.04 | 0.66 | 0.33 |
| H-SST5 | 1.43 | 0.26 | 2.26 | 1.35 | 0.69 | 0.29 |
| H-SST6 | 0.79 | 0.69 | 0.12 | 1.19 | 0.68 | 0.30 |
| H-SST7 | 0.98 | 1.01 | 1.37 | 1.69 | 0.66 | 0.40 |
| H-SST8 | 1.40 | 0.68 | 1.72 | 1.76 | 0.67 | 0.40 |
| Mean | 0.90 | 0.87 | 1.98 | 1.19 | 0.68 | 0.33 |
| Sd | 0.27 | 0.47 | 1.20 | 0.42 | 0.01 | 0.05 |
| CS | 1.64 | 3.827 | 1.427 | 1.514 | - | - |

**Table 7-13. Rejection probabilities, means, and standard deviations (Sd) of indices of radial homogeneity computed from horizontal slice faces of homogeneous gyratory compacted (H-SST) specimens**

| Sample ID | z-Test on Frequency Proportion | $\chi^2$ Test on Frequency | t-Test on Total Area | t-Test on Frequency |
|---|---|---|---|---|
| H-SST1 | 0.209 | 0.178 | 0.032 | 0.283 |
| H-SST2 | 0.243 | 0.368 | 0.000 | 0.108 |
| H-SST3 | 0.202 | 0.460 | 0.007 | 0.126 |
| H-SST4 | 0.179 | 0.280 | 0.043 | 0.109 |
| H-SST5 | 0.174 | 0.620 | 0.014 | 0.065 |
| H-SST6 | 0.304 | 0.408 | 0.434 | 0.085 |
| H-SST7 | 0.140 | 0.310 | 0.055 | 0.039 |
| H-SST8 | 0.080 | 0.411 | 0.032 | 0.035 |
| Mean | 0.191 | 0.379 | 0.077 | 0.106 |
| Sd | 0.067 | 0.132 | 0.145 | 0.079 |

The rejection probabilities provide additional insight to the accuracy of the tests. For the H-SST specimens, the rejection probabilities from the horizontal slice faces are given in Table 7-13. It is shown from the table that although t-tests on total area and frequency provided six and two individual rejection probabilities below 5%, respectively, the rejection probabilities in average were all greater than 5%, indicating homogeneity. Also, it is indicated that the rejection probabilities of H-SST specimens are all smaller than those of L-SST specimens, showing presence of slight but not significant level of radial inhomogeneity in homogeneous gyratory compacted specimens. From the comparison of the rejection probabilities in Table 7-11 and Table 7-13 it is indicated that both the z-test and the $\chi^2$ test provided all individual rejection probabilities above 5%; however, the z-test on frequency proportion provided the largest difference between the rejection probabilities of the L-SST and H-SST specimens.

The computed test statistics of the radially inhomogeneous gyratory compacted (I-SST) specimens using the horizontal slice faces are provided in Table 7-14, whereas the critical statistics are provided at the bottom of the tables. All tests identified inhomogeneity correctly by providing all computed statistics above the critical statistic. For the I-SST specimens, the rejection probabilities from the horizontal slice faces are given in Table 7-15. The table indicates that the rejection probabilities were extremely small, indicating that the proposed tests are equally reliable in the measurement of inhomogeneity when applied to horizontal slice faces.

In summary, the suggested tests detected both homogeneity and inhomogeneity. The L-SST and I-SST specimens were identified most accurately by the tests. Fewer tests were successful in identifying the level of homogeneity of the H-SST specimens. This

**Table 7-14. Computed indices of radial homogeneity, the means, standard deviations (Sd), and the critical statistics (CS) using the horizontal slice faces of radially inhomogeneous gyratory compacted (I-SST) specimens**

| Sample ID | z-Test on Frequency Proportion | $\chi^2$ Test on Frequency | t-Test on Total Area | t-Test on Frequency | Eccentricity | Moment of Inertia |
|---|---|---|---|---|---|---|
| I-SST1 | 3.57 | 5.38 | 9.09 | 4.34 | 0.70 | 0.38 |
| I-SST2 | 2.97 | 11.21 | 5.51 | 4.76 | 0.71 | 0.37 |
| I-SST3 | 3.61 | 3.25 | 11.11 | 6.36 | 0.70 | 0.33 |
| I-SST4 | 2.82 | 6.29 | 10.06 | 3.96 | 0.70 | 0.36 |
| I-SST5 | 2.65 | 4.57 | 6.09 | 8.78 | 0.71 | 0.33 |
| I-SST6 | 3.22 | 6.55 | 4.60 | 3.19 | 0.73 | 0.32 |
| I-SST7 | 2.80 | 8.36 | 5.47 | 4.26 | 0.72 | 0.23 |
| I-SST8 | 3.12 | 10.10 | 5.69 | 7.33 | 0.74 | 0.30 |
| Mean | 3.10 | 6.96 | 7.20 | 5.37 | 0.71 | 0.33 |
| Sd | 0.36 | 2.74 | 2.48 | 1.92 | 0.01 | 0.05 |
| CS | 1.64 | 3.83 | 1.427 | 1.514 | - | - |

**Table 7-15. Rejection probabilities, means, and standard deviations (Sd) of indices of radial homogeneity computed from horizontal slice faces of radially inhomogeneous gyratory compacted (I-SST) specimens**

| Sample ID | z-Test on Frequency Proportion | $\chi^2$ Test on Frequency | t-Test on Total Area | t-Test on Frequency |
|---|---|---|---|---|
| I-SST1 | 0.000 | 0.021 | 0.000 | 0.000 |
| I-SST2 | 0.001 | 0.001 | 0.000 | 0.000 |
| I-SST3 | 0.000 | 0.073 | 0.000 | 0.000 |
| I-SST4 | 0.002 | 0.013 | 0.000 | 0.000 |
| I-SST5 | 0.004 | 0.033 | 0.000 | 0.000 |
| I-SST6 | 0.001 | 0.011 | 0.000 | 0.004 |
| I-SST7 | 0.003 | 0.004 | 0.000 | 0.000 |
| I-SST8 | 0.001 | 0.001 | 0.000 | 0.000 |
| Mean | 0.002 | 0.020 | 0.000 | 0.001 |
| Sd | 0.001 | 0.024 | 0.000 | 0.001 |

might be the result of actual inhomogeneity of some of the H-SST specimens. However, this statement cannot be emphasized since inhomogeneity in H-SST specimens was not indicated by all of the tests. While, it can be highlighted that the average statistics were distinct for the L-SST and H-SST specimens, indicating a slight but not significant level of radial inhomogeneity in H-SST specimens. Based on the identification of both homogeneity and inhomogeneity, using horizontal faces, it seems that the $z$-test on frequency proportion is the most accurate test. The test provided all correct decisions. It identified the L-SST and H-SST specimens as homogeneous and the I-SST specimens as inhomogeneous. Additionally, the test best distinguished between the level of homogeneity of L-SST and H-SST specimens.

### 7.6.1.4   *Comparison of the Tests on Vertical Slice Faces*

The computed test statistics and the corresponding rejection probabilities for the measurement of radial inhomogeneity from vertical slice faces are given in Table 7-16 through Table 7-21. Five tests were used for the measurement of radial inhomogeneity using vertical slice faces: the z-test on frequency proportion, the chi-square test on frequency, the t-test on total area proportion, the t-test frequency density, and the inner-outer average diameter test. The inner-outer average diameter statistic provided highly variable values and did not provide sufficient distinction between homogeneous and inhomogeneous specimens. The following discussions are made based on the computed test statistics and the rejection probabilities of the four remaining test statistics.

The computed test statistics of the L-SST specimens using vertical slice faces are provided in Table 7-16, whereas the critical statistics are provided at the bottom of the

tables. As it is observed from the table, except for one case of the t-statistic on total area proportion, the computed statistics are all below the critical statistic, indicating that the tests on vertical slice faces are reliable for the detection of radial homogeneity.

For the L-SST specimens, the rejection probabilities for the tests from the vertical slice faces are given in Table 7-17. The t-test on total area, which misidentified one specimen, provided the mean rejection probability of 37%. All other tests identified all eight homogeneous specimens correctly. The $\chi^2$ test provided the highest rejection probability (60%), the z-test provided the second highest mean rejection probability (44%), and the t-test on frequency had the mean rejection probability of 39%.

For the H-SST specimens, the computed statistics from the vertical slice faces are given in Table 7-18. The values were in average smaller than the critical statistics; however, some individual values exceeded the critical statistics. The t-test on total area misidentified three specimens as being homogeneous and the t-test on frequency misidentified two specimens as being homogeneous. The z-test and the $\chi^2$ test identified all specimens as being homogeneous. All of the tests provided larger computed statistics for the H-SST specimens than for the L-SST specimens, indicating a slight radial inhomogeneity in the H-SST specimens. Among the tests, which identified all individual specimens correctly, the z-test indicated the greatest difference between the computed statistic of L-SST and H-SST specimens.

For the H-SST specimens, the rejection probabilities for the tests from vertical slice faces are given in Table 7-19. It is shown in the table that all of the mean rejection Probabilities are above 5%, indicating homogeneity. However, some individual rejection probabilities of both t-tests are below 5%, indicating inhomogeneity. The z-test on

**Table 7-16. Computed indices of radial homogeneity, the means, standard deviations (Sd), and the critical statistics (CS) using the vertical slice faces of linear kneading compacted (L-SST) specimens**

| Sample ID | z-Test on Frequency Proportion | $\chi^2$ Test on Frequency | t-Test on Total Area Proportion | t-Test on Frequency Density | Inner-outer Average Diameter |
|---|---|---|---|---|---|
| **L-SST1** | 0.79 | 0.49 | 1.82 | 1.71 | 25.30 |
| **L-SST2** | 0.26 | 0.12 | 0.52 | 0.30 | 0.29 |
| **L-SST3** | 0.17 | 0.69 | -0.43 | -0.70 | 11.43 |
| **L-SST4** | 0.56 | 0.32 | 0.91 | -0.03 | -7.96 |
| **L-SST5** | -0.18 | 0.07 | -0.13 | 0.89 | -2.58 |
| **L-SST6** | 0.31 | 0.14 | 0.64 | 0.32 | 7.09 |
| **L-SST7** | -0.43 | 0.46 | -0.36 | -0.96 | -0.46 |
| **L-SST8** | 0.14 | 0.63 | 0.55 | 1.64 | -3.40 |
| **Mean** | 0.20 | 0.37 | 0.44 | 0.40 | 3.71 |
| **Sd** | 0.39 | 0.24 | 0.75 | 0.98 | 10.64 |
| **CS** | 2.480 | 4.079 | 1.752 | 1.755 | - |

**Table 7-17. Rejection probabilities, means, and standard deviations (Sd) of indices of radial homogeneity computed from vertical slice faces of the linear kneading compacted (L-SST) specimens**

| Sample ID | z-Test on Frequency Proportion | $\chi^2$ Test on Frequency | t-Test on Total Area Proportion | t-Test on Frequency Density |
|---|---|---|---|---|
| **L-SST1** | 0.291 | 0.500 | 0.042 | 0.051 |
| **L-SST2** | 0.423 | 0.738 | 0.304 | 0.384 |
| **L-SST3** | 0.449 | 0.422 | 0.662 | 0.754 |
| **L-SST4** | 0.347 | 0.589 | 0.186 | 0.512 |
| **L-SST5** | 0.554 | 0.830 | 0.553 | 0.192 |
| **L-SST6** | 0.410 | 0.720 | 0.264 | 0.375 |
| **L-SST7** | 0.620 | 0.514 | 0.640 | 0.826 |
| **L-SST8** | 0.457 | 0.447 | 0.295 | 0.058 |
| **Mean** | 0.444 | 0.595 | 0.368 | 0.394 |
| **Sd** | 0.105 | 0.151 | 0.225 | 0.293 |

**Table 7-18. Computed indices of radial homogeneity, the means, standard deviations (Sd), and the critical statistics (CS) using the vertical slice faces of homogeneous gyratory compacted (H-SST) specimens**

| Sample ID | z-Test on Frequency Proportion | $\chi^2$ Test on Frequency | t-Test on Total Area Proportion | t-Test on Frequency Density | Inner-outer Average Diameter |
|---|---|---|---|---|---|
| H-SST1 | 1.07 | 0.97 | 1.80 | 0.92 | -0.01 |
| H-SST2 | 0.63 | 0.91 | 1.38 | 1.82 | 4.96 |
| H-SST3 | 0.66 | 0.33 | 0.92 | 0.32 | 21.09 |
| H-SST4 | 0.77 | 1.14 | 1.52 | 1.68 | -1.00 |
| H-SST5 | 0.97 | 0.49 | 2.48 | 2.12 | 20.29 |
| H-SST6 | 0.34 | 0.26 | 0.93 | 0.22 | 4.73 |
| H-SST7 | 1.24 | 0.62 | 2.51 | 0.91 | 12.27 |
| H-SST8 | 0.64 | 1.18 | 1.39 | 1.62 | 2.36 |
| Mean | 0.79 | 0.74 | 1.62 | 1.20 | 8.09 |
| Sd | 0.29 | 0.36 | 0.62 | 0.71 | 8.76 |
| CS | 2.480 | 4.079 | 1.752 | 1.755 | - |

**Table 7-19. Rejection probabilities, means, and standard deviations (Sd) of indices of radial homogeneity computed from vertical slice faces of the homogeneous gyratory compacted specimens (H-SST) specimens**

| Sample ID | z-Test on Frequency Proportion | $\chi^2$ Test on Frequency | t-Test on Total Area Proportion | t-Test on Frequency Density |
|---|---|---|---|---|
| H-SST1 | 0.232 | 0.342 | 0.044 | 0.185 |
| H-SST2 | 0.329 | 0.357 | 0.092 | 0.042 |
| H-SST3 | 0.322 | 0.583 | 0.184 | 0.377 |
| H-SST4 | 0.295 | 0.303 | 0.072 | 0.054 |
| H-SST5 | 0.253 | 0.500 | 0.011 | 0.023 |
| H-SST6 | 0.402 | 0.627 | 0.182 | 0.413 |
| H-SST7 | 0.199 | 0.451 | 0.010 | 0.187 |
| H-SST8 | 0.327 | 0.296 | 0.090 | 0.061 |
| Mean | 0.295 | 0.432 | 0.086 | 0.168 |
| Sd | 0.065 | 0.128 | 0.068 | 0.154 |

frequency proportions and the $\chi^2$ test both provided the individual rejection probabilities above 5%. It is also shown in the table that the rejection probabilities of the tests for the H-SST specimens are all smaller than those of the L-SST specimens, indicating slight but not significant amount of radial inhomogeneity in the H-SST specimens. Among the tests, which identified all H-SST specimens as homogeneous, the z-test better distinguished between the level of homogeneity of the L-SST and H-SST specimens by providing greater difference between the rejection probabilities of the two sets.

For the inhomogeneous gyratory compacted specimens (I-SST), the computed statistics from the vertical slice faces are given in Table 7-20. As it is indicated from the table, any of the suggested tests misidentified one or more specimens. All individual values of the $\chi^2$ statistic and 7 out of 8 values of z statistic are below the critical statistic, which indicate homogeneity. The t-test on total area, and the t-test on frequency each provided one and four individual statistics lower than the critical statistic, respectively. However, in average the computed t statistics indicated inhomogeneity.

For the I-SST specimens, the rejection probabilities for the tests from vertical slice faces are given in Table 7-21. In agreement with the critical values, all rejection probabilities of the $\chi^2$ statistics and seven rejection probabilities of the z statistic are below 5%, meaning that the tests misidentified inhomogeneity. Despite several individual rejection probabilities above 5%, the average rejection probabilities of the t-test on total area and the t-test on frequency were below 5% indicating inhomogeneity of the I-SST specimens correctly.

Based on the identification of inhomogeneity, using horizontal and vertical faces, it seems that radial inhomogeneity is better measured using horizontal slice faces than

**Table 7-20. Computed indices of radial homogeneity, the means, standard deviations (Sd), and the critical statistics (CS) using the vertical slice faces of radially inhomogeneous gyratory compacted (I-SST) specimens**

| Sample ID | z-Test on Frequency Proportion | $\chi^2$ Test on Frequency | t-Test on Total Area Proportion | t-Test on Frequency Density | Inner-outer Average Diameter |
|---|---|---|---|---|---|
| I-SST1 | 2.69 | 2.72 | 4.16 | 2.91 | 18.86 |
| I-SST2 | 2.24 | 2.36 | 4.56 | 2.30 | 18.36 |
| I-SST3 | 1.89 | 1.31 | 2.94 | 1.10 | 2.51 |
| I-SST4 | 2.20 | 2.70 | 2.61 | 2.18 | 10.97 |
| I-SST5 | 0.94 | 2.74 | 1.59 | 2.16 | 9.82 |
| I-SST6 | 2.05 | 2.38 | 2.80 | 1.66 | -19.29 |
| I-SST7 | 2.04 | 2.29 | 2.46 | 1.72 | 12.40 |
| I-SST8 | 1.22 | 3.30 | 3.12 | 1.71 | 11.95 |
| Mean | 1.91 | 2.47 | 3.03 | 1.97 | 8.20 |
| Sd | 0.57 | 0.57 | 0.95 | 0.54 | 12.23 |
| CS | 2.480 | 4.079 | 1.752 | 1.755 | - |

**Table 7-21. Rejection probabilities, means, and standard deviations (Sd) of indices of radial homogeneity computed from vertical slice faces of the radially inhomogeneous gyratory compacted (I-SST) specimens**

| Sample ID | z-Test on Frequency Proportion | $\chi^2$ Test on Frequency | t-Test on Total Area Proportion | t-Test on Frequency Density |
|---|---|---|---|---|
| I-SST1 | 0.037 | 0.108 | 0.000 | 0.004 |
| I-SST2 | 0.068 | 0.134 | 0.000 | 0.016 |
| I-SST3 | 0.101 | 0.270 | 0.004 | 0.142 |
| I-SST4 | 0.070 | 0.110 | 0.008 | 0.021 |
| I-SST5 | 0.349 | 0.107 | 0.064 | 0.021 |
| I-SST6 | 0.085 | 0.132 | 0.006 | 0.057 |
| I-SST7 | 0.086 | 0.140 | 0.012 | 0.051 |
| I-SST8 | 0.060 | 0.077 | 0.003 | 0.052 |
| Mean | 0.107 | 0.135 | 0.012 | 0.046 |
| Sd | 0.100 | 0.058 | 0.021 | 0.044 |

using vertical slice faces. When horizontal slice faces were used, 10 out of 96 cases were misidentified; however when vertical slices were used 23 out of 96 cases were misidentified. The greater reliability of the results using horizontal faces is caused by the orientation of the aggregates. The aggregates in gyratory compacted specimens are preferred to orient in horizontal direction (Azari et al., 2003; Masad et al., 1998) and as result, their appearance on the horizontal slice faces are better representative of their size and arrangement.

Based on the detection of both homogeneity and inhomogeneity, using horizontal slice faces, it seems that the z test on horizontal slice faces is the most accurate test. The test, in addition to identifying all specimens correctly, clearly distinguished between the level of homogeneity of the L-SST, H-SST, and I-SST specimens. As a general statement, the selection of a test for inhomogeneity is not an arbitrary decision. Test accuracy can be quite variable. Although, the power of the z, chi-square, and the t-tests were 100% for most cases, it was evident that not all of the tests yield the same finding, homogeneity or inhomogeneity. Two factors explain the occasional discrepancies in the simulated and actual results. One factor is the sampling variation of the limited number of specimens. The small sample size that is generally available makes it difficult to evaluate the true precision of the tests. Another factor is the differences between the simulated and fabricated specimens. There are factors in fabrication and testing of actual specimens that are not captured in simulation, merely because the factors are not thoroughly quantified. Factors such as orientation and distribution of the aggregates in gyratory compacted specimens need to be quantified and incorporated in the simulation.

# CHAPTER 8 - COMPRESSIVE TESTING OF SPECIMENS USING SIMPLE PERFORMANCE TESTS

## 8.1 INTRODUCTION

To examine the effect of vertical inhomogeneity on the mechanical performance of the mixture, the appropriate laboratory tests had to be selected. The selected tests must have two important characteristics. Firstly, the test must have been approved by the professional community for characterizing asphalt mixture performance. Secondly, the specimens for the tests should retain the created vertical inhomogeneity after the compacted specimens are cut and cored to the required test specimen geometry. Based on these characteristics, simple performance tests (SPT) were selected. The simple performance tests, which involve a compression mode of loading, have been suggested by NCHRP projects 9-19 and 9-29 to verify the performance characteristics of Superpave mixture designs. The parameters computed from the SPT measurements are used as inputs to mechanistic-empirical pavement design methods and support the predictive performance models developed as part of NCHRP project 1-37A (2004). The simple performance tests have also been suggested as the potential quality control-quality assurance testing of asphalt mixtures in the field.

In addition to the importance of the simple performance tests for generating important performance parameters, the geometry of the test specimens makes the tests good candidates for the evaluation of the effect of inhomogeneity. The required specimen geometry for simple performance tests would retain the vertical inhomogeneity that was originally created in the gyratory specimens. The inhomogeneously compacted gyratory

271

specimens can be cut and cored to the shape and size of SPT specimens and yet maintain their inhomogeneous characteristics.

Equally sized and shaped homogeneous and vertically inhomogeneous specimens referred to as H-SPT and I-SPT, respectively, were prepared and tested according to the standard method for the simple performance tests (NCHRP 2002). A review of the procedures for preparing and testing of asphalt mixture specimens to determine the mixture compressive properties using simple performance tests is provided in Chapter 2.

Although H-SPT and I-SPT specimens were prepared with the same gradation, asphalt content, and air void content, the distributions of the aggregates, asphalt, and as a result, the distribution of the air voids in the I-SPT specimens were intended to be significantly different from those of H-SPT specimens. The selected constituent materials, the mixture design parameters for H-SPT specimens, and the altered mixture parameters for the I-SPT specimens were explained in Chapter 7.

The H-SPT and I-SPT specimens were subjected to two simple performance tests: the dynamic modulus and the repeated axial load (flow number) tests. The dynamic modulus test was conducted at intermediate and high temperatures of 21°C and 45°C, and the flow number test was conducted at a high temperature of 45°C.

The dynamic modulus test yields a compressive modulus (E*), which is the measured peak stress divided by the measured peak strain, and the phase angle ($\phi$), which is the lag in time between the peak stress and the peak strain responses of the material. E* and $\phi$ were used to compute three performance properties: the E*sin$\phi$ and sin$\phi$/E* at intermediate temperature, and the sin$\phi$/E* at high temperature. The E*sin$\phi$ at intermediate temperature represents the damage or the dissipated energy in a

strain-controlled mode of loading and is indicative of susceptibility for fatigue cracking in thin pavement layers. The $\sin\phi/E^*$ at intermediate temperature represents the damage or the dissipated energy in a stress-controlled mode of loading and is indicative of the susceptibility for fatigue cracking in thick pavement layers. When measured at a high temperature, $\sin\phi/E^*$ is indicator of the susceptibility for permanent deformation.

The repeated axial load test yields the flow number ($F_N$), which is the number of cycles to reach the minimum change in permanent strain. The flow number is another performance parameter that evaluates the susceptibility of the material to permanent deformation. Table 8-1 and Table 8-2 provide the measured and computed compressive properties of the eight homogeneous and eight inhomogeneous specimens.

A comparison of the compressive properties of the homogeneous and inhomogeneous specimens would indicate the effect of vertical inhomogeneity on the compressive performance of the material. The comparison would be made based on statistical analyses and physical evaluations. The statistical analyses include an F-test on variances and a two-sample t-test on the mean compressive properties of the homogeneous (H-SPT) and vertically inhomogeneous (I-SPT) specimens. The physical evaluation would address the possible impact of vertical inhomogeneity on the design and performance prediction of a pavement layer. Table 8-3 provides the results of the statistical analyses and the decisions on the significance of the difference between the properties of the H-SPT and I-SPT specimens.

To further investigate the effect of vertical inhomogeneity on the compressive performance, the relationship between each compressive property and the homogeneity index, z, was evaluated. The z statistic was used since it was selected as the most accurate

**Table 8-1. Dynamic modulus (E\*), phase angle (ϕ), stress controlled fatigue damage (sinϕ/E\*) measured at 21°C, strain controlled fatigue damage (E\*sinϕ) measured at 21°C, permanent deformation damage (sinϕ/E\*) measured at 45°C, and flow number ($F_N$) of eight homogeneous (H-SPT) specimens, "Sd" represents standard deviation and "CV" represents coefficient of variation**

| Sample ID | 21°C | | | | 45°C | | | |
|---|---|---|---|---|---|---|---|---|
| | $E^*x10^6$ (kPa) | ϕ | sin(ϕ)/E\* $x10^{-8}$ (1/kPa) | $E^*sin(ϕ)$ $x10^6$ (kPa) | $E^*x10^5$ (kPa) | ϕ | sin(ϕ)/E\* $x10^{-7}$ (1/kPa) | $F_N$ |
| H-SPT1 | 6.61 | 29.97 | 7.56 | 3.30 | 6.58 | 35.42 | 8.81 | 4394 |
| H-SPT2 | 7.00 | 27.01 | 6.49 | 3.18 | 8.48 | 33.72 | 6.55 | 4864 |
| H-SPT3 | 5.01 | 27.67 | 9.28 | 2.32 | 5.31 | 35.70 | 11.00 | 3202 |
| H-SPT4 | 4.95 | 28.75 | 9.73 | 2.38 | 5.74 | 38.96 | 10.95 | 3375 |
| H-SPT5 | 4.79 | 27.96 | 9.78 | 2.25 | 6.25 | 37.92 | 9.84 | 3013 |
| H-SPT6 | 5.70 | 29.51 | 8.64 | 2.81 | 5.28 | 38.04 | 11.68 | 3455 |
| H-SPT7 | 5.53 | 28.54 | 8.63 | 2.64 | 5.48 | 36.87 | 10.95 | 3563 |
| H-SPT8 | 6.55 | 33.95 | 8.53 | 3.66 | 5.54 | 33.07 | 9.84 | 2963 |
| Average | 5.77 | 29.17 | 8.58 | 2.82 | 6.08 | 36.21 | 9.95 | 3604 |
| Sd | 0.85 | 2.16 | 1.11 | 0.52 | 1.07 | 2.11 | 1.65 | 677 |
| CV (%) | 14.80 | 7.39 | 12.98 | 18.30 | 17.63 | 5.83 | 16.55 | 18.79 |

**Table 8-2. Dynamic modulus (E\*), phase angle (ϕ), stress controlled fatigue damage (sinϕ/E\*) measured at 21°C, strain controlled fatigue damage (E\*sinϕ) measured at 21°C, permanent deformation damage (sinϕ/E\*) measured at 45°C, and flow number ($F_N$) of eight inhomogeneous (I-SPT) specimens, "Sd" represents standard deviation and "CV" represents coefficient of variation**

| Sample ID | 21°C | | | | 45°C | | | |
|---|---|---|---|---|---|---|---|---|
| | $E^*x10^6$ (kPa) | ϕ | sin(ϕ)/E\* $x10^{-8}$ (1/kPa) | $E^*sin(ϕ)$ $x10^6$ (kPa) | $E^*x10^5$ (kPa) | ϕ | sin(ϕ)/E\* $x10^{-7}$ (1/kPa) | $F_N$ |
| I-SPT1 | 5.06 | 27.17 | 9.02 | 2.31 | 3.76 | 40.06 | 17.13 | 3588 |
| I-SPT2 | 4.08 | 29.14 | 11.93 | 1.99 | 4.83 | 27.41 | 9.53 | 1067 |
| I-SPT3 | 3.85 | 26.50 | 11.58 | 1.72 | 8.19 | 36.75 | 7.30 | 4739 |
| I-SPT4 | 6.26 | 27.78 | 7.44 | 2.92 | 7.39 | 36.34 | 8.02 | 5166 |
| I-SPT5 | 6.79 | 26.67 | 6.61 | 3.05 | 4.66 | 37.16 | 12.95 | 3164 |
| I-SPT6 | 5.26 | 26.16 | 8.38 | 2.32 | 5.15 | 37.96 | 11.95 | 4350 |
| I-SPT7 | 4.64 | 26.96 | 9.76 | 2.11 | 6.04 | 34.70 | 9.42 | 4331 |
| I-SPT8 | 4.79 | 22.87 | 8.11 | 1.86 | 7.94 | 34.23 | 7.08 | 5082 |
| Average | 5.09 | 26.66 | 9.11 | 2.28 | 6.00 | 35.58 | 10.42 | 3936 |
| STD | 1.01 | 1.79 | 1.89 | 0.48 | 1.67 | 3.77 | 3.42 | 1349 |
| CV | 19.81 | 6.71 | 20.78 | 20.96 | 27.77 | 10.60 | 32.86 | 34.29 |

**Table 8-3. The computed F and computed t for the comparison of the variances ($s^2$) and the means of compressive properties for homogeneous (H-SPT) and inhomogeneous (I-SPT) specimens at various test temperatures (T)**

| Test | T (°C) | Property | Sample | Mean | $s^2$ | F* | t | $t_{cr}$ | Decision | Rejection Probability (%) |
|---|---|---|---|---|---|---|---|---|---|---|
| Dynamic Modulus | 21 | $E^* \times 10^6$ (kPa) | H-SPT | 5.77 | 0.72 | 1.41 | 1.76 | 2.14 | Accept | 17.1 |
| | | | I-SPT | 5.09 | 1.02 | | | | | |
| | | $\sin(\phi)/E^* \times 10^{-8}$ (1/kPa) | H-SPT | 8.58 | 1.23 | 2.89 | 0.68 | 2.14 | Accept | 50.88 |
| | | | I-SPT | 9.11 | 3.57 | | | | | |
| | | $\sin(\phi)E^* \times 10^6$ (kPa) | H-SPT | 2.82 | 0.27 | 0.86 | 2.15 | 2.14 | Reject | 4.99 |
| | | | I-SPT | 2.28 | 0.23 | | | | | |
| Dynamic Modulus | 45 | $E^* \times 10^5$ (kPa) | H-SPT | 6.08 | 1.14 | 2.41 | 0.12 | 2.14 | Accept | 90.3 |
| | | | I-SPT | 6.00 | 2.79 | | | | | |
| | | $\sin(\phi)/E^* \times 10^{-7}$ (1/kPa) | H-SPT | 9.95 | 2.72 | 4.32 | 0.35 | 1.81 | Accept | 36.62 |
| | | | I-SPT | 10.42 | 11.70 | | | | | |
| Repeated Axial | 45 | $F_N$ | H-SPT | 3604 | 458329 | 3.97 | 0.62 | 1.81 | Accept | 27.38 |
| | | | I-SPT | 3936 | 181989 | | | | | |

*Critical F for equality of the variances is 3.79.

statistic for the measurement of homogeneity (Chapter 7). The discussion on the results of compressive testing and the effect of inhomogeneity on the measured compressive properties are presented for each test at each test temperature.

## 8.2  COMPARISON OF DYNAMIC MODULUS TEST PROPERTIES AT 21°C

### 8.2.1  Comparison of E* of H-SPT and I-SPT Specimens

The compressive modulus (E*) of the asphalt mixture material is an important parameter that determines the ability of the material to resist compressive strain as it is subjected to cyclic compressive loading and unloading. The measured E* values were compared for homogeneous and inhomogeneous specimens at a test temperature of 21°C, where the behavior of the mixture is hypothesized to be greatly dominated by binder stiffness.

The E* values for the eight specimens, for both groups, were ranked from highest to lowest. Figure 8-1 indicates that at 21°C the E* values of homogeneous specimens were all slightly higher than those of the inhomogeneous specimens, which indicates a slightly higher ability of homogeneous specimens to resist compressive strain. The mean E* values are shown in Table 8-1 and Table 8-2, with the values being $5.77 \times 10^6$ kPa for H-SPT and $5.09 \times 10^6$ kPa for I-SST specimens. It is also indicated that the variability in the E* values of the H-SPT specimens is lower than the variability in the E* values of the I-SPT specimens, with the coefficients of variation being 14.80% versus 19.81%, respectively. The higher coefficient of variation indicates less stability in the test measurements of the inhomogeneous specimens.

Statistical tests were conducted to evaluate the significance of the difference between the variances and the means of the two sets of specimens. An F test on the variances was applied to determine if the variability in the E* values of the two sets of specimens were significantly different. The computed F value of 1.41 was compared with the critical F value of 3.79 for a 5 % level of significance, which indicated that the difference in the variances was not significant.

A two-sample t-test assuming equal variances was then conducted on the mean E* values of H-SPT and I-SPT specimens to examine if the observed difference in the means was significant. Using a 5% level of significance, a computed t value of 1.76 was compared to the critical t value of 2.14, which indicates that the difference in the mean E* values was not significant. The computed t value of 1.76 corresponds to a 17.1% rejection probability. Therefore, from a statistical standpoint, the measured moduli of homogeneous and inhomogeneous mixtures are not different.
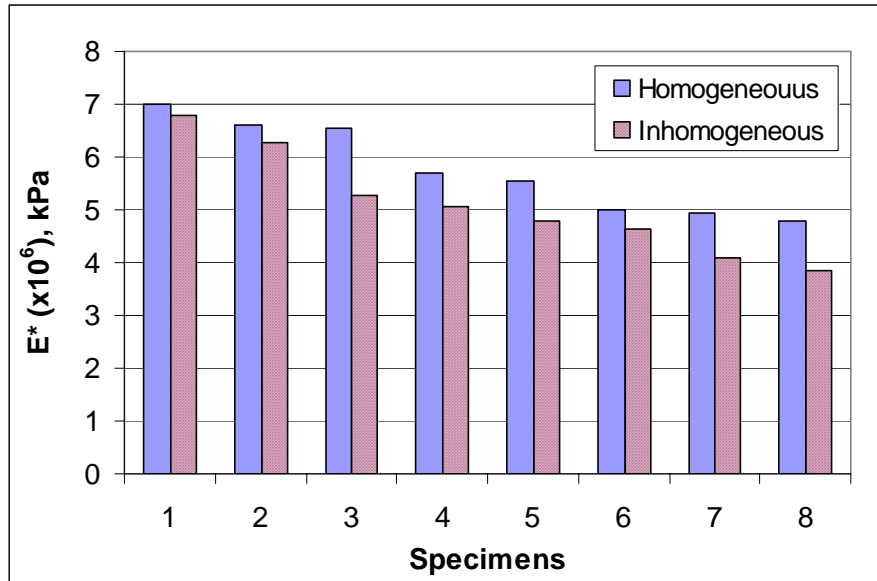
**Figure 8-1. Comparison of E\* of homogeneous and inhomogeneous specimens, 21°C**

### 8.2.2    Comparison of $\sin\phi/E^*$ of H-SPT and I-SPT Specimens

The fatigue damage in a stress controlled mode of loading or the susceptibility of

the mixture to fatigue cracking in a thick layer is evaluated by $\sin\phi/E^*$ at intermediate

temperatures. The higher the $\sin\phi/E^*$, the greater the likelihood that the material is

susceptible to fatigue damage when it is placed in a thick layer. Values of the $\sin\phi/E^*$

parameter for homogeneous and inhomogeneous specimens were compared to examine

the effect of vertical inhomogeneity on estimates of fatigue susceptibility of the material

when placed in a thick overlay.

The $\sin\phi/E^*$ values for the eight specimens, for both groups, were ranked from

highest to lowest. Figure 8-2 indicates that at 21°C, five out of eight $\sin\phi/E^*$ values for

homogeneous specimens were smaller than those of inhomogeneous specimens. The

mean $\sin\phi/E^*$ for homogeneous specimens is also lower than that of inhomogeneous

specimens, with values of $8.58\times10^{-8}$ kPa versus $9.11\times10^{-8}$ kPa, respectively (Table 8-1
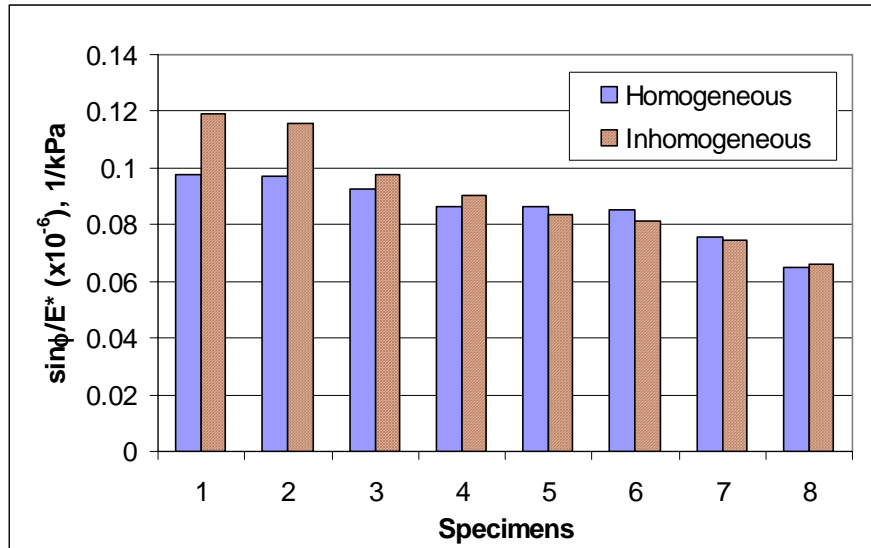
**Figure 8-2. Comparison of sinϕ/E\* of homogeneous and inhomogeneous specimens, 21°C**

and Table 8-2). The higher mean sinϕ/E\* value of inhomogeneous specimens indicates

that the material would be estimated to be more susceptible to fatigue damage when it is

placed in a thick layer. From Table 8-1 and Table 8-2, it is also indicated that the

variability in the sinϕ/E\* values of the inhomogeneous specimens is higher than the

variability in the sinϕ/E\* values of the homogeneous specimens, with coefficients of

variation of 20.78% versus 12.98%, respectively. The higher coefficient of variation of

the inhomogeneous specimens indicates less stability in the test measurements.

Statistical tests were conducted to evaluate the significance of the difference

between the variances and the means of the two sets of specimens. An F test on the

variances was applied to determine if the variability in the sinϕ/E\* values of the

homogeneous and inhomogeneous groups were significantly different. The computed F

value of 2.89 was compared with the critical F value of 3.79 for a 5% level of

significance, which indicated that the difference in the variances was not significant.

278

A two-sample t-test assuming equal variances was then conducted on the mean $\sin\phi/E^*$ values of inhomogeneous and homogeneous specimens to examine if the observed difference between the means is significant. Using a 5% level of significance, a computed t value of 0.68 was compared to the critical t value of 2.14, which indicated that the difference in the means was not significant. The computed t value of 0.68 corresponds to a 50.88% rejection probability. This indicates that based on the results of the dynamic modulus test the susceptibility of the material to fatigue damage in a thick layer would not be overestimated even if the tested specimens were extremely inhomogeneous.

## 8.2.3 Comparison of E*sin$\phi$ of H-SPT and I-SPT Specimens

The fatigue damage in a strain controlled mode of loading or the susceptibility of the mixture to fatigue cracking in a thin pavement layer is represented by E*sin$\phi$ measured at an intermediate temperature. The higher the E*sin$\phi$, the more the material would be susceptible to fatigue damage when it is placed in a thin layer. The E*sin$\phi$ values were compared for homogeneous and inhomogeneous specimens to examine the effect of vertical inhomogeneity on the estimate of the fatigue susceptibility of the material when placed in a thin overlay.

The E*sin$\phi$ values for the eight specimens, for both groups, were ranked from the highest to lowest. Figure 8-3 indicates that at 21°C, the E*sin$\phi$ values of homogeneous specimens were all higher than those of inhomogeneous specimens. Table 8-1 and Table 8-2 also show that the mean E*sin$\phi$ values of H-SPT specimens is greater than that of I-SPT specimens, with the values of $2.82 \times 10^6$ kPa for H-SPT and $2.28 \times 10^6$ kPa for I-SPT specimens. This means that based on E*sin$\phi$ values of inhomogeneous specimens the material would be estimated to be less susceptible to fatigue cracking when it is placed in
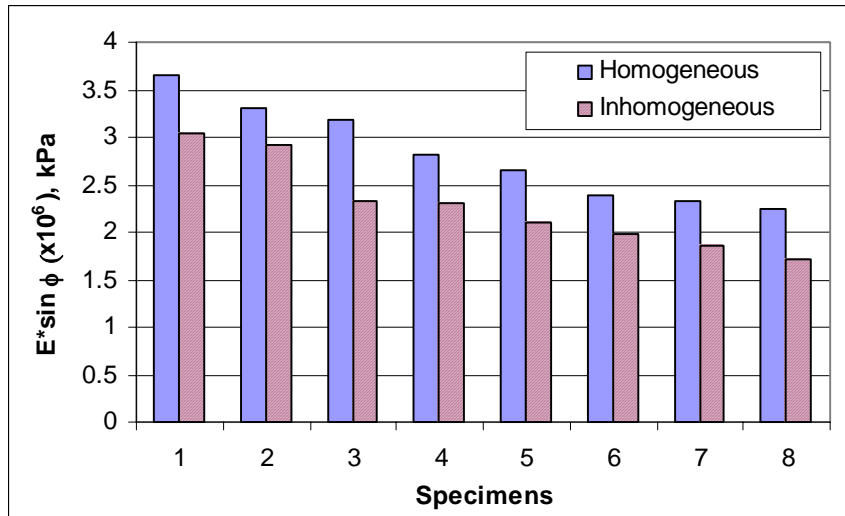
**Figure 8-3. Comparison of sinφ E\* of homogeneous and inhomogeneous specimens, 21°C**

a thin layer. Table 8-1 and Table 8-2 also show the variability of the E\*sinφ values. The

E\*sinφ values of inhomogeneous specimens are slightly more variable than those of

homogeneous (H-SPT) specimens, with coefficients of variation of 20.96% for I-SPT and

18.30% for H-SPT specimens. The higher coefficient of variation of the inhomogeneous

specimens indicates less stability in the test measurements.

Statistical tests were conducted to evaluate the significance of the difference

between the variances and the means of the two sets of specimens. An F test on the

variances was applied to determine if the variability in the E\*sinφ values of the

homogeneous and inhomogeneous groups were significantly different. The computed F

value of 0.86 was compared with the critical F value of 3.79 for a 5% level of

significance, which indicated that the difference in the variances was not significant.

A two-sample t-test assuming equal variances was then conducted on the mean E\*sinφ

values of the homogeneous and inhomogeneous specimens to examine if the observed

difference in the means was significant. Using a 5% level of significance, a computed t

value of 2.15 was compared to the critical t value of 2.14, which indicates a significant difference. The computed t value of 2.15 corresponds to a 4.99 % rejection probability. This indicates that the effect of inhomogeneity on the estimate of fatigue susceptibility of the material in a thin layer is significant.

In the testing of asphalt mixtures, the possibility of inhomogeneity exists. The test results may provide smaller E*sin$\phi$ values than that expected. The use of smaller E*sin$\phi$ values would result in over-predictions of the fatigue performance of the material and under-design of a thin layer, which could result in premature failure of the layer.

In summary, the statistical analyses indicated that vertical inhomogeneity has significant impact on measured E*sin$\phi$ values, which might impact the prediction of the fatigue performance of a thin pavement layer. The fatigue performance of a thin layer based on the laboratory measurement of inhomogeneous E*sin$\phi$ values might be over predicted, which could result in the premature failure of an overlay.

## 8.3 COMPARISON OF DYNAMIC MODULUS PROPERTIES AT 45°C

### 8.3.1 Comparison of E* of H-SPT and I-SPT Specimens

The compressive modules (E*) of the asphalt mixtures were compared for homogeneous and inhomogeneous specimens at a test temperature of 45°C, where the behavior of the mixture is hypothesized to be mostly dominated by the aggregate structure. Therefore, the effect of inhomogeneity is expected to be more evident at high test temperatures.

The E* values for the eight specimens, for both groups, were ranked from highest to lowest. Figure 8-4 shows that at 45°C, five out of eight E* values of homogeneous
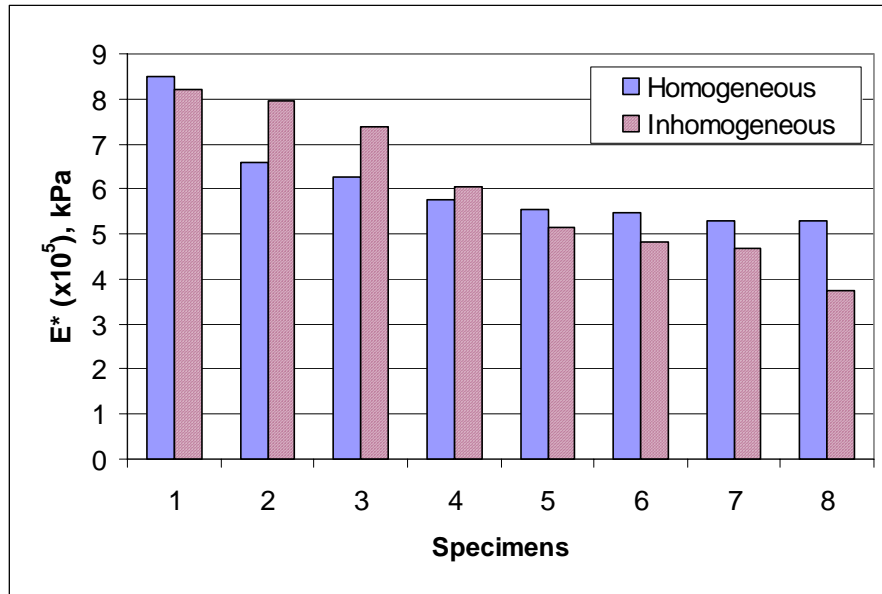
**Figure 8-4. Comparison of E\* of homogeneous and inhomogeneous specimens, 45°C**

specimens were higher than those of inhomogeneous specimens. Table 8-1 and Table 8-2 indicate that the mean E\* value of H-SPT specimens is slightly higher than that of I-SPT specimens, with the values being $6.08 \times 10^5$ kPa and $6.00 \times 10^5$ kPa, respectively. The tables also show that the variability in the E\* values of the H-SPT specimens is lower than that of the I-SPT specimens, with coefficients of variation of 17.63% versus 27.7%, respectively. The higher coefficient of variation indicates less stability in the test measurements of the inhomogeneous specimens.

Comparison of the variability of the E\* values at 21°C and 45°C provides additional information on the effect of inhomogeneity. It is evident from Table 8-1 and Table 8-2 that the variability in the E\* values is greater at 45°C test temperature than at 21°C. The variabilities of 14.80% and 17.63% at 21°C are compared with 19.81% and 27.77% at 45°C for the H-SPT and I-SPT specimens, respectively. The higher coefficient of variation indicates less stability in the test measurements at a high test temperature.

Statistical tests were conducted to evaluate the significance of the difference between the variances and the means of the two sets of specimens. An F test on the variances was applied to determine if the variability in the E* values of the homogeneous and inhomogeneous groups were significantly different. The computed F value of 2.41 was compared with the critical F value of 3.79 for a 5% level of significance, which indicated that the difference in the variances was not significant.

A two-sample t-test that assumes equal variances was made on the mean E* values of the inhomogeneous and homogeneous specimens to examine if the observed difference in the means was significant. Using a 5% level of significance, a computed t value of 0.12 was compared to the critical t value of 2.14, which indicates that the difference in the means was not significant. The computed t value of 0.12 corresponds to a 90.3% rejection probability. Therefore, from a statistical standpoint, the means and variances of the stiffness values of the homogeneous and inhomogeneous mixtures at high test temperatures are not significantly different.

A comparison of the values of the dynamic modulus of homogeneous and inhomogeneous specimens at intermediate and high test temperatures would show if the effect of inhomogeneity is different at the two temperatures. The results indicate that the difference between the E* values of the H-SST and I-SST specimens at the high test temperature is smaller than the difference at intermediate temperature. This is specified from the rejection probabilities of 90.3% and 17.1% for E* comparisons at the high and intermediate temperatures, respectively.

In summary, based on the statistical evaluations, the differences between the means and variances of the E* values of homogeneous and inhomogeneous specimens

were not significant, which means that inhomogeneity does not have an effect on the load

capacity of the material either at intermediate or high temperatures. However,

inhomogeneity might be the cause for the smaller difference in the dynamic modulus

values of the homogeneous and inhomogeneous specimens at high temperature than at

intermediate temperature. The smaller difference in modulus values at 45°C is caused by

the smaller rate of decrease in modulus with the increase in test temperature for the

inhomogeneous specimens. This might have been caused by the coarser mixture in the

lower portion of inhomogeneous specimens resisting more of the axial load than the

homogeneous mixture. Therefore, the hypothesis that the effect of aggregate structure is

more evident at high-test temperature is valid.

### 8.3.2 Comparison of sin$\phi$/E* of H-SPT and I-SPT Specimens

The susceptibility of the material for permanent deformation (rutting) was

evaluated by sin$\phi$/E* measured at high temperatures. The higher the measured sin$\phi$/E*,

the more the material should be susceptible to permanent deformation. The sin$\phi$/E*

parameter of H-SPT and I-SPT specimens were compared to examine the effect of

vertical inhomogeneity on the estimate of rutting potential of the material.

The sin$\phi$/E* values for the eight specimens, for both groups, were ranked from the

highest to lowest. Figure 8-5 indicates that at 45°C, four out of eight sin$\phi$/E* values of

homogeneous specimens were smaller than those of inhomogeneous specimens. Table

8-1 and Table 8-2 show that the mean sin$\phi$/E* for homogeneous specimens is smaller

than that of inhomogeneous specimens, with values of $9.95 \times 10^{-7}$ kPa for H-SST and

$10.42 \times 10^{-7}$ for I-SST specimens. The higher mean sin$\phi$/E* value indicates that I-SPT

specimens are more susceptible to permanent deformation damage. The tables also
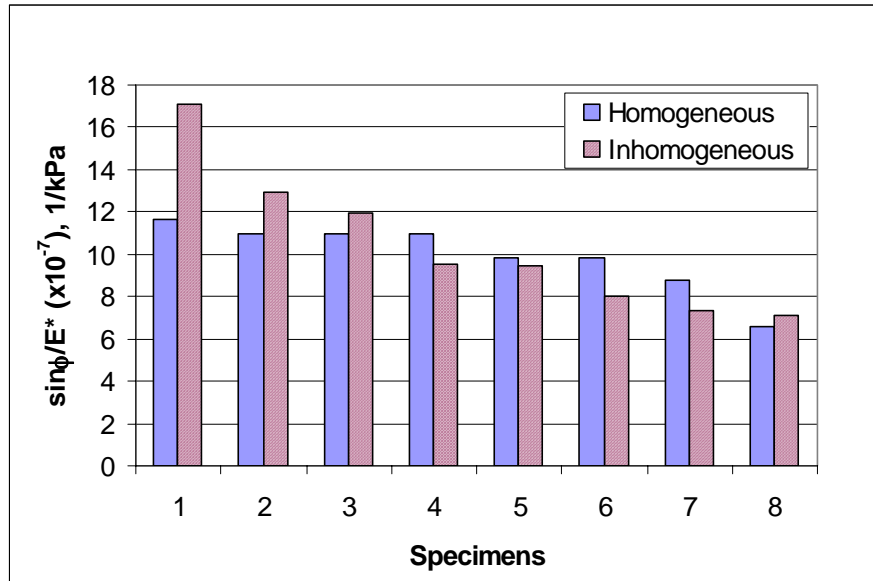
**Figure 8-5. Comparison of sinφ/E\* of homogeneous and inhomogeneous specimens, 45°C**

indicate that the variability in the sinφ/E\* values of the H-SPT specimens is smaller than

the variability in the sinφ/E\* values of the I-SPT specimens, with coefficients of variation

of 16.55% and 32.86%, respectively. The higher coefficients of variation indicate less

stability in the test measurements of the inhomogeneous specimens.

Statistical tests were conducted to evaluate the significance of the differences

between the variances and the means of the two sets of specimens. An F test on the

variances was applied to determine if the variability in the sinφ/E\* values of the H-SPT

and I-SPT specimens were significantly different. The computed F value of 4.32 was

compared with the critical F value of 3.79 for a 5 % level of significance, which indicated

that the difference in the variances of the sinφ/E\* of the two groups was significant.

A two-sample t-test that assumes unequal variances was then conducted on the

mean sinφ/E\* values of H-SST and I-SST specimens to examine if the observed

difference in the means was significant. Using a 5% level of significance, a computed t

value of 0.35 was compared to the critical t value of 1.81, which indicated that the difference in the means was not significant. The computed t value of 0.35 corresponds to a 36.62 % rejection probability. This indicates that from a statistical standpoint, homogeneous and inhomogeneous specimens have similar responses in permanent deformation. As a result, the prediction of the permanent deformation performance of a pavement layer based on the measurements of $\sin\phi/E^*$ from inhomogeneous specimens could be valid.

In summary, based on the statistical evaluation, the performance prediction of a pavement layer using laboratory measurement of $\sin\phi/E^*$ could be valid even if an extreme level of vertical inhomogeneity was present. This occurs because the difference between the mean $\sin\phi/E^*$ values for homogeneous and inhomogeneous specimens was not significant.

## 8.4 COMPARISON OF FLOW NUMBER TEST RESULTS

In addition to the $\sin\phi/E^*$ parameter, the resistance of a mixture to permanent deformation can be measured using the flow number ($F_N$) from the repeated axial load test. The flow number is the number of load cycles at which the rate of change of the cumulative axial permanent strain is minimum. The higher the $F_N$ value, the more resistant the material is to permanent deformation. The $F_N$ values of the homogeneous and inhomogeneous specimens were compared to examine the effect of inhomogeneity on the estimate of permanent deformation potential of the material.

The $F_N$ values of the eight specimens for both groups were ranked from the highest to the lowest. Figure 8-6 shows that seven out of eight $F_N$ values for H-SPT
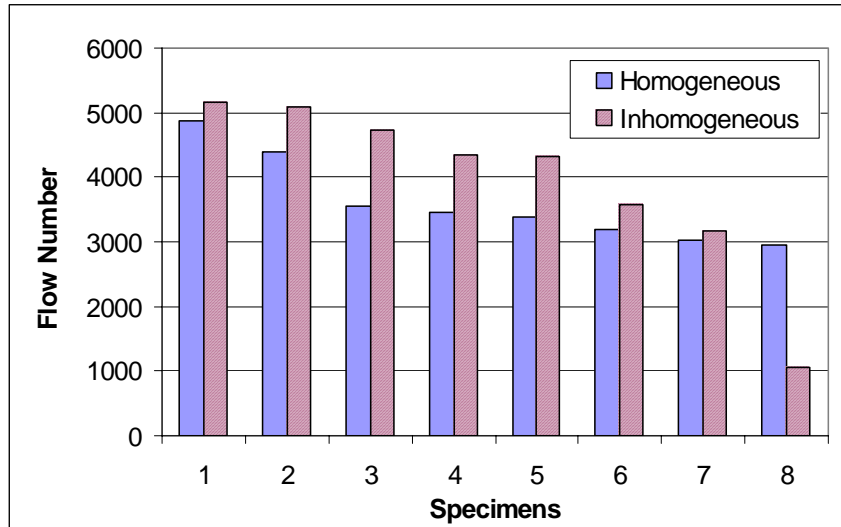
**Figure 8-6. Comparison of F$_N$ values of homogeneous and inhomogeneous specimens**

specimens were smaller than those for I-SPT specimens. Table 8-1 and Table 8-2 also

show that the mean F$_N$ value of H-SPT specimens is smaller than that of I-SPT

specimens, with values of 3604 for H-SST and 3936 for I-SST specimens. This means

that the homogeneous specimens failed after a smaller number of load cycles than the

inhomogeneous specimens. The tables show that the variance of F$_N$ values of H-SPT

specimens is lower than that of I-SPT specimens, with coefficients of variation of 18.79%

and 34.29 %, respectively. The higher coefficient of variation indicates less stability in

the test measurements of the inhomogeneous specimens.

Statistical tests were conducted to evaluate the significance of the difference

between the variances and the means of the two sets of specimens. An F test on the

variances was applied to determine if the variability in the F$_N$ values of the homogeneous

and inhomogeneous groups were significantly different. The computed F value of 3.97

was compared with the critical F value of 3.79 for a 5% level of significance, which

indicated that the difference was significant.

A two-sample t-test that assumes unequal variances was conducted on the mean $F_N$ values of H-SST and I-SST specimens to examine if the observed difference in the means was significant. Using a 5% level of significance, a computed t value of 0.62 was compared to the critical t value of 1.81, which indicated that the difference in the means was not significant. The computed t value of 0.62 corresponds to a 27.38 % rejection probability. This indicates that based on $F_N$ measurements the prediction of the rutting performance of the material could be valid even if the tested specimens were extremely inhomogeneous.

Although the difference between the $F_N$ values was shown to be statistically insignificant, the physical impact of the difference on the performance prediction of a pavement layer needed to be addressed. Since in testing of asphalt mixtures the possibility of inhomogeneity exists, large $F_N$ values might be measured. Therefore, the performance of a pavement layer based on the measured $F_N$ values could be over predicted. A premature failure of the layer could occur if the selection of the overlay materials were based on the $F_N$ values of inhomogeneous specimens.

In summary, the statistical analyses indicated that the performances of homogeneous and inhomogeneous specimens in permanent deformation were not significantly different. Therefore, statistically, the performance prediction of a pavement layer based on the laboratory measurement of $F_N$ would be reliable even if an extreme level of vertical inhomogeneity was present. However, from a physical standpoint, the performance of a layer in permanent deformation might be over predicted if the tested specimens were extremely inhomogeneous. A premature failure of the layer might occur

if the materials for a pavement layer were selected based on the $F_N$ values of inhomogeneous specimens.

It is also observed that although both $F_N$ and $\sin\phi/E^*$ at 45°C evaluate the permanent deformation performance of the material, they provided opposite decisions regarding the effect of inhomogeneity. Based on the $\sin\phi/E^*$ values of inhomogeneous specimens, the performance of a pavement layer would be under predicted, while the use of $F_N$ values would result in over prediction of the performance. It appears that the response of the material is a function of the test type, which is characterized by magnitude, frequency, and duration of the load. Therefore, the design engineer needs to be aware of the specific effect of inhomogeneity on the property of interest and to adjust design and performance prediction accordingly.

## 8.5  RELATIONSHIP BETWEEN SPT RESULTS AND INHOMOGENEITY

It is of interest to evaluate the relationship between compressive properties and the aggregate inhomogeneity to improve the reliability of the design and performance prediction of pavement layers. The existence of such relationship would make it possible to improve the models for the prediction of the compressive properties of asphalt mixtures. A correlation analysis provides the means to examine the relationship between the compressive properties and inhomogeneity and to draw conclusions about the strength of the relationship. The correlation analyses include graphical analyses and computation of the correlation coefficient, R. The graphical analysis provides the visual inspection of the data that would indicate the degree to which compressive properties and the aggregate inhomogeneity are related. The correlation coefficient, R, is the quantitative

measure of the degree to which variation in inhomogeneity can be used to explain the variation in compressive properties.

To examine the relationship between compressive properties and index of homogeneity, the measured and computed compressive properties in Table 8-1 and Table 8-2 and the computed z statistic in Tables 7-6 and 7-8 were used. The z statistic was selected among the tested indices of homogeneity since in addition to showing a statistical power of 100% (Chapter 6), it provided a high rejection probability in the measurement of homogeneity and low rejection probability in the measurement of inhomogeneity. The z statistic also indicated the greatest distinction between homogeneous and inhomogeneous specimens (Chapter 7). Each of the compressive properties was then plotted versus the computed z values to visually investigate a trend between the two sets of variables. The correlation coefficient between the computed z values and each of the compressive properties was also computed.

The discussion is divided based on the test type and test temperature, since the compressive response of the specimens was different with respect to different tests and at different temperatures. Two types of correlations will be discussed: (1) the correlation between computed z values and each compressive property within each set of homogeneous and inhomogeneous specimens and (2) the correlation between the computed z values and each of the compressive properties between the two sets of homogeneous and inhomogeneous specimens. The computed correlation coefficients, R, within the homogeneous set, within the inhomogeneous set, and between the homogeneous and inhomogeneous sets for the two temperatures of 21°C and 45°C are provided in Table 8-4. To examine the statistical significance of the correlations, the

computed values of Table 8-4 are compared to the critical correlation coefficients for a 5% level of significance.

## 8.5.1  Relationship between z Statistics and E* Properties at 21°C

At 21°C the relationship between the z statistic and three compressive properties of E*, sinϕ/E*, and E*sinϕ were evaluated within H-SPT, within I-SPT, and between H-SPT and I-SPT sets. The coefficients in Table 8-4 indicate that within either homogeneous or inhomogeneous sets the compressive properties are not correlated with the z statistic. This indicates that the variability within compressive properties of either H-SST or I-SST specimens measured at 21°C was not explained by the variability in the aggregate distribution. This observation was expected since the range of z statistic for each set of specimens is very narrow.

The relationship of the compressive properties and the z statistics between the H-SPT and I-SPT sets are shown in Figure 8-7 through Figure 8-9. In this case, a higher correlation between the compressive properties and the z statistic is expected since the range of z values is much wider for the two sets than the range within each set of

**Table 8-4. Correlation coefficients, R, between the z statistic and the compressive properties**

| Test Temperature | Test | Property | Within Homogeneous | Within Inhomogeneous | Between Homogeneous and Inhomogeneous |
|---|---|---|---|---|---|
| 21°C | Dynamic Modulus | E* | -0.141 | -0.063 | -0.367 |
| | | sin(ϕ)/E* | 0.000 | 0.055 | 0.184 |
| | | E*sin(ϕ) | -0.187 | -0.032 | -0.499* |
| 45°C | Dynamic Modulus | E* | -0.344 | 0.625 | -0.063 |
| | | sin(ϕ)/E* | 0.341 | -0.780* | 0.045 |
| 45°C | Flow Number | FN | -0.344 | 0.565 | 0.063 |

* The computed R indicates that the correlation is statistically significant when compared with the critical correlation coefficient of 0.707 for n=8 and 0.497 for n=16.

specimens. Values in Table 8-4 indicate that R values for the correlation between the two sets are greater than the correlations within each set of specimens. However, among the three compressive properties, only the correlation between E*sin$\phi$ and z (|R| of 0.499) was above the critical R of 0.497. Figure 8-7 through Figure 8-9 also indicate that despite clear distinction between homogeneous and inhomogeneous z statistics, the change in compressive properties with respect to the change in z statistic is small. In summary, among the compressive properties of the specimens as measured by the dynamic modulus test at 21C°, only E*sin$\phi$ was affected by specimen inhomogeneity.

## 8.5.2 Relationship between z Statistics and E* Properties at 45°C

The relationship of the z statistic and the two compressive properties of E* and sin$\phi$/E* measured at 45°C were evaluated because the strength of the relationship at high test temperatures was of interest. It is hypothesized that at high-test temperatures the mechanical response of the material is more dominated by the aggregate structure than at
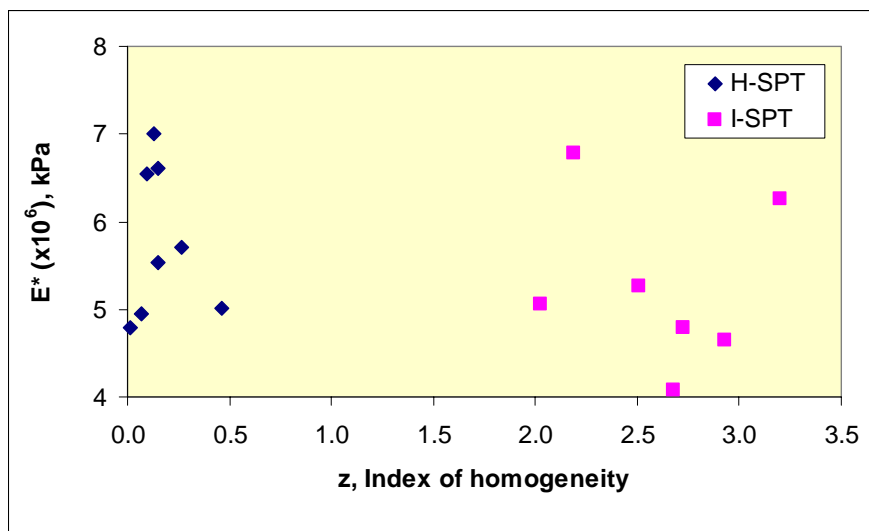


**Figure 8-7. Relationship between "z" and E* of homogeneous and inhomogeneous sets, 21°C; H-SPT stands for homogeneous and I-SPT stands for inhomogeneous specimens**
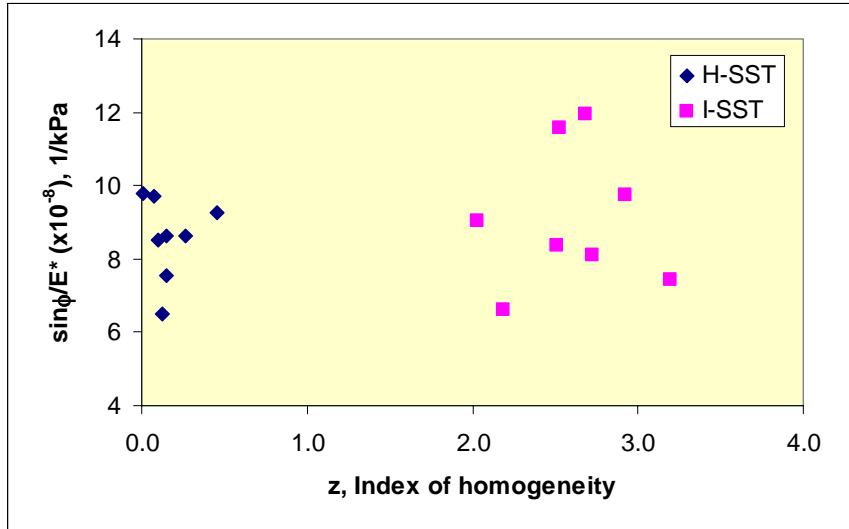
**Figure 8-8. Relationship between "z" and sinφ/E\* of homogeneous and inhomogeneous sets, 21°C; H-SPT stands for homogeneous and I-SPT stands for inhomogeneous specimens**
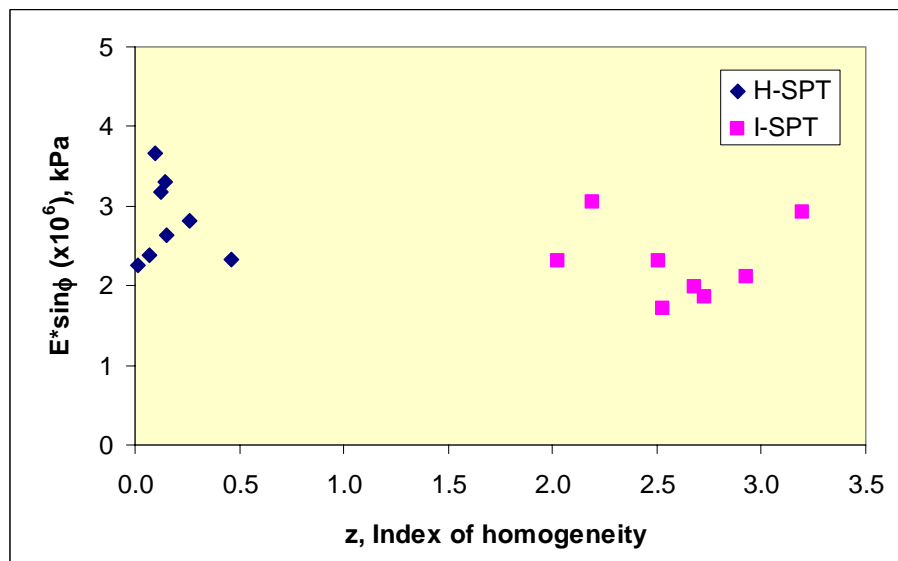


**Figure 8-9. Relationship between "z" and E\*sinφ of homogeneous and inhomogeneous sets, 21°C; H-SPT stands for homogeneous and I-SPT stands for inhomogeneous specimens**

intermediate temperatures. Therefore, a higher correlation between the compressive

properties and z statistic would be expected. The evaluations were conducted for

specimens within the H-SPT set, within the I-SPT set, and between the H-SPT and I-SPT

sets.

The correlation of each property with the computed z statistic within each set of

specimens is provided in Table 8-4. As indicated from the R values within the H-SPT

specimens, low correlations exist between the homogeneity index (z) and each of the

compressive properties. However, a comparison of the computed and critical R values

indicated that none of the correlations were statistically significant. The R values within

the I-SPT specimens indicated that the correlations are either insignificant (between E*

and z) or they have incorrect directions. The direction of the relationship (between

$\sin\phi$/E* and z is counter to the expected direction of the trend (R= -0.780). This is the

result of sampling variation for the small sample. However the trend implies that, at a

high-test temperature, the variability in the compressive properties within each set of

specimens was not explained by the variation in aggregate distribution.

The relationships of compressive properties and the homogeneity indices for all

specimens, homogeneous and inhomogeneous, are shown in Figure 8-10 and Figure 8-11.

As shown in the figures and indicated by the R values of Table 8-4, the correlations

between the z statistic and each of the compressive properties are very small. Despite the

expectation of higher correlations for a wider range of z values, the difference between

the compressive properties of homogeneous and inhomogeneous specimens was not

explained by the level of inhomogeneity. The reason for the low correlations between the

compressive properties measured at a high test temperature and the index of homogeneity

is the small change in the compressive properties of the mixture with the increase in the level of inhomogeneity.

### 8.5.3    Relationship between the z Statistics and the Flow Number

The correlation of the flow numbers from the repeated axial load test at 45°C with the z statistic was investigated. The correlations were evaluated for specimens within H-SST, within I-SST, and between H-SST and I-SST sets. A higher correlation between the compressive properties and the z statistic should be expected since at high test temperatures the mechanical response of the material is hypothesized to be more dominated by the aggregate structure than at an intermediate temperature.

The correlations of $F_N$ and the z statistic within the H-SST and within I-SST specimens are provided in Table 8-4. As observed from the R values, the correlations within each set are not significant. The variability in the result of the flow number test within either homogeneous or inhomogeneous group was not explained by the variation in the aggregate distribution.

The relationship of $F_N$ and homogeneity index for all specimens, homogeneous and inhomogeneous, is shown in Figure 8-12. As shown in the figure and indicated in Table 8-4, the correlation between the z statistic and flow number is very low. Despite the expectation of a higher correlation for a wider range of z values, the differences between the $F_N$ values of the two sets of specimens were not explained by inhomogeneity. The reason for the insignificant correlation between flow number and the index of homogeneity is the insignificant change in the flow number of the mixture with the increase in the level of inhomogeneity.
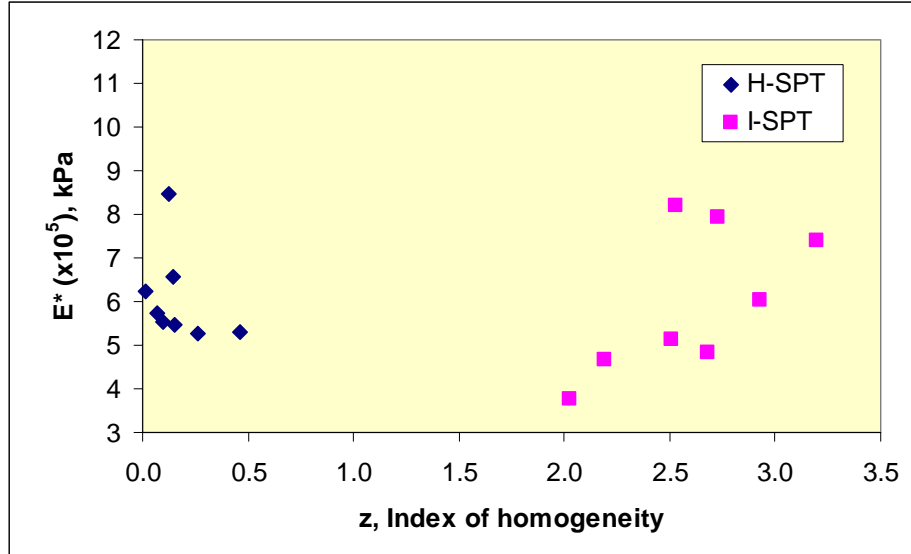
**Figure 8-10. Relationship between "z" and E* for homogeneous and inhomogeneous sets, 45°C; H-SPT stands for homogeneous and I-SPT stands for inhomogeneous specimens**
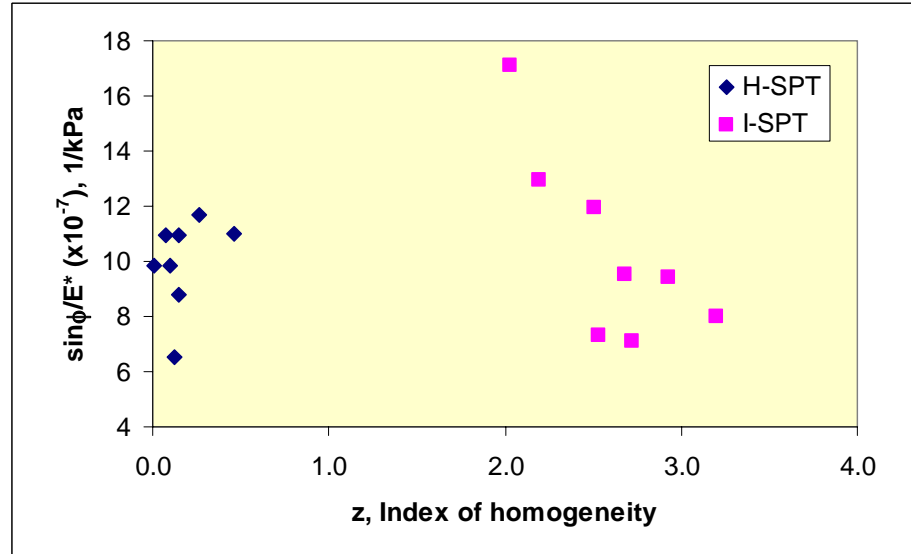


**Figure 8-11. Relationship between "z" and sin$\phi$/E* for homogeneous and inhomogeneous sets, 45°C; H-SPT stands for homogeneous and I-SPT stands for inhomogeneous specimens**
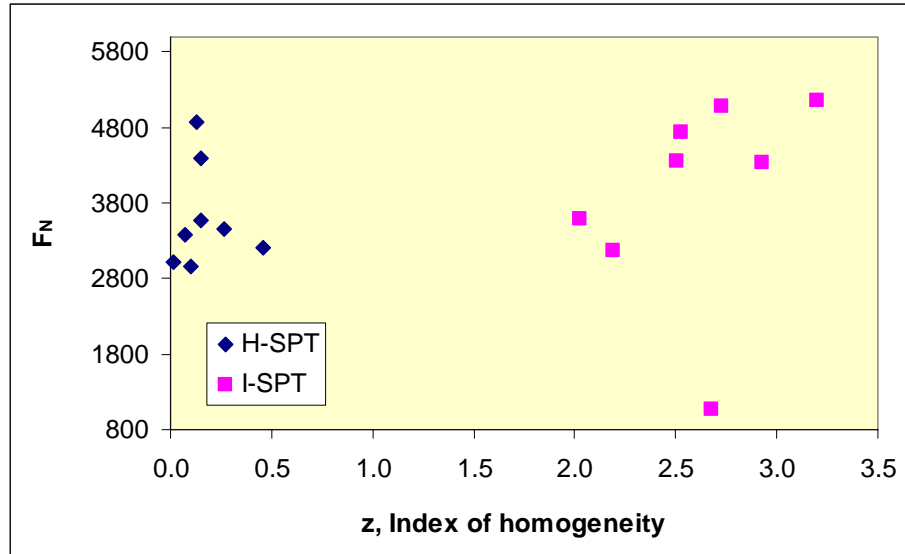
**Figure 8-12. Relationship between "z" and $F_N$ for homogeneous and inhomogeneous sets; H-SPT stands for homogeneous and I-SPT stands for inhomogeneous specimens**

## 8.6 SUMMARY OF THE CHAPTER

In this chapter the results of simple performance tests (SPT), which included the dynamic modulus and the repeated axial load (flow number) tests, were presented. The simple performance tests (SPT) were selected for the evaluation of the effect of vertical inhomogeneity on the mechanical performance of the asphalt mixture specimens for two reasons: first, the importance of the parameters that are measured from the tests and second, the suitability of the geometry of the test specimens. The compressive modulus (E*) of asphalt mixture as measured using SPT is an important parameter for the design and analysis of a pavement. Also, the cumulative deformation obtained from the flow number test is an indicator of permanent deformation characteristic of the asphalt mixture and is used in prediction of the high temperature performance of a pavement layer.

The geometry of the test specimens is the second advantage of the test. The SPT specimens, which are 150 mm in height by 100 mm in diameter, maintain the vertical

inhomogeneity that might have been developed during the specimen fabrication. In other words, the test specimen retains the original vertical inhomogeneity after it is cut and cored from the gyratory size to the standard test size.

The results of SPT for homogeneous and inhomogeneous specimens were statistically compared to evaluate if the difference between the means and variances of the two sets are significant. The results of the SPT tests were also used to evaluate the possible physical impact of inhomogeneity on the design and performance predictions, i.e., if the use of the measured dynamic modulus and flow number in design and performance prediction is valid when inhomogeneity is present. In addition, the correlation between various compressive properties and the level of inhomogeneity was evaluated. The observations in this chapter might be used to reevaluate the emphasis on homogeneity of the fabricated specimens in order to obtain the true compressive properties of a mixture. The findings of the chapter are summarized as follows:

1. At 21°C, the dynamic modulus of homogeneous specimens was higher than those of inhomogeneous specimens, but not significantly. From a statistical point of view, pavement layers can be reliably designed for fatigue cracking using the E* of vertically inhomogeneous specimens.

2. At 45°C, the dynamic modulus of homogeneous specimens was higher than those of inhomogeneous specimens, but not significantly. From the statistical point of view, a pavement layer can be reliably designed for permanent deformation using the E* of vertically inhomogeneous specimens.

3. The difference between E* of homogeneous and inhomogeneous specimens was smaller at a high temperature than at an intermediate temperature. This is indicated

by the larger rejection probability of the t-statistic at the high temperature than at the intermediate temperature (90.3% versus 17.1%, respectively). This shows that inhomogeneity lowers the rate of decrease in the modulus with the increase in temperature.

4. The $\sin\phi/E^*$ value measured at 21°C, which represents the fatigue susceptibility in thick pavement layer, increases with inhomogeneity, but not significantly, with the rejection probability of 50.88%. This means that from the statistical point of view the fatigue damage in a thick layer might be reliably predicted based on $\sin\phi/E^*$ of even extremely inhomogeneous laboratory specimens.

5. The $\sin\phi E^*$ value measured at 21°C, which represents the fatigue damage in thin layer, was smaller for inhomogeneous specimens. The rejection probability of 4.99% indicated that the difference is significant but marginally so. Therefore, the fatigue performance of a thin pavement layer based on $\sin\phi E^*$ values of inhomogeneous specimens might be over predicted, which might involve the risk of premature failure of the layer.

6. The mean $\sin\phi/E^*$ value measured at 45°C, which represents the susceptibility for permanent deformation, is measured slightly higher for inhomogeneous than for homogeneous specimens, with the rejection probability of 73.03%. From a statistical standpoint the permanent deformation of a pavement layer might be reliably predicted based on $\sin\phi/E^*$ of inhomogeneous laboratory specimen.

7. The flow number, which is the number of repetitions to failure, was greater for inhomogeneous than for homogeneous specimens, meaning that the performance of the material in permanent deformation improves with the increase in the level of

inhomogeneity. However, the rejection probability of 54.4% indicated that the difference was not significant. From a statistical point of view the performance of a pavement layer for permanent deformation can be reliably predicted based on the flow number values of inhomogeneous specimens. However, from the physical standpoint, the possibility exists that the rutting performance of a pavement layer is over predicted if the test specimens are inhomogeneous.

8.  Although $\sin\phi/E^*$ and $F_N$ both represent the potential for permanent deformation, they did not provide the same decision regarding the effect of inhomogeneity (items 6 and 7). It can be concluded that the effect of inhomogeneity on mechanical performance of a mixture is test dependant. The design engineer needs to be aware of the specific effect of inhomogeneity on the property of interest and to adjust design and performance prediction accordingly.

9.  The correlation between dynamic modulus test properties measured at 21°C and homogeneity index (z) within sets of homogeneous and inhomogeneous specimens were generally low. This indicates that the variability in compressive properties of homogeneous specimens was not explained by the variability in aggregate distribution.

10. The correlation between dynamic modulus test properties measured at 45°C and homogeneity index (z) within the homogeneous specimens were generally low. This indicates that even at high-test temperatures the variability in compressive properties of homogeneous specimens was not explained by the variability in aggregate distribution.

11. The correlations between dynamic modulus test properties measured at 45°C and the z index within inhomogeneous specimens were fair, with a significant correlation between z and $\sin\phi/E^*$ (R of 0.780). However, the observed direction did not agree with the expected direction of the trend (Item 6). It can be concluded that the significance of the correlation might be due to the sampling variation.

12. The correlation between dynamic modulus test properties and homogeneity index (z) between the two groups of homogeneous and inhomogeneous specimens for the two test temperatures were generally very low, meaning that the compressive properties of asphalt mixtures as measured by the dynamic modulus test are not a function of specimen inhomogeneity.

13. The correlation between $F_N$ and homogeneity index (z) within the homogeneous, within the inhomogeneous set, and between the homogeneous and inhomogeneous specimens was low. This indicates that the variability in cumulative deformation measurements using the axial load test was not explained by the variability in aggregate structure.

From the summary above, it can be concluded that the created level of vertical inhomogeneity that was accurately measured by normal proportion statistic (z), was not conclusively evident from the results of the simple performance tests. It can be assumed then that the simple performance tests are not sensitive to various arrangements of the aggregates even at high-test temperatures. Therefore, the tests are dependable in characterizing the properties of asphalt materials, since they measure some overall mixture properties regardless of the inhomogeneity in aggregate distribution. The observations in this chapter would raise the question: Should methods of laboratory

fabrication ensure homogeneity of specimens in order to obtain reliable compressive

properties of a mixture?

# CHAPTER 9 - TESTING OF SPECIMENS USING SUPERPAVE SHEAR TESTER

## 9.1 INTRODUCTION

To examine the effect of radial inhomogeneity on the mechanical performance of the mixture, the appropriate laboratory test needs to be selected. The selected test should have two important characteristics. First, it should be a robust test that has been recommended by professional associations for testing of asphalt mixture specimens. Second, the geometry of the required test specimen should retain the created radial inhomogeneity. Based on these characteristics, the simple shear tests (SST) were selected to evaluate the effect of radial inhomogeneity on mechanical performance of asphalt mixture specimens. The SST tests have been suggested by AASHTO (1998) for determining the permanent deformation and fatigue cracking characteristics of hot mix asphalt. The tests have been frequently used for characterizing the asphalt mixtures at the Turner-Fairbank Highway Research Center (TFHRC) Laboratory of Federal Highway Administration (FHWA). The asphalt mixture properties measured by the SST have been used as major parameters for the design and performance prediction applications. The SST results have also shown to agree well with the performance of Accelerated Loading Facility (ALF) test sections of FHWA (Stuart et al. 1999).

In addition to the applicability of the SST in characterizing asphalt mixtures, the geometry of the test specimens was a factor in the selection of the test. The required specimens for SST would retain the radial inhomogeneity that was originally created in the gyratory specimens. The inhomogeneously compacted gyratory specimens can be cut to the shape and size of SST specimens and yet keep their inhomogeneous characteristics.

Radially inhomogeneous and corresponding homogeneous specimens were fabricated and tested according to the standard test methods of simple shear tests (AASHTO, 1998). A summary of the procedures for preparing and testing asphalt mixture specimens to determine the mixture shear properties is provided in Chapter 2. Although the prepared homogeneous and inhomogeneous specimens were equal in size and shape, the distribution of the aggregates, asphalt, and as a result the distribution of air voids in the radially inhomogeneous specimens were intended to be significantly different from the homogeneous specimens. The selected constituent materials, the mixture design parameters for homogeneous specimens, and the altered mixture parameters for the inhomogeneous specimens were explained in Chapter 7. Three sets of eight specimens were prepared using two methods of compaction. The first set was cored from homogeneous linear kneading compacted slabs and is referred to as L-SST. Specimens of this set were assumed to be radially homogeneous. The second set of specimens was fabricated homogeneously according to the Superpave method of specimen preparation using a gyratory compactor. The as-compacted specimens were cut into the SST size specimens of 150 mm in diameter and 50 mm in height and are referred to as H-SST. This set was fabricated to be as homogeneous as possible; however, it was inevitable for some radial inhomogeneity to develop during the gyration process (Chapter 7). The third set of specimens that were cut from gyratory compacted specimens was purposely fabricated to reflect an extreme level of radial inhomogeneity and is referred to as I-SST.

The three sets of specimens were subjected to a shear mode of loading. Using the Superpave Shear Tester, two types of tests were conducted: the frequency sweep at a

constant height (FSCH) and the repeated shear test at a constant height (RSCH) (AASHTO, 1998). The FSCH test is a strain-controlled test that characterizes the constitutive behavior of the asphalt-aggregate mixture in shear. The RSCH test is a stress-controlled test that evaluates the mechanical performance of the asphalt mixtures by measuring the cumulative permanent deformation ($\varepsilon_p$) and the number of load repetitions to failure ($N_f$). The FSCH test was conducted at intermediate and high temperatures of 25°C and 50°C, respectively, and the RSCH test was conducted at the high temperature of 50°C.

A number of shear properties were computed using the shear stress, shear strain, and the phase angle ($\delta$), which were measured from the FSCH tests. The stiffness of the material is evaluated by the shear modulus, $G^*$, which is the shear stress divided by the shear strain. The damage or the dissipated energy in a strain-controlled mode of loading is measured by $G^*\sin\delta$. This is an indicator of fatigue damage in thin pavement layers at an intermediate pavement temperature. The damage or the dissipated energy for a stress controlled mode of loading is measured by $\sin\delta/G^*$. This represents the fatigue cracking susceptibility in thick layers at intermediate temperatures. When measured at a high temperature, $\sin\delta/G^*$ is an indicator of the permanent deformation susceptibility.

During the RSCH test, a repeated sinusoidal shear load was applied to the specimen to ensure failure. The strains after 5000 load cycles and the number of cycles that causes 2% strain in the specimen were the properties that were measured. The average shear properties from the FSCH test at a frequency of 10 Hz and the performance properties from the RSCH test are provided in Table 9-1 through Table 9-3.

The results of the FSCH and RSCH tests were analyzed to investigate the differences in the shear properties at the three different levels of radial inhomogeneity. One-way analyses of variance (ANOVA) were conducted to assess the difference. The comparison reflects the following hypotheses for the three groups of specimens:

*$H_o$: The mean shear property for the three levels of inhomogeneity is equal*

(5-101)

*$H_A$: The mean shear property for the three levels of inhomogeneity is not equal*

(5-102)

The ANOVA test uses an F statistic to test for the significance of the differences in the means. The decision would be based on the comparison of the critical and computed F values, with the critical value obtained from an F table. If the computed F exceeds the critical F, then the alternative hypothesis $H_A$ is assumed to be valid. The computed F statistics and the decisions made on the acceptance or the rejection of the null hypothesis are provided in Table 9-4. The comparisons are presented separately for each pair of specimen sets, while "LH" represents comparison of the linear kneading compacted and homogeneous gyratory compacted specimens, "LI" represents the comparison of the linear kneading compacted and inhomogeneous gyratory compacted specimens, and "HI" represents comparison of the homogeneous gyratory compacted and inhomogeneous gyratory compacted specimens.

In addition to the ANOVA F test, a correlation analysis, which characterizes the relationship of each shear property and the homogeneity index, was conducted. The correlation analysis included graphical study and computation of the correlation coefficient, R. The graphical study would reveal the soundness of the trends and the

**Table 9-1. Shear modulus (G\*), phase angle (δ), fatigue damage in stress-controlled mode (sinδ/G\* at 25°C), fatigue damage in strain-controlled mode (G\*sinδ), permanent deformation (sinδ/G\* at 50°C), repetition to failure (N$_f$), and permanent strain after 5000 cycles of linear kneading compacted (L-SST) specimens; "Sd" represents standard deviation and "CV" represents coefficient of variation**

| Sample ID | 25°C | | | | 50°C | | | N$_f$ | ε$_p$, % |
|---|---|---|---|---|---|---|---|---|---|
| | G\*x10$^5$ (kPa) | δ | sin(δ)/G\* x10$^{-4}$ (1/kPa) | G\*sin(δ) x10$^2$ (kPa) | G\*x10$^4$ (kPa) | δ | sin(δ)/G\* x10$^{-2}$ (1/kPa) | | |
| L-SST1 | 9.06 | 48.35 | 8.24 | 6.77 | 3.86 | 71.54 | 2.46 | 732 | 3.62 |
| L-SST2 | 9.10 | 45.95 | 7.89 | 6.54 | 2.72 | 67.44 | 3.39 | 946 | 4.46 |
| L-SST3 | 7.72 | 44.65 | 9.45 | 5.64 | 3.74 | 71.58 | 2.51 | - | - |
| L-SST4 | 8.26 | 46.91 | 8.87 | 6.05 | 3.97 | 69.8 | 2.35 | 3298 | 2.24 |
| L-SST5 | 7.76 | 47.1 | 9.47 | 5.70 | 3.47 | 68.84 | 2.74 | 1051 | 4.37 |
| L-SST6 | 8.55 | 47.31 | 8.43 | 6.16 | 4.29 | 72.07 | 2.21 | 1273 | 3.77 |
| L-SST7 | 8.23 | 46.13 | 8.68 | 5.89 | 4.11 | 71.12 | 2.30 | - | - |
| L-SST8 | 7.22 | 45.66 | 10.19 | 5.32 | 3.48 | 71.48 | 2.67 | - | - |
| Average | 8.24 | 47.43 | 8.90 | 6.01 | 3.71 | 68.68 | 2.58 | 1460 | 3.69 |
| Sd | 0.66 | 46.51 | 0.76 | 0.48 | 0.49 | 70.48 | 0.37 | 1046 | 0.89 |
| CV | 8.01 | 1.11 | 8.51 | 7.99 | 13.17 | 1.64 | 14.49 | 71.63 | 24.11 |

**Table 9-2. Shear modulus (G\*), phase angle (δ), stress-controlled fatigue damage (sinδ/G\* at 25°C), strain-controlled fatigue damage (G\*sinδ), permanent deformation (sinδ/G\* at 50°C), repetitions to failure (N$_f$), and permanent strain after 5000 cycles of homogeneous gyratory compacted (H-SST) specimens; "Sd" represents standard deviation and "CV" represents coefficient of variation**

| Sample | 25°C | | | | 50°C | | | N$_f$ | ε$_p$, % |
|---|---|---|---|---|---|---|---|---|---|
| | G\*x10$^5$ (kPa) | δ | sin(δ)/G\* x10$^{-4}$ (1/kPa) | G\*sin(δ) x10$^2$ (kPa) | G\*x10$^4$ (kPa) | δ | sin(δ)/G\* x10$^{-2}$ (1/kPa) | | |
| H-SST1 | 8.04 | 44.55 | 8.75 | 5.65 | 4.67 | 69.67 | 2.01 | 993 | 3.41 |
| H-SST2 | 8.50 | 44.73 | 8.25 | 5.96 | 4.88 | 69.95 | 1.92 | 834 | 4.17 |
| H-SST3 | 8.98 | 43.45 | 7.64 | 6.16 | 5.53 | 68.49 | 1.65 | 926 | 3.83 |
| H-SST4 | 8.17 | 43.32 | 8.42 | 5.61 | 5.18 | 65.86 | 1.80 | 1015 | 3.64 |
| H-SST5 | 9.32 | 43.07 | 7.52 | 6.54 | 5.41 | 68.25 | 1.72 | 952 | 3.72 |
| H-SST6 | 8.95 | 44.56 | 7.63 | 6.11 | 5.28 | 68.69 | 1.76 | 1176 | 3.55 |
| H-SST7 | 10.40 | 43.14 | 6.65 | 7.20 | 5.07 | 69.28 | 1.84 | - | - |
| H-SST8 | 8.88 | 43.82 | 7.70 | 6.07 | 5.20 | 68.79 | 1.80 | - | - |
| Average | 8.90 | 46.51 | 7.82 | 6.16 | 5.15 | 68.62 | 1.81 | 983 | 3.72 |
| Sd | 0.74 | 0.69 | 0.65 | 0.51 | 0.28 | 1.26 | 0.11 | 114 | 0.26 |
| CV | 8.36 | 1.48 | 8.29 | 8.29 | 5.38 | 1.84 | 6.24 | 11.59 | 7.07 |

**Table 9-3. Shear modulus (G\*), phase angle (δ), stress-controlled fatigue damage (sinδ/G\* at 25°C), strain-controlled fatigue damage (sinδG\*), permanent deformation (sinδ/G\* at 50°C), repetitions to failure (N$_f$), and permanent strain after 5000 cycles of inhomogeneous gyratory compacted (I-SST) specimens; "Sd" represents standard deviation and "CV" represents coefficient of variation**

| Sample | 25°C | | | | 50°C | | | | |
|---|---|---|---|---|---|---|---|---|---|
| | G\*x10$^5$ (kPa) | δ | sin(δ)/G\* x10$^{-4}$ (1/kPa) | G\*sin(δ) x10$^2$ (kPa) | G\*x10$^4$ (kPa) | δ | sin(δ)/G\* x10$^{-2}$ (1/kPa) | N$_f$ | ε$_p$, % |
| I-SST1 | 9.85 | 42.01 | 7.17 | 6.96 | 5.11 | 71.10 | 1.83 | 9372 | 1.48 |
| I-SST2 | 10.68 | 44.99 | 6.26 | 7.15 | 4.82 | 69.22 | 1.96 | 7953 | 1.58 |
| I-SST3 | 15.07 | 43.45 | 4.57 | 10.38 | 5.68 | 69.03 | 1.60 | 5448 | 1.74 |
| I-SST4 | 10.78 | 43.57 | 6.38 | 7.41 | 5.39 | 65.68 | 1.73 | 4027 | 1.93 |
| I-SST5 | 10.72 | 43.72 | 6.33 | 7.28 | 5.87 | 70.84 | 1.59 | 6970 | 1.68 |
| I-SST6 | 10.26 | 42.79 | 6.73 | 7.09 | 5.01 | 68.84 | 1.89 | 5957 | 1.73 |
| I-SST7 | 12.17 | 41.36 | 5.32 | 7.89 | 5.32 | 69.59 | 1.76 | 4820 | 2.02 |
| I-SST8 | 11.44 | 40.41 | 5.78 | 7.55 | 5.97 | 69.72 | 1.57 | 8118 | 1.83 |
| Average | 11.37 | 42.79 | 6.07 | 7.71 | 5.40 | 69.25 | 1.74 | 6583 | 1.75 |
| Sd | 1.65 | 1.47 | 0.82 | 1.12 | 0.42 | 1.66 | 0.15 | 1832 | 0.18 |
| CV | 14.52 | 3.43 | 13.56 | 14.48 | 7.69 | 2.39 | 8.41 | 27.82 | 10.11 |

**Table 9-4. The computed ANOVA F and critical F values for comparison of shear properties for the two test temperatures (T) and pairs of homogeneity levels. "L" represents linear kneading compacted specimens, "H" represents homogeneous gyratory compacted specimens, "I" represents inhomogeneous gyratory compacted specimens, and "Sd" represents standard deviation of the shear properties**

| Property | Test | T (°C) | Sets | Mean | Sd | Pairs | Computed F | Critical F | Decision |
|---|---|---|---|---|---|---|---|---|---|
| G\* x10$^5$, kPa | FSCH | 25 | L | 8.25 | 0.66 | LH | 0.72 | 3.46 | Accept |
| | | | H | 8.91 | 0.74 | LI | 15.84 | 3.46 | Reject |
| | | | I | 11.4 | 1.65 | HI | 9.81 | 3.46 | Reject |
| G\*sinδ x10$^2$, kPa | FSCH | 25 | L | 6.01 | 0.48 | LH | 0.08 | 3.46 | Accept |
| | | | H | 6.16 | 0.51 | LI | 10.06 | 3.46 | Reject |
| | | | I | 7.71 | 1.11 | HI | 8.31 | 3.46 | Reject |
| Sinδ/G\* x10$^{-4}$, 1/kPa | FSCH | 25 | L | 8.90 | 0.76 | LH | 4.20 | 3.46 | Reject |
| | | | H | 7.82 | 0.65 | LI | 28.79 | 3.46 | Reject |
| | | | I | 6.07 | 0.82 | HI | 10.99 | 3.46 | Reject |
| G\* x10$^4$, kPa | FSCH | 50 | L | 3.71 | 0.49 | LH | 25.75 | 3.46 | Reject |
| | | | H | 5.15 | 0.28 | LI | 35.25 | 3.46 | Reject |
| | | | I | 5.40 | 0.42 | HI | 0.75 | 3.46 | Accept |
| Sinδ/G\* x10$^{-2}$, 1/kPa | FSCH | 50 | L | 2.58 | 0.37 | LH | 20.31 | 3.46 | Reject |
| | | | H | 1.81 | 0.11 | LI | 24.22 | 3.46 | Reject |
| | | | I | 1.74 | 0.15 | HI | 0.17 | 3.46 | Accept |
| ε$_p$@ 5000, % | RSCH | 50 | L | 3.69 | 0.89 | LH | 0.01 | 3.63 | Accept |
| | | | H | 3.72 | 0.26 | LI | 24.89 | 3.63 | Reject |
| | | | I | 1.75 | 0.18 | HI | 28.54 | 3.63 | Reject |
| N$_f$ | RSCH | 50 | L | 1460 | 1046 | LH | 0.18 | 3.63 | Accept |
| | | | H | 983 | 114 | LI | 23.14 | 3.63 | Reject |
| | | | I | 6583 | 1832 | HI | 30.81 | 3.63 | Reject |

direction of the trends between shear properties and the index of radial homogeneity. The coefficient of correlation, R, would evaluate the strength of the relationships.

## 9.2  COMPARISON OF THE FSCH TEST RESULTS AT 25°C

### 9.2.1   Comparison of G* of SST Specimens

The shear stiffness of the material that is represented by G* determines the amount of shear strain in the mixtures as they are subjected to cyclic shear loading and unloading. The G* values were compared for homogeneous linear kneading compacted (L-SST), homogeneous gyratory compacted (H-SST), and inhomogeneous gyratory compacted (I-SST) specimens at test temperature of 25°C. The G* values for the eight specimens of each of the three groups were ranked from highest to lowest and represented in Figure 9-1. As it is observed in the figure, the G* values of I-SST specimens were all considerably higher than those of H-SST and L-SST specimens and the G* values of H-SST specimens were slightly higher than those of L-SST specimens. This trend is also observed from the mean G* values in Table 9-1 through Table 9-3, with the mean values of $8.24 \times 10^5$ kPa for L-SST, $8.90 \times 10^5$ kPa for H-SST, and $11.37 \times 10^5$ kPa for I-SST specimens. This indicates that at 25°C, the shear modulus of the material increases with the increase in the level of inhomogeneity. The tables also indicate that the variability in G* values of inhomogeneous specimens is higher than the variability in G* values of the homogeneous specimens, with coefficients of variation of 14.52% for I-SST versus 8.01% and 8.36% for L-SST and H-SST specimens, respectively. The higher coefficient of variation indicates less stability in the test measurements of the inhomogeneous specimens.

**Figure 9-1. Comparison of G\* of homogeneous and inhomogeneous specimens at 25°C; L-SST stands for linear kneading compacted, H-SST stands for homogeneous gyratory compacted, and I-SST stands for inhomogeneous gyratory compacted specimens**

An F test was conducted on the mean G\* values of the three sets of specimens to assess if the observed differences in the means are significant. To evaluate the significance of the difference in the means of any pair, the computed F value was compared to the critical F for a 5% level of significance. The comparison of the mean G\* values of the L-SST and H-SST specimens is designated as "LH" in Table 9-4. A computed F of 0.72 for the LH comparison was compared to the critical F value of 3.46, which indicates that the difference between G\* values of L-SST and H-SST specimens is not significant. This implies that, when tested at 25°C, the responses of H-SST and L-SST specimens are not different.

The comparison of the G\* values of the L-SST and I-SST specimens is designated as "LI" in Table 9-4. A computed F value of 15.81 for the LI comparison indicates that the difference between mean G\* values of L-SST and I-SST specimens is significant. The computed F value of 15.81 corresponds to a rejection probability of a less than 1%. This

implies that radial inhomogeneity causes a significant increase in the shear stiffness of the material.

The comparison of the mean G* values of the H-SST and I-SST specimens is designated as "HI" in Table 9-4. A computed F value of 9.81 for the HI comparison indicates that the difference between G* values of H-SST and I-SST specimens is significant. The computed F value of 9.81 corresponds to a rejection probability of less than 1%. Therefore, the shear response of homogeneous gyratory specimens is different from the response of radially inhomogeneous specimens.

In summary, at a test temperature of 25°C, the responses of the two sets of L-SST and H-SST specimens are not different when loaded in shear. On the other hand, inhomogeneous I-SST specimens exhibit significantly greater shear moduli than the other two sets of specimens. This implies that the design of a pavement layer based on G* values of gyratory compacted specimens would be reliable. However, if specimens are extremely inhomogeneous, it is probable to under design a thick layer and over design a thin layer for fatigue based on the measured G* values.

### 9.2.2 Comparison of sinδ/G* of SST Specimens

The susceptibility of the mixture to fatigue cracking in a thick pavement layer is evaluated by sinδ/G* at the intermediate temperature. The higher the sinδ/G* value, the more the material is susceptible to fatigue cracking in a thick pavement layer. The sinδ/G* parameter was compared for L-SST, H-SST, and I-SST specimens to examine the effect of radial inhomogeneity on the fatigue performance of the material. The sinδ/G* values for the eight specimens, for the three groups, were ranked from highest to lowest in Figure 9-2. The figure indicates that at 25°C, the sinδ/G* values of I-SST
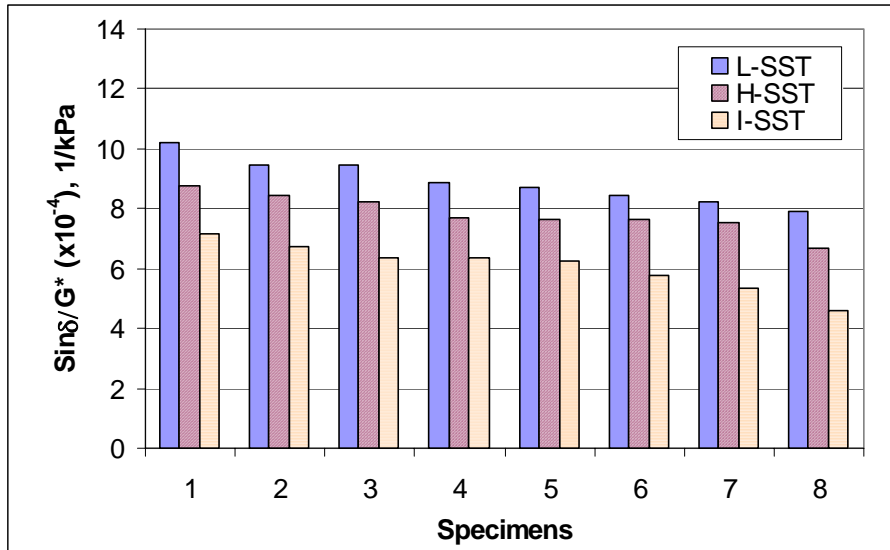
**Figure 9-2. Comparison of sinδ/G* of homogeneous and inhomogeneous specimens at 25°C. L-SST stands for linear kneading compacted, H-SST stands for homogeneous gyratory compacted, and I-SST stands for inhomogeneous gyratory compacted specimens**

specimens were all lower than those of H-SST and L-SST specimens and the sinδ/G* values of H-SST specimens were all lower than those of L-SST specimens. This trend is also observed from the mean sinδ/G* values in Table 9-1 through Table 9-3, with mean values of $8.90 \times 10^{-4}$ 1/kPa for L-SST, $7.82 \times 10^{-4}$ 1/kPa for H-SST, and $6.07 \times 10^{-4}$ 1/kPa for I-SST specimens. This indicates that the potential for stress-controlled fatigue cracking (in a thick layer) decreases with an increase in the level of radial inhomogeneity. It is also indicated from the tables that the variability in sinδ/G* values of I-SST specimens is higher than the variability in sinδ/G* values of the L-SST and H-SST specimens, with coefficients of variation of 13.56% for I-SST versus 8.51% and 8.29% for L-SST and H-SST specimens, respectively. The higher coefficient of variation indicates less stability in the test measurements of the inhomogeneous specimens.

312

An F-test was conducted on the mean $\sin\delta/G^*$ values of the three groups of specimens to examine if the observed differences in the means are significant. The computed F value was compared to the critical F for a 5% level of significance. The comparison of the mean $\sin\delta/G^*$ values of the L-SST and H-SST specimens is designated as "LH" in Table 9-4. A computed F of 4.20 for the LH comparison was compared to the critical F value of 3.46, which indicates that the difference between $\sin\delta/G^*$ values of the two sets is significant. The computed F value of 4.20 corresponds to a 4% rejection probability. This implies that the fatigue damage potential of a material in a thick layer would be estimated to be lower based on $\sin\delta/G^*$ of gyratory compacted specimens than based on $\sin\delta/G^*$ of linearly kneaded specimens.

The comparison of the $\sin\delta/G^*$ values of the L-SST and I-SST specimens is designated as "LI" in Table 9-4. A computed F value of 28.79 for the LI comparison indicates that the difference between mean $\sin\delta/G^*$ values of L-SST and I-SST specimens is significant. The rejection probability of the computed F value of 28.79 is less than 1%. Therefore, the potential of the material for fatigue damage in a thick layer is under estimated if the test specimen is radially inhomogeneous.

The comparison of the mean $G^*$ values of the H-SST and I-SST specimens is designated as "HI" in Table 9-4. A computed F value of 10.99 for the HI comparison indicates that the difference between mean $\sin\delta/G^*$ values of H-SST and I-SST specimens is significant. The rejection probability of the computed F value of 10.99 is less than 1%. This indicates that, at a test temperature of 25°C, an increase in the level of radial inhomogeneity of the test specimens would result in a lower estimate of a fatigue damage potential of the material in a thick layer.

In summary, for the three sets of specimens, three significantly different sinδ/G* values were measured. This means that a lower estimate of the fatigue damage potential of the material is obtained with the increase in the level of radial inhomogeneity of the test specimens. From the physical standpoint, if tested specimens are inhomogeneous, the fatigue performance of a thick layer might be overestimated, which could result in premature failure of the layer.

### 9.2.3    Comparison of G*sinδ of SST Specimens

The susceptibility of the mixture to fatigue cracking in a thin pavement layer is represented by sinδG* at intermediate temperatures. The G*sinδ parameter was compared for L-SST, H-SST, and I-SST specimens to examine the effect of radial inhomogeneity on fatigue performance of the material. The G*sinδ values for the eight specimens, for the three groups, were ranked from the highest to lowest in Figure 9-3. The figure indicates that at 25°C, the G*sinδ values of I-SST specimens were all considerably higher than those of L-SST and H-SST specimens. Also, six out of eight G*sinδ values of H-SST specimens were slightly higher than those of L-SST specimens. Table 9-1 through Table 9-3 show that the mean G*sinδ value of H-SST is slightly higher than that of L-SST specimens ($6.12 \times 10^2$ kPa versus $6.01 \times 10^2$ kPa) and the mean G*sinδ value of I-SST specimens ($7.70 \times 10^2$ kPa) is considerably higher than those of L-SST and H-SST specimens. This indicates that the potential for strain-controlled fatigue damage (in a thin layer) increases with the increase in the level of radial inhomogeneity. It is also observed from the tables that the variability in G*sinδ values of inhomogeneous specimens is higher than the variability in G*sinδ values of the other two sets, with

314

**Figure 9-3. Comparison of G\*sinδ values of homogeneous and inhomogeneous specimens at 25°C; L-SST stands for linear kneading compacted, H-SST stands for homogeneous gyratory compacted, and I-SST stands for inhomogeneous gyratory compacted specimens**

coefficients of variation of 14.48% for I-SST versus 7.99% and 8.29% for L-SST and H-SST specimens, respectively. The higher coefficient of variation indicates less stability in the test measurements of the inhomogeneous specimens.
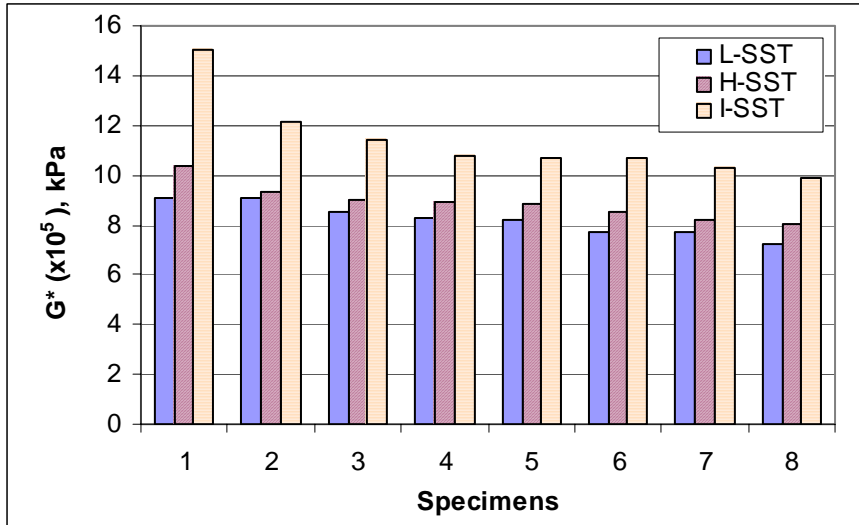
An F test was conducted on the mean G\*sinδ values of the three sets of specimens to examine if the observed differences in the means are significant. The computed F value was compared to the critical F for a 5% level of significance. The comparison of the mean G\*sinδ values of the L-SST and H-SST specimens is designated as "LH" in Table 9-4. A computed F of 0.08 for the LH comparison was compared to the critical F value of 3.46, which indicates that the difference between G\*sinδ values of L-SST and H-SST specimens is not significant. This implies that the estimate of the fatigue damage potential of the material in a thin overlay based on G\*sinδ values of homogeneous gyratory specimens is valid.

The computed F value was compared to the critical F for the comparison of the G*sinδ values of the L-SST and I-SST specimens designated as "LI" in Table 9-4. A computed F value of 10.06 for the LI comparison indicates that the difference between mean G*sinδ values of L-SST and I-SST specimens is significant. The rejection probability of the computed F value of 10.06 is less than 1%. This implies that the fatigue damage potential of a material in a thin layer is significantly overestimated if the tested specimens are radially inhomogeneous.

The computed F value was compared to the critical F for the comparison of the mean G*sinδ values of the H-SST and I-SST specimens designated as "HI" in Table 9-4. A computed F value of 8.31 for the HI comparison indicates that the difference between G*sinδ values of H-SST and I-SST specimens is significant. The computed F value of 8.31 corresponds to a rejection probability less than 1%. This implies that the estimate of the fatigue performance of a thin layer based on G*sinδ values of homogeneous gyratory compacted specimens would be valid. Only when the tested specimens are extremely inhomogeneous, can the fatigue performance of the material in a thin layer be underestimated.

In summary, at a test temperature of 25°C, the G*sinδ of homogeneous gyratory specimens is not different from that of linear kneading compacted specimens and significantly different from that of radially inhomogeneous specimens. This implies that the estimate of fatigue damage potential of a material in a thin layer based on G*sinδ values of homogeneous gyratory specimens is valid. However, if the specimens are extremely inhomogeneous, the fatigue damage potential of a thin layer could be overestimated. To reduce the fatigue damage potential of the layer, the materials with

which the layer was originally designed can be changed. However, this might increase the susceptibility of the material to another type of damage. For example, if a softer asphalt binder is selected, the fatigue damage would be reduced but the rutting potential of the layer would be increased.

The significantly different shear performance of homogeneous and radially inhomogeneous specimens can be explained based on the difference in the aggregate structures of the three sets of specimens. Two hypotheses were assumed: first, the core of the specimen mostly controls the performance of the material and second, the ring of the specimen mostly controls the performance of the material. The former is supported by the non-uniformity of the stress distribution across the specimen. The lack of confinement at the sides of specimens in a Superpave shear tester introduces a non-uniform shear stress distribution across the top and the bottom surfaces. The experimental measurements and analytical analyses by Masad and Bahia (2002), Ansell and Brown (1978), and Duncan and Dunlop (1969) indicated that only the middle third (core) of the specimen receives uniform shear stress. Therefore, the shear performance of the material is determined mainly by the response of the core portion, which is stressed the most. Since the core of an inhomogeneous specimen is comprised of a very dense material with low air content, the resistance of the specimen to the applied shear load would be higher than that of a homogeneous specimen.

The second hypothesis is that the ring of the specimen controls the shear performance of the material. Since the coarser gradation of the ring has more aggregate-to-aggregate and more aggregate-to-platen contact than the finer mixture in the core, gluing the top and bottom of the specimen to the platens introduces more

confinement at the edges than in the middle of the specimen. However, for homogeneous specimens, the confinement of the top and bottom surfaces is constant through the ring and the core. As a result higher shear stiffness is measured for the radially inhomogeneous specimen than for the homogeneous specimen.

Although the factor responsible for the behavior of the homogeneous and inhomogeneous specimens is not known, it is important to acknowledge and account for it in laboratory analyses. Failure to account for the effect of radial inhomogeneity, even if it is only moderate, could result in under or over prediction of the field performance and consequently the over or under design of the pavement layers, respectively.

## 9.3  COMPARISON OF THE FSCH TEST RESULTS AT 50°C

### 9.3.1  Comparison of G* of SST Specimens

The shear modulus (G*) of the asphalt mixture material were compared for L-SST, H-SST, and I-SST specimens at test temperature of 50°C, where the behavior of the mixtures is hypothesized to be mostly dominated by the structure of the aggregates. Therefore, the difference in performance of the homogeneous and inhomogeneous mixtures is hypothesized to be more evident at high-test temperatures.

The G* values for the eight specimens in each of the three groups were ranked from highest to lowest. Figure 9-4 indicates that at 50°C, the G* values of I-SST specimens were all considerably higher than those of L-SST specimens and, unlike the observation at 25°C, only slightly higher than those of H-SST specimens. This is also observed from the mean values provided in Table 9-1 through Table 9-3, with the values of $3.71 \times 10^4$ kPa for L-SST, $5.15 \times 10^4$ kPa for H-SST, and $5.40 \times 10^4$ kPa for I-SST
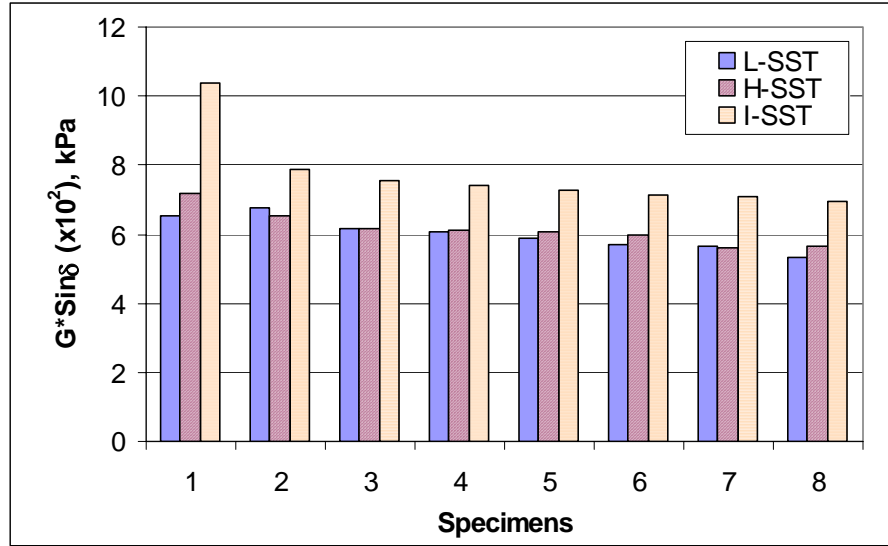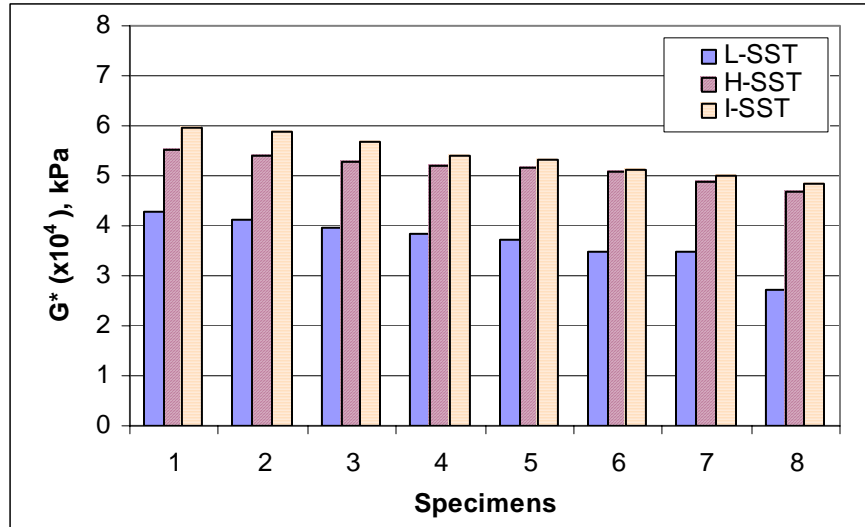
**Figure 9-4. Comparison of the G\* values of homogeneous and inhomogeneous specimens at 50°C; L-SST stands for linear kneading compacted, H-SST stands for homogeneous gyratory compacted, and I-SST stands for inhomogeneous gyratory compacted specimens**

specimens. This indicates that at 50°C, the response of homogeneous gyratory specimens in shear is different from the response of homogeneous linearly kneaded and similar to the response of inhomogeneous gyratory specimens. Unlike the variability in G\* values at 25°C, the variability in G\* values of homogeneous L-SST specimens at 50°C is higher than those of H-SST and I-SST specimens. The coefficient of variation of 13.17% for L-SST is compared with the coefficients of variation of 5.38% and 7.69% for H-SST and I-SST specimens, respectively. The higher coefficient of variation indicates less stability in the shear test measurements of the homogeneous L-SST specimens at higher test temperatures.

An F-test was conducted on the mean G\* values of L-SST, H-SST, and I-SST specimens to examine if the observed differences in the means was significant. The computed F values were compared to the critical F for a 5% level of significance for the three sets of comparisons. The comparison of the mean G\* values of the L-SST and

H-SST specimens is designated as "LH" in Table 9-4. A computed F of 25.75 for the LH comparison was compared to the critical F value of 3.46, which indicates that the difference between the G* values of L-SST and H-SST specimens is significant. The rejection probability of the computed F value of 25.75 is less than 1%. This implies that at a test temperature of 50°C the slight inhomogeneity that was introduced by gyratory compactor causes a significant increase in the shear modulus of the material.

The computed F value was compared to the critical F for the comparison of the mean G* values of the L-SST and I-SST specimens designated as "LI" in Table 9-4. A computed F value of 32.25 for the LI comparison indicates that the difference between mean G* values of L-SST and I-SST specimens is significant. It is also noted that the computed F value of 32.25 is greater than that for the LI comparison at 25°C (F value of 15.84). This implies that the same level of radial inhomogeneity would cause a greater resistance of the material to shear load at a high test temperature than at an intermediate temperature.

The computed F value was compared to the critical F for the comparison of the mean G*sinδ values of the H-SST and I-SST specimens designated as "HI" in Table 9-4. A computed F value of 0.75 for the HI comparison indicates that the difference between G* values of H-SST and I-SST specimens is not significant. This implies that at 50°C, homogeneous and inhomogeneous gyratory compacted specimens resist the shear load similarly.

Since testing of asphalt mixtures is mainly on gyratory compacted specimens, the physical impact of testing gyratory compacted specimens for the design of a pavement needs to be addressed. In designing an overlay to resist permanent deformation in high

temperature, G* is directly proportional to the performance, i.e., a mixture with higher

modulus is preferable to reduce the permanent deformation. Based on the modulus of

gyratory compacted specimens, which is greater than the modulus of radially

homogeneous specimens (e.g., L-SST), the thickness of a pavement layer might be under

designed. As a result, premature failure of the layer in permanent deformation might be

an outcome.

In summary, the comparisons of the G* values at 50°C indicate that the

homogeneous gyratory compacted specimens behave significantly different from the

linearly kneaded specimens. A small amount of inhomogeneity causes significant

increase in shear resistance of the material at high temperature. Therefore, based on G*

values of gyratory compacted specimens; a layer would be under-designed, which

involves the risk of premature failure of the pavement layer.

### 9.3.2 Comparison of sinδ/G* of SST Specimens

The susceptibility of the material for permanent deformation (rutting) is evaluated

by sinδ/G* measured in high temperature. The higher the sinδ/G* value, the more

permanent deformation is estimated for a pavement layer. The sinδ/G* parameter of

L-SST, H-SST, and I-SST were compared to examine the effect of radial inhomogeneity

on the performance of the material in permanent shear deformation. The sinδ/G* values

for the eight specimens, for the three groups, were ranked from highest to lowest. Figure

9-5 indicates that at 50°C, the sinδ/G* values of L-SST specimens are considerably

higher than those of H-SST and I-SST specimens and the sinδ/G* values of H-SST

specimens are slightly higher than those of I-SST specimens. This trend is also indicated

from the mean sinδ/G* values in Table 9-1 through Table 9-3, with the mean values of

2.58x10$^{-2}$ 1/kPa for L-SST, 1.81x10$^{-2}$ 1/kPa for H-SST, and 1.74x10$^{-2}$ 1/kPa for I-SST

specimens. This indicates that the response of homogeneous gyratory specimens in

permanent deformation is different from the response of homogeneous linearly kneaded

specimens and similar to the response of inhomogeneous gyratory specimens. It is also

observed from the tables that the variability in sinδ/G* values of L-SST specimens is

higher than the variability in sinδ/G* values of H-SST and I-SST specimens, with

coefficients of variation of 14.49% for L-SST versus 6.24% and 8.41% for H-SST and

I-SST specimens, respectively. The higher coefficient of variation indicates less stability

in the shear test measurements of the homogeneous L-SST specimens at higher test

temperatures.

An F-test was conducted on the mean sinδ/G* values of the three sets of

specimens to examine if the observed differences in the means are significant. The

computed F values were compared to the critical F for a 5% level of significance for the
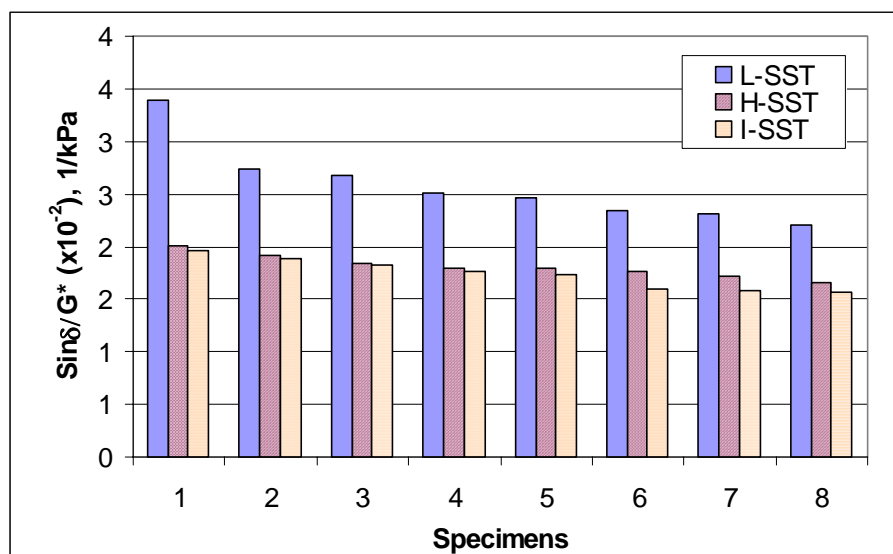


**Figure 9-5. Comparison of sinδ/G* of L-SST, H-SST, I-SST specimens at 50°C; L-SST stands for linear kneading compacted, H-SST stands for homogeneous gyratory compacted, and I-SST stands for inhomogeneous gyratory compacted specimens**

322

three sets of comparisons. The comparison of the mean sinδ/G* values of the L-SST and H-SST specimens is designated as "LH" in Table 9-4. A computed F of 20.31 for the LH comparison was compared to the critical F value of 3.46, which indicates that the difference between sinδ/G* values of L-SST and H-SST specimens is significant. Therefore, a slight level of radial inhomogeneity in gyratory compacted specimens would result in a significantly lower estimate of the rutting potential of the material.

The comparison of the sinδ/G* values of the L-SST and I-SST specimens is designated as "LI" in Table 9-4. A computed F value of 24.22 for the LI comparison indicates that the difference between the mean sinδ/G* values of L-SST and I-SST specimens are significant. The computed F value of 24.22 corresponds to a rejection probability of less than 1%. This implies that the estimate of the susceptibility of the material to permanent deformation is lowered when the level of radial inhomogeneity of the laboratory specimens is increased.

The comparison of the mean sinδ/G* values of the H-SST and I-SST specimens is designated as "HI" in Table 9-3. A computed F value of 0.17 for the HI comparison indicates that the difference between sinδ/G* values of H-SST and I-SST specimens is not significant. Therefore, the response of homogeneous and inhomogeneous gyratory specimens in shear is not different. This implies that the susceptibility of the material to permanent deformation based on shear testing of H-SST specimens is significantly underestimated.

In summary, the comparisons of the sinδ/G* values at 50°C indicate that homogeneous gyratory compacted specimens with an insignificant amount of radial inhomogeneity behave similar to the inhomogeneous gyratory compacted specimens

when loaded in shear. Homogeneous gyratory (H-SST) and inhomogeneous (I-SST) specimens have significantly lower $\sin\delta/G^*$ values than the radially homogeneous (L-SST) specimens. Therefore, the susceptibility of the material to permanent deformation, based on $\sin\delta/G^*$ values of H-SST and I-SST specimens, would be underestimated, which would involve the risk of premature failure of the pavement layer.

At 50°C the behavior of the mixtures was hypothesized to be mostly dominated by the structure of the aggregates. Therefore, the difference in performance of the homogeneous and inhomogeneous mixtures was expected to be more evident at high test temperatures. This hypothesis, to some extent, was supported by the result of the FSCH test at 50°C. The slight level of inhomogeneity in H-SST specimens was not affecting the shear stiffness properties of the specimens at intermediate temperature. However, at a high test temperature the same level of radial inhomogeneity caused a significant increase in shear modulus and as a result a significant increase in the permanent deformation resistance.

## 9.4  COMPARISON OF THE RSCH TEST RESULTS

### 9.4.1  Comparison of $N_f$ Values of SST Specimens

The resistance of the material to permanent deformation can be evaluated using repeated shear at constant height (RSCH) test conducted at 50°C. The number of load cycles ($N_f$) in RSCH test that cause 2% cumulative shear strain in a specimen is used to evaluate the resistance of the material to permanent deformation. The higher the $N_f$ value, the more the material is resistant to shear failure. The $N_f$ values of L-SST, H-SST, and I-SST specimens were compared to examine the effect of radial inhomogeneity on the

resistance of the material to permanent deformation. The $N_f$ values of the eight specimens

for each of the three groups were ranked from highest to lowest. Figure 9-6 shows three

out of eight L-SST specimens and two out of eight H-SST specimens failed at the early

stages of the test while the I-SST specimens reached the 2% failure criteria after a

considerable number of load cycles. Table 9-1 through Table 9-3 also show that the mean

$N_f$ value of I-SST specimens is much higher than the mean $N_f$ values of L-SST and

H-SST specimens, with the values of 6583 for I-SST specimens versus 1460 and 983 for

L-SST and H-SST specimens, respectively. This indicates that radial inhomogeneity

increases the resistance of the material to permanent shear deformation.  It is also

indicated from the tables that the variability in $N_f$ values of L-SST specimens is

considerably higher than those of the other sets, with coefficients of variations of 71.63

for L-SST, 9.95 for H-SST, and 18.49 for I-SST specimens. A higher coefficient of
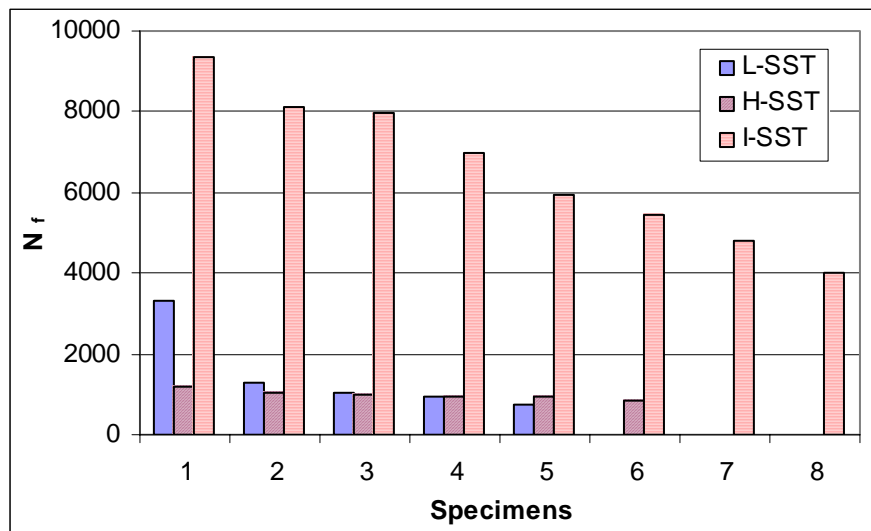


**Figure 9-6. Comparison of $N_f$ values of homogeneous and inhomogeneous specimens; L-SST stands for linear kneading compacted, H-SST stands for homogeneous gyratory compacted, and I-SST stands for inhomogeneous gyratory compacted specimens**

An F-test was conducted on the mean $N_f$ values of L-SST, H-SST, and I-SST specimens to examine if the observed differences in the means are significant. The computed F value for unequal sample sizes was compared to the critical F for a 5% level of significance for the three sets of comparisons. The comparison of the mean $N_f$ values of the L-SST and H-SST specimens is designated as "LH" in Table 9-4. A computed F of 0.18 for the LH comparison was compared to the critical F value of 3.46, which indicates that the difference between $N_f$ values of L-SST and H-SST specimens is not significant. This implies that in resisting the repeated shear load homogeneous gyratory specimens and radially homogeneous specimens behave similarly. Therefore, the prediction of the rutting performance of a pavement layer based on $N_f$ values of homogeneous gyratory specimens is valid.

The comparison of the $N_f$ values of the L-SST and I-SST specimens is designated as "LI" in Table 9-4. A computed F value of 23.14 for the LI comparison indicates that the difference between the mean $N_f$ values of L-SST and I-SST specimens is significant. The computed F value of 23.14 corresponds to a rejection probability of less than 1%. This implies that radial inhomogeneity in RSCH specimens would cause a significant overestimation of the resistance of the material to permanent shear strain.

The comparison of the mean $N_f$ values of the H-SST and I-SST specimens is designated as "HI" in Table 9-4. A computed F value of 30.81 for the HI comparison indicates that the difference between $N_f$ values of H-SST and I-SST specimens is significant. The computed F value of 30.81 corresponds to a rejection probability of less than 1%. This indicates that H-SST specimens behave significantly different from radially inhomogeneous specimens in resisting permanent shear strain. Therefore, the

prediction of the rutting performance of a pavement layer based on $N_f$ values of homogeneous gyratory specimens is valid.

In summary, the comparison of the $N_f$ values indicated that in the RSCH test, homogeneous gyratory and linearly kneaded specimens performed similarly in resisting the permanent shear deformation. As a result, the prediction of the performance of a pavement layer in resisting permanent deformation based on $N_f$ values of gyratory compacted specimens would be reliable. However, if specimens were extremely inhomogeneous, the resistance of the material to permanent shear deformation would be significantly overestimated.

### 9.4.2   Comparison of $\varepsilon_p$ of SST Specimens

The resistance of the material to permanent deformation can also be evaluated using the permanent cumulative shear strain ($\varepsilon_p$) after 5000 load cycles measured from the repeated shear at constant height (RSCH) test. The smaller the $\varepsilon_p$, the more the material is resistant to shear failure. The $\varepsilon_p$ values of L-SST, H-SST, and I-SST specimens were compared to examine the effect of radial inhomogeneity on the permanent deformation of the mixture. The $\varepsilon_p$ values of the eight specimens for the three groups were ranked from highest to lowest. Figure 9-7 shows that three out of eight L-SST specimens and two out of eight H-SST specimens reached the maximum strain level at the early stages of the test, while the amount of cumulative strain for I-SST specimens after 5000 cycles were considerably lower than those of the L-SST and H-SST specimens. Table 9-1 through Table 9-3 also show that the mean $\varepsilon_p$ value of I-SST
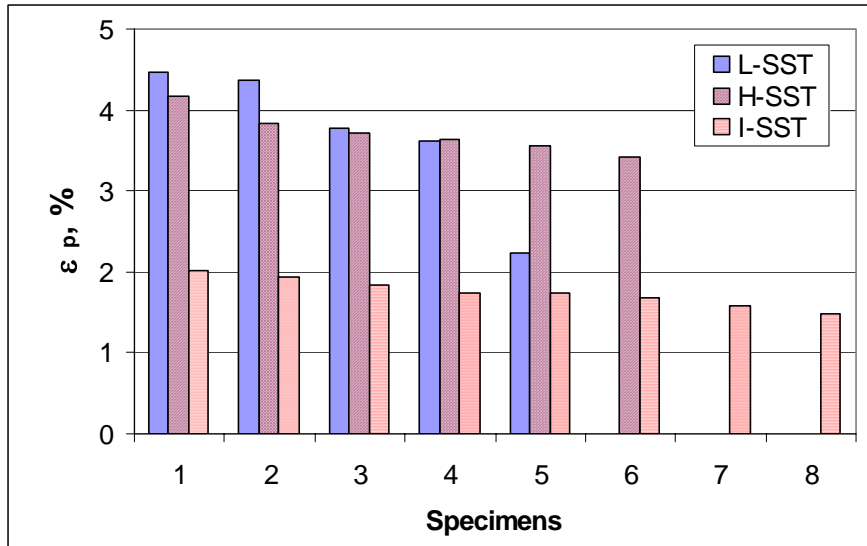
**Figure 9-7. Comparison of $\varepsilon_p$ values of homogeneous and inhomogeneous specimens; L-SST stands for linear kneading compacted, H-SST stands for homogeneous gyratory compacted, and I-SST stands for inhomogeneous gyratory compacted specimens**

specimens are much smaller than the mean $\varepsilon_p$ value of L-SST and H-SST specimens, with the values of 1.75% for I-SST specimens versus 3.69% and 3.72% for L-SST and H-SST specimens, respectively. This indicates that radial inhomogeneity increases the resistance of the material to permanent shear deformation. The tables also include the variability of the $\varepsilon_p$ measurements. The variability in $\varepsilon_p$ values of L-SST specimens is considerably higher that those of H-SST and I-SST specimens, with coefficients of variation of 24.11 for L-SST versus 6.46 and 7.11 for H-SST and I-SST specimens, respectively.

An F-test was conducted on the mean $\varepsilon_p$ values of L-SST, H-SST, and I-SST specimens to examine if the observed differences in the means are significant. The computed F value for unequal sample sizes was compared to the critical F for a 5% level of significance for the three cases. The comparison of the mean $\varepsilon_p$ values of the L-SST and H-SST specimens is designated as "LH" in Table 9-4. A computed F of 0.01 for the

328

LH comparison was compared to the critical F value of 3.46, which indicates that the difference between $\varepsilon_p$ values of L-SST and H-SST specimens is not significant. This indicates that slight inhomogeneity in H-SST specimens did not affect the resistance of the material to permanent deformation as measured by RSCH test.

The comparison of the $\varepsilon_p$ values of the L-SST and I-SST specimens is designated as "LI" in Table 9-4. A computed F value of 24.89 for the LI comparison indicates that the difference between mean $\varepsilon_p$ values of the two sets is significant. The computed F value of 24.89 corresponds to a rejection probability of less than 1%. This implies that radial inhomogeneity would increase the resistance of the material to permanent deformation.

The comparison of the mean $\varepsilon_p$ values of the H-SST and I-SST specimens is designated as "HI" in Table 9-4. A computed F value of 28.54 for this comparison indicates that the difference between $\varepsilon_p$ values of H-SST and I-SST specimens is significant. The computed F value of 28.54 corresponds to a rejection probability of less than 1%. This implies that homogeneous gyratory specimens respond significantly different from the radially inhomogeneous specimens when subjected to repeated shear load. Therefore, the prediction of the rutting performance of the material based on the RSCH properties of homogeneous specimens would be valid.

In summary, when subjected to the RSCH test at a test temperature of 50°C, L-SST and H-SST specimens perform similarly. The slight level of inhomogeneity that is caused by a gyratory compactor would not change the performance of the material in resisting permanent deformation. Therefore, the decisions that are made based on $\varepsilon_p$ measurements of the homogeneous gyratory specimens would be valid. However, a high

level of radial inhomogeneity would significantly increase the resistance of the material to permanent deformation. Therefore, the RSCH test on highly inhomogeneous specimens would indicate elevated resistance of the material to permanent deformation, which would cause overestimation of the performance of the material in the field.

A comparison of the results of the FSCH and RSCH tests would indicate that the response of a material is a function of the test type. Both $\sin\delta/G^*$, as measured by the FSCH at 50°C, and $\varepsilon_p$, as measured by the RSCH, are measures of permanent deformation. The two parameters are interchangingly used by the asphalt industries for the evaluation of the permanent deformation performance of asphalt mixtures. Although the same results were expected from $\sin\delta/G^*$ and $\varepsilon_p$, they led to opposite conclusions regarding the effect of radial inhomogeneity. In FSCH at 50°C, the $\sin\delta/G^*$ values of H-SST specimens were similar to those of inhomogeneous (I-SST) specimens, while in RSCH tests, the $\varepsilon_p$ values of H-SST specimens were similar to those of radially homogeneous (L-SST) specimens. The difference in the behavior of the H-SST specimens as measured in FSCH at 50°C and RSCH might be due to the different loading frequencies and loading patterns of the two tests. In the FSCH test, the cyclic load was applied without any rest; while in the RSCH test, the cyclic load was applied in 0.1 second followed by 0.6 second rest period. It seems that aggregates show more resistance to the shear load if it is applied continuously (i.e., in the FSCH test). Therefore, it can be stated that the slight inhomogeneity in H-SST specimens increases the load carrying capacity of the specimens more prominently in the FSCH test than in the RSCH test.

330

## 9.5 RELATIONSHIP BETWEEN SST RESULTS AND INHOMOGENEITY

It is of interest to evaluate the relationship between shear properties and the

aggregate inhomogeneity to improve the reliability of the design and performance

predictions. A correlation analysis was utilized to evaluate the strengths of the

relationships between SST measurements and the level of radial inhomogeneity. The

correlation analysis includes the graphical study and the computation of correlation

coefficients. The graphical study provides the visual inspection of the data that would

indicate the degree to which shear properties and the aggregate inhomogeneity are

related. The correlation coefficient, R, is a quantitative measure of the degree to which

variation in inhomogeneity can be used to explain the variation in shear properties.

To examine the correlation between shear properties and index of homogeneity,

the measured and computed shear properties in Table 9-1 through Table 9-3 and the

computed z statistic in Tables 7-10, 7-12, and 7-14 were used. The z statistic was selected

as the index of homogeneity since (1) it indicated a statistical power of 100% (Chapter 6),

(2) it showed a low rejection probability in detecting radial inhomogeneity of I-SST

specimens and a high rejection probability in detecting the homogeneity of L-SST

specimens, and (3) it provided the greatest distinction between the levels of homogeneity

of the three sets of L-SST, H-SST, and I-SST specimen. The values of each shear

property were plotted versus the computed z values to visually investigate whether or not

a trend existed between the two sets of variables. The correlation coefficient, R, was

computed between the shear properties and the computed z values to examine the degree

to which the shear properties are affected by the radial inhomogeneity. Additionally, R

values were computed between the shear properties and the ring and core air void

contents to examine if the core or the ring was more responsible for resisting the shear load.

The discussion of the correlations is divided based on the test type (FSCH, RSCH), test temperature (25°C, 50°C), and the correlation variables (shear properties versus z, shear properties versus air void content). For each test, three types of correlations would be discussed: (1) the correlation of the computed z values and each shear property within each set of L-SST, H-SST, and I-SST specimens, (2) the correlation of computed z values and each shear property between the three sets of L-SST, H-SST, and I-SST specimens, and (3) the correlation of the ring and core air void contents and each shear property between the three sets of L-SST, H-SST, and I-SST specimens. The computed correlation coefficients, R, within each set and between the three sets for the two test temperatures are provided in Table 9-5.

### 9.5.1 Relationships between z Statistics and FSCH Properties at 25° C

From the FSCH test at 25°C, the relationship between z statistic and the three compressive properties of G*, sinδ/G*, and G*sinφ were evaluated within each and between the three sets of L-SST, H-SST, and I-SST specimens. The computed correlation coefficients in Table 9-5 indicate that the correlations of the shear properties and the z statistic within each set are very low. The small ranges of z values within each set of specimens are responsible for the low correlations. In summary, the variations in shear properties within H-SST, L-SST, and I-SST specimens as measured by the FSCH test at 25°C were not explained by the variations in the aggregate distribution.

The relationship of the shear properties and the z statistics between the three sets of specimens are shown in Figure 9-8 through Figure 9-10. In this case, a higher

**Table 9-5. Correlation coefficients, R, between the z statistic and the shear properties and between the ring and core air voids and the shear properties**

| Property | Test | T °C | z (L-SST) | z (H-SST) | z (I-SST) | z (All sets) | Ring Air void (All sets) | Core Air Void (All sets) |
|---|---|---|---|---|---|---|---|---|
| G* | FSCH | 25 | -0.26 | -0.45 | 0.33 | 0.78 | 0.58 | -0.71 |
| Sinδ/G* | FSCH | 25 | 0.40 | 0.46 | -0.10 | -0.81 | -0.59 | 0.76 |
| G*sinδ | FSCH | 25 | -0.14 | -0.40 | 0.14 | 0.73 | 0.53 | -0.65 |
| G* | FSCH | 50 | 0.17 | 0.03 | -0.14 | 0.71 | 0.58 | -0.55 |
| Sinδ/G* | FSCH | 50 | -0.35 | 0.35 | 0.52 | -0.71 | -0.56 | 0.48 |
| $\varepsilon_p$@ 5000 | RSCH | 50 | -0.87 | 0.48 | -0.48 | -0.89 | -0.66 | 0.82 |
| $N_f$ | RSCH | 50 | 0.69 | -0.81 | 0.35 | 0.87 | 0.57 | -0.83 |

The critical correlation coefficient (R) for n= 8 is 0.71 and for n=24 is 0.40.

correlation between the compressive properties and the z statistic was expected since the range of z values is much wider than the range of values within each set of specimens. The figures indicate that the relationship between shear properties at 25°C and the z statistic are well defined. For the three distinguished sets of z statistics, the shear properties of the sets are noticeably different. Table 9-5 shows that, when all 24 specimens are included, the computed R values are much greater than the R values computed within each set of eight specimens. The comparison of the computed R values of 0.78 for G*, -0.81 for sinδ/G*, and 0.73 for G*sinδ with the critical R value of 0.40 indicates that all three shear properties are significantly correlated with the z statistic.

## 9.5.2 Relationships between z Statistics and FSCH Properties at 50°C

The relationships between the z statistic and two compressive properties of G* and sinδ/G* obtained from the FSCH test at 50°C were evaluated. The evaluations were conducted for specimens within each set of L-SST, H-SST, and I-SST, and between the three sets of specimens. It is hypothesized that at high test temperatures the mechanical response of the material is more dominated by the aggregate structure than at

**Figure 9-8. Relationship between "z" and G\* of L-SST, H-SST, and I-SST groups at 25°C; L-SST stands for linear kneading compacted, H-SST stands for homogeneous gyratory compacted, and I-SST stands for inhomogeneous gyratory compacted specimens**
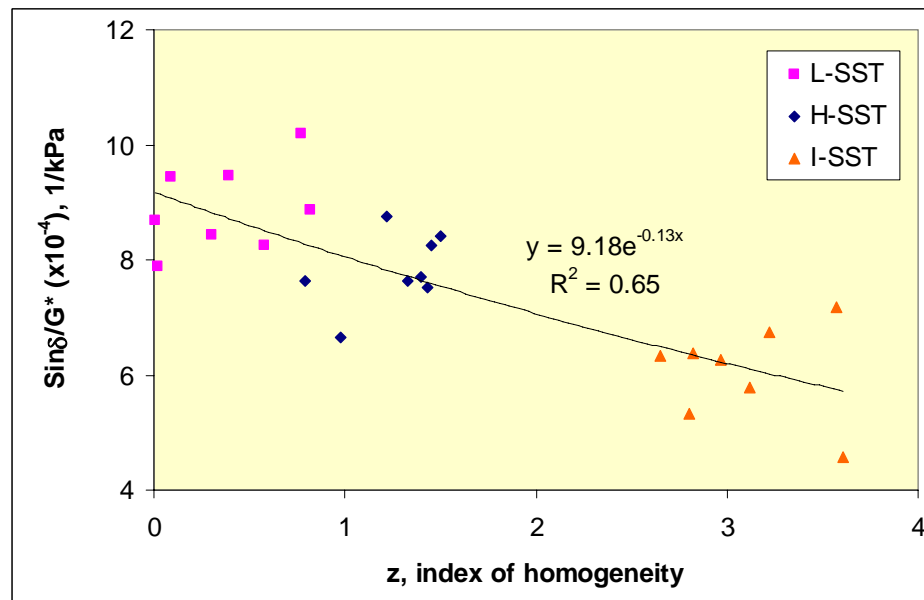


**Figure 9-9. Relation between "z" and sinδ/G\* of L-SST, H-SST, and I-SST groups at 25°C; L-SST stands for linear kneading compacted, H-SST stands for homogeneous gyratory compacted, and I-SST stands for inhomogeneous gyratory compacted specimens**
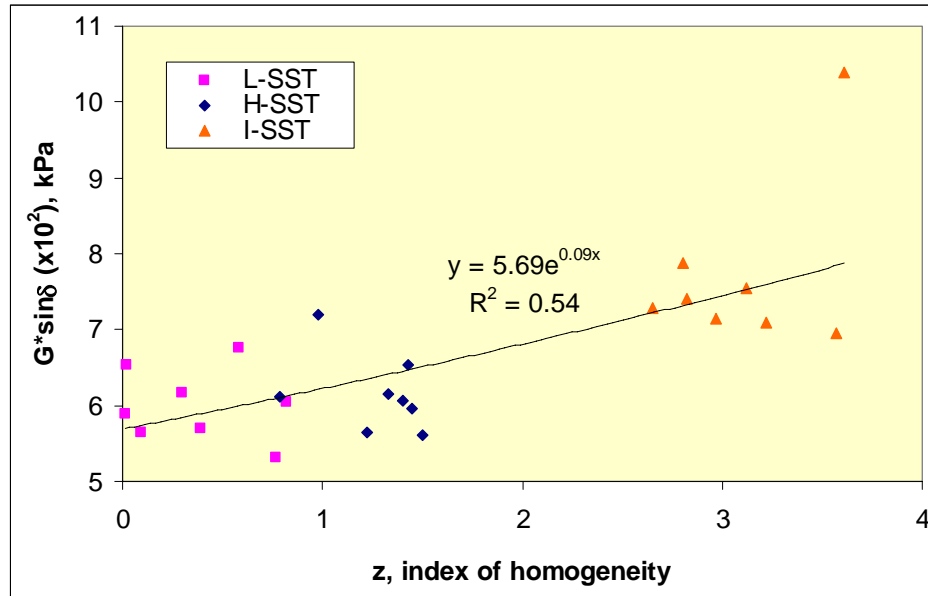
**Figure 9-10. Relation between "z" and G\*sinδ of L-SST, H-SST, and I-SST groups at 25°C; L-SST stands for linear kneading compacted, H-SST stands for homogeneous gyratory compacted, and I-SST stands for inhomogeneous gyratory compacted specimens**

intermediate temperatures. Therefore, a higher correlation between the shear properties and z statistic should be expected.

Correlation coefficients between the FSCH properties at 50°C and the z statistic within each set of specimens are included in Table 9-5. The values in the table indicate that the correlations are either low or have inaccurate directions. This results from the small ranges of the z values within each set of specimens. In summary, the variation in the shear properties within the L-SST, H-SST, and I-SST specimens as measured by the FSCH test at 50°C was not explained by the variation in radial distribution of the aggregates.

The relationship of the shear properties at 50°C and the z statistic between the three sets of specimens are shown in Figure 9-11 and Figure 9-12. As indicated from the figures, the trends of the relationships exhibit greater nonlinearity than the trends at 25°C
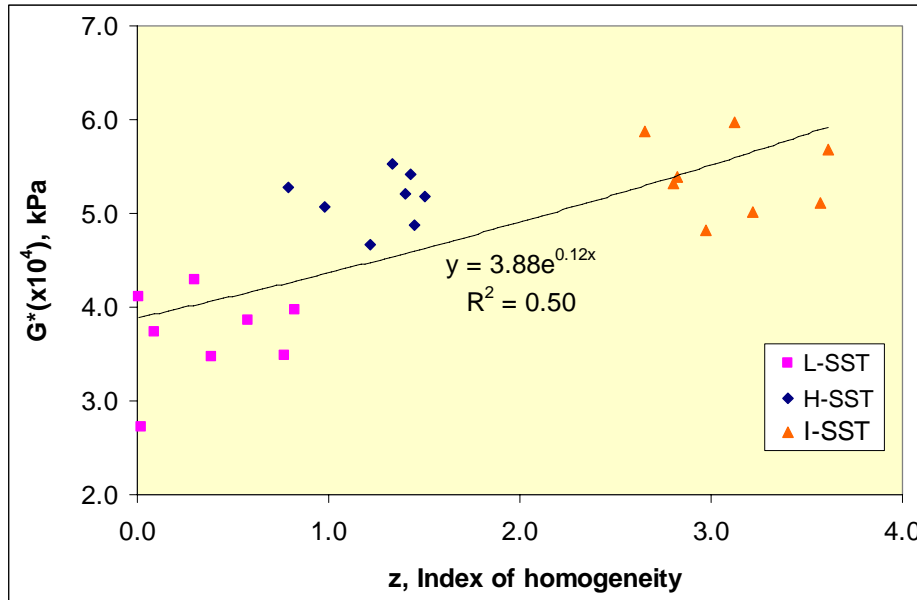
**Figure 9-11. Relationship between "z" and G\* of L-SST, H-SST, and I-SST sets at 50°C; L-SST stands for linear kneading compacted, H-SST stands for homogeneous gyratory compacted, and I-SST stands for inhomogeneous gyratory compacted specimens**
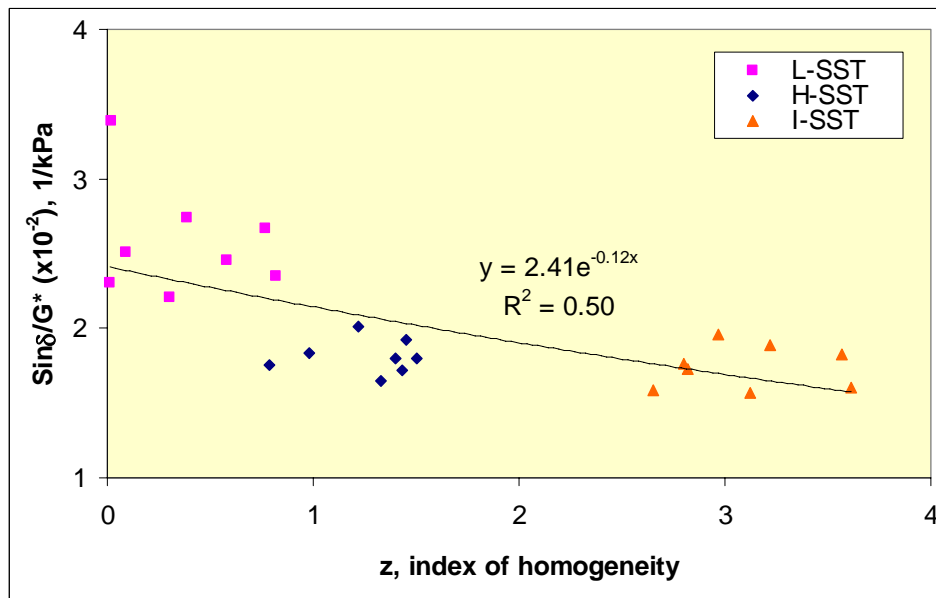


**Figure 9-12. Relationship between "z" and sinδ/G\* of L-SST, H-SST, and I-SST sets at 50°C; L-SST stands for linear kneading compacted, H-SST stands for homogeneous gyratory compacted, and I-SST stands for inhomogeneous gyratory compacted specimens**

(Figure 9-8 through Figure 9-10). The difference in the trends at the two test temperatures results because the H-SST specimens responded differently at different test temperatures. The responses of H-SST specimens at the intermediate temperature were very similar to those of L-SST specimens; however, at high temperature the responses of the H-SST specimens were very similar to those of I-SST specimens. In addition, as indicated from Table 9-5, lower correlations were observed between the FSCH properties and the z statistic at 50°C than at 25°C.

In summary, the shear properties of the specimens as measured by the FSCH test at 50°C were significantly correlated with the level of radial inhomogeneity. However, the correlations were lower than those at 25°C. The trends of the relationships between z values and FSCH properties at 50°C were curvilinear, indicating a greater difference between the shear responses of the L-SST and H-SST specimens than between the shear responses of H-SST and I-SST specimens at 50°C.

### 9.5.3   Relationships between z Statistics and the RSCH Properties

The relationships between the z statistic and the two shear properties of $\varepsilon_p$ and $N_f$ obtained from the RSCH test at 50°C were evaluated. The evaluations were conducted for specimens within each set of L-SST, H-SST, and I-SST, and between the three sets of specimens. It is hypothesized that at high-test temperatures the mechanical response of the material is more dominated by the aggregate structure than at intermediate temperatures. Therefore, a higher correlation between the compressive properties and z statistic should be expected.

The relationships between the two shear properties and the computed z statistic within each set of L-SST, H-SST, and I-SST specimens are included in Table 9-5. The

correlation coefficients in Table 9-5 show that correlation of $\varepsilon_p$ and z within L-SST

specimens is significant. For other cases the correlations are either low or have inaccurate

directions. The small ranges of the z values within each set of specimens are responsible

for insignificant correlations. In summary, the variation in the shear properties within the

L-SST, H-SST, and I-SST specimens as measured by the RSCH test at 50°C was not

explained by the variation in radial distribution of the aggregates.

The relationships of $\varepsilon_p$ and $N_f$ versus z statistic for the three sets of specimens are shown

in Figure 9-13 and Figure 9-14. As indicated from the figures, the relationships between z

and the RSCH properties are well defined. For the three distinct levels of inhomogeneity,

three different sets of shear properties were measured. Table 9-5 shows that the highest

correlation between any of the shear properties and the z statistic was observed between z

and the RSCH properties, with an R of -0.89 for z versus $\varepsilon_p$ and an R of 0.87 for z versus

$N_f$. In summary, the shear properties of the specimens as measured by the RSCH test

were significantly correlated with the levels of radial inhomogeneity. The higher

correlation between RSCH parameters and the z statistic indicates that this test is more

responsive to the differences in aggregate structure than the FSCH test.

### 9.5.4 Relationships between the Air Void Distribution and the Shear Properties

The correlation between the measured air void contents of the core and the ring

and the shear properties for each specimen was evaluated. The correlation would assess if

the core or the ring mixture was responsible for the changes in shear properties when

inhomogeneity was present. Image analyses were applied to all specimens to provide

independent measurements of the air void contents of the core and the ring portions of
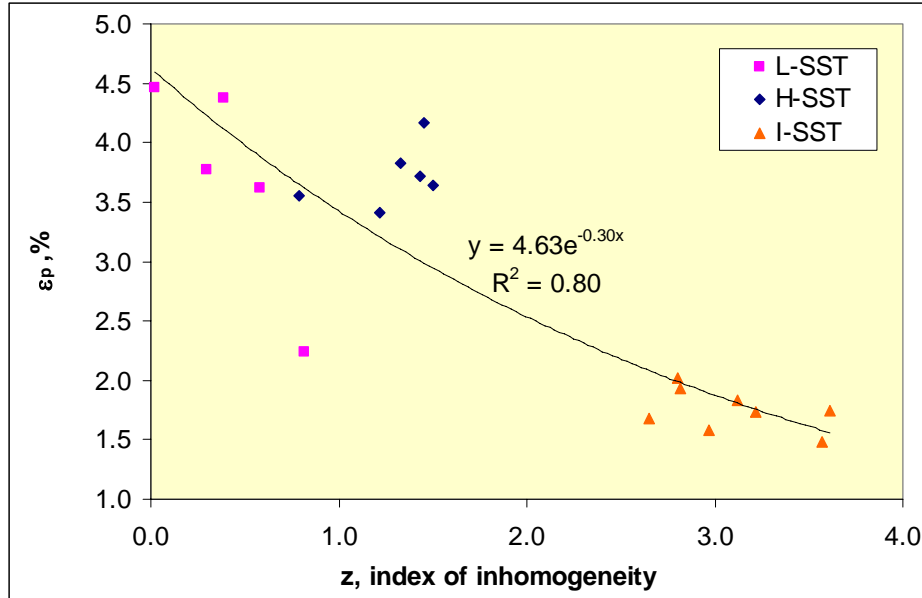
**Figure 9-13. Relationship between "z" and $\epsilon_p$ of L-SST, H-SST, and I-SST sets at 50°C; L-SST stands for linear kneading compacted, H-SST stands for homogeneous gyratory compacted, and I-SST stands for inhomogeneous gyratory compacted specimens**
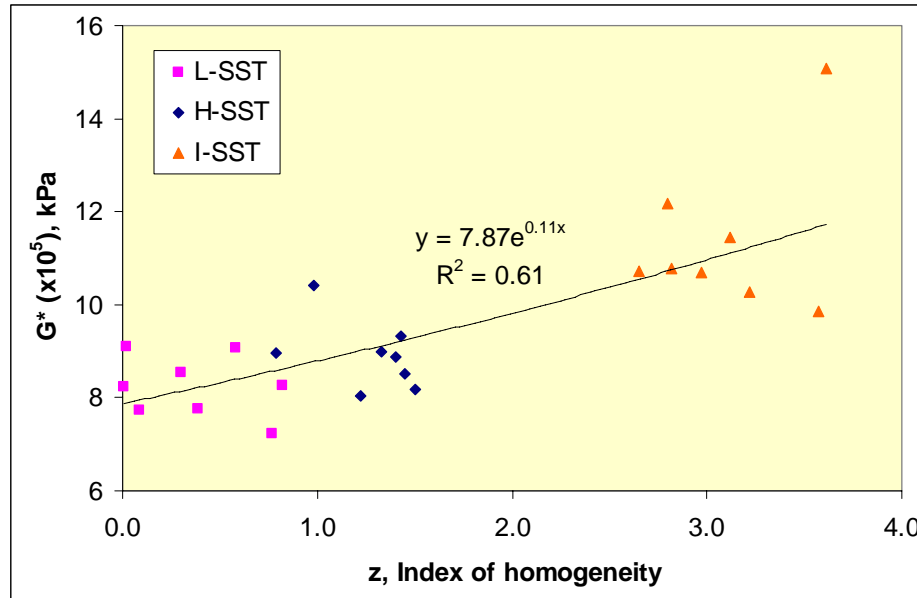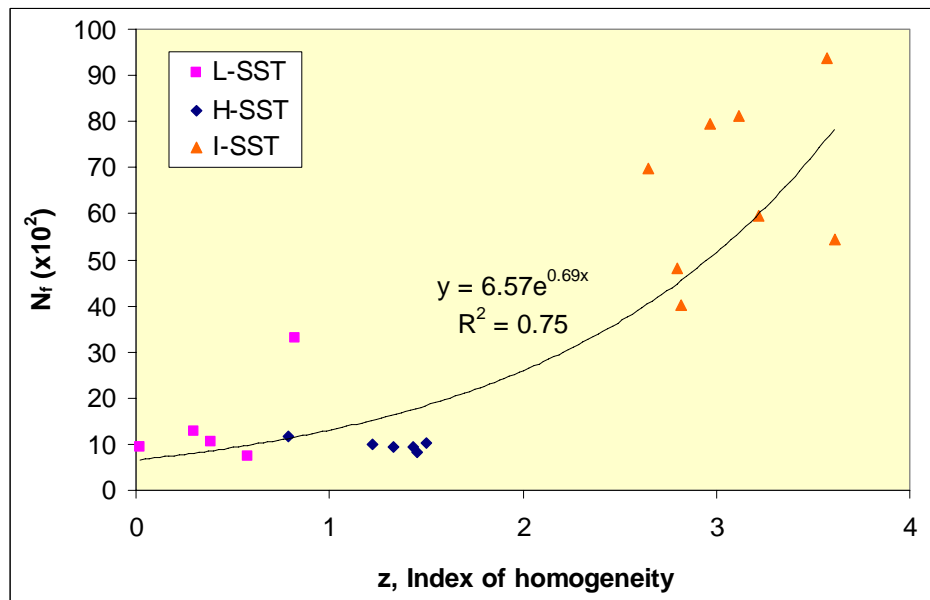


**Figure 9-14. Relationship between "z" and $N_f$ of L-SST, H-SST, and I-SST sets at 50°C; L-SST stands for linear kneading compacted, H-SST stands for homogeneous gyratory compacted, and I-SST stands for inhomogeneous gyratory compacted specimens**

each specimen. The results of air void measurement using analysis of x-ray computed tomography images are provided in Appendix E.

The correlation coefficients of the core and the ring air void contents with the shear properties were computed between the three sets of specimens. The computed correlation coefficients are provided in Table 9-5. The coefficients indicate moderate correlation between both the core air voids and the shear properties and between the ring air voids and the shear properties. Additional specific findings are: First, the direction of the correlations between shear properties and the core air voids are opposite of those between shear properties and the ring air voids. In other words, if a property has a positive correlation with the core air void content, the correlation with the ring air void content would be negative. This indicates that each portion works separately to resist the shear load. Second, the directions of the correlations show that the decrease in the core air void and increase in the ring air void would increase the shear stiffness. This indicates that a combination of a dense core and a coarse ring would result in a high shear resistant material. Third, the shear properties from FSCH at 25°C are more correlated with the core air void content than with the ring air void content (R = -0.71 versus R= 0.58 for G*), which indicates that the core is more responsible for carrying the shear load in the FSCH test at 25°C. Fourth, the shear properties from FSCH at 50°C are more highly correlated with the ring air void content than with the core air void content (R = −0.56 vs. R = 0.48 for sinδG*), which indicates that in the FSCH test at 50°C, the ring of the specimens is more responsible for resisting the shear load. Fifth, similar to the FSCH test at 25°C, the properties measured in the RSCH test are more highly correlated with the core air void content than with the ring air void content (R = -0.83 vs. R = 0.57 for $N_f$),

which indicates that in RSCH, the core of the specimens are more responsible for carrying the shear load.

## 9.6  SUMMARY OF THE CHAPTER

This chapter intended to evaluate the effect of the radial inhomogeneity that is specific to gyratory compacted specimens on permanent deformation and fatigue properties of the asphalt mixture material. Three sets of homogeneous and radially inhomogeneous specimens were created in the laboratory using linear kneading and Superpave gyratory compactors. Despite a low level of radial inhomogeneity that was observed in the homogeneous gyratory compacted specimens, they are still considered to be homogeneous. Among various statistics that were computed and tested in Chapters 6 and 7, the values of the z statistic were used for the correlation analyses. The z statistic was selected since: (1) it indicated a statistical power of 100%, (2) it showed low rejection probabilities in detecting radial inhomogeneity of I-SST specimens and high rejection probabilities in detecting the homogeneity of L-SST specimens, and (3) it provided the greatest distinction between the levels of homogeneity of the three sets of L-SST, H-SST, and I-SST specimens.

The three sets of specimens were subjected to a shear mode of loading. Using the Superpave Shear Tester, the frequency sweep test at a constant height (FSCH) at temperatures of 25°C and 50°C, and the repeated shear test at a constant height (RSCH) at 50°C was conducted. A number of shear properties were obtained from the FSCH and RSCH tests. Using the shear stress, shear strain, and the phase angle measured from the FSCH test at 25°C, the shear stiffness (G*), the stain controlled fatigue damage (G*sinδ),

and the stress controlled fatigue damage ($\sin\delta/G^*$) were computed. From the FSCH test at 50°C, the shear stiffness ($G^*$) and the permanent deformation damage ($\sin\delta/G^*$) were computed. From the RSCH test, the strains ($\varepsilon_p$) after 5000 load cycles and the number of cycles ($N_f$) that caused 2% strain in the specimen were measured.

Several statistical analyses were conducted in order to draw logical conclusions based on the measured and computed data. An F test on the means was used to test the significance of the change in the shear properties with the change in the level of inhomogeneity. In addition, the correlation analysis was used to examine the strength of the relationship between the shear properties and the level of inhomogeneity. Several findings resulted from this study:

First, the shear properties from the FSCH test at 25°C indicate that the shear modulus ($G^*$) increased, the stress controlled fatigue damage ($\sin\delta/G^*$) decreased, and the strain controlled fatigue damage ($G^* \sin\delta$) increased with the increase in the level of inhomogeneity. All three shear properties of inhomogeneous (I-SST) specimens were significantly different than those of L-SST and H-SST specimens. This indicates that based on the FSCH properties of highly inhomogeneous specimens, the fatigue performance of a thin layer would be underestimated and that of a thick layer would be overestimated, with the later resulting in premature failure of the layer. Comparison of the properties of L-SST and H-SST specimens indicated that $G^*$ and $G^*\sin\delta$ were not significant; however, the $\sin\delta/G^*$ of H-SST specimens was significantly lower than that of the L-SST specimens. This indicates that based on $\sin\delta/G^*$ of H-SST specimens the performance of a thick layer in fatigue might be overestimated.

Second, the comparisons of the G* and sinδ/G* values from FSCH test at 50°C indicate that the shear modulus (G*) increased and the permanent deformation damage (Sinδ/G*) decreased with the increase in the level of inhomogeneity. The homogeneous gyratory compacted (H-SST) specimens that have slight radial inhomogeneity behaved significantly different from the homogeneous (L-SST) specimens and similar to the radially inhomogeneous (I-SST) specimens. In other words, at a high temperature, a slight amount of inhomogeneity caused significant increases in G* and significant decreases in permanent deformation damage (Sinδ/G*) of the material. Therefore, the performance of a pavement layer for permanent deformation, based on the shear properties of gyratory compacted specimens would be over predicted, which would involve the risk of premature failure of the pavement.

Third, the comparison of the $N_f$ and $\varepsilon_p$ values from RSCH test indicates that I-SST specimens are performing significantly better than L-SST and H-SST specimens in resisting the shear deformation. The L-SST and H-SST specimens are performing similarly in resisting permanent shear deformation. Therefore, it is concluded that a slight inhomogeneity that is present in a gyratory compacted specimen would not change the performance of the material in permanent deformation as measured by the RSCH test. As a result, the prediction of the performance of a pavement layer based on $N_f$ and $\varepsilon_p$ values of gyratory compacted specimens in resisting permanent deformation would be valid.

Fourth, the correlations of the shear properties and the level of radial inhomogeneity within each set of specimens were very low or the direction of the trend was not accurate. In other words, the variation in the shear properties of the specimens was not explained by the variation in radial distribution of the aggregates. The reason for

343

the low correlations is the small range of the homogeneity index values for each set of specimens.

Fifth, the correlations of the shear properties and the level of radial inhomogeneity between the three sets of specimens were significant, where the test type and test temperature determined the trends of the correlations. The relationship of the FSCH test at 25°C and the RSCH test with the index of homogeneity exhibited very small nonlinearity, indicating that H-SST specimens behaved more similar to homogeneous specimens than to inhomogeneous specimens. However, the relationships between FSCH properties at 50°C and the z statistics were more nonlinear, indicating that H-SST specimens behaved more similar to inhomogeneous specimens than to homogeneous specimens.

Sixth, the correlation coefficients of the shear properties and the air void content of the ring and the core of all specimens indicated that the shear properties from the FSCH test at 25°C and from the RSCH test correlated better with the core air void content. The shear properties from the FSCH test at 50°C slightly better correlated with the ring air void content.

Seventh, the direction of the correlation between the shear properties and the core air void content is opposite to the direction of the correlation between the shear properties and the ring air void content. In other words, if a property has a positive correlation with the core air void content, it would have a negative correlation with the ring air void content, indicating that each portion works separately to resist the shear load.

# CHAPTER 10 - CONCLUSIONS

## 10.1 INTRODUCTION

The goal of this research was to evaluate the effects of inhomogeneity on the mechanical response of an asphalt mixture. The objectives of the study were to develop statistical indices for the measurement of homogeneity, to demonstrate that the indices could reliably distinguish between homogeneity and inhomogeneity, and to indicate that the indices could be used as performance indicators by correlating the mechanical response of an asphalt mixture to a level of inhomogeneity.

Since reliable material characterization is important for the support of the performance prediction models of the NCHRP Mechanistic-Empirical Design Guide (2004), this study was directed towards quantifying inhomogeneity and examining its effect on the mechanical response of asphalt mixture material. This involved measurement of the distribution of coarse aggregates by analyses of the cross-sectional images of homogeneous and inhomogeneous specimens captured nondestructively using 3-D x-ray computed tomography (XCT), followed by the mechanical testing of the specimens. The reliable measurement of homogeneity necessitated evaluation of existing methods of analysis and testing of new statistical tests using 3-D computer simulation.

## 10.2 EVALUATION OF EXISTING INDICES

The first step in characterizing the effect of inhomogeneity was to evaluate existing methods of measuring inhomogeneity. Some of the existing tests had conceptual problems that would reduce their statistical power. In addition, the indices by Yue et al.

(1995) and Masad et al. (1998) lacked a known statistical distribution. Therefore, statistical significance of sample values of the computed indices could not be tested. Critical values of these indices are needed to distinguish between the conditions of homogeneity and inhomogeneity. Thus, systematic decisions are not possible until the distributions are identified. The lack of critical values for the selected levels of significance also prevent the assessment of the power of the tests, which is important in evaluating the best tests to use.

## 10.3   NEW INDICES OF HOMOGENEITY

Based on the need for reliable measurements of inhomogeneity, which is a common problem in laboratory specimens, several new statistics (indices) were proposed. Values of the proposed indices could be computed using the geometric properties of the coarse aggregates. The properties used to define the indices were the frequency, area, and centroid distances of the aggregates. Based on the rationality of index values, a number of tests were selected as the final candidates to be tested by simulation. The selected tests were the t-test on total area, the t-test on frequency, the t-test on nearest neighbor distance, the z test on frequency proportion, and the chi-square test on frequency. Computer simulation was used to assess the selected tests. Virtual specimens with various aggregate structures were simulated and values of the indices of the proposed statistical tests were computed, from which the power of the tests and the critical statistics for three levels of significance of 10%, 5%, and 1% were obtained. The power of each test reflects the accuracy of the test, while the critical statistics enable homogeneous and inhomogeneous specimens to be distinguished.

### 10.3.1  Power of Tests of Vertical Homogeneity

The tests of vertical homogeneity were evaluated using both horizontal and vertical slice faces. The homogeneity tests on horizontal slice faces included the t-test on total area, the t-test on frequency, the t-test on nearest neighbor distance, and the chi-square test on frequency. The statistical power of the tests indicated that the frequency-based indices provided very high power, the distance-based index provided medium power, and the area-based index provided the lowest power in the measurement of vertical inhomogeneity. The chi-square test and the t-test on frequency provided powers of 99.9% and 90.1%, respectively, the t-test on nearest neighbor provided a power of 75%, and the t-test on total area provided a power of 18%. Therefore, among the four proposed tests, the two frequency based tests are most reliable for the detection of vertical homogeneity when horizontal slice faces are used.

The difference in the powers of the t-tests can be explained based on the rational examination of the t-statistic and the nature of frequency, distance, and area properties. The value of a t-statistic is a function of the difference between the mean geometric properties, the pooled variance of the means, and the sample size. The numerator of the statistic represents the difference between the means of the slice face properties within the coarser and finer portions of specimens. The denominator of the statistic represents the sampling variation of the slice face properties within the coarser and finer portions. The sample size, which is included in the denominator, also affects the computed index values. A large sample size would result in a small standard error of the mean and the greater accuracy estimator of homogeneity. Therefore, for a sufficient number of slices in the coarser and finer portions, if the difference between the mean geometric properties of the coarser and finer portions is large and the variability in the measured properties

within the two portions is small, a large index value would result. If the difference between the mean properties is large but the variability of the measured properties within the coarser and finer portions is also large, a computed index could be small. A low power of a test would result from a small index value and a high power of a test would result from a large index value for the state of inhomogeneity.

The nature of the area and distance properties as well as the rationale of the t statistic as explained above could be used to explain the lower power of the area-based and distance-based t-index. When large aggregates are sliced through, circular cross-sections with diameters less than or equal to 19 mm are formed, with only cross sections with diameters in the range of 4.75 mm to 19 mm entering into the analysis. Depending on the location of the slices through aggregates, a wide range of total aggregate areas and mean centroid distances would then be measured from the slices. This would yield large sampling variation in the aggregate area and mean centroid distance measurements of the slices. The large variation would yield a small value of the t-statistic for the inhomogeneous specimens and, therefore, the low power of the t-test on the area and distance properties.

The nature of the frequency property as well as the rationale of the t statistic could be used to explain the large power of the frequency-based t-index. Regardless of the locations of the slices through coarse aggregates, the frequency of the aggregates with cross-sections in the range of 4.75 mm to 19 mm in diameter would be recorded similarly. This means that the frequency of the aggregates cross sections would not be biased by their size. Therefore, there would be less variability in the frequency

measurements of the slice faces. This would yield a large t value, which result in the high power of the frequency-based tests.

Vertical homogeneity was also evaluated using vertical slice faces. The homogeneity tests using vertical faces included the t-test on total area, the t-test on frequency, the chi-square test on frequency, and the z test on frequency proportion. All indices of vertical homogeneity computed from vertical slice faces indicated a power of 100%. Therefore, all of the proposed tests are equally accurate for the measurement of vertical inhomogeneity when applied to vertical slice faces.

The rationale of the t-statistic and the trend of the coarse aggregate location in vertical and lateral directions are used to explain the 100% power of the t-tests when applied to vertical slices. Vertically inhomogeneous specimens were simulated in such a way that coarse aggregates are distributed with varying probability in the vertical direction and equal probability in lateral directions. This would yield a large difference in the means and small sampling variation of the coarse aggregate properties measured from lower and upper portions of vertical slice faces. As a result, a large t value and consequently a high power of the t-test would be computed from vertical slice faces.

Based on the findings of simulation for tests of vertical homogeneity, all of the tests proposed for vertical slice faces are accurate. When applied to horizontal slice faces, other than the t-test on total area, all other selected tests are accurate for testing of vertical homogeneity. However, the selection of the best vertical homogeneity index would need to account for the results of verification process, which involves testing of actual specimens.

### 10.3.2  Power of Tests of Radial Homogeneity

The power of the indices for measurement of radial homogeneity was evaluated using both horizontal and vertical slice faces. The tests included the t-test on total area, the t-test on frequency, the chi-square test on frequency, and the z test on frequency proportion. The analysis of the simulation results indicated that the power of the indices applied to both horizontal and vertical slice faces were 100%, meaning that the proposed tests are equally accurate when computed from either slice face direction.

The rationale of the t-statistic and the distribution of coarse aggregates within the specimen can be used to explain the 100% power of the t-statistics using either horizontal or vertical slice faces. Radially inhomogeneous specimens are simulated in such a way that coarse aggregates have equal probability of being located at any vertical position. This would cause a small sampling variation in the measured properties from horizontal slice faces, which represents the vertical trend in coarse aggregate arrangement. The small sampling variation would result in a small-pooled variance in denominator, a large value of the t-statistic, and consequently the high power of the test. On the other hand, the coarse aggregates are positioned with different probabilities in lateral direction. Therefore, the sampling variation in the properties measured from vertical slice faces, which represents the lateral trend in coarse aggregate arrangement, would be higher than that from the horizontal slice faces. However, the relatively higher variability is overshadowed by the larger number of vertical slice faces, which is nine, compared to the number of horizontal slice faces, which is three. This would cause the indices to have 100% power in the measurement of radial homogeneity using both horizontal and vertical slice faces.

The results of simulation indicate that, when testing for radial homogeneity, the use of both vertical and horizontal slice faces is acceptable. In both cases, any of the proposed tests would accurately measure radial homogeneity. However, the final selection of the best test statistic and most appropriate slice face direction would need to account for the results of the tests on actual specimens.

### 10.3.3 Determination of the Number of Slice Faces Using Simulation

To quantify the homogeneity of a specimen, the number of slices that should be used had to be determined. For the gradation used in this study, McCuen and Azari (2001) showed that a 10-mm spacing is necessary for independency of the slices. When cylindrical specimens are sliced horizontally, the slice faces have equal areas, and if taken in the right position, the slices would be from the same population. Therefore, each slice face is equally important in the computation of the statistics. Since a greater number of slices provide more reliable statistics, the maximum number of independent slices was used in analysis involving horizontal slice faces. The maximum number of independent horizontal slices was 12 for the evaluation of vertical inhomogeneity but only three for the evaluation of radial inhomogeneity.

When cylindrical specimens are sliced vertically, the cross sections of the slices are not the same. The middle slice face provides the largest cross-sectional area, while the area of a cross section decreases as the distance from the center slice increases. Based on the required 10-mm spacing between the slices and meaningful size of the sampling areas, the maximum number of vertical slices for evaluation of both vertical and radial homogeneity was determined to be nine. However, the unequal areas of the slice faces raised the question of whether all nine slices were necessary for reliable determination of

the statistics. To answer the question, the test statistics for each specimen were computed using five, seven, and nine slice faces, and the values of the statistics and the power of the tests were compared.

A comparison of the computed statistics from sets of five, seven, and nine slices revealed a change in the values of the statistics with the change in the number of slices. If the differences between the computed statistics were not significant, then it would be more efficient to conduct the analysis using a smaller number of slices. The comparison revealed that only the z statistic changed significantly with the increase in the number of slice faces, all other statistics did not change significantly. For example, with the change in the number of slices from five to nine, the chi-square statistic changed in the range of 4.59 to 4.71 and the t-statistic changed in the range of 1.77 to 1.86, both of which represent a very small difference in probability. However, the z statistic changed in the range of 1.59 to 2.24, which represents a significant difference in probability. The reason for the significant change in the z value could be explained in terms of the rationale of the z statistic (Equations 4-81 and 4-82). The increase in the number of slices would increase the expected maximum frequency of coarse aggregates in the sampling portions. This would result in a significant decrease in the sampling variation that is reflected in the denominator of the z statistic and consequently a significant increase in the z value.

Based on the results, all nine vertical slices are required for the accurate measurement of both vertical and radial homogeneity when the z proportion test is applied. On the other hand, five slices would be adequate to achieve the maximum accuracy of the chi-square and the t-tests. This implies that it would be more efficient to apply the chi-square and t-tests to five slice faces than to apply the z-test to nine slice

faces. However, the greater complexity of the z index (use of more geometric properties and larger number of slices) might be necessary to achieve adequate accuracy with homogeneity measurements of limited number of actual specimens. Therefore, the final decision on the number of slices would be made based on selection of the optimum test statistic, which is determined with consideration to the results of the tests on actual specimens. If homogeneity of the actual specimens was more accurately detected by the z test, then use of all nine slices would be necessary.

The findings in this section reemphasize that the selection of the number of vertical slice faces is not an arbitrary decision and needs to be determined using simulation. Therefore, the tests that are available in the literature might not accurately detect inhomogeneity since the number of slices for the suggested tests was not selected based on simulation.

### 10.3.4 Comparison of the Critical Statistics from Simulation and Standard Tables

The critical values computed from simulation were compared with the critical values from the standard statistical tables in order to examine if they were significantly different. To examine the difference, the exceedance probabilities of the simulated critical values were compared with 10%, 5%, and 1% levels of significance that correspond to the critical values in the standard tables. The comparison indicated that for some statistics, the exceedance probabilities and the corresponding levels of significance were similar, while for others they were very different. For example, the exceedance probabilities and the corresponding levels of significance of the chi-square statistic for testing radial homogeneity were similar. For a 5% level of significance, the exceedance probability was 4.7%. However, the values of the t test on total area were very different.

For a 5% level of significance, the exceedance probability was 10.9%. Therefore, it would be incorrect to automatically use the standard tables just because the form of a standard test statistic is used. This practice could lead to erroneous decisions.

The difference in the simulated and tabled values can be explained in terms of the properties that are being tested. The measured geometric properties such as aggregate area and aggregate frequency are very different from the properties on which the statistical tests were developed. Therefore, although each test of homogeneity was structured based on the standard z, t, and chi-square tests, the critical values for any new test must be obtained through simulation. This conclusion reemphasizes that tests identified in the literature that use the form of the z or t test might not accurately detect inhomogeneity if their critical values were determined from existing tables and not verified by simulation.

Computer simulation was necessary for derivation of the critical test statistics and the identification of the factors that influence the accuracy of the tests. Factors such as the slice face direction and the number of slices were found to be important. In addition, simulation was necessary to determine the critical values of the indices that are specific to the properties that are being measured and to the geometry of the test specimens. However, to ensure that the proposed tests and the selected factors provide correct decisions on the homogeneity of a limited number of laboratory specimens, their application to the actual specimens needs to be verified.

## 10.4   HOMOGENEITY TESTING OF ACTUAL SPECIMENS

The indices of homogeneity were computed using homogeneous and inhomogeneous laboratory specimens in order to verify the applicability of the proposed

tests to actual specimens. Evaluation of actual specimens for homogeneity requires measurement of the geometric properties of the constituent aggregates, which were obtained by analysis of the x-ray computed tomography (XCT) scanned images. The indices were then computed using the measured geometric properties. The homogeneity of the specimens was then determined by comparison of the computed indices with the critical index values or comparison of the rejection probabilities with the 5% level of significance. The rejection probabilities from actual specimens in combination with the power of the tests from simulation would be used to select the optimum indices of vertical and radial inhomogeneity.

## 10.4.1  Testing of Vertical Homogeneity

The application of the indices of vertical homogeneity to the actual specimens revealed the following facts: First, the proposed indices of vertical homogeneity detected the homogeneity of the homogeneous (H-SPT) specimens correctly using both vertical and horizontal slice faces. The average values of the test statistics were all below the critical values. Other than the t-statistic on total area applied to horizontal slice faces, which incorrectly identified one homogeneous specimen to be inhomogeneous, all individual values of the statistics were below the critical value. For example, the computed z values using vertical slice faces of H-SPT specimens were all less than the critical z, with the average z of 0.17 compared to the critical z of 1.59, and an average rejection probability of 0.45 compared to 0.05. This indicated that the specimens prepared to be homogeneous and compacted using Superpave gyratory compactor were in fact vertically homogeneous.

Second, in the testing of vertically inhomogeneous specimens (I-SPT), all average computed statistics were above the critical statistics, which indicated that the specimens were not homogeneous. Other than the chi-square test applied to vertical slice faces, which resulted in three computed statistics to be below the critical value, all other tests correctly identified the inhomogeneity of individual specimens. The reason for the incorrect decisions by the chi-square test might be that the test is excessively sensitive to the sampling variation that results during specimen preparation and the testing of a limited number of actual specimens.

Third, the homogeneity test when applied to vertical slice faces of actual specimens showed that among the tests that identified all individual specimens correctly, the z statistic, provided the greatest discrimination between homogeneity and inhomogeneity. This was shown by the difference in the average rejection probabilities of the homogeneous and inhomogeneous specimens. The difference in the computed rejection probabilities was in the range of 0.260 to 0.419, with the upper range value belonging to the z statistic.

The results of homogeneity tests on actual specimens confirmed that the proposed indices of vertical homogeneity are reliable for distinguishing between homogeneity and inhomogeneity. Other than one case of t-test on total area and three cases of chi-square test, all other actual cases were in agreement with the critical values developed with simulation. Both simulation and actual testing recommended the use of the z test and frequency based t test. Similar to the simulation results, the t-test on total area is more accurate when computed from vertical slice faces than from horizontal slice faces of actual specimens.

**10.4.2  Testing of Radial Homogeneity**

The application of the indices of radial homogeneity to the actual specimens revealed three facts: First, horizontal slice faces provide more accurate measurement of radial homogeneity than vertical slice faces. Although simulation indicated maximum power of the proposed tests with the use of both slice face directions, the indices computed from actual specimens were more accurate when computed from horizontal slice faces. Thirty-three out of 72 cases were misidentified using vertical slice faces while only 11 cases were misidentified using horizontal slice faces. The reason for this is the larger sampling variation in the measured geometric properties from vertical slice faces of actual specimens, which is caused by the trend in the coarse aggregate arrangement in the lateral direction. Therefore, for measurement of radial homogeneity, using horizontal slice faces is recommended.

Second, other than the z test, all of the tests applied to horizontal slice faces misidentified one or more specimens. Out of 24 L-SST, H-SST, and I-SST specimens, the chi-square test misidentified one, the t-test on total area misidentified six, and the t-test on frequency misidentified four of the specimens. As the z test did not result in any misidentifications, it is considered to be the most reliable for detecting radial homogeneity.

Third, the z index identified three distinct levels of homogeneity for the three sets of specimens. The computed indices for the linearly kneaded (L-SST), homogeneous gyratory (H-SST), and inhomogeneous gyratory compacted specimens (I-SST) were 0.19, 0.90, and 3.10, respectively. This indicates that the z index is accurate for test of homogeneity.

Fourth, the computed z statistics indicated that specimens prepared homogeneously (L-SST and H-SST) were in fact homogeneous and the I-SST set that was prepared to be inhomogeneous was correctly identified as being inhomogeneous. The computed indices for L-SST specimens were all below the critical statistic (the average z of 0.19 was much less than the critical z of 2.48). For H-SST specimens, the computed indices were all greater than those for the L-SST specimens but still below the critical z (the average z of 0.90 was less than the critical z of 2.48), which indicated that, despite the tendency of more coarse aggregates to be in the periphery of gyratory compacted specimens, they are still homogeneous. The z index measured significant amounts of radial inhomogeneity in the I-SST specimens. The computed indices were all greater than the critical z (the average z of 3.10 exceeded the critical z of 2.48), which indicated that the tests accurately measured radial inhomogeneity.

The fabrication of test specimens is not a perfect process. Sampling variation is expected to occur. Discrepancies between the test accuracies of actual and simulated analyses can, therefore, result because of the variation inherent to the fabrication of actual specimens. These variations were not included in the simulation. Although, the simulated and actual specimens were fabricated based on the same gradations and same overall aggregate structure, the material handling and compaction process affects the orientation and distribution of the aggregates. This can produce actual-specimen indices that are different from those generated by simulation, even though the differences are expected to be small. The orientation and distribution of the aggregates were not included in the simulation because the extent of these factors in laboratory specimens is not yet fully understood and therefore, has not been well quantified. The z index that uses both the

358

area and the frequency of the aggregates was less affected by such factors and provided the required accuracy when applied to actual specimens.

The application of the tests of homogeneity to actual specimens was beneficial in confirming and refining the results of the simulations. The refinement of the simulation findings is necessary since factors exist in preparation and homogeneity testing of actual specimens that are not included in the simulation. Including the results of the verification process in the final selection of the test statistics as well as the selection of the number and direction of slices provides more assurance in the use of the tests. Pavement engineers can use the proposed indices of homogeneity with more confidence, since the applicability of the statistics generated from simulation have been demonstrated by the actual specimens.

## 10.5 EFFECT OF INHOMOGENEITY ON MECHANICAL PROPERTIES

Subsequent to the inhomogeneity testing, the specimens were subjected to mechanical loading to examine the effect of inhomogeneity on the compressive and shear performance of the material. The following are the results of the mechanical tests:

### 10.5.1 Effect of Vertical Inhomogeneity on Compressive Properties of the Mixtures

The effect of vertical inhomogeneity on the compressive properties of the asphalt mixtures was examined by subjecting homogeneous (H-SPT) and vertically inhomogeneous (I-SPT) specimens to the dynamic modulus (E*) and flow number ($F_N$) of the simple performance tests (SPT). The E* test was conducted at intermediate and high temperatures of 21°C and 45°C, and the $F_N$ test was conducted at the high test temperature of 45°C.

Statistical analyses were conducted on the measured and computed mechanical properties in order to evaluate the significance of the difference between the mechanical response of the homogeneous and inhomogeneous specimens. The results of t-tests on the SPT measurements indicated that (1) I-SPT specimens had lower, but not significantly lower, dynamic moduli (E*) than H-SPT specimens at both intermediate and high-test temperatures. (2) I-SPT specimens had higher, but not significantly higher, potential for rutting using the dynamic modulus test (Sinφ/E* at 45°C); (3) I-SPT specimens had higher, but not significantly higher, potential for fatigue damage in a thick layer using the dynamic modulus test (Sinφ/E* at 21°C); (4) I-SPT specimens had significantly lower potential for fatigue damage in a thin layer using the dynamic modulus test (E*sinφ at 21°C); and (5) I-SPT specimens had lower, but not significantly lower, potential for rutting using cycles to failure ($F_N$) at 45°C.

A correlation analysis was used to evaluate the relationship between the z index and the compressive responses of the material. In agreement with the t-test, correlation analyses indicated that the only correlation that was significant was the fatigue potential for a thin layer (E*sinφ at 21ºC). All other correlations were insignificant. The insignificant correlations are caused by the insignificant differences between the compressive responses of the homogeneous and inhomogeneous specimens as measured by the simple performance tests. This would imply that the parameters of the simple performance tests, which are commonly used for the evaluation of the asphalt mixture quality, might not always be sufficiently sensitive to the differences in aggregate structures. For this mixture, sampling variation in the laboratory that leads to

inhomogeneity may not affect the measurement of the compressive properties of the material and would not be a major concern.

Another observation from the results is the contradiction between the permanent deformation potential of the material as measured by $\sin\varphi/E^*$ from the dynamic modulus test and by $F_N$ from the flow number test. Although $\sin\varphi/E^*$ and $F_N$ are often considered to be interchangeable when characterizing high temperature performance of asphalt materials, they indicated an opposite trend when inhomogeneity was present. The design engineer needs to be aware of the specific effect of inhomogeneity on the property of interest and to adjust design and performance prediction accordingly.

A word of caution must be given on the use of $E^*\sin\varphi$ and $F_N$ values of inhomogeneous specimens for performance prediction. Since the $E^*\sin\varphi$ values of the vertically inhomogeneous specimens were smaller than those of the homogeneous ones, fatigue performance of the material in a thin layer would be overestimated. Similarly, using the higher $F_N$ values of the vertically inhomogeneous specimens, the permanent deformation performance of a layer would be overestimated. Therefore, in both cases, premature failure of a layer could occur. To increase the reliability of the performance prediction for both fatigue and rutting, a factor of safety proportional to the amount of inhomogeneity of the specimens is suggested to be applied to the $E^*\sin\varphi$ and $F_N$ values.

## 10.5.2 Effect of Radial Inhomogeneity on Shear Properties of the Mixtures

The effect of radial inhomogeneity on the shear properties of the asphalt mixtures was examined by subjecting linearly kneaded (L-SST), homogeneous gyratory compacted (H-SST), and radially inhomogeneous (I-SST) specimens to Superpave shear tests (SST). The SST included frequency sweep at constant height (FSCH) and repeated

shear at constant height (RSCH) tests. The FSCH test was conducted at intermediate and high-test temperatures of 25°C and 50°C, and the RSCH test was conducted at 50°C.

Statistical analyses were conducted on the measured and computed shear properties in order to evaluate the significance of the difference between the shear responses of the three sets. The results of F tests indicated that at the intermediate temperature, the increase in the level of radial inhomogeneity of the gyratory compacted specimens caused significant increases in the shear modulus (G*), significant decreases in fatigue damage potential of the material in thick layers ($\sin\delta/G^*$), and significant increases in fatigue damage potential of the material in thin layers (G* $\sin\delta$). These are contrary to the observations made from the axial compression tests (SPT), where inhomogeneous specimens indicated lower dynamic modulus (E*), higher fatigue damage potential in thick layers ($\sin\phi/E^*$), and lower fatigue damage potential in thin layers (E*$\sin\phi$), with only E*$\sin\phi$ being significant. This might imply that the response of an inhomogeneous asphalt material is dependent on the mode of loading (axial or shear). Therefore, design engineers need to take into account the effect of inhomogeneity with consideration to the mode of loading that was used to measure the mechanical properties.

Homogeneous gyratory specimens (H-SST) behaved similarly to radially homogeneous specimens (L-SST) in fatigue, measured at the intermediate temperature, while they behaved similarly to radially inhomogeneous specimens (I-SST) in rutting, measured at the high-test temperature. This might imply that there is an interaction between inhomogeneity and test temperature, which causes the trend in which the material behaves to be different at different test temperatures. Therefore, the effect of inhomogeneity should be taken into consideration with respect to the test temperature,

362

which has been determined based on the expected damage in the field. Thus, the effect of inhomogeneity should consider the type of damage for which the layer is being analyzed or designed.

As measured by the RSCH test, homogeneous gyratory (H-SST) and linearly compacted (L-SST) specimens had similar cycles to failure ($N_f$), while inhomogeneous specimens had significantly higher $N_f$ values than the two homogeneous sets. This might imply that for a specific mode of loading in the laboratory (e.g., shear), in addition to the test temperature, the loading pattern (cyclic load with or without rest period) has a significant effect on the trend in which the material responses. Therefore, the effect of inhomogeneity on performance prediction should consider the laboratory test-loading pattern. The findings above imply that pavement design engineers need to take into account the effect of inhomogeneity with respect to the mode of loading (shear or axial), test temperature (intermediate or high), and the loading pattern (continuous or with rest period), where these factors have been determined based on loading configuration and the damage expected in the field.

A correlation analysis was used to evaluate the relationship between the z index and the shear responses of the material. The analyses indicated that all correlations were significant. The significant correlations are the result of significant differences between the shear responses of the L-SST, H-SST, and I-SST specimens as measured by the Superpave shear tests. However, the trends of the correlation were different for the two test temperatures of 25°C and 50°C and the two loading patterns in the FSCH and RSCH tests. In the FSCH test at intermediate temperature, homogeneous gyratory compacted specimens responded more closely to homogeneous linearly compacted specimens, which

resulted in slightly nonlinear relationship between shear properties and z statistic with the correlation coefficient of 0.78. In the FSCH test at the high temperature, homogeneous gyratory compacted specimens responded more closely to inhomogeneous gyratory compacted specimens, which resulted in a curvilinear relationship between shear properties and the z statistic with the correlation coefficient of 0.71. In the RSCH test, the relationships between shear properties and the z statistic was slightly nonlinear with the highest correlation coefficient of 0.88.

Several findings can be drawn from the correlations. First, the highest correlations with the RSCH parameters indicate that the repeated shear test is most affected by the variations in aggregate structure. Second, the trend of the relationship between FSCH properties and the z statistic at the intermediate temperature and between RSCH properties and the z statistic indicates that gyratory specimens need to be highly inhomogeneous to exhibit significant changes in shear properties. Third, the trend of the relationship between FSCH properties and the z statistic at the high temperature indicates that even a slight amount of radial inhomogeneity that is created during specimen preparation significantly increases the shear resistance of the material in permanent deformation. This implies that the amount of radial inhomogeneity in gyratory compacted specimens should be minimized in order to prevent the overestimation of the rutting performance of the material in the field. In addition to the careful preparation of the specimens, application of a factor of safety to the shear properties of gyratory compacted specimens would ensure the reliability of the performance prediction. The value of the factor of safety should be proportional to the level of inhomogeneity of the specimens.

# CHAPTER 11 - RECOMMENDATIONS

Additional research is needed to further verify the findings of this study. The suggested recommendations are expected to improve our understanding of the interaction between asphalt mixture inhomogeneity and mechanical behavior. Since this research was a laboratory study, it needs to be extended to the field.

## 11.1   FIELD MEASUREMENT OF INHOMOGENEITY

This research focused on developing and testing indices that measure the inhomogeneity of laboratory-prepared asphalt specimens. It is recommended to extend the applicability of the suggested indices for the field measurement of inhomogeneity. An approach similar to the one taken for the measurement of laboratory inhomogeneity could provide an effective, nondestructive method for the measurement of inhomogeneity in the field. The approach includes collecting data on the mixture properties of the asphalt mixture layers from various locations of a pavement section followed by the computation of homogeneity indices. To obtain the mixture properties, a device similar to a high frequency ground penetrating radar (GPR) could be used to nondestructively capture 2-D cross-sectional density map images from various locations of a pavement section. Using image analysis tools, the density information would then be measured from the cross-sectional images. Statistical testing would be used to examine the significance of the difference in the mixture densities at various portions of a pavement layer. Statistical testing includes computation of the index of homogeneity, such as the z index, using the collected density data and making a decision on the homogeneity of a pavement section based on the comparison of the computed and critical index values.  Research is needed

to evaluate the critical values of the indices that are specific to the field. Computer simulation of homogeneous and inhomogeneous test sections can be used to determine the distributions of the test statistics, their critical values, and the power of the tests.

## 11.2   HOMOGENEITY INDICES AS PERFORMANCE INDICATORS

Inhomogeneity has been associated with poor performance, reduced durability, and shorter life (Stroup-Gardiner and Brown, 1999). Thus, an accurate estimate of field inhomogeneity would be of value to evaluate the performance of an existing pavement under loading and environmental influences.

To ensure the suitability of the index of homogeneity as a performance indicator, the relationship between homogeneity and the mechanical performance of a pavement section must be assessed.  The assessment would include collecting homogeneity and performance data starting from the early stages in the life of a pavement layer until signs of distress develop. The z index on density data from the asphalt mixture layer is suggested for the measurement of homogeneity. The use of density data is recommended since the differences in density result from the differences in the aggregate and air void distributions that are indications of inhomogeneity. In addition, density can be easily measured nondestructively by several different means, such as GPR, nuclear density gauges, and pavement quality indicator (PQI) device. The performance data could be obtained by measurement of the modulus of the pavement layer shortly after construction and at monthly intervals. A device such as a Portable Seismic Pavement Analyzer (PSPA) can be used for the quick measurement of moduli of the layers. The initial moduli and the reduction in moduli, which indicates the deterioration of the layer with the

366

application of the loads, can be measured and correlated to the level of homogeneity of the section. The use of an accelerated loading device, such as the Miniature Mobile Load Simulator (MMLS), is recommended to intensify the loading and expedite the deterioration of the sections. If a significant correlation between the values of the homogeneity index and the change in moduli is established, then the suggested index can be used as a measure of the performance of a pavement.

## 11.3   HOMOGENEITY INDEX FOR QUALITY CONTROL AND ACCEPTANCE

The quality of new asphalt concrete pavement construction is traditionally assessed from the results of asphalt content, air void, and aggregate gradation measurements of cored samples. Deviations of the measured values from the mixture design criteria have been the basis for quality control and acceptance of pavement layers. Since inhomogeneity has been related to significant changes in the abovementioned quality indicators (Stroup-Gardiner and Brown 1999), a measure of homogeneity, such as the z index, can be used for routine quality control (QC). The z index can be computed using mixture density, which can be measured reliably in the field using GPR, PQI, or nuclear density gauges. The homogeneity of the mixture layer can then be assessed by a comparison of the computed z index with the critical z that was obtained from computer simulation. Any z greater than the critical z requires a penalty to the paving contractors.

## 11.4   EFFECT OF AGGREGATE GRADATION ON INHOMOGENEITY

A dense-graded blend with a 19.5-mm nominal maximum aggregate size (NMAS) was used in this study to form various aggregate structures. The compaction effort caused

an insignificant level of inhomogeneity in specimens that were prepared homogeneously. It is of interest to know if compaction causes significant levels of inhomogeneity in mixtures with other aggregate gradations. This would identify mixtures that are prone to inhomogeneity, which would identify the gradations that require greater care in the process of specimen preparation. A knowledge of the correlation between mixture gradations and inhomogeneity would make improvements in design and performance decisions based on gradation information.

## 11.5   INDICES FOR THE MEASUREMENT OF RANDOM INHOMOGENEITY

This research emphasized the characterization of systematic vertical and radial inhomogeneity of laboratory prepared specimens. It is also important to be able to detect and measure random inhomogeneity. Random inhomogeneity, which is the separation of a design mixture into random clusters of coarser and finer mixtures, is hypothesized to be a cause of occasional high or low mechanical property measurements. When mechanical test results are not consistent and inhomogeneity is not identified, it may incorrectly be concluded that factors other than inhomogeneity caused the inconsistency. This could misdirect engineers and technicians.

To test for random inhomogeneity, an approach similar to that taken for the testing of vertical and radial inhomogeneity is recommended. One possible index of random homogeneity can be defined based on the comparison of the geometric properties of coarse aggregates within the openings of a grid imposed on slice faces of the specimens. For the purpose of testing the index, computer simulated and actual

inhomogeneous specimens can be created by randomly placing pockets of coarse aggregates within each specimen.

## 11.6   EXAMINING THE FACTORS THAT AFFECT INHOMOGENEITY

In the gyratory compaction of asphalt mixture specimens, several factors might be responsible for the occurrence of inhomogeneity, factors such as specimen height, the mixing and compaction temperatures, and the angle and pressure of the gyration. To examine the effects of these factors, various heights of asphalt mixture can be compacted at different temperatures, with varying angles and varying vertical pressures. The specimens can then be tested for homogeneity. This study would require a large number of specimens; however, the results would be very beneficial in obtaining the optimum gyratory setting to fabricate specimens with a minimum amount of inhomogeneity.

## 11.7   EFFECT OF INHOMOGENEITY ON TENSILE RESPONSE

In this study, the effect of inhomogeneity on the compressive and shear performance of laboratory specimens was examined. It is of interest to examine the effect of inhomogeneity on other modes of response, specifically the tensile response. In this respect, homogeneous and inhomogeneous specimens can be subjected to a tensile loading in a test set up such as beam fatigue. Inhomogeneous beam specimens are speculated to have less resistance to tensile strain.

To measure the homogeneity of the beams, the z index that was suggested for the measurement of vertical homogeneity could be used. However, application of the index to beam specimens requires assessment of the critical statistics that are specific to the

geometry of the beams using computer simulation. This is because the slice faces of the beams would be different in number and size from those of the cylindrical specimens for which the critical z was computed.

## 11.8   EFFECT OF INDIVIDUAL MIXTURES ON MEASURED PROPERTIES OF INHOMOGENEOUS SPECIMENS

It is of interest to examine if the coarser or the finer mixtures were responsible for the responses of inhomogeneous specimens. In the compression test, the LVDTs extend over both the coarser and the finer portions and are speculated to have provided average strain measurements. Similarly, in shear test, the strain gauges measure an average strain from both the coarser and finer portions.

To examine the effect of individual mixtures on the measured moduli, either the location of the LVDTs or the arrangement of the mixtures can be changed. For the compression test, the location of the LVDTs can be altered. Separate LVDTs can be placed over the coarser and finer mixtures and separate strains for the two portions can be measured. If the strain measurements are not significantly different from each other, it could be concluded that both coarse and fine mixtures are equally responsible for the response of the specimens.

To examine the effect of coarser and finer mixtures on the shear modulus, it is recommended to alter the arrangement of the mixtures. Shear specimens can be created with the coarser mixture in the core and the finer mixture in the ring. The specimens can be tested with the conventional LVDT setup. If different structures provide similar responses, it can be concluded that both mixtures are equally responsible for the response of the specimens.

# APPENDIX A - DETERMINATION OF THE NUMBER OF PARTICLES FOR COMPUTER DEVELOPMENT OF A SPECIMEN

To form virtual specimens as part of the simulation of homogeneity indices, it is necessary to determine the number of particles in each class size in a given size specimen. The information on the design components of asphalt mixtures needs to be used to determine the number of particles. This requires the knowledge of the weight-volume relationship and the volume packing fraction of the asphalt mixture specimens.

## A.1    WEIGHT –VOLUME RELATIONSHIP

In order to obtain realistic results, the computer model of a specimen must adhere to realistic volume-weight constraints. Therefore, the volume of air voids ($V_v$) and the weight fractions of both asphalt ($f_a$) and aggregates ($f_p$) must be used to derive the weight-volume relationship of asphalt mixture specimens. The derivation of the relationship is as follows:

1. The volume of the specimen ($V_s$) equals the sum of the volume of aggregates ($V_p$), asphalt ($V_a$), and air voids ($V_v$):

$$V_s = V_p + V_a + V_v \tag{A-1}$$

2. Both sides of Equation (A-1) are divided by the $V_s$:

$$1 = \frac{V_p}{V_s} + \frac{V_a}{V_s} + r_v \tag{A-2}$$

in which $r_v$ is the volume fraction of the air voids.

3. Rearranging the terms yields the following expression:

$$V_s(1-r_v) = V_a + V_p \tag{A-3}$$

4. Substituting the volumes in the right side of the equation with equivalent weight-specific weight relationships yields the following:

$$V_s(1-r_v) = \frac{W_a}{\gamma_a} + \frac{W_p}{\gamma_p} \tag{A-4}$$

in which $W_a$ and $W_p$ are the weights, and $\gamma_a$ and $\gamma_p$ are the specific weights of asphalt and aggregates, respectively.

5. Writing the weights of aggregates and asphalt in term of the weight of specimen yields the following:

$$V_s(1-r_v) = \frac{f_p W_s}{\gamma_p} + \frac{f_a W_s}{\gamma_a} \tag{A-5}$$

in which $f_p$ and $f_a$ are the specimen weight fractions of aggregates and asphalt.

6. Rearranging the terms yields the following expression that relates the weight and the volume of the specimen:

$$W_s = \frac{(1-r_v)}{\left[\dfrac{f_p}{\gamma_p} + \dfrac{f_a}{\gamma_a}\right]} V_s \tag{A-6}$$

## A.2   VOLUME PACKING FRACTION

Knowledge of the volume packing fraction of an asphalt mixture specimen is an essential component of simulating a realistic number of particles. The derivation of volume packing fraction is as follows:

1. The volume packing fraction ($P_v$) is defined as the ratio of the volume of particles to the volume of the specimen, which yields the following expression:

$$P_v = \frac{V_p}{V_s} = \frac{W_p/\gamma_p}{V_s} = \frac{f_p W_s/\gamma_p}{V_s} \tag{A-7}$$

2. Substituting for $W_s$ from Equation (A-6) and rearranging the terms yields the expression for the volume packing fraction:

$$P_v = \frac{1 - r_v}{1 + \left(\dfrac{f_a}{f_p}\right)\left(\dfrac{\gamma_p}{\gamma_a}\right)} \tag{A-8}$$

## A.3  NUMBER OF PARTICLES

The weight-volume relationship and volume packing fraction are used to derive the equation for computing the number of particles in each gradation level of a specimen. For the purposes of approximating, the particles can be assumed to be spherical with a diameter equal to the average of adjacent sieve sizes.  For example, for adjacent sieve sizes of 25 mm and 19 mm, the particle class diameter would be 22 mm. Derivation of the expression for computing the number of aggregates in each gradation class size is explained as follows:

1. The number of particles ($n_i$) for gradation level $i$ is expressed as the ratio of the volume of all particles in the $i^{th}$ gradation level ($V_i$) to the volume of one particle ($v_i$):

$$n_i = \frac{V_i}{v_i} \tag{A-9}$$

2. Substituting the total volume of the aggregates in the gradation level $i$ with the equivalent weight-specific weight expression and substituting the volume of the particle with volume of a sphere results in the following:

$$n_i = \frac{V_i}{v_i} = \frac{W_i/\gamma_p}{\pi d_i^3/6} \qquad \text{(A-10)}$$

in which $d_i$ is the average particle diameter for level $i$; $W_i$ is the weight of particles

in gradation level $i$; and $\gamma_p$ is the specific weight of the particles.

3. Expressing the weight of the aggregates in the gradation level $i$ in terms of the total

weight of particles yields the following:

$$n_i = \frac{6F_iW_p}{\pi\gamma_p d_i^3} \qquad \text{(A-11)}$$

where $F_i$ is the weight fraction for gradation level $i$ and $W_p$ is the total weight of

particles.

4. Writing the weight of particles ($W_p$) in terms of volume ($V_p$) and specific weight

($\gamma_p$) of the particles and deleting the like terms result in the following:

$$n_i = \frac{6F_i\gamma_p V_p}{\pi\gamma_p d_i^3} = \frac{6F_iV_p}{\pi d_i^3} \qquad \text{(A-12)}$$

5. The volume of the particles can be written in terms of the packing fraction ($P_v$) of

the volume of the specimen:

$$n_i = \frac{6F_iP_vV_s}{\pi d_i^3} \qquad \text{(A-13)}$$

6. Expressing the volume of the solid in terms of the dimensions of the specimen

yields the final expression for computing the number of particles:

$$n_i = \frac{1.5F_iP_vD_s^2H_s}{d_i^3} \qquad \text{(A-14)}$$

in which $D_s$ and $H_s$ are the diameter and height of the specimen, respectively.

# APPENDIX B - ASPHALT CONTENT DETERMINATION BASED ON SPECIFIC SURFACE AREA OF THE AGGREGATES

## B.1    INTRODUCTION

Making inhomogeneous specimens requires separating the design gradation into a coarser and a finer mixture, which requires the knowledge of the gradation and the binder content of each mixture. The coarser and the finer gradations were obtained by modifying the design gradation as explained in Chapter 3. The asphalt contents were determined using the specific surface area method and were adjusted by the level of workability required in the laboratory.

The optimum asphalt content, which is defined as the minimum amount of asphalt content that covers the surface of all aggregates ensures both workability and durability of the asphalt mixture. Therefore, after deducting the amount of asphalt absorbed into the aggregates pores, the optimum asphalt content for a specific gradation can be determined by summing of surface areas of aggregates in all class sizes multiplied by an assumed asphalt film thickness. The following sections explain determination of the optimum binder contents of the coarser and the finer mixtures using the specific surface area method.

## B.2    COMPUTING THE AGGREGATE SURFACE AREA

The surface area measurement method used in this study was adopted from the methods suggested by Christensen (2001) and Kandhal et al. (1997). Table B-1 through

Table B-3 shows the computation of the aggregates total surface area for the three gradations. The steps of the computation are as follows:

1.  The percent retained on each sieve (Column 3) was calculated from the sieve analysis data.

2.  The average particle diameter in each of the class sizes (Column 4) was calculated as the arithmetic average of the smaller and larger sieve openings for each class size. For the passing 0.075-mm fraction, an average particle diameter of 0.0375 mm was assumed.

3.  Based on the assumption that the aggregates are spherical in shape, the volume and surface area of the average particle in each class size was calculated (Columns 5 and 7, respectively).

4.  The weight of each particle (Column 6) was determined based on the specific weight of the aggregates ($\gamma_p$) and the computed volume of each spherical particle (Column 5).

5.  The number of particles per unit weight of each class size (Column 8) was calculated based on the percent weight of the particles retained (Column 3) and the average weight of each particle (Column 6).

6.  The surface area per unit weight of each class size (Column 9) was calculated as the product of the number of particles per unit weight (Column 8) and the surface area of the particles in that class size (Column 7).

7.  The total surface area per unit weight of the aggregates was calculated by summing the unit surface areas of the aggregates in all class sizes; this is provided at the bottom of the tables.

**Table B-1. Specific surface computation for the design gradation**

| (1) | (2) | (3) | (4) | (5) | (6) | (7) | (8) | (9) |
|---|---|---|---|---|---|---|---|---|
| Sieve Opening (mm) | Percent Passing | Retained (kg/kg) | Average Particle Size (mm) | Volume Per Particle (cm³) | Weight Per Particle (kg) | Surface Area Per Particle (m²) | Number of Particles Per Unit Weight ($n_i$/kg) | Surface Area Per Unit Weight m²/kg |
| 19 | 100 | 0.240 | 15.75 | 2.05E+00 | 5.93E-03 | 1.49E-03 | 4.05E+01 | 0.060 |
| 12.5 | 76 | 0.140 | 11 | 6.97E-01 | 2.02E-03 | 7.26E-04 | 6.93E+01 | 0.050 |
| 9.5 | 62 | 0.179 | 7.125 | 1.89E-01 | 5.49E-04 | 3.05E-04 | 3.26E+02 | 0.099 |
| 4.75 | 44.1 | 0.140 | 3.555 | 2.35E-02 | 6.82E-05 | 7.58E-05 | 2.05E+03 | 0.156 |
| 2.36 | 30.1 | 0.078 | 1.77 | 2.90E-03 | 8.42E-06 | 1.88E-05 | 9.26E+03 | 0.174 |
| 1.18 | 22.3 | 0.066 | 0.89 | 3.69E-04 | 1.07E-06 | 4.75E-06 | 6.17E+04 | 0.293 |
| 0.6 | 15.7 | 0.055 | 0.45 | 4.77E-05 | 1.38E-07 | 1.22E-06 | 3.97E+05 | 0.483 |
| 0.3 | 10.2 | 0.031 | 0.225 | 5.96E-06 | 1.73E-08 | 3.04E-07 | 1.79E+06 | 0.544 |
| 0.15 | 7.1 | 0.022 | 0.1125 | 7.46E-07 | 2.16E-09 | 7.59E-08 | 1.02E+07 | 0.773 |
| 0.075 | 4.9 | 0.049 | 0.0375 | 2.76E-08 | 8.01E-11 | 8.44E-09 | 6.12E+08 | 5.163 |

$\gamma_p = 2.89\ E+03\ kg/m^3$
$\gamma_a = 1.02E+03\ kg/m^3$
Total surface area per unit weight= 7.796 m² /kg

**Table B-2. Specific surface computation for the coarser gradation**

| (1) | (2) | (3) | (4) | (5) | (6) | (7) | (8) | (9) |
|---|---|---|---|---|---|---|---|---|
| Sieve Opening (mm) | Percent Passing | Retained (kg/kg) | Average Particle Size (mm) | Volume Per Particle (cm³) | Weight Per Particle (kg) | Surface Area Per Particle (m²) | Number of Particles Per Unit Weight ($n_i$/kg) | Surface Area Per Unit Weight m²/kg |
| 19 | 52.95 | 0.180 | 15.75 | 2.05E+00 | 5.93E-03 | 1.49E-03 | 3.03E+01 | 0.045 |
| 12.5 | 34.95 | 0.105 | 11 | 6.97E-01 | 2.02E-03 | 7.26E-04 | 5.20E+01 | 0.038 |
| 9.5 | 24.45 | 0.134 | 7.125 | 1.89E-01 | 5.49E-04 | 3.05E-04 | 2.44E+02 | 0.074 |
| 4.75 | 11.03 | 0.035 | 3.555 | 2.35E-02 | 6.82E-05 | 7.58E-05 | 5.13E+02 | 0.039 |
| 2.36 | 7.53 | 0.020 | 1.77 | 2.90E-03 | 8.42E-06 | 1.88E-05 | 2.32E+03 | 0.044 |
| 1.18 | 5.58 | 0.017 | 0.89 | 3.69E-04 | 1.07E-06 | 4.75E-06 | 1.54E+04 | 0.073 |
| 0.6 | 3.93 | 0.014 | 0.45 | 4.77E-05 | 1.38E-07 | 1.22E-06 | 9.94E+04 | 0.121 |
| 0.3 | 2.55 | 0.008 | 0.225 | 5.96E-06 | 1.73E-08 | 3.04E-07 | 4.48E+05 | 0.136 |
| 0.15 | 1.78 | 0.006 | 0.1125 | 7.46E-07 | 2.16E-09 | 7.59E-08 | 2.54E+06 | 0.193 |
| 0.075 | 1.23 | 0.012 | 0.0375 | 2.76E-08 | 8.01E-11 | 8.44E-09 | 1.53E+08 | 1.291 |

$\gamma_p = 2.89\ E+03\ kg/m^3$
$\gamma_a = 1.02E+03\ kg/m^3$
Total surface area per unit weight= 2.054 m² /kg

**Table B-3. Specific surface computation for the finer gradation**

| (1) | (2) | (3) | (4) | (5) | (6) | (7) | (8) | (9) |
|---|---|---|---|---|---|---|---|---|
| Sieve Opening (mm) | Percent Passing | Retained (kg/kg) | Average Particle Size (mm) | Volume Per Particle (cm$^3$) | Weight Per Particle (kg) | Surface Area Per Particle (m$^2$) | Number of Particles Per Unit Weight ($n_i$/kg) | Surface Area Per Unit Weight m$^2$/kg |
| 19 | 47.05 | 0.060 | 15.75 | 2.05E+00 | 5.93E-03 | 1.49E-03 | 1.01E+01 | 0.015 |
| 12.5 | 41.05 | 0.035 | 11 | 6.97E-01 | 2.02E-03 | 7.26E-04 | 1.73E+01 | 0.013 |
| 9.5 | 37.55 | 0.045 | 7.125 | 1.89E-01 | 5.49E-04 | 3.05E-04 | 8.15E+01 | 0.025 |
| 4.75 | 33.08 | 0.105 | 3.555 | 2.35E-02 | 6.82E-05 | 7.58E-05 | 1.54E+03 | 0.117 |
| 2.36 | 22.58 | 0.059 | 1.77 | 2.90E-03 | 8.42E-06 | 1.88E-05 | 6.95E+03 | 0.131 |
| 1.18 | 16.73 | 0.050 | 0.89 | 3.69E-04 | 1.07E-06 | 4.75E-06 | 4.62E+04 | 0.220 |
| 0.6 | 11.78 | 0.041 | 0.45 | 4.77E-05 | 1.38E-07 | 1.22E-06 | 2.98E+05 | 0.362 |
| 0.3 | 7.65 | 0.023 | 0.225 | 5.96E-06 | 1.73E-08 | 3.04E-07 | 1.34E+06 | 0.408 |
| 0.15 | 5.33 | 0.017 | 0.1125 | 7.46E-07 | 2.16E-09 | 7.59E-08 | 7.63E+06 | 0.580 |
| 0.075 | 3.68 | 0.037 | 0.0375 | 2.76E-08 | 8.01E-11 | 8.44E-09 | 4.59E+08 | 3.872 |

$\gamma_p$ = 2.89 E+03 kg/m$^3$
$\gamma_a$ = 1.02E+03 kg/m$^3$
Total surface area per unit weight, SSA = 5.742 m$^2$ /kg

## B.3   BINDER CONTENT DETERMINATION

With knowledge of total specific surface area, the optimum binder contents for the three gradations were estimated and provided in Table B-4. The procedure for computation of the asphalt content is as follows:

1.  The weight of asphalt binder per unit weight of aggregates is determined as:

$$P_b = SSA \times T \times \gamma_a \qquad (B-1)$$

where $P_b$ is weight of asphalt per unit weight of aggregate (kg/kg); SSA is the total specific surface area per unit weight of aggregate (m$^2$/kg); T is the asphalt film thickness, which increases with the aggregate size and is assumed in the range of 5.5 to 9 microns; and $\gamma_a$ is the specific weight of asphalt, which is 1.02E+03 kg/m$^3$.

378

2. The percent asphalt content ($f_a$) by weight of total mix is then determined as:

$$f_a(\%) = \frac{P_b}{1+P_b} \times 100 \tag{B-2}$$

**Table B-4.The estimated percent asphalt content of the design, coarser, and the finer gradations.**

| Gradation | SSA m$^2$ /kg | Assumed Film Thickness, $T$ (micron) | Weight of asphalt Per Unit Weight of aggregates, $P_b$ (kg/kg) | Asphalt Content by Total Weight of Mixture, $f_a$ (%) |
|---|---|---|---|---|
| Design | 7.796 | 6.6 | 0.052 | 4.92 |
| Coarser | 2.054 | 9 | 0.019 | 1.85 |
| Finer | 5.742 | 5.5 | 0.032 | 3.12 |

# APPENDIX C - TRANSFORMATION CURVES

## C.1  INTRODUCTION

In order to simulate virtual homogeneous and inhomogeneous specimens, it is necessary to transform uniform random variates to random particle positions within the specimens. Transformation curves are used for this purpose. For example, a uniform variate, 0 to 1, can be transformed to a location (0 to 150 mm) that positions the center of a particle within the vertical boundaries of the specimen. To create virtual specimens that reflect an inhomogeneous condition requires a different transformation curve than would be needed for the homogeneous condition. Also, different forms of inhomogeneity utilize different transformation curves. The purpose of this appendix is to provide details on the development of the transformation curves used herein. Specifically, the sections discuss detailed development of the transformation curves for the homogeneous, vertically inhomogeneous, and radially inhomogeneous specimens.

## C.2  TRANSFORMATION CURVES FOR VERTICAL POSITIONING OF AGGREGATES

### C.2.1  Vertically Homogeneous

In a vertically homogeneous specimen, aggregates have an equal chance of residing in any vertical position throughout the height of the specimen. A first-degree polynomial is utilized to transform a uniform random number between 0 and 1 to a random vertical position through the specimen. The process of developing the relationship that associates a random vertical position to a random number is as follows:

1.  A linear model is selected to represent the transformation curve:

$$h_i = au_i + b \qquad\qquad\qquad\qquad \text{(C-1)}$$

where $h_i$ is the vertical position of the aggregate centroid, $u_i$ is the random number between 0 and 1, and a and b are the coefficients that need to be evaluated.

2. It is necessary to set limits on the specimen height. The top and bottom limits that would ensure that each aggregate lies fully within the specimen are:

$$h_b = {d_i}\!/\!{2} \qquad\qquad\qquad\qquad \text{(C-2)}$$

$$h_t = H_s - {d_i}\!/\!{2} \qquad\qquad\qquad\qquad \text{(C-3)}$$

where $h_b$ is the bottom limit and $h_t$ is the top limit; $H_s$ is the height of the specimen, which is 150 mm; and $d_i$ is the diameter of the aggregates that is being positioned.

3. Solve for a and b in Equation (C-1) by correlating the limits of random numbers (0 and 1) with the top and bottom limits of the specimen:

$$h_i = b = {d_i}\!/\!{2} \qquad\qquad \text{for} \qquad u_i = 0 \qquad\qquad \text{(C-4)}$$

$$h_i = a + b = H_s - {d_i}\!/\!{2} \qquad\qquad \text{for} \qquad u_i = 1 \qquad\qquad \text{(C-5)}$$

4. The values of a and b from Equations (C-4) and (C-5) along with the value of $H_s$ are substituted into Equation (C-1) which produces the transformation curve for the vertically homogeneous specimen:

$$h_i = (150 - d_i)u_i + {d_i}\!/\!{2} \qquad\qquad\qquad\qquad \text{(C-6)}$$

### C.2.2   Two-Layer Vertical Inhomogeneity: Coarse Particles

In two-layer vertical inhomogeneity, coarse aggregates have a greater chance of being positioned in the bottom portion of the specimen. In order to place the coarse aggregates in the specimen, a random number between 0 and 1 is used with each coarse aggregate. A second-degree polynomial is utilized to transform the uniform random number to a vertical position within the specimen so that a large particle has a 75% probability of residing in the bottom portion and a 25% probability of being located in the top portion of the specimen. Based on the estimate of the volume of the coarser mixture, the height of the bottom portion was determined to be 53% of total height of the specimen (Section 3.3.1.3). The process of developing the relationship that relates the vertical position of coarse aggregates to a random number is as follows:

1.  A second-degree polynomial is selected:

    $$h_i = au_i^2 + bu_i + c \tag{C-7}$$

    where $h_i$ is the vertical position of the aggregate centroid; $u_i$ is the random number between 0 and 1; and a, b, and c are the coefficients that need to be evaluated.

2.  Values for $a$, $b$, and $c$ in Equation (C-7) are obtained by associating the limits of random numbers with the top and bottom limits of the specimen (Equations (C-2) and (C-3)) and with the probability of the coarse aggregates being located at the bottom portion of the specimen:

    $$h_i = c = {d_i}/{2} \qquad\qquad \text{for} \qquad u_i = 0 \tag{C-8}$$

    $$h_i = a + b + c = H_s - {d_i}/{2} \qquad\qquad \text{for} \qquad u_i = 1 \tag{C-9}$$

    $$h_i = a(0.75)^2 + b(0.75) + c = 0.53H_s \quad \text{for} \qquad u_i = 0.75 \tag{C-10}$$

3. The values of a, b, and c from Equations (C-8), (C-9), and (C-10) along with the value of $H_s$ are substituted into Equation (C-7) which produces the transformation curve for the placement of the coarse particles in a two-layer vertically inhomogeneous specimen:

$$h_i = (177.6 - 1.33d_i)u_i^2 - (27.6 - 0.33d_i)u_i + \frac{d_i}{2} \qquad \text{(C-11)}$$

## C.2.3 Two-Layer Vertical Inhomogeneity: Fine Particles

In a two-layer vertically inhomogeneous specimen, the fine aggregates that have a diameter smaller than 4.75 mm have a greater chance of being positioned in the upper portion of the specimen than those in the 4.75 to 19 mm range. In order to determine a vertical position of a fine aggregate in the specimen, a random number between 0 and 1 is associated with each fine aggregate. A second-degree polynomial is utilized to transform the random number to a vertical position within the specimen with a 25% probability of the particle to reside in the bottom portion and 75% probability to reside in the top portion of the specimen. The process of developing the relationship that relates the vertical position of the fine aggregate to a random number is as follows:

1. A second-degree polynomial is selected (Equation (C-7)).
2. Values for *a*, *b*, and *c* in Equation (C-7) are obtained by associating the limits of random numbers with the top and bottom limits of the specimen (Equations (C-8) and (C-9)) and with the probability of the fine aggregates in the lower portion of the specimen:

$$h_i = a(0.25)^2 + b(0.25) + c = 0.53H_s \quad \text{for} \quad u_i = 0.25 \qquad \text{(C-12)}$$

383

3. The values of $a$, $b$, and $c$ from Equations (C-8), (C-9), and (C-12), along with the value of $H_s$, are substituted into Equation (C-7) which results in the equation of the transformation curve for the placement of the fine particles in a two-layer vertically inhomogeneous specimen:

$$h_i = (-222.4 + 1.33d_i)u_i^2 + (372.4 - 2.33d_i)u_i + \frac{d_i}{2} \qquad \text{(C-13)}$$

## C.2.4 Three-Layer Vertical Inhomogeneity: Coarse Particles

In three-layer vertical inhomogeneity, the particles in the original gradation are separated into coarse, fine, and medium gradations. The coarse particles have the greatest chance of being positioned in the bottom third portion and the least chance of being in the top third portion of the specimen. The chances of the fine and coarse aggregates to reside in the middle third of the specimen are the same.

To place the coarse aggregates in a three-layer vertically inhomogeneous specimen, a random number between 0 and 1 is used with each coarse aggregate. A second-degree polynomial is utilized to transform the uniform random number to a vertical position within the specimen so that a particle has a 52% probability of residing in the bottom third portion, a 33% probability of being located in the middle third portion, and a 15% probability of being located in the top third portion of the specimen. The height of the bottom portion was determined to be 34%, and the heights of the middle and upper portions were each determined to be 33% of the total height of the specimen. These values were computed based on the estimate of the volume of the coarse, medium, and the fine mixtures (Section 3.3.2.3). The process of developing the

relationship that relates the vertical position of the coarse aggregate in a three-layer

vertically inhomogeneous specimen to a random number is as follows:

1.  A second-degree polynomial is selected (Equation (C-7)).

2.  Values for *a*, *b*, and *c* in Equation (C-7) are obtained by associating the limits of

    random numbers with the top and bottom limits of the specimen (Equations (C-8)

    and (C-9)) and with the probabilities of the coarse aggregates being located in the

    bottom two-thirds and the bottom third of the specimen:

$$h_i = a(0.85)^2 + b(0.85) + c = 0.67H_s \quad \text{for} \quad u_i = 0.85 \tag{C-14}$$

$$h_i = a(0.52)^2 + b(0.52) + c = 0.34H_s \quad \text{for} \quad u_i = 0.52 \tag{C-15}$$

3.  Subtract Equation (C-15) from Equation (C-14) to obtain the relationship between

    the coefficients "a" and "b":

$$a(0.45) + b(0.33) = 0.33H_s \tag{C-16}$$

4.  The values of *a*, *b*, and *c* from (C-8), (C-9), and (C-16) along with the value of $H_s$

    are substituted into Equation (C-7) which produces the transformation curve for

    the placement of the coarse particles in a three-layer vertically inhomogeneous

    specimen:

$$h_i = (2.75d_i)u_i^2 + (150.0 - 3.75d_i)u_i + \frac{d_i}{2} \tag{C-17}$$

### C.2.5  Three-Layer Vertical Inhomogeneity: Fine Particles

In three-layer vertical inhomogeneity, fine aggregates (smaller than 4.75 mm in

diameter) have the smallest chance of being positioned in the bottom third portion and the

highest chance of being in the top third portion of the specimen. To place the fine

aggregates in the specimen a uniform random number between 0 and 1 is used for each

fine aggregate. A second-degree polynomial is utilized to transform the uniform random number to a vertical position within the specimen so that a particle has a 15% probability of residing in the bottom third portion, a 33% probability of being located in the middle third portion, and a 52% probability of being located in the top third portion of the specimen. The height of the lower, middle, and the upper portions are 34%, 33%, and 33% of total height of the specimen, respectively (Section 3.3.2.3). The process of developing the relationship that relates the vertical position of the fine aggregate to a random number is as follows:

1. A second-degree polynomial is selected (Equation (C-7)).

2. Values for $a$, $b$, and $c$ in Equation (C-7) are obtained by associating the limits of random numbers with the top and bottom limits of the specimen (Equations (C-8) and (C-9)) and with the probabilities of the fine aggregates being located at the lower two-third and the lower third of the specimen:

$$h_i = a(0.48)^2 + b(0.48) + c = 0.67H_s \quad \text{for} \quad u_i = 0.48 \qquad \text{(C-18)}$$

$$h_i = a(0.15)^2 + b(0.15) + c = 0.34H_s \quad \text{for} \quad u_i = 0.15 \qquad \text{(C-19)}$$

3. Subtract Equation (C-19) from Equation (C-18) to obtain the relationship between the coefficients "a" and "b":

$$a(0.21) + b(0.33) = 0.33H_s \qquad \text{(C-20)}$$

4. The values of a, b, and c from Equations (C-8), (C-9), and (C-20) along with the value of $H_s$ are substituted into Equation (C-7) which produces the transformation curve for the placement of the fine particles in a three-layer vertically inhomogeneous specimen:

$$h_i = (-2.75d_i)u_i^2 + (150 + 1.75d_i)u_i + {d_i}\big/{2} \qquad \text{(C-21)}$$

## C.3  TRANSFORMATION CURVES FOR RADIAL POSITIONING OF AGGREGATES

### C.3.1  Radial Homogeneity

In a radially homogeneous specimen, all aggregates have an equal chance of being located at any lateral position within the specimen. Assigning a random radial position to a random number requires a linear equation. The process of developing the transformation curve is as follows:

1. A linear equation is selected:

$$r_i = au_i + b \qquad \text{(C-22)}$$

   where $r_i$ is the radial position of the aggregate centroid, $u_i$ is the uniform random number between 0 and 1, and $a$ and $b$ are the coefficients that need to be evaluated.

2. It is necessary to set limit on the outer edge of the specimen. The outer edge limit that would ensure that the aggregates reside fully within the wall of the specimen is:

$$r_e = R_s - {d_i}\big/{2} \qquad \text{(C-23)}$$

   where $r_e$ is the outer limit for positioning the aggregate centroid; $R_s$ is the radius of the specimen, which is 75 mm; and $d_i$ is the diameter of the aggregate that is being positioned.

3. The limits of random numbers are associated with the outer edge limit.

387

$$r_i = b = 0 \qquad\qquad \text{for} \quad u_i = 0 \qquad\qquad \text{(C-24)}$$

$$r_i = a = R_s - {d_i}/{2} \qquad\qquad \text{for} \quad u_i = 1 \qquad\qquad \text{(C-25)}$$

4.  Solve for $a$ and $b$ in Equation (C-22) by substituting them from Equations (C-24) and (C-25), which produces the transformation curve for a radially homogeneous specimen:

$$r_i = (75 - {d_i}/{2})u_i \qquad\qquad \text{(C-26)}$$

## C.3.2  Radial Inhomogeneity: Coarse Particles

In a radially inhomogeneous specimen, the coarse aggregates have a greater chance of being positioned in the ring of the specimen. For positioning the coarse aggregates, a second-degree polynomial is used to transform a uniform random number between 0 and 1 to a radial position such that a particle has a 75% probability of being positioned in the ring and a 25% probability of being located in the core. The thickness of the ring and the radius of the core were determined to be 23.5 mm and 50.5 mm, respectively (Section 3.4.1.3). These values were computed based on the estimates of the volumes of the coarser and the finer mixtures. The process of developing the transformation curve for relating the radial position of a coarse particle to a random number is as follows:

1.  A second-degree polynomial is selected:

$$r_i = au_i^2 + bu_i + c \qquad\qquad \text{(C-27)}$$

where $r_i$ is the radial position of the aggregate centroid; $u_i$ is the random number between 0 and 1; and $a, b$, and $c$ are the coefficients that need to be evaluated.

2. Solve for $a$, $b$, and $c$ in Equation (C-27) by associating the limits of random numbers with the outer and inner limits of the specimen (Equations (C-23) and (C-24)) and with the probability of the aggregates residing in the core of the specimen:

$$r_i = c = 0 \qquad \text{for} \qquad u_i = 0 \qquad\qquad \text{(C-28)}$$

$$r_i = a + b + c = R_s - \frac{d_i}{2} \qquad \text{for} \qquad u_i = 1 \qquad\qquad \text{(C-29)}$$

$$r_i = a(0.25)^2 + b(0.25) + c = 50.5 \qquad \text{for} \qquad u_i = 0.25 \qquad\qquad \text{(C-30)}$$

3. The values of $a$, $b$, and $c$ from (C-28), (C-29), and (C-30) are substituted into Equation (C-27) resulting in the transformation curve for the placement of the coarse particles in a radially inhomogeneous specimen:

$$r_i = (-169.33 - 0.67d_i)u_i^2 + (244.33 + 0.542d_i)u_i \qquad\qquad \text{(C-31)}$$

### C.3.3 Radial Inhomogeneity: Fine Particles

In a radially inhomogeneous specimen, the fine aggregates (smaller than 4.75 mm in diameter) have a greater chance of being in the core of the specimen. A second-degree polynomial is utilized to transform a uniform random number between 0 and 1 to a random radial position in the specimen so that a fine particle has a 75% probability of residing in the core and a 25% probability of being located in the ring of the specimen. The process of developing the transformation curve to relate a fine aggregate radial position to a random number is as follows:

1. A second-degree polynomial is selected (Equation (C-27)).

2. Solve for $a$, $b$, and $c$ in Equation (C-27) by associating the limits of random numbers with the inner and outer limits of the specimen (Equations (C-28) and

(C-29)) and with the probability of the fine aggregates being located in the core of the specimen:

$$h_i = a(0.75)^2 + b(0.75) + c = 50.5 \qquad \text{for} \qquad u_i = 0.75 \qquad \text{(C-32)}$$

3. The values of $a$, $b$, and $c$ from (C-28), (C-29), (C-32) are substituted into Equation (C-27) which produces the transformation curve for the placement of the fine particles in a radially inhomogeneous specimen:

$$r_i = (25.33 - 2d_i)u_i^2 + (49.67 + 1.5d_i)u_i \qquad \text{(C-33)}$$

# APPENDIX D - POSITION OF THE INNER RECTANGLE IN INNER-OUTER AVERAGE DIAMETER METHOD

The inner-outer average diameter method (Tashman et al., 2001) compares the average diameter of the aggregates in the inner and in the outer portions of vertical slice faces of a specimen. The dimensions and the location of the inner rectangle are determined based on two conditions: first, the area of the inner portion is equal to the area of the outer portion; second, the proportion of the dimensions of the inner portion is kept the same as the proportion of the dimensions of the slice face. The determination of the coordinates of the inner and outer rectangles is as follows:

1. The two conditions mentioned above are stated as follow:

$$w_1 h_1 = \frac{1}{2} WH \qquad\qquad \text{(D-1)}$$

$$\frac{w_1}{h_1} = \frac{W}{H} \qquad\qquad \text{(D-2)}$$

   where $w_1$ and $h_1$ are the width and height of the inner rectangle and $W$ and $H$ are the width and height of the slice face.

2. Substituting $w_1$ from Equation (D-1) into Equation (D-2) solves for $h_1$:

$$\frac{WH}{2h_1^2} = \frac{W}{H} \qquad\qquad \text{(D-3)}$$

$$h_1 = \frac{H}{\sqrt{2}} \qquad\qquad \text{(D-4)}$$

3. Substituting $h_1$ from (D-4) into either (D-1) or (D-2) results in $w_1$:

$$w_1 = \frac{W}{\sqrt{2}} \qquad\qquad \text{(D-5)}$$

4. Based on the dimensions of the inner rectangle, the coordinates of the inner rectangle are determined as follows:

$$A : (\frac{W}{2} - \frac{w_1}{2}, \frac{H}{2} - \frac{h_1}{2})$$

$$B : (\frac{W}{2} + \frac{w_1}{2}, \frac{H}{2} - \frac{h_1}{2})$$

$$C : (\frac{W}{2} - \frac{w_1}{2}, \frac{H}{2} + \frac{h_1}{2})$$

$$D : (\frac{W}{2} + \frac{w_1}{2}, \frac{H}{2} + \frac{h_1}{2})$$

5. Substituting $h_1$ and $w_1$ from Equations (D-4) and (D-5), respectively, will result in the coordinates of the inner rectangle in terms of the dimensions of the slice face (W, H):

$$A : (\frac{W}{2} - \frac{W}{2\sqrt{2}}, \frac{H}{2} - \frac{H}{2\sqrt{2}})$$

$$B : (\frac{W}{2} + \frac{W}{2\sqrt{2}}, \frac{H}{2} - \frac{H}{2\sqrt{2}})$$

$$C : (\frac{W}{2} - \frac{W}{2\sqrt{2}}, \frac{H}{2} + \frac{H}{2\sqrt{2}})$$

$$D : (\frac{W}{2} + \frac{W}{2\sqrt{2}}, \frac{H}{2} + \frac{H}{2\sqrt{2}})$$

392
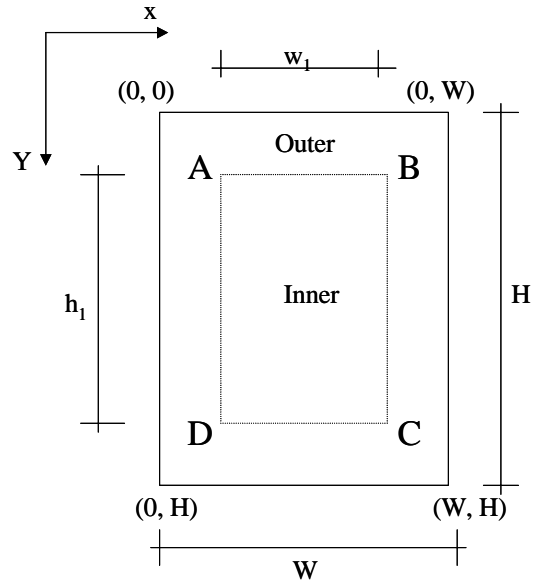
**Figure D-1. Position of the inner rectangle within the vertical slice face**

# APPENDIX E - AIR VOID MEASUREMENTS

## E.1    INTRODUCTION

The air void contents of homogeneous and inhomogeneous specimens were measured to ensure that the overall air void content of the specimens both within and between the homogeneous and inhomogeneous sets was similar. The conventional laboratory method for the measurement of the air void is the saturated-surface dry (SSD) method (AASHTO 1998b), which uses the bulk specific gravity measurements. However, this method is only appropriate for homogeneous specimens. For inhomogeneous specimens where one portion of the specimen is coarser than the other portion, the bulk specific gravity would not be measured correctly. The large surface voids extend through the specimen and connect to the inner voids. Water can then penetrate through the interconnected voids, which causes the air void measurements to be underestimated. Therefore, different methods of measuring air voids were required for the inhomogeneous specimens.

Because of the potential error with the SSD method, two other methods were examined for the air void measurement of inhomogeneous specimens: the vacuum sealing (Corelok) and image analysis methods. In the vacuum-sealing method, a vacuum chamber is used to seal the specimen within a special plastic bag to prevent water from penetrating into the sample. Research by Buchanan (2001) has indicated that the Corelok vacuum-sealing device provides a better measure of internal air void content of coarse graded mixtures than the conventional SSD method.

The image analysis was used to measure the air void content from the x-ray scanned images of the specimens. The advantage of this method is that the air voids are measured using the exact geometric dimensions of the voids at the surface and within the specimen and there is no approximation involved. In addition, image analysis makes possible separate measurements of the air void contents of different portions of the specimens. The air void contents of the coarser and the finer portions of the specimens are additional information on the level of inhomogeneity of the specimens.

## E.2 AIR VOID MEASUREMENT OF SPECIMENS EVALUATED FOR VERTICAL INHOMOGENEITY

The bulk specific gravity of vertically inhomogeneous and corresponding homogeneous specimens was evaluated using SSD, Corelok, and image analyses. The results are provided in Table E-1. It is indicated in the table that the SSD, Corelok, and image analysis methods provided comparable air void measurements of homogeneous specimens (averages of 6.45%, 6.21%, and 6.92%). However, for the inhomogeneous specimens the SSD underestimates the air voids by about 2% (average of 4.84). This results because the surface of inhomogeneous specimens was extremely porous with the pores extensively extended through the specimen. When the specimens are submerged in water during the SSD measurement, the surface pores are filled with water and excluded from the voids. On the other hand, Corelok slightly overestimates the specimen air void contents (average of 7.4 %) because the use of plastic bags as part of the measurement process smoothes out the surface of the specimen, which adds some voids to the existing

**Table E-1- Air void contents (AVC, %) of the homogeneous (H-SPT) and vertically inhomogeneous (I-SPT) specimens using SSD, Corelok, and image analysis methods**

| Specimens | AVC (SSD) | AVC (Corelok) | Image Analysis | Specimens | AVC (SSD) | AVC (Corelok) | Image Analysis |
|---|---|---|---|---|---|---|---|
| H-SPT1 | 6.33 | 6.14 | 6.15 | I-SPT1 | 4.66 | 7.53 | 6.84 |
| H-SPT2 | 6.33 | 6.18 | 6.78 | I-SPT2 | 4.49 | 7.88 | 8.13 |
| H-SPT3 | 6.55 | 6.14 | 7.13 | I-SPT3 | 4.86 | 7.05 | 6.73 |
| H-SPT4 | 6.48 | 5.85 | 7.45 | I-SPT4 | 5.08 | 7.52 | 7.10 |
| H-SPT5 | 6.85 | 6.81 | 7.23 | I-SPT5 | 5.00 | 7.71 | 7.72 |
| H-SPT6 | 6.25 | 6.07 | 6.65 | I-SPT6 | 4.80 | 7.32 | 7.72 |
| H-SPT7 | 6.14 | 5.81 | 6.31 | I-SPT7 | 4.92 | 7.12 | 7.03 |
| H-SPT8 | 6.70 | 6.70 | 7.67 | I-SPT8 | 4.89 | 7.21 | 7.60 |
| AVG | 6.45 | 6.21 | 6.92 | AVG | 4.84 | 7.42 | 7.36 |
| STD | 0.24 | 0.36 | 0.54 | STD | 0.19 | 0.29 | 0.48 |

surface voids. The measurement of the air voids using image analysis was comparable to the Corelok measurements, with the averages of 7.4 % and 7.36% using Corelock and image analysis, respectively. The results of image analysis also indicate that the overall air void values of homogeneous and inhomogeneous specimens were similar (average of 6.92% and 7.36%, respectively), indicating that the intent of having homogeneous and inhomogeneous specimens with similar overall air void contents was satisfied.

In addition to the overall air voids of the specimens, the air voids of the lower and the upper portions were also measured using image analysis (Table E-2). Despite similar overall air voids of homogeneous and inhomogeneous specimens, the difference between the air voids of the lower and the upper portions of inhomogeneous specimens was significantly greater than those of homogeneous specimens with an average difference of 11% compared to the average difference of 1%.

**Table E-2- Overall air void contents and air void contents of the coarser and the finer portions of homogeneous gyratory compacted specimens (H-SPT) and vertically inhomogeneous gyratory compacted specimens (I-SPT) using image analysis of CT images**

| Specimens | Lower | Upper | Overall | Specimens | Lower | Upper | Overall |
|-----------|-------|-------|---------|-----------|-------|-------|---------|
| H-SPT1 | 7.52 | 6.15 | 6.84 | I-SPT1 | 13.31 | 0.36 | 6.84 |
| H-SPT2 | 8.17 | 6.78 | 7.48 | I-SPT2 | 13.73 | 2.54 | 8.13 |
| H-SPT3 | 8.58 | 7.13 | 7.86 | I-SPT3 | 13.06 | 0.41 | 6.73 |
| H-SPT4 | 7.87 | 7.45 | 7.66 | I-SPT4 | 13.09 | 1.11 | 7.10 |
| H-SPT5 | 8.82 | 7.23 | 8.03 | I-SPT5 | 12.10 | 3.34 | 7.72 |
| H-SPT6 | 7.48 | 6.65 | 7.07 | I-SPT6 | 12.89 | 2.55 | 7.72 |
| H-SPT7 | 7.74 | 6.31 | 7.03 | I-SPT7 | 12.66 | 1.40 | 7.03 |
| H-SPT8 | 7.89 | 7.67 | 7.78 | I-SPT8 | 12.83 | 2.37 | 7.60 |
| AVG | 8.01 | 6.92 | 7.47 | AVG | 12.96 | 1.76 | 7.36 |
| STD | 0.48 | 0.54 | 0.44 | STD | 0.48 | 0.48 | 0.48 |

## E.3    AIR VOID MEASUREMENT OF SPECIMENS EVALUATED FOR RADIAL INHOMOGENEITY

The bulk specific gravity of radially inhomogeneous specimens was evaluated using SSD, Corelok, and image analyses. Since the air void values of homogeneous specimens were not different when measured with SSD and Corelok, the air void measurements for this set of specimens were only conducted by SSD and image analysis. The air void values are provided in Table E-3. As indicated in the table, the air void values of the radially inhomogeneous specimens were underestimated by SSD (average of 4.03%) and overestimated by the Corelok (average of 8.65%). The values provided by the image analysis were on average in agreement with the design air void values and

**Table E-3- Air void contents (AVC, %) of the homogeneous linearly kneaded specimen (L-SST), homogeneous gyratory compacted specimen (H-SST), and radially inhomogeneous gyratory compacted specimens (I-SST); "S" represents specimens**

| S | AVC (SSD) | Image Analysis | S | AVC (SSD | Image Analysis | S | AVC (SSD) | AVC (Corelok) | Image Analysis |
|---|---|---|---|---|---|---|---|---|---|
| L-SST1 | 6.99 | 8.57 | H-SST1 | 6.54 | 7.08 | I-SST1 | 4.72 | 8.66 | 5.60 |
| L-SST2 | 6.60 | 8.03 | H-SST2 | 6.75 | 5.91 | I-SST2 | 3.67 | 9.03 | 6.84 |
| L-SST3 | 6.83 | 7.03 | H-SST3 | 7.39 | 7.16 | I-SST3 | 4.87 | 8.14 | 5.68 |
| L-SST4 | 6.22 | 7.08 | H-SST4 | 6.50 | 6.34 | I-SST4 | 3.11 | 8.88 | 5.46 |
| L-SST5 | 6.81 | 6.25 | H-SST5 | 6.85 | 6.91 | I-SST5 | 4.62 | 7.92 | 7.16 |
| L-SST6 | 6.11 | 6.09 | H-SST6 | 6.07 | 6.85 | I-SST6 | 3.42 | 9.47 | 5.74 |
| L-SST7 | 6.99 | 5.63 | H-SST7 | 6.93 | 6.75 | I-SST7 | 4.53 | 7.66 | 6.20 |
| L-SST8 | 6.55 | 8.75 | H-SST8 | 6.27 | 6.93 | I-SST8 | 3.27 | 9.47 | 7.13 |
| AVG | 6.64 | 7.18 | AVG | 6.66 | 6.74 | AVG | 4.03 | 8.65 | 6.23 |
| STD | 0.33 | 1.17 | STD | 0.41 | 0.42 | STD | 0.73 | 0.69 | 0.72 |

were comparable for the homogeneous linearly kneaded, homogeneous gyratory compacted, and inhomogeneous specimens (averages of 7.18, 6.74, and 6.23, respectively).

In addition to the overall air voids, the air voids of the ring and the core portions were measured separately using image analysis. The results are provided in Table E-4. The analyses indicated that there is no difference between the air voids of the ring and the core portions of the homogeneous linear kneading specimens (averages of 7.02 and 7.38, respectively). However, analyses of the homogeneous gyratory compacted specimens and radially inhomogeneous specimens indicated that the air void contents of the ring and core portions are significantly difference. The air void of the ring portion of the

**Table E-4- Overall air void contents and air void contents of the coarser and the finer portions of homogeneous linearly kneaded (L-SST), homogeneous gyratory compacted (H-SST), and radially inhomogeneous gyratory compacted (I-SST) specimens measured using image analysis of CT scanned images; "S" represents specimens**

| S | Ring | Core | Overall | S | Ring | Core | Overall | S | Ring | Core | Overall |
|---|------|------|---------|---|------|------|---------|---|------|------|---------|
| L-SST1 | 8.68 | 8.42 | 8.57 | H-SST1 | 9.37 | 4.35 | 7.08 | I-SST1 | 9.79 | 0.35 | 5.60 |
| L-SST2 | 8.29 | 7.70 | 8.03 | H-SST2 | 7.66 | 3.35 | 5.91 | I-SST2 | 12.14 | 0.22 | 6.84 |
| L-SST3 | 7.52 | 6.41 | 7.03 | H-SST3 | 10.70 | 3.85 | 7.16 | I-SST3 | 10.00 | 0.29 | 5.68 |
| L-SST4 | 6.91 | 7.30 | 7.08 | H-SST4 | 9.31 | 3.65 | 6.34 | I-SST4 | 9.75 | 0.11 | 5.46 |
| L-SST5 | 5.69 | 6.95 | 6.25 | H-SST5 | 9.37 | 3.93 | 6.91 | I-SST5 | 11.01 | 2.34 | 7.16 |
| L-SST6 | 6.11 | 6.06 | 6.09 | H-SST6 | 9.49 | 3.75 | 6.85 | I-SST6 | 10.07 | 0.32 | 5.74 |
| L-SST7 | 5.03 | 6.39 | 5.63 | H-SST7 | 8.82 | 4.02 | 6.75 | I-SST7 | 9.34 | 2.27 | 6.20 |
| L-SST8 | 7.92 | 9.78 | 8.75 | H-SST8 | 9.05 | 4.44 | 6.93 | I-SST8 | 11.40 | 1.80 | 7.13 |
| AVG | 7.02 | 7.38 | 7.18 | AVG | 9.22 | 3.92 | 6.74 | AVG | 10.44 | 0.96 | 6.23 |
| STD | 1.31 | 1.24 | 1.17 | STD | 0.84 | 0.36 | 0.42 | STD | 0.97 | 0.99 | 0.72 |

homogeneous gyratory specimens were on average 2.5 times greater than the air void of the core portion, indicating that the gyratory compactor induces inhomogeneity in the air void distribution of the compacted specimens. The air void contents of the ring portions of radially inhomogeneous specimens was on average ten times greater than the air void contents of the core portions, which was the result of the intended radial inhomogeneity that was created.

# APPENDIX F - ABBREVIATIONS AND NOTATIONS

$A_{hl}$ = Total area of six horizontal slice faces in the lower sampling portion of a specimen evaluated for two-layer vertical inhomogeneity.

$A_{hu}$ = Total area of six horizontal slice faces in the upper sampling portion of a specimen evaluated for two-layer vertical inhomogeneity.

$A_{hT}$ = Total area of 12 horizontal slice faces in a specimen evaluated for two-layer vertical inhomogeneity.

$A_{hv}$ = Area of one horizontal slice face of a specimen evaluated for two-layer vertical inhomogeneity.

$A_{hj}$ = Total area of four horizontal slices in the $j^{th}$ portion of a specimens evaluated for three-layer inhomogeneity.

$A_{lvi}$ = Area of the lower portion of the $i^{th}$ vertical slice face of a specimen evaluated for two-layer vertical inhomogeneity.

$A_{uvi}$ = Area of the upper portion of the $i^{th}$ vertical slice face of a specimen evaluated for two-layer vertical inhomogeneity.

$A_{lv}$ = Total area of lower portions of nine vertical slice faces of a specimen evaluated for two-layer vertical inhomogeneity.

$A_{uv}$ = Total area of upper portions of nine vertical slice faces of a specimen evaluated for two-layer vertical inhomogeneity.

$A_{rh}$ = Total area of the rings on the three horizontal slice faces of a specimen evaluated for radial inhomogeneity.

$A_{ch}$ = Total area of the cores on the three horizontal slice faces of a specimen evaluated for radial inhomogeneity.

$A_{hh}$ = Total area of the rings and cores of the three horizontal slice faces of a specimen evaluated for radial inhomogeneity.

$A_{rvi}$ = Area of the ring on the $i^{th}$ vertical slice face of a specimen evaluated for radial inhomogeneity.

$A_{cvi}$ = Area of the core on the $i^{th}$ vertical slice face of a specimen evaluated for radial inhomogeneity.

$A_{rv}$ = Total area of the rings on the nine vertical slice faces of a specimen evaluated for radial inhomogeneity.

$A_{cv}$ = Total Area of the cores on the nine vertical slice faces of a specimen evaluated for radial inhomogeneity.

$A_{vh}$ = Total area of the rings and cores of nine vertical slice faces of a specimen evaluated for radial inhomogeneity.

$\overline{A}_{l2}$ = Population value of the total coarse aggregate area in the lower portion of specimens evaluated for two-layer vertical inhomogeneity.

$\overline{A}_{u2}$ = Population value of the total coarse aggregate area in the upper portion of specimens evaluated for two-layer vertical inhomogeneity.

$\overline{A}_{l3}$ = Population value of the total coarse aggregate area in the lower portion of a specimen evaluated for three-layer vertical inhomogeneity.

$\overline{A}_{m3}$ = Population value of the total coarse aggregate area in the middle portion of a specimen evaluated for three-layer vertical inhomogeneity.

$\overline{A}_{u3}$ = Population value of total coarse aggregate area in the upper portion of a specimen evaluated for three-layer vertical inhomogeneity.

$\overline{A}_r$ = Population value of total coarse aggregate area in the ring portion of specimens evaluated for radial inhomogeneity.

$\overline{A}_c$ = Population value of the total coarse aggregate area in the core portion of specimens evaluated for radial inhomogeneity.

$a_{hli}$ = Total area of coarse aggregates on the $i^{th}$ horizontal slice face in the lower portion of a specimen evaluated for two-layer vertical inhomogeneity, where i = 1, 2, 3, 4, 5, 6.

$a_{hui}$ = Total area of coarse aggregates on the $i^{th}$ horizontal slice face in the upper portion of a specimen evaluated for two-layer vertical inhomogeneity, where i = 1, 2, 3, 4, 5, 6.

$a_{hl}$ = Total coarse aggregate area on six horizontal slice faces in the lower portion of a specimen evaluated for two-layer vertical inhomogeneity.

$a_{hu}$ = Total coarse aggregate area on six horizontal slice faces in the upper portion of a specimen evaluated for two-layer vertical inhomogeneity.

$a_{hv}$ = Total coarse aggregate area from the 12 horizontal slice faces of a specimen evaluated for two-layer vertical inhomogeneity.

$a_{hji}$ = The total area of coarse aggregates in the $i^{th}$ horizontal slice face of the $j^{th}$ portion of a specimen evaluated for three-layer vertical inhomogeneity, where i= 1, 2, 3, 4 and j = 1, 2, 3.

$a_{lvi}$ = Total area of the coarse aggregates on the lower portion of the $i^{th}$ vertical slice face of a specimen evaluated for two-layer vertical inhomogeneity.

$a_{uvi}$ = Total area of the coarse aggregates on the upper portion of the $i^{th}$ vertical slice face of a specimen evaluated for two-layer vertical inhomogeneity.

$a_{lv}$ = Total coarse aggregate area in the lower portions of the nine vertical slice faces of a specimen evaluated for two-layer vertical inhomogeneity.

$a_{uv}$ = Total coarse aggregate area in the upper portions of the nine vertical slice faces of a specimen evaluated for two-layer vertical inhomogeneity.

$a_{vv}$ = Total coarse aggregate area from the lower and upper portions of nine vertical slices of a specimen evaluated for two-layer vertical inhomogeneity.

$a_{pli}$ = Aggregate area proportion in lower portion of the $i^{th}$ vertical slice face of a specimen evaluated for two-layer vertical inhomogeneity.

$a_{pui}$ = Aggregate area proportion in upper portion of the $i^{th}$ vertical slice face of a specimen evaluated for two-layer vertical inhomogeneity.

$a_{rhi}$ = Total area of coarse aggregates on the ring portion of the $i^{th}$ horizontal slice face of a specimen evaluated for radial inhomogeneity, where i = 1, 2, 3.

$a_{chi}$ = Total area of coarse aggregates on the core portion of the $i^{th}$ horizontal slice face of a specimen evaluated for radial inhomogeneity, where i = 1, 2, 3.

$a_{hhi}$ = Total area of coarse aggregates on the ring and core portions of the $i^{th}$ horizontal slice face of a specimen evaluated for radial inhomogeneity, where i = 1, 2, 3.

$a_{hh}$ = Total coarse aggregate area from the ring and core portions of three horizontal slice faces of a specimen evaluated for radial inhomogeneity.

$a_{r1i}$ = Total area of coarse aggregates on the first ring strip of the $i^{th}$ vertical slice face of a specimen evaluated for radial inhomogeneity, where i = 1, 2, …, 9.

$a_{r2i}$ = Total area of coarse aggregates on the second ring strip of the $i^{th}$ vertical slice face of a specimen evaluated for radial inhomogeneity, where i = 1, 2, …, 9.

$a_{rvi}$ = Total area of coarse aggregates on the two ring portions of the $i^{th}$ vertical slice face of a specimen evaluated for radial inhomogeneity, where i = 1, 2, …, 9.

$a_{cvi}$ = Total area of coarse aggregates on the core portion of the $i^{th}$ vertical slice face of a specimen evaluated for radial inhomogeneity, where i = 1, 2, …, 9.

404

$a_{vhi}$ = Total area of coarse aggregates on ring and core portions of the $i^{th}$ vertical slice of a specimen evaluated for radial inhomogeneity, where i = 1, 2, …, 9.

$a_{vh}$ = Total coarse aggregate area from the ring and core portions of nine vertical slice faces of a specimen evaluated for radial inhomogeneity.

$a_{pri}$ = Total coarse aggregate area proportion from the ring portion of the $i^{th}$ vertical slice face of a specimen evaluated for radial inhomogeneity.

$a_{pci}$ = Total coarse aggregate area proportion from the core portion of the $i^{th}$ vertical slice face of a specimen evaluated for radial inhomogeneity.

$\overline{a_l}$ = Mean of total coarse aggregate areas from the six horizontal slices in the lower portion of a specimen evaluated for two-layer vertical inhomogeneity.

$\overline{a_u}$ = Mean of total coarse aggregate areas from the six horizontal slices in the upper portion of a specimen evaluated for two-layer vertical inhomogeneity.

$\overline{a_{hj}}$ = Mean of total coarse aggregate area from the four horizontal slice faces in the $j^{th}$ sampling portion of a specimen evaluated for three-layer vertical inhomogeneity, where j = 1, 2, 3.

$\overline{a_h}$ = Grand mean of total aggregate areas from the twelve horizontal slices in the three sampling portions of a specimen evaluated for three-layer vertical inhomogeneity.

$\overline{a_{vv}}$ = Mean coarse aggregate area from the lower and upper portions of nine vertical slice faces of a specimen evaluated for two-layer vertical inhomogeneity.

$\overline{a}_{pl}$ = Mean of total aggregate area proportion in the lower portions of the nine vertical slices of a specimen evaluated for two-layer vertical inhomogeneity.

$\overline{a}_{pu}$ = Mean of total aggregate area proportion in the upper portions of the nine vertical slices of a specimen evaluated for two-layer vertical inhomogeneity.

$\overline{a}_{hh}$ = Mean of coarse aggregate area from the ring and core portions of the three horizontal slice faces of a specimen evaluated for radial inhomogeneity.

$\overline{a}_r$ = Mean of total coarse aggregate areas from the ring portions of three horizontal slice faces of a specimen evaluated for radial inhomogeneity.

$\overline{a}_c$ = Mean of total coarse aggregate areas from the core portions of the three horizontal slice faces of a specimen evaluated for radial inhomogeneity.

$\overline{a}_{vh}$ = Mean coarse aggregate area from ring and core portions of the nine vertical slice faces of a specimen evaluated for radial inhomogeneity.

$\overline{a}_{pr}$ = Mean of total coarse aggregate area proportion from the ring portions of nine vertical slice faces of a specimen evaluated for radial inhomogeneity.

$\overline{a}_{pc}$ = Mean of total coarse aggregate area proportion from the core portions of nine vertical slice faces of a specimen evaluated for radial inhomogeneity.

$D_v$ = Diameter of a specimen evaluated for two-layer vertical inhomogeneity, which is 100 mm.

$D_c$ = Diameter of the core of a horizontal slice face of a specimen evaluated for radial inhomogeneity, which is 101 mm.

$D_h$ = Diameter of a specimen evaluated for radial inhomogeneity, which is 150 mm.

$\overline{D}_{l2}$ = Population value of the mean coarse aggregate nearest neighbor distance in the lower portion of specimens evaluated for two-layer vertical inhomogeneity.

$\overline{D}_{u2}$ = Population value of the coarse aggregate mean nearest neighbor distance in the upper portion of specimens evaluated for two-layer vertical inhomogeneity.

$\overline{D}_{l3}$ = Population value of the coarse aggregate mean nearest neighbor distance in the lower portion of specimens evaluated for three-layer vertical inhomogeneity.

$\overline{D}_{m3}$ = Population value of the coarse aggregate mean nearest neighbor distance in the middle portion of specimens evaluated for three-layer vertical inhomogeneity.

$\overline{D}_{u3}$ = Population value of the coarse aggregate nearest mean neighbor distance in the upper portion of specimens evaluated for three-layer vertical inhomogeneity.

$d_i$ = Distance between the $i^{th}$ vertical slice face and the middle of a specimen measured along a radii that is perpendicular to the slice face.

$\overline{d}_{hli}$ = Mean nearest neighbor distance of the coarse aggregates on the $i^{th}$ horizontal slice face in the lower portion of a specimen evaluated for two-layer vertical inhomogeneity, where i = 1, 2, 3, 4, 5, 6.

$\overline{d}_{hui}$ = Mean nearest neighbor distance of the coarse aggregates on the $i^{th}$ horizontal slice face in the upper portion of a specimen evaluated for two-layer vertical inhomogeneity, where i = 1, 2, 3, 4, 5, 6.

$\overline{d}_{l}$ = Average of the mean nearest neighbor distances in six horizontal slices in the lower portion of a specimen evaluated for two-layer vertical inhomogeneity.

$\overline{d}_{u}$ = Average of the mean nearest neighbor distances in six horizontal slices in the upper portion of a specimen evaluated for two-layer vertical inhomogeneity.

$\overline{d}_{hji}$ = Mean nearest neighbor distance of coarse aggregates in the $i^{th}$ horizontal slice face of the $j^{th}$ portion of a specimen evaluated for three-layer vertical inhomogeneity, where i= 1, 2, 3, 4 and j = 1, 2, 3.

$\overline{d}_{hj}$ = Average of the mean nearest neighbor distances from the four horizontal slice faces in the $j^{th}$ sampling portion of a specimen evaluated for three-layer vertical inhomogeneity, where j = 1, 2, 3.

$\overline{d}_{h}$ = Grand mean of the mean nearest neighbor distances from the twelve horizontal slice faces in the three sampling portions of a specimen evaluated for three-layer vertical inhomogeneity.

$\overline{d}_{lvi}$ = The mean nearest neighbor distance of the coarse aggregates on the lower portion of the $i^{th}$ vertical slice face of a specimen evaluated for two-layer vertical inhomogeneity.

$\overline{d}_{uvi}$ = The mean nearest neighbor distance of the coarse aggregates on the upper portion of the $i^{th}$ vertical slice face of a specimen evaluated for two-layer vertical inhomogeneity.

$\overline{d}_{dli}$ = Mean nearest neighbor distance density in the lower portion of the $i^{th}$ vertical slice of a specimen evaluated for two-layer vertical inhomogeneity.

$\overline{d}_{dui}$ = Mean nearest neighbor distance density in the upper portion of the $i^{th}$ vertical slice of a specimen evaluated for two-layer vertical inhomogeneity.

$\overline{d}_{dl}$ = Average of the mean nearest neighbor distance densities in the lower portions of the nine vertical slice faces of a specimen evaluated for two-layer vertical inhomogeneity.

$\overline{d}_{du}$ = Average of the mean nearest neighbor distance densities in the upper portions of the nine vertical slice faces of a specimen evaluated for two-layer vertical inhomogeneity.

$F_a$ = F statistic on total coarse aggregate area for evaluation of three-layer vertical inhomogeneity using horizontal slice faces.

$F_d$ = F statistic on the coarse aggregate mean nearest neighbor distance for evaluation of three-layer vertical inhomogeneity.

$F_f$ = F statistic on coarse aggregate frequency for evaluation of three-layer vertical homogeneity.

$F_{a\alpha}$ = Critical $F_a$ value for separating homogeneous and three-layered vertically inhomogeneous specimens for a selected level of significance.

$F_{d\alpha}$ = Critical $F_d$ value for separating homogeneous and three-layered vertically inhomogeneous specimens for a selected level of significance.

$F_{f\alpha}$ = Critical $F_f$ value for separating homogeneous and three-layered vertically inhomogeneous specimens for a selected level of significance.

$\overline{F}_b$ = Population value of the coarse aggregate frequency in the bottom portion of specimens evaluated for two-layer vertical inhomogeneity.

$\overline{F}_t$ = Population value of the coarse aggregate frequency in the top portion of specimens evaluated for two-layer vertical inhomogeneity.

$\overline{F}_l$ = Population value of the coarse aggregate frequency on the horizontal slice faces in the lower portion of a three-layer vertical inhomogeneity, where j = 1, 2, 3.

$\overline{F}_m$ = Population value of the coarse aggregate frequency on the horizontal slice faces in the middle portion of a three-layer vertical inhomogeneity, where j = 1, 2, 3.

$\overline{F}_u$ = Population value of the coarse aggregate frequency on the horizontal slice faces in the upper portion of a three-layer vertical inhomogeneity, where j = 1, 2, 3.

$\overline{F}_r$ = Population value of the coarse aggregate frequency in the ring portion of homogeneous specimens evaluated for radial inhomogeneity.

$\overline{F}_c$ = Population value of the coarse aggregate frequency in the core portion of homogeneous specimens evaluated for radial inhomogeneity.

$f_{hli}$ = Frequency of coarse aggregates on the $i^{th}$ horizontal slice face in the lower portion of a specimen evaluated for two-layer vertical inhomogeneity, where i = 1, 2, 3, 4, 5, 6.

$f_{hui}$ = Frequency of coarse aggregates on the $i^{th}$ horizontal slice face in the upper portion of a specimen evaluated for two-layer vertical inhomogeneity, where i = 1, 2, 3, 4, 5, 6.

$f_{hl}$ = Total coarse aggregate frequency on the six horizontal slice faces in the lower portion of a specimen evaluated for two-layer vertical inhomogeneity.

$f_{hu}$ = Total coarse aggregate frequency on the six horizontal slice faces in the upper portion of a specimen evaluated for two-layer vertical inhomogeneity.

$f_{hv}$ = Total frequency on the 12 horizontal slice faces in the lower and upper portions of a specimen evaluated for two-layer vertical inhomogeneity.

$f_{hji}$ = Frequency of coarse aggregates in the $i^{th}$ horizontal slice face of $j^{th}$ portion of a specimen evaluated for three-layer vertical inhomogeneity, where i=1, 2, 3, 4 and j = 1, 2, 3.

$f_{hj}$ = Summation of the coarse aggregate frequencies on four horizontal slices of the $j^{th}$ sampling portion of a specimen evaluated for three-layer vertical inhomogeneity, where j = 1, 2, 3.

$f_h$ = Total coarse aggregate frequency from the 12 horizontal slices in the three portions of a specimen evaluated for three-layer vertical inhomogeneity.

$f_{lvi}$ = Frequency of the coarse aggregates on the lower portion of the $i^{th}$ vertical slice of a specimen for two-layer vertical inhomogeneity.

$f_{uvi}$ = Frequency of the coarse aggregates on the upper portion of the $i^{th}$ vertical slice of a specimen for two-layer vertical inhomogeneity.

$f_{lv}$ = Total coarse aggregate frequency on the lower portions of the nine vertical slice faces in a specimen evaluated for two-layer vertical inhomogeneity.

$f_{uv}$ = Total coarse aggregate frequency on the upper portions of nine vertical slice faces of a specimen evaluated for two-layer vertical inhomogeneity.

$f_{vv}$ = Total frequency from lower and upper portions of nine vertical slice faces of a specimen evaluated for two-layer vertical inhomogeneity.

$f_{dli}$ = Aggregate frequency density in the lower portion of the $i^{th}$ vertical slice face of a specimen evaluated for two-layer vertical inhomogeneity.

$f_{dui}$= Aggregate frequency density in the upper portion of the $i^{th}$ vertical slice face of a specimen evaluated for two-layer vertical inhomogeneity.

$f_{rhi}$ = Frequency of coarse aggregates on the ring portion of the $i^{th}$ horizontal slice face of a specimen evaluated for radial inhomogeneity, where i = 1, 2, 3.

$f_{chi}$ = Frequency of coarse aggregates on the core portion of the $i^{th}$ horizontal slice face of a specimen evaluated for radial inhomogeneity, where i = 1, 2, 3.

$f_{hhi}$ = Frequency of coarse aggregates on the ring and core portions of the $i^{th}$ horizontal slice of a specimen for radial inhomogeneity, where i = 1, 2, 3.

$f_{rh}$ = Total coarse aggregate frequency on the ring portions of the three horizontal slice faces of a specimen evaluated for radial inhomogeneity.

$f_{ch}$ = Total coarse aggregate frequency on the core portions of the three horizontal slice faces of a specimen evaluated for radial inhomogeneity.

$f_{hh}$ = Total frequency on the ring and core portions of the three horizontal slice faces of a specimen evaluated for radial inhomogeneity.

$f_{r1i}$ = Frequency of the coarse aggregates on the first ring strip of the $i^{th}$ vertical slice face of a specimen evaluated for radial inhomogeneity, where i = 1, 2, …, 9.

$f_{r2i}$ = Frequency of the coarse aggregates on the second ring strip of the $i^{th}$ vertical slice face of a specimen evaluated for radial inhomogeneity, where i = 1, 2, …, 9.

$f_{rvi}$ = Frequency of the coarse aggregates on the two ring strips of the $i^{th}$ vertical slice face of a specimen evaluated for radial inhomogeneity, where i = 1, 2, …, 9.

$f_{cvi}$ = Frequency of coarse aggregates on the core portion of the $i^{th}$ vertical slice face of a specimen evaluated for radial inhomogeneity, where i = 1, 2, …, 9.

$f_{dri}$ = Frequency density of the coarse aggregates on the ring portion of the $i^{th}$ vertical slice face of a specimen evaluated for radial inhomogeneity, where i = 1, 2, …, 9.

$f_{dci}$ = Frequency density of the coarse aggregates on the core portion of the $i^{th}$ vertical slice face of a specimen evaluated for radial inhomogeneity, where i = 1, 2, …, 9.

413

$f_{vhi}$ = Frequency of coarse aggregates on the ring and core portions of the $i^{th}$ vertical slice of a specimen evaluated for radial inhomogeneity, where i = 1, 2, …, 9.

$f_{rv}$ = Total coarse aggregate frequency on the ring portions of nine vertical slice faces of a specimen evaluated for radial inhomogeneity.

$f_{cv}$ = Total coarse aggregate frequency on the core portions of nine vertical slice faces of a specimen evaluated for radial inhomogeneity.

$f_{vh}$ = Total coarse aggregate frequency on the ring and core portions of the nine vertical slices of a specimen evaluated for radial inhomogeneity.

$\overline{f}_l$ = Mean coarse aggregate frequency of the six horizontal slice faces in the lower portion of a specimen evaluated for two-layer vertical inhomogeneity.

$\overline{f}_u$ = Mean coarse aggregate frequency of the six horizontal slice faces in the upper portion of a specimen evaluated for two-layer vertical inhomogeneity.

$\overline{f}_{hj}$ = Mean aggregate frequency of the four horizontal slices in the $j^{th}$ portion of a specimens for three-layer vertical inhomogeneity, where j = 1, 2, 3.

$\overline{f}_h$ = Grand mean of aggregate frequency of the twelve horizontal slices in the three sampling portions of a specimen for three-layer vertical inhomogeneity.

$\overline{f}_{dl}$ = Mean of the coarse aggregate frequency densities in the lower portions of nine vertical slice faces of a specimen for two-layer vertical inhomogeneity.

414

$\overline{f}_{du}$ = Mean of the coarse aggregate frequency densities in the upper portions of nine vertical slice faces of a specimen for two-layer vertical inhomogeneity.

$\overline{f}_{r}$ = Mean coarse aggregate frequency on the ring portions of three horizontal slice faces of a specimen evaluated for radial inhomogeneity.

$\overline{f}_{c}$ = Mean coarse aggregate frequency on the core portions of three horizontal slice faces of a specimen evaluated for radial inhomogeneity.

$\overline{f}_{dr}$ = Mean coarse aggregate frequency density on the ring portions of nine vertical slice faces of a specimen evaluated for radial inhomogeneity.

$\overline{f}_{dc}$ = Mean coarse aggregate frequency density on the core portions of nine vertical slice faces of a specimen evaluated for radial inhomogeneity.

$h_v$ = Height of the lower or upper portion of a vertical slice face of a specimen evaluated for two-layer vertical inhomogeneity, which is 60 mm.

$h_h$ = Height of vertical slices of a specimen evaluated for radial inhomogeneity, which is 50 mm.

H-SPT = Homogeneous gyratory compacted specimens evaluated for vertical homogeneity and subjected to simple performance tests (SPT).

I-SPT = Inhomogeneous gyratory compacted specimens evaluated for vertical homogeneity and subjected to simple performance tests (SPT).

L-SST == Homogeneous linear kneading compacted specimens evaluated for radial homogeneity and subjected to Superpave shear tests (SST).

H-SST = Homogeneous gyratory compacted specimens evaluated for radial homogeneity and subjected to Superpave shear tests (SST).

I-SST = Inhomogeneous gyratory compacted specimens evaluated for radial homogeneity and subjected to Superpave shear tests (SST).

$MS_{ba}$ = Between mean square as a parameter of total area F statistic.

$MS_{wa}$ = Within mean square as a parameter of the total area F statistic.

$MS_{bd}$ = Between mean square as a parameter of the nearest neighbor F statistic.

$MS_{wd}$ = Within mean square as a parameter of the nearest neighbor F statistic.

$MS_{bf}$ = Between mean square as a parameter of the frequency F statistic.

$MS_{wf}$ = Within mean square as a parameter of the frequency F statistic.

$n_{hl}$ = Number of horizontal slice faces in the lower portion of a specimen evaluated for two-layer vertical inhomogeneity, which is six.

$n_{hu}$ = Number of horizontal slice faces in the upper portion of a specimen evaluated for two-layer vertical inhomogeneity, which is six.

$n_{lv}$ = Number of lower sampling portions on vertical slice faces of a specimen evaluated for two-layer vertical inhomogeneity, which is nine.

$n_{uv}$ = Number of upper sampling portions on vertical slice faces of a specimen evaluated for two-layer vertical inhomogeneity, which is nine.

$n_p$ = Number of sampling portions in a specimen evaluated for three-layer vertical inhomogeneity, which is three.

$n_s$ = Number of horizontal slices in each of the three portions of a specimen evaluated for three-layer vertical inhomogeneity, which is four.

$n_{vv}$ = Number of vertical slices made in a specimen evaluated for vertical inhomogeneity, which is nine.

$n_{rh}$ = Number of ring portions on horizontal slice faces of a specimen evaluated for radial inhomogeneity, which is three.

$n_{ch}$ = Number of core portions on horizontal slice faces of a specimen evaluated for radial inhomogeneity, which is three.

$n_{hh}$ = Number of horizontal slice faces of a specimen evaluated for radial inhomogeneity, which is three.

$n_{rv}$ = Number of ring portions on vertical slice faces of a specimen evaluated for radial inhomogeneity, which is nine.

$n_{cv}$ = Number of core portions on vertical slice faces of a specimen evaluated for radial inhomogeneity, which is nine.

$\overline{P}_l$ = Population value of the coarse aggregate frequency proportions in the lower portion of a specimen evaluated for two-layer vertical inhomogeneity.

$\overline{P}_u$ = Population value of the coarse aggregate frequency proportions in the upper portion of a specimen evaluated for two-layer vertical inhomogeneity.

$\overline{P}_r$ = Population value of the coarse aggregate frequency proportions in the ring portion of a specimen evaluated for radial inhomogeneity.

$\overline{P}_c$ = Population value of the coarse aggregate frequency proportions in the core portion of a specimen evaluated for radial inhomogeneity.

$\hat{p}_{lv}$ = Frequency proportion of the coarse aggregates in the lower portions of the nine vertical slices of a specimen for two-layer vertical inhomogeneity.

$\hat{p}_{uv}$ = Frequency proportion of the coarse aggregates in the upper portions of the nine vertical slices of a specimen for two-layer vertical inhomogeneity.

$\hat{p}_{vv}$ = Frequency proportion of the coarse aggregates in the lower and upper portions of the vertical slice faces in a specimen evaluated for two-layer vertical inhomogeneity.

$\hat{p}_{rh}$ = Coarse aggregate frequency proportion from the ring portion of horizontal slice faces of a specimen evaluated for radial inhomogeneity.

418

$\hat{p}_{ch}$ = Coarse aggregate frequency proportion from the core portion of horizontal slice faces of a specimen evaluated for radial inhomogeneity.

$\hat{p}_{hh}$ = Proportion of coarse aggregate frequency from the ring and core portions of horizontal slice faces of a specimen evaluated for radial inhomogeneity.

$\hat{p}_{rv}$ = Coarse aggregate frequency proportion from the ring portions of nine vertical slice faces of a specimen evaluated for radial inhomogeneity.

$\hat{p}_{cv}$ = Coarse aggregate frequency proportion from the core portions of nine vertical slice faces of a specimen evaluated for radial inhomogeneity.

$\hat{p}_{vh}$ = Coarse aggregate frequency proportion from the ring and core portions of nine vertical slice faces of a specimen evaluated for radial inhomogeneity.

$R_v$ = Radius of the specimen evaluated for two-layer and three-layer vertical inhomogeneity, which is 50 mm.

$r_{hl}$ = Ratio of the area of the horizontal slice faces in the lower portion to the area of the slice faces in entire specimen evaluated for two-layer vertical inhomogeneity, which is 0.5.

$r_{hu}$ = Ratio of the area of the horizontal slice faces in the upper portion to the area of the slice faces in entire specimen evaluated for two-layer vertical inhomogeneity, which is 0.5.

$r_{hj}$ = Ratio of the area of four horizontal slices in the $j^{th}$ portion of a specimens to the total area of the slices in the three portions of a specimen evaluated for three-layer inhomogeneity, which is one-third.

$r_{lv}$ = Ratio of the area of the lower portions of the nine vertical slice faces to the area of both lower and upper portions of a specimen evaluated for two-layer vertical inhomogeneity, which is 0.5.

$r_{uv}$ = Ratio of the area of the upper portions of the nine vertical slice faces to the area of both lower and upper portions of a specimen evaluated for two-layer vertical inhomogeneity, which is 0.5.

$r_{rh}$ = Ratio of the area of the rings to the area of the rings and cores on horizontal slices of a specimen evaluated for radial inhomogeneity, which is 0.5.

$r_{ch}$ = Ratio of the area of the cores to the area of the ring and cores on horizontal slices of a specimen evaluated for radial inhomogeneity, which is 0.5.

$r_{rv}$ = Ratio of the area of the rings to the area of the rings and cores on nine vertical slices of a specimen evaluated for radial inhomogeneity.

$r_{cv}$ = Ratio of the area of the cores to the area of the rings and cores on nine vertical slices of a specimen evaluated for radial inhomogeneity.

$s_{al}$ = Standard deviation of the total coarse aggregate areas of the six horizontal slice faces in the lower portion of a specimen evaluated for two-layer vertical inhomogeneity.

$s_{au}$ = Standard deviation of total coarse aggregate areas of the six horizontal slice faces in the upper portion of a specimen evaluated for two-layer vertical inhomogeneity.

$s_{dl}$ = Standard deviation of the mean nearest neighbor distances in six horizontal slices in the lower portion of a specimen evaluated for two-layer vertical inhomogeneity.

$s_{du}$ = Standard deviation of the mean nearest neighbor distances in six horizontal slices in the upper portion of the specimen evaluated for two-layer vertical inhomogeneity.

$s_{fl}$ = Standard deviation of the coarse aggregate frequencies on the six horizontal slice faces in the lower portion of a specimen evaluated for two-layer vertical inhomogeneity.

$s_{fu}$ = Standard deviation of the coarse aggregate frequencies on the six horizontal slice faces in the upper portion of a specimen evaluated for two-layer vertical inhomogeneity.

$s_{av}$ = Square root of the pooled variance of the total coarse aggregate areas from the horizontal slice faces in the lower and upper portions of a specimen evaluated for two-layer vertical inhomogeneity.

$s_{dv}$ = Square root of the pooled variance of the coarse aggregate mean nearest neighbor distances from the horizontal slice faces in the lower and upper portions of a specimen evaluated for two-layer vertical inhomogeneity.

$s_{fv}$= Square root of the pooled variance of total coarse aggregate frequencies from the horizontal slice faces in the lower and upper portions of a specimen evaluated for two-layer vertical inhomogeneity.

$s_{apl}$ = Standard deviation of the total coarse aggregate area proportions from the lower portions of the nine vertical slice faces of a specimen evaluated for two-layer vertical inhomogeneity.

$s_{apu}$ = Standard deviation of the total coarse aggregate area proportions from the upper portions of the nine vertical slice faces of a specimen evaluated for two-layer vertical inhomogeneity.

$s_{ddl}$= Standard deviation of the mean nearest neighbor distance densities from the lower portions of the nine vertical slice faces of a specimen evaluated for two-layer vertical inhomogeneity.

$s_{ddu}$ = Standard deviation of the mean nearest neighbor distance densities from the upper portions of the nine vertical slice faces of a specimen evaluated for two-layer vertical inhomogeneity.

$s_{fdl}$ = Standard deviation of the coarse aggregate frequency densities from the lower portions of the nine vertical slice faces of a specimen evaluated for two-layer vertical inhomogeneity.

$s_{fdu}$ = Standard deviation of the coarse aggregate frequency densities from the upper portions of the nine vertical slice faces of a specimen evaluated for two-layer vertical inhomogeneity.

$s_{apv}$ = Square root of the pooled variance of total coarse aggregate area proportions in the lower and upper portions of the vertical slice faces of a specimen evaluated for two-layer vertical inhomogeneity.

$s_{ddv}$ = Square root of the pooled variance of the mean nearest neighbor distance densities in the lower and upper portions of the vertical slice faces of a specimen evaluated for two-layer vertical inhomogeneity.

$s_{fdv}$ = Square root of the pooled variance of the coarse aggregate frequency densities from the lower and upper portions of vertical slice faces of a specimen evaluated for two-layer vertical inhomogeneity.

$s_{pvv}$ = Square root of the pooled variance of the coarse aggregate frequency proportions in the lower and upper portions of the vertical slice faces of a specimen evaluated for two-layer vertical inhomogeneity.

$s_{ar}$ = Standard deviation of total coarse aggregate areas on the ring portions of the three horizontal slices of a specimen evaluated for radial inhomogeneity.

$s_{ac}$ = Standard deviation of total coarse aggregate areas on the core portions of the three horizontal slices of a specimen evaluated for radial inhomogeneity.

$s_{fr}$ = Standard deviation of the coarse aggregate frequencies in the ring portions of the three horizontal slice faces of a specimen evaluated for radial inhomogeneity.

$s_{fc}$ = Standard deviation of the coarse aggregate frequencies in the core portions of the three horizontal slice faces of a specimen evaluated for radial inhomogeneity.

$s_{ahh}$ = Square root of the pooled variance of the total coarse aggregate areas from the horizontal slice faces of a specimen evaluated for radial inhomogeneity.

$s_{fhh}$ = Square root of the pooled variance of total coarse aggregate frequencies from the horizontal slice faces of a specimen evaluated for radial inhomogeneity.

$s_{phh}$ = Square root of the pooled variance of the coarse aggregate frequency proportions from the horizontal slice faces of a specimen evaluated for radial inhomogeneity.

$s_{apr}$ = Standard deviation of the total coarse aggregate area proportion on the ring portions of the nine vertical slices of a specimen evaluated for radial inhomogeneity.

$s_{apc}$ = Standard deviation of the total coarse aggregate area proportion on the core portions of the nine vertical slices of a specimen evaluated for radial inhomogeneity.

$s_{fdr}$ = Standard deviation of the coarse aggregate frequency densities in the ring portions of the nine vertical slice faces of a specimen evaluated for radial inhomogeneity.

$s_{fdc}$ = Standard deviation of the coarse aggregate frequency densities in the core portions of the nine vertical slice faces of a specimen evaluated for radial inhomogeneity.

$s_{aph}$ = Square root of the pooled variance of the total coarse aggregate area proportion from the ring and core portions of the nine vertical slice faces of a specimen evaluated for radial inhomogeneity.

$s_{fdh}$ = Square root of the pooled variance of coarse aggregate frequency density from the ring and core portions of the nine vertical slice faces of a specimen evaluated for radial inhomogeneity.

$s_{pvh}$ = Square root of the pooled variance of the coarse aggregate frequency proportions from the ring and core portions of the nine vertical slice faces of a specimen evaluated for radial inhomogeneity.

$t_{av}$ = t statistic on the total coarse aggregate area from the horizontal slice faces, as an index of homogeneity of a specimen evaluated for two-layer vertical inhomogeneity.

$t_{dv}$ = t statistic on the mean nearest neighbor distance from the horizontal slice faces, as the index of homogeneity of a specimen evaluated for two-layer vertical inhomogeneity.

$t_{fv}$ = t statistic on the coarse aggregate frequency from the horizontal slice faces, as the index of homogeneity of a specimen evaluated for two-layer vertical inhomogeneity.

$t_{av\alpha}$ = Critical $t_{av}$ value, which separates homogeneous from two-layer vertically inhomogeneous specimens.

$t_{dv\alpha}$ = Critical $t_{dv}$ value, which separates homogeneous from two-layer vertically inhomogeneous specimens.

$t_{fv\alpha}$ = Critical $t_{fv}$ value, which separates homogeneous from two-layer vertically inhomogeneous specimens.

$t_{apv}$ = t statistic on the total area proportion measured from vertical slice faces of a specimen evaluated for two-layer vertical inhomogeneity.

$t_{ddv}$ = t statistic on the nearest neighbor distance density from the vertical slice faces of a specimen evaluated for two-layer vertical inhomogeneity.

$t_{fdv}$ = t statistic on the coarse aggregate frequency density from the vertical slice faces of a two-layer vertical inhomogeneity.

$t_{ap\alpha}$ = Critical $t_{ap}$ value, which separates homogeneous specimens from the two-layer vertically inhomogeneous specimens.

$t_{fdv\alpha}$ = Critical $t_{fd}$ value, which separates homogeneous specimens from the two-layer vertically inhomogeneous specimens.

$t_{ddv\alpha}$ = Critical $t_{dd}$ value, which separates homogeneous specimens from the two-layer vertically inhomogeneous specimens.

$t_{ah}$ = t statistic on the total coarse aggregate area from the horizontal slice faces, as an index of homogeneity of a specimen evaluated for radial inhomogeneity.

$t_{fh}$ = t statistic on the coarse aggregate frequency from the horizontal slice faces, as the index of homogeneity of a specimen evaluated for radial inhomogeneity.

$t_{ah\alpha}$ = Critical $t_{ah}$ value, which separates homogeneous from radially inhomogeneous specimens.

$t_{fh\alpha}$ = Critical $t_{fh}$ value, which separates homogeneous from radially

inhomogeneous specimens.

$t_{aph}$ = t statistic on the total coarse aggregate area proportion from the vertical slice

faces, as an index of homogeneity of a specimen evaluated for radial inhomogeneity.

$t_{fdh}$ = t statistic on the coarse aggregate frequency density from the vertical slice

faces, as the index of homogeneity of a specimen evaluated for radial inhomogeneity.

$t_{aph\alpha}$ = Critical $t_{aph}$ value, which separates homogeneous from radially

inhomogeneous specimens.

$t_{fdh\alpha}$ = Critical $t_{fdh}$ value, which separates homogeneous from radially

inhomogeneous specimens.

$v_{3x}$ = Degree of freedom for the $\chi^2_{3vh}$ test for evaluation of three-layer vertical

inhomogeneity using horizontal slice faces, which is the number of sampling portions

minus 1, which is $3 - 1 = 2$.

$v_{2x}$ = Degree of freedom for the $\chi^2_{2vh}$ test for evaluation of two-layer vertical

inhomogeneity using horizontal slice faces, which is number of sampling portions minus

1, which is $2 - 1 = 1$.

$w_{vi}$ = Width of the $i^{th}$ vertical slice face of a specimen evaluated for two-layer and

three-layer vertical inhomogeneity, which is also the width of the corresponding sampling

portion on the $i^{th}$ vertical slice faces.

427

$w_{hi}$ = Width of the $i^{th}$ vertical slice face of a specimen evaluated for radial inhomogeneity.

$w_{ci}$ = Width of the core strip of the $i^{th}$ vertical slice face of a specimen evaluated for radial inhomogeneity.

$w_{ri}$ = Width of one of the two ring strips of the $i^{th}$ vertical slice face of a specimen evaluated for radial inhomogeneity.

$w_{ti}$ = Width of one of the two transition strips on the $i^{th}$ vertical slice face of a specimen evaluated for radial inhomogeneity.

$\chi^2_{hv}$ = Chi-square frequency statistic from the horizontal slices, as the index of homogeneity of a specimen evaluated for two-layer vertical inhomogeneity.

$\chi^2_{hv\alpha}$ = Critical $\chi^2_{hv}$ value, which separates homogeneous specimens from two-layer vertically inhomogeneous specimens.

$\chi^2_{3h}$ = Chi-square frequency statistic for evaluating three-layer vertical inhomogeneity using horizontal slice faces.

$\chi^2_{3h\alpha}$ = Critical $\chi^2_{3h}$ value, which separates homogeneous specimens from the three-layered inhomogeneous specimens for the selected level of significance.

$\chi^2_{vv}$ = Chi-square frequency statistic measured from the vertical slice faces of a specimen evaluated for two-layer vertical inhomogeneity.

$\chi^2_{vv\alpha}$ = Critical $\chi^2_{vv}$ value, which separates homogeneous specimens from

two-layer vertically inhomogeneous specimens.

$\chi^2_{hh}$ = Chi-square frequency statistic from the horizontal slice faces, as the index

of homogeneity of a specimen evaluated for radial inhomogeneity.

$\chi^2_{hh\alpha}$ = Critical $\chi^2_{hh}$ value, which separates homogeneous specimens from radially

inhomogeneous specimens.

$\chi^2_{vh}$ = Chi-square frequency statistic from the vertical slice faces, as the index of

homogeneity of a specimen evaluated for radial inhomogeneity.

$\chi^2_{vh\alpha}$ = Critical $\chi^2_{vh}$ value, which separates homogeneous specimens from radially

inhomogeneous specimens.

$x_{lv}$ = Expected maximum frequency on the lower portions of the nine vertical slice

faces of a specimen evaluated for two-layer vertical inhomogeneity.

$x_{uv}$ = Expected maximum frequency on the upper portions of nine vertical slice

faces of a specimen evaluated for two-layer vertical inhomogeneity.

$x_{rh}$ = Expected maximum coarse aggregate frequency on the three ring portions of

horizontal slice faces of a specimen evaluated for radial inhomogeneity.

$x_{ch}$ = Expected maximum coarse aggregate frequency on the three core portions of

horizontal slice faces of a specimen evaluated for radial inhomogeneity.

429

$x_{rv}$ = Expected maximum coarse aggregate frequency on the ring portions of nine vertical slice faces of a specimen evaluated for radial inhomogeneity.

$x_{cv}$ = Expected maximum coarse aggregate frequency on the core portions of nine vertical slice faces of a specimen evaluated for radial inhomogeneity.

$z_{vv}$ = Frequency proportion index measured from vertical slice faces of a specimen evaluated for two-layer vertical inhomogeneity, which has standard normal distribution.

$z_{vv\alpha}$ = Critical $z_{vv}$ value, which separates homogeneous specimens from two-layer vertically inhomogeneous specimens.

$z_{hh}$ = Frequency proportion index from horizontal slice faces of a specimen evaluated for radial inhomogeneity, which has standard normal distribution.

$z_{hh\alpha}$ = Critical $z_{hh}$ value, which separates homogeneous specimens from radially inhomogeneous specimens.

$z_{vh}$ = Frequency proportion index from vertical slice faces of a specimen evaluated for radial inhomogeneity, which has standard normal distribution.

$z_{vh\alpha}$ = Critical $z_{vh}$ value, which separates homogeneous specimens from radially inhomogeneous specimens.

# REFERENCES

1. American Association of State Highway and Transportation Officials (AASHTO). (1997). "Segregation causes and cures for hot mix asphalt." *AASHTO/NAPA Joint Task Force on Asphalt Segregation*, Washington, D.C.

2. American Association of State Highway and Transportation Officials (AASHTO). (1998). "Method for determining the permanent deformation and fatigue cracking characteristics of hot mix asphalt (HMA) using the simple shear test (SST) device." *AASHTO Provisional Standards TP7-98*, Washington, D.C.

3. American Association of State Highway and Transportation Officials (AASHTO). (2000). "Method for preparing and determining the density of hot mix asphalt (HMA) specimens by means of the Superpave gyratory compactor." *AASHTO Provisional Standards TP4-00*, Washington, D.C.

4. American Association of State Highway and Transportation Officials (AASHTO). (2003). "Determining dynamic modulus of hot-mix asphalt concrete mixtures." *AASHTO Provisional Standards TP62-03*, Washington, D.C.

5. Ansell, P. and Brown, S. F. (1978). "Cyclic simple shear apparatus for dry granular materials." *Geotechnical Testing Journal*, 1(2), 91-92.

6. Ayyub, B. M. and McCuen, R. H. (1997). *Probability, statistics, & reliability for engineers*, CRC Press, Boca Raton, Florida.

7. Azari, H., McCuen, R. H., and Stuart, K. D. (2003). "Optimum compaction temperature for modified binders." *Journal of Transportation Engineering, ASCE*, 129(5), 531-537.

8. Besag, J. E. and Gleave, J. T. (1974). "On the detection of spatial pattern in plant communities." *Bulletin of the International Statistical Institute,* 45(1), 153-158.

9. Buchanan, M. S. (2000). "An evaluation of selected methods for measuring the bulk specific gravity of compacted hot mix asphalt (HMA)." *Journal of the Association of Asphalt Paving Technologists,* 69, 608-634.

10. Busters, M., Saxl, I., Kohutek, I., and Sulleiova, K. (1996). "Analysis of spatial arrangement of particles in thin foil of Al-$Al_4C_3$ composite." *Institute of Materials Research*, Slovak Academy of Sciences, Watsonova, Slovak Republic.

11. Byth, K. and Ripley, B. D. (1980). "On sampling spatial patterns by distance methods." *Biometrics*, 36, 279-284.

12. Christensen, D. W. (2001). "Requirements for voids in mineral aggregates for Superpave mixtures." *Interim NCHRP Report 90-25*, National Cooperative Highway Research Program (NCHRP), Washington, D.C.

13. Cressie, N. (1993). *Statistics for spatial data*, John Wiley and Sons, New York, New York.

14. Chang, C., Baladi, G., and Wolff, T. (2000). "Detecting segregation in bituminous pavements." *Transportation Research Record 1813*, Transportation Research Board, Washington, D.C., 77-86.

15. Cross, S. A. and Brown, E. R. (1993). "Effect of segregation on performance of hot mix asphalt." *Transportation Research Record 1417*, Transportation Research Board, Washington, D.C., 117-126.

16. Curray, J. R. (1956). "Analysis of two-dimensional orientation data." *Journal of Geology*, 64, 117-131.

17. Diggle, P. J. (1977). "A note on robust density estimation for spatial point patterns." *Biometrika*, 64, 91-95

18. Diggle, P. J. (1979). "On parameter estimation and goodness-of-fit testing for spatial point patterns." *Biometrics*, 35, 87-101.

19. Diggle, P. J. (1983). *Statistical analysis of spatial point patterns,* Academic Press.

20. Diggle, P. J., Besag, J. E., and Gleaves, J. T. (1976). "Statistical analysis of spatial point patterns by means of distance methods." *Biometrics*, 32, 659-667.

21. Duncan, J. M. and Dunlop, P. (1969). "Behavior of soils in simple shear tests." *Proceeding, International Conference On Soil Mechanics and Foundation Engineering*, Mexico, 101-109.

22. Edwards, S. F. and Wilkinson, D. R. (1980). "The deduction of the probability distribution of sphere sizes in a random assembly from measurements on a cross-section through the assembly." *Journal of Physics (London). D: Applied Physics* 13: L209-L211.

23. Eriksen, K. (1992). "Homogeneity of air voids in asphalt-aggregate mixtures compacted by different methods at different temperatures." *Strategic Highway*

*Research Program,* SHRP-88-AIIR-13, National Research Council, Washington, D.C.

24. Hanisch, K. H. and Stoyan, D. (1981). "Stereological estimation of the radial distribution function of centers of spheres." *Journal of Microscopy,* 122, 131-141.

25. Harvey, J., Eriksen, K., Sousa, J., and Monismith, C. (1994). "Effects of laboratory specimen preparation on aggregate-asphalt structure, air-void content measurements, and repetitive simple shear test results." *Transportation Research Record 1454*, Transportation Research Board, National Research Council, Washington, D.C., 113-121.

26. Heltshe, J. F. and Ritchey, T. A. (1984). "Spatial pattern detection using quadrat samples." *Biometrics*, 40, 877-885.

27. Hilliard, J. E. and Anacker, D. C. (1974). "Estimation of the size and orientation distribution of filamentary features from measurements on a two-dimensional section." *Journal of Microscopy,* 102(1), 41-48.

28. Holgate, P. (1965). "Some new tests of randomness." *Journal of Ecology,* 53, 261-266.

29. Image-Pro Plus Version 4.5. (2001). Media Cybernetics, Silver Spring, MD.

30. Instrotek Inc. (2001). Corelok Operator Guide Version 10, Raleigh, NC.

31. Kandhal, P. S., Foo, K. Y., and Mallick, R. B. (1997). "Critical review of voids in mineral aggregate requirements in Superpave." *Transportation Research Record 1609*, Transportation Research Board, National Research Council, Washington, D.C., 21-27.

32. Kennedy, W. J. and Gentle, J. E. (1980). *Statistical computing*. New York: Marcel Dekker.

33. Ketcham, R. A. and Carlson, W. D. (2000). "Quantitative characterization of asphalt concretes using high-resolution x-ray computed tomography (CT)." *NCHRP-IDEA Project 64,* Transportation Research Board, National Research Council, Washington, D.C.

34. Ketcham, R. A. and Carlson, W. D. (2001). "Acquisition, optimization and interpretation of x-ray computed tomographic imagery: Applications to the geosciences." *Journal of Computers and Geosciences,* 27, 381-400.

35. Khedaywi, T. S. and White, T. D. (1994). "Development and analysis of laboratory techniques for simulating segregation." *Transportation Research Record* 1492, Transportation Research Board, National Research Council, Washington, D.C., 36-45.

36. Khedaywi, T. S. and White, T. D. (1996). "Effect of segregation on fatigue performance of asphalt paving mixtures." *Transportation Research Record 1543*, Transportation Research Board, National Research Council, Washington, D.C., 63-70.

37. Landis, E. N., Nagy, E. N., and Keane, D. T. (2003). "Microstructure and fracture in three dimensions." *Engineering Fracture Mechanics*, 70(7), 911-925.

38. Lin, H. C. (1997). "Javamesh- A two dimensional triangular mesh generator for finite elements." *Master of Science Thesis*, University of Pittsburgh.

39. Mardia, K.V., Edwarda, R., and Puri, M. L. (1977). "Analysis of central place theory." *Bulletin of the International Statistical Institute*, 47, 93-110.

40. Masad, E. and Bahia, H. (2002). "Effect of loading configuration and material properties on non-linear response of asphalt mixtures." *Journal of the Association of Asphalt Paving Technologists*, 71, 575- 607.

41. Masad, E., Muhunthan, B., Shashihar, N., and Harman, T. (1998). "Aggregate orientation and segregation in asphalt concrete." *ASCE, Geotechnical Special Publication*, 85, 69-80.

42. Masad, E. and Tashman, L. (2001). "Internal structure analysis of asphalt mixes to improve the simulation of Superpave gyratory compaction to field condition." *Final Report*, Washington Center for Asphalt Technology, Pullman, Washington.

43. Mathieu, O., Cruz-Orive, L. M., Hoppeler, H., and Weibel, E. R. (1980). "Measuring error and sampling variation in stereology: Comparison of the efficiency of various methods for planer image analysis." *Journal of Microscopy*, 121, 75-88.

44. McCuen, R. H. (1985). *Statistical methods for engineers*. Prentice-Hall, Inc., Englewood Cliffs, N. J.

45. McCuen, R. H. (2003). *Modeling hydrologic change*, Lewis Publishers, Boca Raton, FL.

46. McCuen, R. H. and Azari, H. (2001). "Assessment of asphalt specimen homogeneity." *Journal of Transportation Engineering,* ASCE, 127(5), 363-369.

47. McCuen, R. H., Azari, H., and Shashidhar, N. (2001). "Computer simulation of statistical characterization of aggregate inhomogeneity in asphalt concrete."

*Transportation Research Record 1757*, Transportation Research Board, National Research Council, 119-126.

48. Meakin, P. and Jullien, R. (1991)."Simulation of particle deposition and segregation." *Physics of Granular Media.* Nova Science, New York, N.Y.

49. Miles, R. E. (1970). "On the homogeneous planar poisson point process." *Mathematical Biosciences*, 6, 85-127.

50. Miles, R. E. (1978). "The sampling, by quadrats, of planar aggregates." *Journal of Microscopy,* 113(3), 257-267.

51. Miles, R. E. and Davy, P. (1977). "On the choice of quadrats in stereology." *Journal of Microscopy*, 110, 27-44.

52. National Cooperative Highway Research Program (NCHRP). (2002). " Simple performance test for Superpave mix design." *NCHRP Report 465*, Washington, D.C.

53. National Cooperative Highway Research Program (NCHRP). (2004). " Guide for mechanistic-empirical design of new and rehabilitated pavement structure." *NCHRP Report 1-37A*, Washington, D.C.

54. Nolan, G. T. and Kavanagah, P. E. (1993). "Computer simulation of random packings of spheres with log-normal distribution." *Powder Technology*, 76, 309-316.

55. Oda, M. (1972). "Initial fabric and their relations to mechanical properties of granular material." *Soils and Foundations*, 12(1), 17-36.

56. Okabe, A., Boots, B., and Kokichi, S. (1992). *Spatial tessellations*. John Wiley & Sons, New York, N.Y.

57. Ripley, B. D. (1981). *Spatial statistics*. John Wiley & Sons, New York, N.Y.

58. Romero, P. and Anderson, M. (2000). "Variability of superpave shear tester repeated shear at constant height test." *In-house FHWA Study*, Draft version.

59. Romero, P. and Masad, E. (2001). "Relationship between the representative volume element and mechanical properties of asphalt concrete." *Journal of Materials in Civil Engineering*, ASCE, 13(1), 77-84.

60. Russ, J. C. (1994). *The Image processing handbook*. 2$^{nd}$ edition. CRC Press, Inc., Boca Raton, FL.

61. Russ, J. C. (1999). *Image analysis tutorial*. Third Edition. A hands-on Workshop on Image Processing and Analysis Techniques using Image-Pro Plus, Media Cybernetics, L. P., Silver Spring, MD.

62. Shashidhar, N. (2000). "X-ray tomography of asphalt concrete." *Transportation Research Record 1681*, Transportation Research Board, National Research Council, Washington, D.C., 186-191.

63. Sobel', I. M. (1994). *A primer for the Monte Carlo method*. CRC Press, Boca Raton, FL.

64. Stroup-Gardiner, M. and Brown, E. R. (1999). "Segregation in hot mix asphalt pavements." *Report 441, National Cooperative Highway Research Program.* Transportation Research Board, Washington, D.C.

65. Stuart, K. D. (2000). "On the Superpave asphalt binder specification for fatigue cracking performance." *In-house FHWA Technical Memorandum*, Federal Highway Administration, McLean, VA.

66. Stuart, K. D. and Mogawer, W. S. (2001). "Understanding the performance of modified binders in mixtures: Permanent deformation using a mixture with diabase aggregates." *In-House Report, FHWA-RD-02-042*, Federal Highway Administration, McLean, VA.

67. Stuart, K. D., Mogawer, W. S., and Romero, P. (1999). "Validation of asphalt binder and mixture tests that measure rutting susceptibility using the accelerated loading facility." *In-House Report, FHWA-RD-99-204*, Federal Highway Administration, McLean, VA.

68. Tallis, G. M. (1970). "Estimating the distribution of spherical and elliptical bodies in conglomerates from plane sections." *Biometrics,* 26, 87-103.

69. Tashman, L., Masad, E., D'Angelo, J., Bukowski, J., and Harman, T. (2002). "X-ray tomography to characterize air void distribution in Superpave gyratory compacted specimens." *International Journal of Pavement*, 3(1), 19-28.

70. Tashman, L. Masad, E., Peterson, R., and Saleh, H. (2001). "Internal structure analysis of asphalt mixes to improve the simulation of Superpave gyratory compaction to field conditions." *Journal of the Association of Asphalt Paving Technologists,* 70, 605-634.

71. Tashman, L., Masad, E., Zbib, H., Little, D., and Kaloush, K. (2005). "Microstructural viscoplastic continuum model for permanent deformation in asphalt pavements." *Journal of Engineering Mechanics*, 131(1), 48-57.

72. Taylor, C. C. (1983). "A new method for unfolding sphere size distributions." *Journal of Microscopy*, 132(1), 57-66.

73. Tobita, Y. (1989). "Fabric tensors in constitutive equations for granular materials." *Soils and Foundations*, 29(4), 99-104.

74. Vincent, P. J., Collins, R., Griffiths, J., and Howarth, J. (1983). "Statistical geometry of geographical point patterns." *Geographia Polonica*, 45, 109-125.

75. Vincent, P. J., Howarth, J., Griffiths, J., and Collins, R. (1976). "The detection of randomness in plant patterns." *Journal of Biogeography*, 3, 373-380.

76. Vincent, P. J., Howarth, J., Griffiths, J., and Collins, R. (1977). "Urban settlement patterns and the properties of the simplicial graph." *The Professional Geographer*, 29, 21-25.

77. Wang, L. B., Wang, Y. P., Mohammed, L., and Harman, T. (2002). "Voids distribution and performance of asphalt concrete." *International Journal of Pavement*, 1(3), 22-33.

78. Williams, R. C., Duncan, G., and White, T. D. (1996). "Hot-mix asphalt segregation: Measurement and effects." *In Transportation Research Record, 1543*, Transportation Research Board, National Research Council, Washington, D.C., 97-105.

79. Witczak, M.W., Bonaquist, R., Von Quintus, H., and Kaloush, K. (2000). "Specimen geometry and aggregate size effects in uniaxial compression and constant height shear tests." *Journal of the Association of Asphalt Paving Technologists,* 69, 733-793.

80. Wojnar, L. (1998). *Image analysis*. CRC Press, Boca Raton, Florida.

81. Yue, Z. Q., Bekking, W., and Morin, I. (1995). "Application of digital image processing to quantitative study of asphalt concrete microstructure." *In*

*Transportation Research Record, 1492*, Transportation Research Board,

National Research Council, Washington, D.C., 53-60